ISSN 0031 - 9465

PHYTOPATHOLOGIA MEDITERRANEA

Plant health and food safety

Volume 63 • No. 2 • August 2024

The international journal of the
Mediterranean Phytopathological Union

FIRENZE UNIVERSITY PRESS

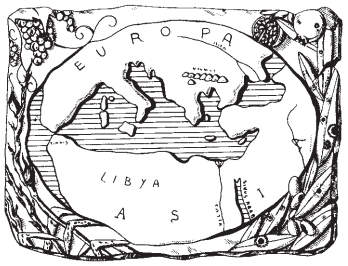

PHYTOPATHOLOGIA MEDITERRANEA

Plant health and food safety

The international journal edited by the Mediterranean Phytopathological Union
founded by A. Ciccarone and G. Goidànich

Phytopathologia Mediterranea is an international journal edited by the Mediterranean Phytopathological Union The journal's mission is the promotion of plant health for Mediterranean crops, climate and regions, safe food production, and the transfer of knowledge on diseases and their sustainable management.
The journal deals with all areas of plant pathology, including epidemiology, disease control, biochemical and physiological aspects, and utilization of molecular technologies. All types of plant pathogens are covered, including fungi, nematodes, protozoa, bacteria, phytoplasmas, viruses, and viroids. Papers on mycotoxins, biological and integrated management of plant diseases, and the use of natural substances in disease and weed control are also strongly encouraged. The journal focuses on pathology of Mediterranean crops grown throughout the world.
The journal includes three issues each year, publishing Reviews, Original research papers, Short notes, New or unusual disease reports, News and opinion, Current topics, Commentaries, and Letters to the Editor.

PHYTOPATHOLOGIA MEDITERRANEA

The international journal of the Mediterranean Phytopathological Union

Volume 63, August, 2024

Firenze University Press

***Phytopathologia Mediterranea*. The international journal of the Mediterranean Phytopathological Union**
https://www.fupress.com/pm

Direttore Responsabile: **Giuseppe Surico**, University of Florence, Italy

Published by Firenze University Press

Firenze University Press
Università degli Studi di Firenze
via Cittadella, 7, 50144 Firenze, Italy
www.fupress.com

Phytopathologia Mediterranea
The international journal of the
Mediterranean Phytopathological Union

Firenze University Press
www.fupress.com/pm

Research Papers

Diversity of *Colletotrichum* species on strawberry (*Fragaria* × *ananassa*) in Germany

Christiane ROSE[1], Ulrike DAMM[2,*]

[1] *Hochschule Geisenheim University, Von-Lade-Straße 1, D-65366 Geisenheim, Germany*
[2] *Senckenberg Museum of Natural History Görlitz, PF 300 154, 02806 Görlitz, Germany*
*Corresponding author. E-mail: ulrike.damm@senckenberg.de

Summary. Anthracnose caused by *Colletotrichum* species is an important disease of strawberries (*Fragaria* × *ananassa*), but the species causing this disease in Germany have not been investigated based on modern systematics. By using multi-locus phylogenetic analyses (ITS, *act*, *gapdh*, *chs-1*, *his3*, *tub2*), 58 *Colletotrichum* isolates from previous and recent collections, obtained mainly from fruit anthracnose of cultivated strawberries in Germany, were identified or re-identified as *C. fioriniae*, *C. godetiae* and *C. nymphaeae* (*C. acutatum* species complex) as well as *C. anthrisci* and *C. lineola* (*C. dematium* complex). *Colletotrichum nymphaeae* was dominant; most of the isolates belonged to one clonal lineage that occurs on strawberries throughout Europe, the United States of America, and some African and Asian countries. One of the other two haplotypes was distantly related and only represented by recently collected material. All other species, each of one haplotype, had only been isolated once or twice from German strawberries. This is the first report of *C. anthrisci* in Germany and for the genus *Fragaria* worldwide; all the other isolated fungi are newly reported for this genus in Germany. Comparisons of morphological characteristics of the species identified demonstrate that these features are of limited use for identification, even to species complex level. In pathogenicity tests, all five species caused anthracnose symptoms on ripe fruit of *Fragaria* × *ananassa* 'Asia'.

Keywords. Anthracnose, *Colletotrichum acutatum*, *C. dematium*, multi-locus phylogeny, pathogenicity.

OPEN ACCESS

Citation: Rose, C., & Damm, U. (2024) Diversity of *Colletotrichum* species on strawberry (*Fragaria × ananassa*) in Germany. *Phytopathologia Mediterranea* 63(2): 155-178. doi: 10.36253/phyto-15094

Accepted: May 2, 2024

Published: July 17, 2024

Data Availability Statement: All relevant data are within the paper and its Supporting Information files.

Competing Interests: The Author(s) declare(s) no conflict of interest.

Editor: Vladimiro Guarnaccia, DiSAFA - University of Torino, Italy.

ORCID
CR: 0009-0003-6767-5547
UD: 0000-0002-2252-5196

INTRODUCTION

Strawberries (*Fragaria* × *ananassa*, *Rosaceae*) are the most common fruit crops after apples in Germany, with a harvested volume of 133,135 t in 2022 (Lehari, 2002; Statistisches Bundesamt, 2023). Intensive strawberry breeding, which has been primarily aimed at high yields, influenced the gene structure and thus immunity to pathogens in strawberries (Hardigan *et al*., 2018), so strawberry cultivation is associated with high production risks. In the presence of warm temperatures and high humidity, rapid outbreaks of anthracnose caused by *Colletotrichum* species can be expected (Howard *et al*., 1992). Trading of young plantlets with latent infections can rapidly spread the disease over long distances (Howard *et al*., 1992). Anthracnose of strawberry

fruit is characterised as brown, sunken spots, in which orange conidial mucilage develops. Main symptoms of green tissues (runners, leaves and stalks) include dark, sunken, necrotic areas (Howard *et al*., 1992).

Brooks (1931) reported a new strawberry disease in Florida, United States of America (USA), called anthracnose, and described the causative pathogen as *C. fragariae*. In the 1980s, *C. acutatum sensu lato* was first reported from strawberries in the USA (Smith and Black, 1986). Anthracnose symptoms in strawberry fields in Germany (Baden, Palatinate) and other European countries including France, Bulgaria, Sweden, Denmark, Spain and Belgium have been reported at least since the 1990s and attributed to *C. acutatum* and *C. gloeosporioides*, while *C. fragariae* was only found within material from the USA (Denoyes and Baudry, 1995; Laun and Fried, 1996; Bobev *et al*., 2002; Nilsson *et al*., 2005; Sundelin *et al*., 2005; Garrido *et al*., 2008; Debode *et al*., 2009). The first molecular study of *Colletotrichum* in Germany by Nirenberg *et al.* (2002) focusing on *C. lupini*, included a strain from strawberry in Germany that had also been identified as *C. acutatum* based on ITS sequence data. Within this investigation, several *Colletotrichum* strains from different hosts and countries, including from strawberries in Germany, had been collected and are maintained at the culture collection of the Biologische Bundesanstalt für Land- und Forstwirtschaft (BBA) Berlin, now Julius Kühn-Institut (JKI), Bundesforschungsinstitut für Kulturpflanzen (Federal Research Centre for Cultivated Plants), Institut für Epidemiologie und Pathogendiagnostik, Braunschweig, Germany.

The systematics of *Colletotrichum* has changed within the last 20 years, due to application of molecular data, especially in multi-locus DNA sequence analyses. *Colletotrichum acutatum* and *C. gloeosporioides* that had been previously regarded as causal agents of strawberry anthracnose were shown to be large species complexes (Damm *et al*., 2012a; Weir *et al*., 2012). The number of accepted *Colletotrichum* species, those that have been revised or newly described based on multi-locus DNA sequences, is constantly increasing; more than 300 *Colletotrichum* species in at least 15 species complexes and more than ten further species are currently accepted (Liu *et al*., 2022; Talhinhas and Baroncelli, 2023). To date, at least 22 species are known from strawberry, belonging to the *C. acutatum*, *C. boninense*, *C. coccodes*, *C. dematium*, *C. gloeosporioides* and *C. truncatum* species complexes (Farr and Rossman, 2024). *Colletotrichum acutatum sensu stricto* is only confirmed from strawberry in Australia (Damm *et al*., 2012a), while most reports of *C. acutatum* on strawberry in the USDA Fungal Databases (Farr and Rossman, 2024), including that from Germany (Nirenberg *et al*., 2002), date back to the pre-molecular era, or were from before *C. acutatum* was shown to be a species complex (Damm *et al*., 2012a). Therefore, these fungi should be considered as *C. acutatum sensu lato* and could include other species within this complex.

To date, only *Colletotrichum* strains infecting a few random, often exotic host plants collected in Germany have been identified or described based on modern systematics (e.g. Damm *et al*., 2012a, b, 2014, 2019; Weir *et al*., 2012); while there are no records of *Colletotrichum* species from *Fragaria* hosts in Germany identified on the same basis.

The aims of the present study were to investigate the diversity of *Colletotrichum* on strawberries from all over Germany based on multi-locus sequence data, to characterise the species morphologically and to test their pathogenicity to fruit of cultivated strawberry (*Fragaria* × *ananassa*) 'Asia'.

MATERIALS AND METHODS

Isolates

Symptomatic material of cultivated strawberry plants (*Fragaria* × *ananassa*) was collected in different regions of Germany, including Saxony (Dresden, Görlitz, Ore Mountains), Brandenburg (Spreewald), North Rhine-Westphalia (Münsterland), Lower Saxony (Lüdersfeld) and Mecklenburg-Western Pomerania (Mecklenburg Lake District). The collected material also included fruit bought at markets in Germany (some of Polish origin) and one sample from wild strawberry (*Fragaria vesca*).

Most of the newly collected material consisted of infected fruit of *F.* × *ananassa*, which had symptoms of brown, sunken spots of necrotic tissue that spread radially. Orange conidial masses sometimes developed in the centres of these spots. Flat, pale to dark mouse-grey mycelium often formed at the edges and sometimes over the entire infection sites. Elongated dark brown necroses initially formed on host stems and petioles, which spread and developed into stem-encompassing necroses and constrictions, on which conidia were sometimes observed. On affected leaves of *F.* × *ananassa*, roundish to oval necrotic areas were observed, each with dark brown irregular edges and a light brown centre, which partially merged. Symptoms of the *F. vesca* leaf sample were similar; grey-brown spots of various sizes and shapes with paler centres and darker irregular margins formed especially at the edges of affected leaves.

To obtain single-conidium isolates, conidia formed on the necrotic host tissues were spread on the surface

of petri dishes with synthetic nutrient-poor agar (SNA; Nirenberg, 1976) using a drop of sterile water. On the following day, single germinating conidia were transferred to oatmeal agar (OA; Crous *et al*., 2019). Plant parts, on which no conidia were present, were surface sterilised (1 min in 3.5% NaClO, 30 s in 70% ethanol), washed in sterile water and placed in petri dishes on sterile filter paper with sterile water until conidia were formed, from which single-conidium isolates were produced.

A further 22 isolates from the culture collection of the former BBA had been collected more than 20 years ago in the federal states of Mecklenburg-Western Pomerania, Saxony, Baden-Württemberg, Hesse, Rhineland-Palatinate and Brandenburg and included one strain bought in a supermarket that originated from the Netherlands.

Although it was not possible to complete and confirm all collection data, it is assumed that all the BBA isolates originated from anthracnose symptoms, especially from fruit rot, because the material had been deposited by plant protection offices in different German federal states in the years when strawberry anthracnose spread across Europe. For one of the isolates from Saxony there was information provided that a 2-year-old stock of 'Selva' (imported plants) was very heavily infested, and a 1-year-old stock was over 50% infected. Most of the strawberry runners from which isolates had been obtained were characterised as necrotic, while one isolate had a noticeable reddish discolouration at the infection site. Two isolates originated from brown roots of *F. vesca* var. *semperflorens*. There was no information on the leaf symptom and no further information on fruit symptoms than fruit rot.

The isolates were stored in the culture collection of the Senckenberg Museum of Natural History Görlitz, Germany (GLMC; Table 1). Selected isolates were deposited in the German Collection of Microorganisms and Cell Cultures (DSMZ), Braunschweig, Germany.

Morphological analyses

The *Colletotrichum* strains were cultivated on SNA with autoclaved filter paper and double-autoclaved stems of *Anthriscus sylvestris* and on OA. Cultures were incubated at 20°C under near UV light (12 h daily photoperiod) for 10 d. Microscopic preparations were made in clear lactic acid. Measurements of microscopic structures of the fungi were carried out according to Damm *et al*. (2007), with 30 measurements per structure and strain, using a Nikon SMZ1000 dissecting microscope (DM) and a Nikon Eclipse 80i compound microscope with differential interference contrast (DIC). Appressoria were observed on the reverse sides of the SNA cultures. Colony features on SNA and OA were observed after the incubation period. To calculate colony growth rates, the diameters of the colonies were determined after 7 and 10 d. Colony colour was characterised according to Rayner (1970).

Phylogenetic analyses

Genomic DNA was extracted from cultures according to Damm *et al*. (2008). The 5.8S nuclear ribosomal RNA gene with the two flanking internal transcribed spacers (ITS), a 200-bp intron of the glyceraldehyde-3-phosphate dehydrogenase (*gapdh*) and partial sequences of the chitin synthase 1 (*chs-1*), histone H3 (*his3*), actin (*act*) and beta-tubulin (*tub2*) genes were amplified and sequenced using the respective primer pairs ITS-1F (Gardes and Bruns, 1993) + ITS-4 (White *et al*., 1990), GDF1 + GDR1 (Guerber *et al*., 2003), CHS-354R + CHS-79F (Carbone and Kohn, 1999), CYLH3F + CYLH3R (Crous *et al*., 2004), ACT-512F + ACT-783R (Carbone and Kohn, 1999) and T1 (O'Donnell and Cigelnik, 1997) + Bt-2b (Glass and Donaldson, 1995) or T1 + BT4R (Woudenberg *et al*., 2009). DNA amplifications were carried out in a Mastercycler® pro S (Eppendorf), each in a total volume of 20 µL. The PCR reaction mixture contained 1 µL of 1:10 diluted genomic DNA, 2.5 µL of 10× buffer (Peqlab), 1 µL of each primer (10 mM), 2.5 µL of $MgCl_2$ (25 mM), 2.5 µL of dNTPs (2 mM), 0.7 µL of DMSO and 0.1 µL of *Taq* DNA polymerase (0.5 U; Peqlab). Conditions for PCR of *gapdh*, *chs-1*, *his3*, *act*, and *tub2* included an initial denaturation step of 5 min at 94°C, followed by 40 cycles each of 30 s at 94°C, 30 s at 52°C and 30 s at 72°C, and a final denaturation step of 7 min at 72°C. ITS PCR was carried out as described by Woudenberg *et al*. (2009). PCR products were visualised on a 1% agarose gel and sequenced by the Senckenberg Biodiversity and Climate Research Centre (BiK-F) laboratory (Frankfurt, Germany). The DNA sequences generated with forward and reverse primers were used to obtain consensus sequences, using BioNumerics v. 7.6.3 (Applied Maths, St-Marthens-Lathem, Belgium), and the alignments were assembled and adjusted manually using Sequence Alignment Editor v. 2.0a11 (Rambaut, 2002). Sequences derived in this study were lodged at NCBI GenBank (www.ncbi.nlm.nih.gov).

For preliminary identification and selection of reference strains, blastn searches were carried out with ITS sequences in NCBI GenBank. Maximum parsimony (MP) analyses were carried out on the multi-locus alignments (ITS, *gapdh*, *chs-1*, *his3*, *act*, *tub2*) with Phy-

logenetic Analysis Using Parsimony (PAUP) v. 4.0b10 (Swofford, 2003), using the heuristic search option with 100 random sequence additions and tree bisection and reconstruction as the branch-swapping algorithm. Alignment gaps were treated as missing, and all characters were unordered and of equal weight. No more than ten trees of score (length) greater than or equal to ten were saved in each replicate. Tree length, consistency index (CI), retention index (RI), rescaled consistency index (RC) and homoplasy index (HI) were calculated for the resulting trees. The robustness of the obtained trees was evaluated by 10,000 bootstrap replications, using the fast-stepwise addition algorithm (Hillis and Bull, 1993). Maximum likelihood (ML) analyses were calculated online using IQ-TREE 1.6 (http://iqtree.cibiv.univie.ac.at; Nguyen *et al*., 2015; Trifinopoulos *et al*., 2016) and model testing under the Bayesian information criterion (BIC) (Kalyaanamoorthy *et al*., 2017). Branch support was obtained by 5000 replicates of ultrafast bootstrap (ufb; Hoang *et al*., 2018; Minh *et al*., 2013). Support values ≥ 95% were considered relevant, following Guindon *et al.* (2010).

Pathogenicity tests

Selected *Colletotrichum* isolates were incubated on OA at 20°C under near UV light for 10 d. To harvest the conidia, 10 mL of sterile distilled water was added to an OA culture of each isolate and swirled thoroughly. The resulting conidium suspensions were adjusted to a final concentration of 2×10^4 conidia mL^{-1}. Ripe fruit of *F.* × *ananassa* 'Asia' (Obsthof Rüdiger, Dresden, Germany) of the quality standard EU No. 543/2011 class Extra (Anonymous, 2011) were surface sterilised with 1% NaClO for 6 min, washed three times with sterile distilled water and placed under sterile conditions on moist filter paper in covered glasses (Gourmet glass, round edge, 300 mL, Weck). Each fruit was inoculated with a 5 µL droplet of conidium suspension (without wounding) or treated with 5 µL of sterile distilled water (experimental control). Five repetitions (fruit) were made for each *Colletotrichum* strain and the control. The covered glasses with inoculated strawberries were placed randomly in a climate cabinet (20°C, 14 h fluorescent light/10 h dark daily cycle, humidity up to 100%). The experiment was carried out twice. Seven d post inoculation (dpi), resulting lesion sizes were determined by counting infected unit squares on a grid placed over scaled photographs. Symptoms were evaluated visually and photographed 7 dpi or, in the case of delayed infection development, 10 dpi. Re-isolations were made from lesion edges and resulting fungi were identified.

RESULTS

Phylogenetic analyses

Based on preliminary morphological examinations and blastn searches of the ITS sequences on NCBI GenBank, 56 of the 58 isolates were identified as belonging to the *C. acutatum* species complex. The other two isolates were identified as belonging to the *C. dematium* complex.

In the multi-locus phylogenetic analyses of the *C. acutatum* species complex (gene boundaries of ITS: 1–546, *gapdh*: 557–829, *chs-1*: 840–1121, *his3*: 1132–1519, *act*: 1530–1777, *tub2*: 1788–2285) 181 isolates, including a selection of 32 (of the 56) newly sequenced isolates from strawberry, 147 reference strains of the *C. acutatum* species complex, and the outgroup *C. orchidophilum* CBS 632.80 and IMI 309357 (Table 1, Supplementary table 1) and 2285 characters including the alignment gaps were processed. Of these, 429 characters were parsimony-informative, 154 parsimony-uninformative and 1702 constant. After a heuristic search using PAUP, the maximum of 590 equally most parsimonious trees were retained (length = 1203 steps, CI = 0.615, RI = 0.947, RC = 0.582, HI = 0.385). One of these trees is shown in Figure 1. The topology of these trees was similar, which was verified for a large section of trees. They differed in the position of taxa within subclades. The consensus tree of the ML analysis confirmed the tree topology obtained with parsimony. The bootstrap values of the two analyses generally agreed with each other. The phylogeny consists of five main clades representing clades 1 to 5 in Damm *et al.* (2012a). Most of the isolates clustered within *C. nymphaeae* (clade 2), where they formed three haplotype groups; most of the strains were of one haplotype. This was the same as several other isolates from strawberry in Europe, Northern America and Africa. According to a preliminary analysis, 46 isolates from the present study belonged to this haplotype, and 24 of these isolates were included in the final analyses. Isolates GLMC 2599, GLMC 2600 and GLMC 2606 represented a second haplotype with other strains from strawberry in Europe and the USA and a strain from *Anemone* in the Netherlands. The third haplotype included isolates GLMC 2653, GLMC 2654 and a strain from *Fragaria* in the USA, forming a distinct subclade (bootstrap support MP/ML: -/100). Two isolates (GLMC 2660, GLMC 2661) clustered in *C. fioriniae* (clade 3); the haplotype was the same as that of a strain from apple in Italy and from *Grevillea* in Germany. Three further strains, two from Germany (GLMC 2589, GLMC 2590) and one from the Netherlands (GLMC 2583), grouped with *C. godetiae* (clade 5). This haplotype was the same as that of strains

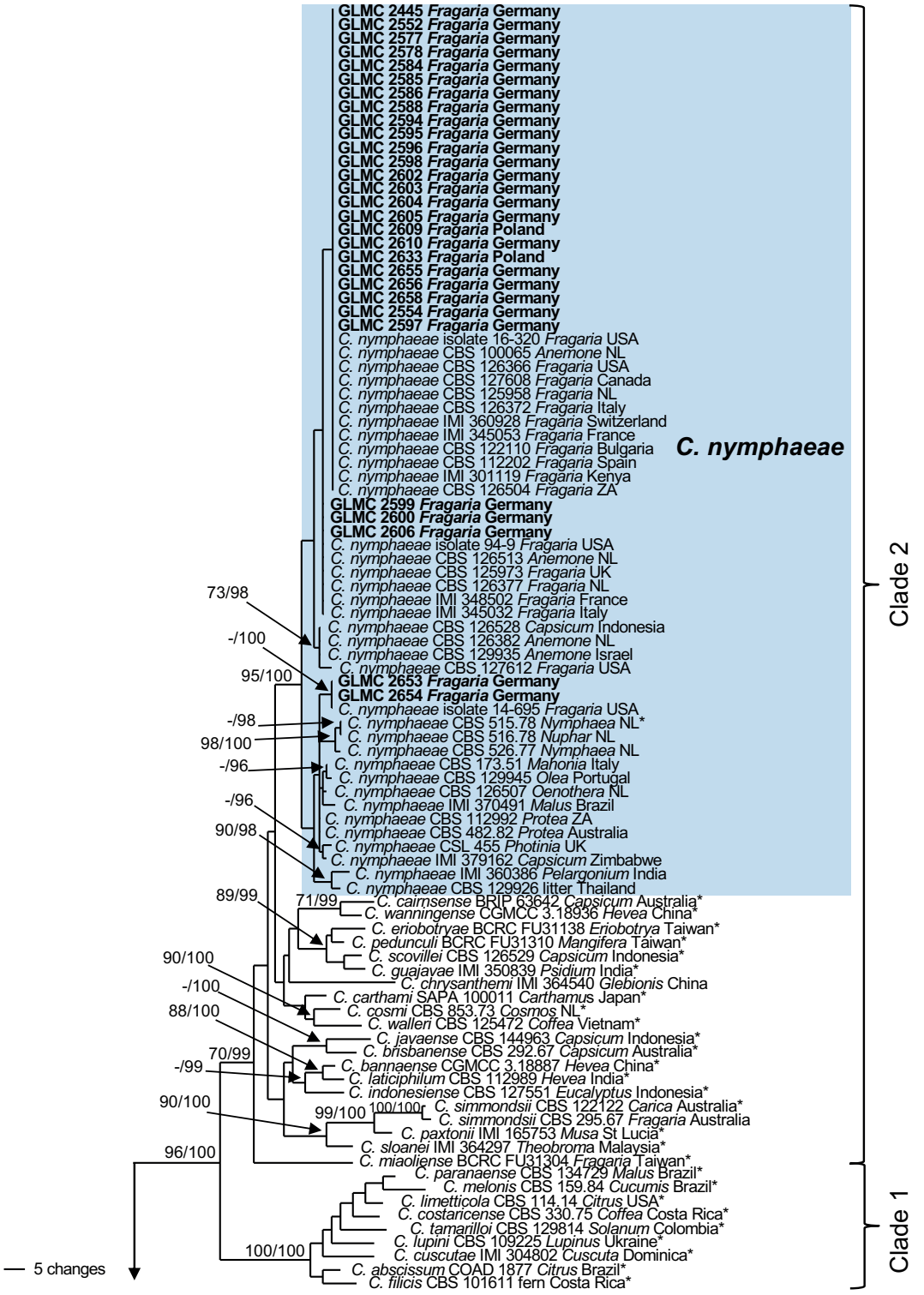

Figure 1. The first of 590 most parsimonious trees obtained from a heuristic search of the combined ITS, *act*, *gapdh*, *chs-1*, *his3*, *tub2* sequence alignment of *Colletotrichum* isolates from *Fragaria* and representative strains of the *C. acutatum* species complex. Bootstrap support values of the MP analysis >70% and of the ML analysis >95% are shown at the nodes. *Colletotrichum orchidophilum* CBS 632.80 and IMI 309357 were used as outgroup. Numbers of ex-type strains are indicated by an asterisk. Isolates obtained or sequenced in this study are shown in bold font. Strain numbers are followed by substrate (host genus) and country of origin (NL = Netherlands, NZ = New Zealand, ZA = South Africa). (Continued)

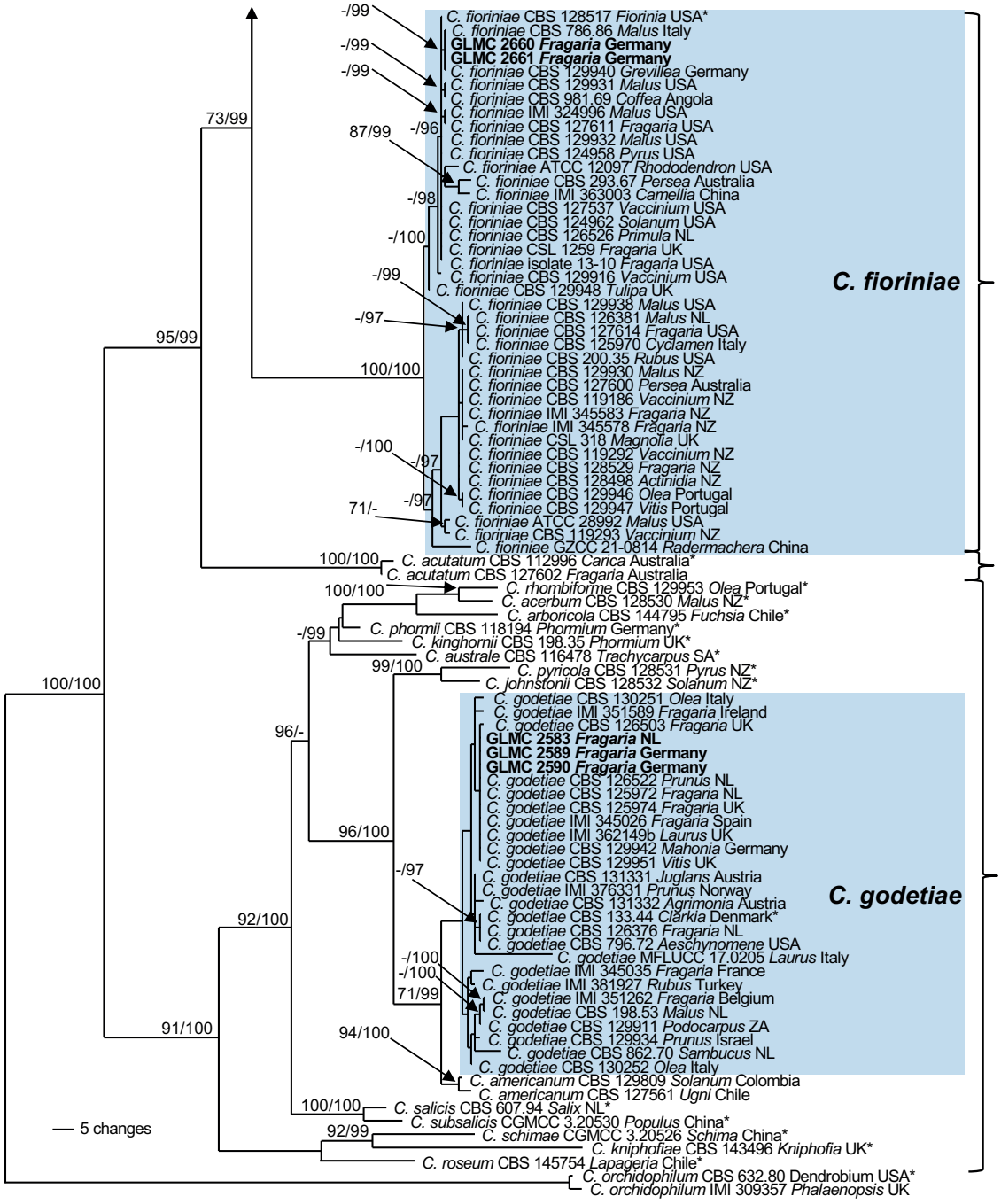

Figure 1. (Continued).

from strawberry and other hosts from other European countries, including an isolate from *Mahonia* in Germany.

In the multi-locus phylogenetic analyses of the *C. dematium* species complex (gene boundaries of ITS: 1–530, *gapdh*: 541–821, *chs-1*: 832–1082, *his3*: 1093–1489, *act*: 1500–1768, *tub2*: 1779–2298), 36 isolates, including the two newly sequenced isolates from strawberry, 33 reference strains and the outgroup *C. chlorophyti* IMI 103806 (Table 1, Supplementary table 1), along with 2298 characters including the alignment gaps were processed. Of these, 415 characters were parsimony-informative, 205 parsimony-uninformative and 1678 constant. After a heuristic search using PAUP, the maximum of 440 equal-

Table 1. Strains of *Colletotrichum* spp. used in this study, with collection details and GenBank accession numbers.

Species	Accession No.[a]	Host/Substrate	Country and Federal State of Germany	GenBank No.[b]					
				ITS	*gapdh*	*chs-1*	*his3*	*act*	*tub2*
C. anthrisci	GLMC 2616, DSM 115225	*Fragaria vesca*, leaf spots	Germany, Saxony	PP069452	PP115710	PP115876	PP115916	PP115767	PP115825
C. fioriniae	GLMC 2660, DSM 115228	*Fragaria* × *ananassa*, fruit rot	Germany, Saxony	PP069446	PP115704	PP115870	—	PP115761	PP115819
C. fioriniae	GLMC 2661, DSM 115229	*Fragaria* × *ananassa*, fruit rot	Germany, Saxony	PP069447	PP115705	PP115871	PP115911	PP115762	PP115820
C. godetiae	GLMC 2589, BBA 70063, DSM 115222	*Fragaria* × *ananassa*, runner with necroses	Germany, Baden-Württemberg	PP069449	PP115707	PP115873	PP115913	PP115764	PP115822
C. godetiae	GLMC 2590, BBA 71234, DSM 115223	*Fragaria* × *ananassa*, fruit	Germany, Mecklenburg-Western Pomerania	PP069450	PP115708	PP115874	PP115914	PP115765	PP115823
C. godetiae	GLMC 2583, BBA 68320	*Fragaria* × *ananassa*, fruit	Netherlands, bought at Plus Markt Berlin, Germany	PP069448	PP115706	PP115872	PP115912	PP115763	PP115821
C. lineola	GLMC 2587, BBA 71830, DSM 115221	*Fragaria* × *ananassa*	Germany, Brandenburg	PP069451	PP115709	PP115875	PP115915	PP115766	PP115824
C. nymphaeae	GLMC 2597, BBA 70822	*Fragaria* × *ananassa*, fruit	Germany, Hesse	PP069424	PP115682	PP115848	—	PP115739	PP115797
C. nymphaeae	GLMC 2554	*Fragaria* × *ananassa*, 'Jive', fruit rot	Germany, Lower Saxony	PP069409	PP115667	PP115833	—	PP115725	PP115782
C. nymphaeae	GLMC 2605, BBA 70094	*Fragaria* × *ananassa*	Germany, Saxony	PP069431	PP115689	PP115855	—	PP115746	PP115804
C. nymphaeae	GLMC 2585, BBA 67865	*Fragaria* × *ananassa*, runner with necroses	Germany, Baden-Württemberg	PP069418	PP115676	PP115842	—	PP115734	PP115791
C. nymphaeae	GLMC 2602, BBA 67859	*Fragaria* × *ananassa*, leaf	Germany, Baden-Württemberg	PP069428	PP115686	PP115852	PP115896	PP115743	PP115801
C. nymphaeae	GLMC 2603, BBA 67866	*Fragaria* × *ananassa*, runner with necroses	Germany, Baden-Württemberg	PP069429	PP115687	PP115853	PP115897	PP115744	PP115802
C. nymphaeae	GLMC 2595, BBA 68394	*Fragaria* × *ananassa*, fruit	Germany, Baden-Württemberg?	PP069422	PP115680	PP115846	PP115891	—	PP115795
C. nymphaeae	GLMC 2596, BBA 70766	*Fragaria* × *ananassa*	Germany, Brandenburg	PP069423	PP115681	PP115847	PP115892	PP115738	PP115796
C. nymphaeae	GLMC 2653, DSM 115226	*Fragaria* × *ananassa*, fruit rot	Germany, Brandenburg	PP069439	PP115697	PP115863	PP115904	PP115754	PP115812
C. nymphaeae	GLMC 2654	*Fragaria* × *ananassa*, fruit rot	Germany, Brandenburg	PP069440	PP115698	PP115864	PP115905	PP115755	PP115813
C. nymphaeae	GLMC 2655	*Fragaria* × *ananassa*, fruit rot	Germany, Brandenburg	PP069441	PP115699	PP115865	PP115906	PP115756	PP115814
C. nymphaeae	GLMC 2598, BBA 70821	*Fragaria* × *ananassa*, fruit	Germany, Hesse	PP069425	PP115683	PP115849	PP115893	PP115740	PP115798
C. nymphaeae	GLMC 2599, BBA 72544	*Fragaria vesca* var. *semperflorens*, brown roots	Germany, Hesse	PP069426	PP115684	PP115850	PP115894	PP115741	PP115799
C. nymphaeae	GLMC 2600, BBA 72543, DSM 115224	*Fragaria vesca* var. *semperflorens*, brown roots	Germany, Hesse	PP069427	PP115685	PP115851	PP115895	PP115742	PP115800
C. nymphaeae	GLMC 2604, BBA 72341	*Fragaria* × *ananassa*, runner with reddish discoloration	Germany, Hesse	PP069430	PP115688	PP115854	PP115898	PP115745	PP115803
C. nymphaeae	GLMC 2552	*Fragaria* × *ananassa*, 'Jive', fruit rot	Germany, Lower Saxony	PP069407	PP115665	PP115831	PP115881	PP115723	PP115780
C. nymphaeae	GLMC 2553	*Fragaria* × *ananassa*, 'Jive', fruit rot	Germany, Lower Saxony	PP069408	PP115666	PP115832	PP115882	PP115724	PP115781

(Continued)

Table 1. (Continued).

Species	Accession No.[a]	Host/Substrate	Country and Federal State of Germany	GenBank No.[b]					
				ITS	*gapdh*	*chs-1*	*his3*	*act*	*tub2*
C. nymphaeae	GLMC 2555	*Fragaria* × *ananassa*, 'Jive', fruit rot	Germany, Lower Saxony	PP069410	PP115668	PP115834	PP115883	PP115726	PP115783
C. nymphaeae	GLMC 2556	*Fragaria* × *ananassa*, 'Jive', fruit rot	Germany, Lower Saxony	PP069411	PP115669	PP115835	PP115884	PP115727	PP115784
C. nymphaeae	GLMC 2557	*Fragaria* × *ananassa*, 'Jive', fruit rot	Germany, Lower Saxony	PP069412	PP115670	PP115836	PP115885	PP115728	PP115785
C. nymphaeae	GLMC 2558	*Fragaria* × *ananassa*, 'Jive', fruit rot	Germany, Lower Saxony	PP069413	PP115671	PP115837	PP115886	PP115729	PP115786
C. nymphaeae	GLMC 2559	*Fragaria* × *ananassa*, 'Jive', fruit rot	Germany, Lower Saxony	PP069414	PP115672	PP115838	PP115887	PP115730	PP115787
C. nymphaeae	GLMC 2610	*Fragaria* × *ananassa*, fruit rot	Germany, Mecklenburg-Western Pomerania	PP069434	PP115692	PP115858	PP115901	PP115749	PP115807
C. nymphaeae	GLMC 2611	*Fragaria* × *ananassa*, fruit rot	Germany, Mecklenburg-Western Pomerania	PP069435	PP115693	PP115859	—	PP115750	PP115808
C. nymphaeae	GLMC 2612	*Fragaria* × *ananassa*, fruit rot	Germany, Mecklenburg-Western Pomerania	PP069436	PP115694	PP115860	PP115902	PP115751	PP115809
C. nymphaeae	GLMC 2656, DSM 115227	*Fragaria* × *ananassa*, 'Asia', petiole with brown spots	Germany, North Rhine-Westphalia	PP069442	PP115700	PP115866	PP115907	PP115757	PP115815
C. nymphaeae	GLMC 2657	*Fragaria* × *ananassa*, 'Asia', petiole with brown spots	Germany, North Rhine-Westphalia	PP069443	PP115701	PP115867	PP115908	PP115758	PP115816
C. nymphaeae	GLMC 2658	*Fragaria* × *ananassa*, 'Asia', leaf spots	Germany, North Rhine-Westphalia	PP069444	PP115702	PP115868	PP115909	PP115759	PP115817
C. nymphaeae	GLMC 2659	*Fragaria* × *ananassa*, 'Asia', leaf spots	Germany, North Rhine-Westphalia	PP069445	PP115703	PP115869	PP115910	PP115760	PP115818
C. nymphaeae	GLMC 2588, BBA 68332	*Fragaria* × *ananassa*, fruit	Germany, Rhineland-Palatinate?	PP069420	PP115678	PP115844	PP115890	PP115736	PP115793
C. nymphaeae	GLMC 2594, BBA 68333	*Fragaria* × *ananassa*, fruit	Germany, Rhineland-Palatinate?	PP069421	PP115679	PP115845	—	PP115737	PP115794
C. nymphaeae	GLMC 2445, DSM 115220	*Fragaria* × *ananassa*, 'Asia', fruit rot	Germany, Saxony	PP069396	PP115654	PP115827	PP115877	PP115712	PP115769
C. nymphaeae	GLMC 2446	*Fragaria* × *ananassa*, 'Asia', fruit rot	Germany, Saxony	PP069397	PP115655	—	—	PP115713	PP115770
C. nymphaeae	GLMC 2447	*Fragaria* × *ananassa*, 'Faith', fruit rot	Germany, Saxony	PP069398	PP115656	—	—	PP115714	PP115771
C. nymphaeae	GLMC 2448	*Fragaria* × *ananassa*, 'Faith', fruit rot	Germany, Saxony	PP069399	PP115657	PP115828	PP115878	PP115715	PP115772
C. nymphaeae	GLMC 2449	*Fragaria* × *ananassa*, 'Diana', fruit rot	Germany, Saxony	PP069400	PP115658	PP115829	PP115879	PP115716	PP115773
C. nymphaeae	GLMC 2450	*Fragaria* × *ananassa*, fruit rot	Germany, Saxony	PP069401	PP115659	—	—	PP115717	PP115774

(Continued)

Table 1. (Continued).

Species	Accession No.[a]	Host/Substrate	Country and Federal State of Germany	GenBank No.[b]					
				ITS	*gapdh*	*chs-1*	*his3*	*act*	*tub2*
C. nymphaeae	GLMC 2451	*Fragaria* × *ananassa*, fruit rot	Germany, Saxony	PP069402	PP115660	—	—	PP115718	PP115775
C. nymphaeae	GLMC 2452	*Fragaria* × *ananassa*, fruit rot	Germany, Saxony	PP069403	PP115661	—	—	PP115719	PP115776
C. nymphaeae	GLMC 2453	*Fragaria* × *ananassa*, fruit rot	Germany, Saxony	PP069404	PP115662	—	—	PP115720	PP115777
C. nymphaeae	GLMC 2454	*Fragaria* × *ananassa*, stem with brown spots	Germany, Saxony	PP069405	PP115663	—	—	PP115721	PP115778
C. nymphaeae	GLMC 2455	*Fragaria* × *ananassa*, stem with brown spots	Germany, Saxony	PP069406	PP115664	PP115830	PP115880	PP115722	PP115779
C. nymphaeae	GLMC 2577, BBA 70090	*Fragaria* × *ananassa*	Germany, Saxony	PP069415	PP115673	PP115839	—	PP115731	PP115788
C. nymphaeae	GLMC 2584, BBA 70095	*Fragaria* × *ananassa*	Germany, Saxony	PP069417	PP115675	PP115841	—	PP115733	PP115790
C. nymphaeae	GLMC 2586, BBA 70092	*Fragaria* × *ananassa*	Germany, Saxony	PP069419	PP115677	PP115843	PP115889	PP115735	PP115792
C. nymphaeae	GLMC 2606, BBA 70093	*Fragaria* × *ananassa*	Germany, Saxony	PP069432	PP115690	PP115856	PP115899	PP115747	PP115805
C. nymphaeae	GLMC 2578, BBA 70091	*Fragaria* × *ananassa*, 'Selva', fruit rot	Germany, Saxony, young plants imported from France via Netherlands	PP069416	PP115674	PP115840	PP115888	PP115732	PP115789
C. nymphaeae	GLMC 1819, 494-99	*Fragaria* × *ananassa*	Germany?, Brandenburg?	PP069395	PP115653	PP115826	—	PP115711	PP115768
C. nymphaeae	GLMC 2609	*Fragaria* × *ananassa*, fruit rot	Poland, bought at the market in Görlitz, Germany	PP069433	PP115691	PP115857	PP115900	PP115748	PP115806
C. nymphaeae	GLMC 2633	*Fragaria* × *ananassa*, fruit rot	Poland, bought at the market in Görlitz, Germany	PP069437	PP115695	PP115861	PP115903	PP115752	PP115810
C. nymphaeae	GLMC 2634	*Fragaria* × *ananassa*, fruit rot	Poland, bought at the market in Görlitz, Germany	PP069438	PP115696	PP115862	—	PP115753	PP115811

[a] GLMC: Culture collection of Senckenberg Museum of Natural History Görlitz, Görlitz, Germany; BBA: Culture collection of the Biologische Bundesanstalt für Land und Forstwirtschaft, Berlin, Germany; DSM: German Collection of Microorganisms and Cell Cultures, Braunschweig, Germany. [b] ITS, 5.8S nuclear ribosomal RNA gene with the two flanking internal transcribed spacers; *gapdh*, 200-bp intron of the glyceraldehyde-3-phosphate dehydrogenase gene; *chs-1*, partial sequences of the chitin synthase 1 gene; *his3*, partial sequences of the histone H3 gene; *act*, partial sequences of the actin gene; *tub2*, partial sequences of the β-tubulin gene.

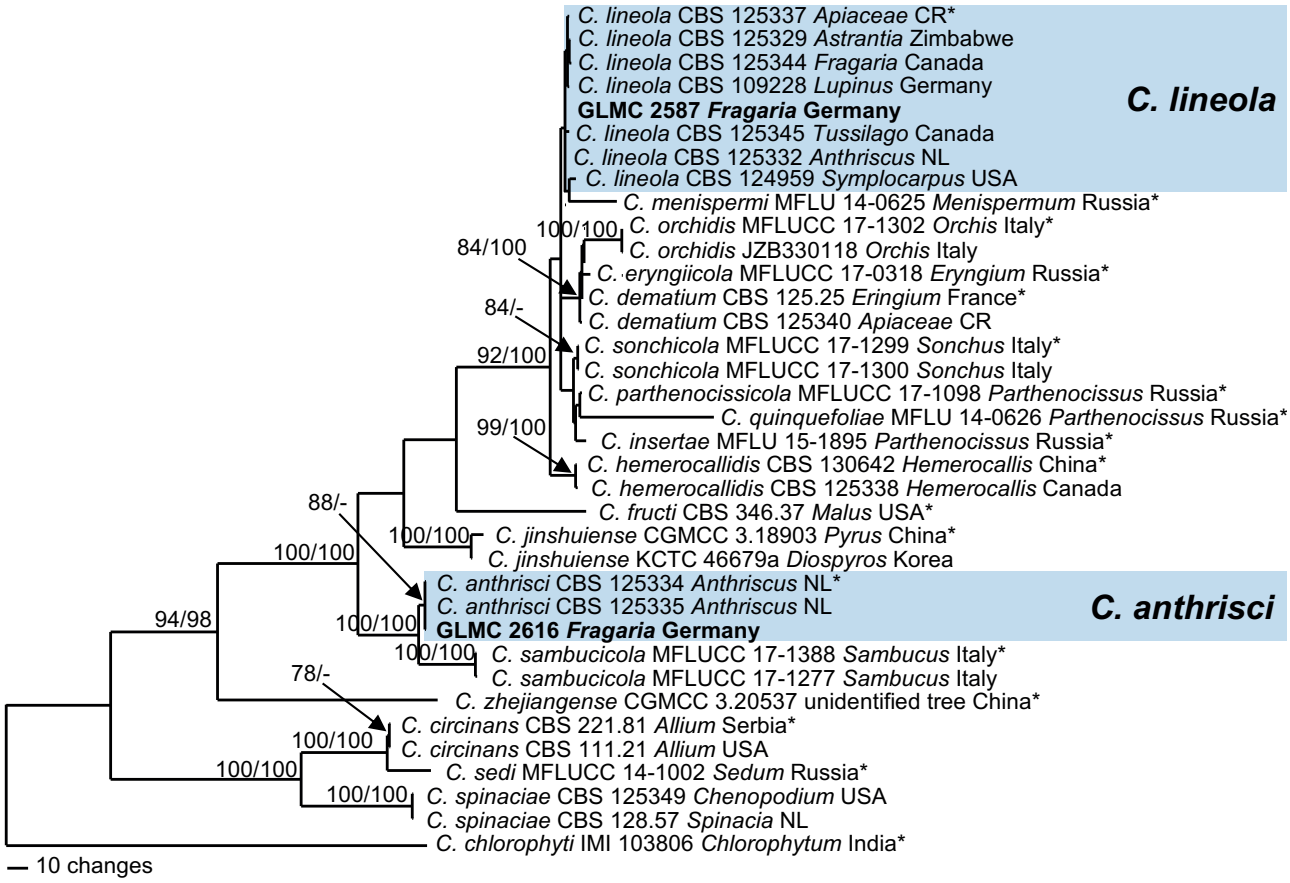

Figure 2. The first of 440 most parsimonious trees obtained from a heuristic search of the combined ITS, *act*, *gapdh*, *chs-1*, *his3*, *tub2* sequence alignment of *Colletotrichum* isolates from *Fragaria* and representative strains of the *C. dematium* species complex. Bootstrap support values of the MP analysis >70% and of the ML analysis >95% are shown at the nodes. *Colletotrichum chlorophyti* IMI 103806 was used as outgroup. Numbers of ex-type strains are indicated by an asterisk. Strains obtained or sequenced in this study are emphasised in bold font. Strain numbers are followed by substrate (host genus) and country of origin (NL = Netherlands, CR = Czech Republic).

ly most parsimonious trees were retained (length = 1062 steps, CI = 0.760, RI = 0.862, RC = 0.655, HI = 0.240). One of them is shown in Figure 2. The topology of these trees was similar, which was verified for a large section of trees. They differed in the position of taxa within subclades. The consensus tree of the ML analysis confirmed the tree topology obtained with parsimony. The bootstrap values of the two analyses generally agreed with each other. Isolate GLMC 2587 clustered with *C. lineola* strains within a big clade (MP/ML: 92/100), which consisted of several closely related species. Isolate GLMC 2616 clustered within *C. anthrisci* (MP/ML: 88/-), forming a sister clade to *C. sambucicola* (MP/ML: 100/100).

Taxonomy

As a result of the multi-locus molecular analyses, the 58 isolates were assigned to five species, of which *C. nymphaeae*, *C. godetiae* and *C. fioriniae* belong to the *C. acutatum* species complex; *C. anthrisci* and *C. lineola* are in the *C. dematium* species complex. Isolates of all these species were studied in culture, and their characteristics are outlined below.

Colletotrichum anthrisci Damm, P.F. Cannon & Crous, *Fungal Diversity* **39**: 56 (2009). (Figure 3)

Sexual morph not observed. *Asexual morph on SNA*. *Vegetative hyphae* 2–5.5 µm diam., hyaline, smooth-walled, septate, branched. *Conidiomata* acervular, conidiophores and setae formed on pale brown angular to roundish basal cells. *Setae* dark brown, 125–165 µm long, bases conical to slightly inflated, 11–15.5 µm diam., tapering to acute apices. *Conidiophores* hyaline to pale brown, smooth-walled, septate. *Conidiogenous cells* hyaline to pale brown, smooth-walled, cylindrical to clavate, 8–14 × 2.5–3 µm, opening up to 2 µm diam.,

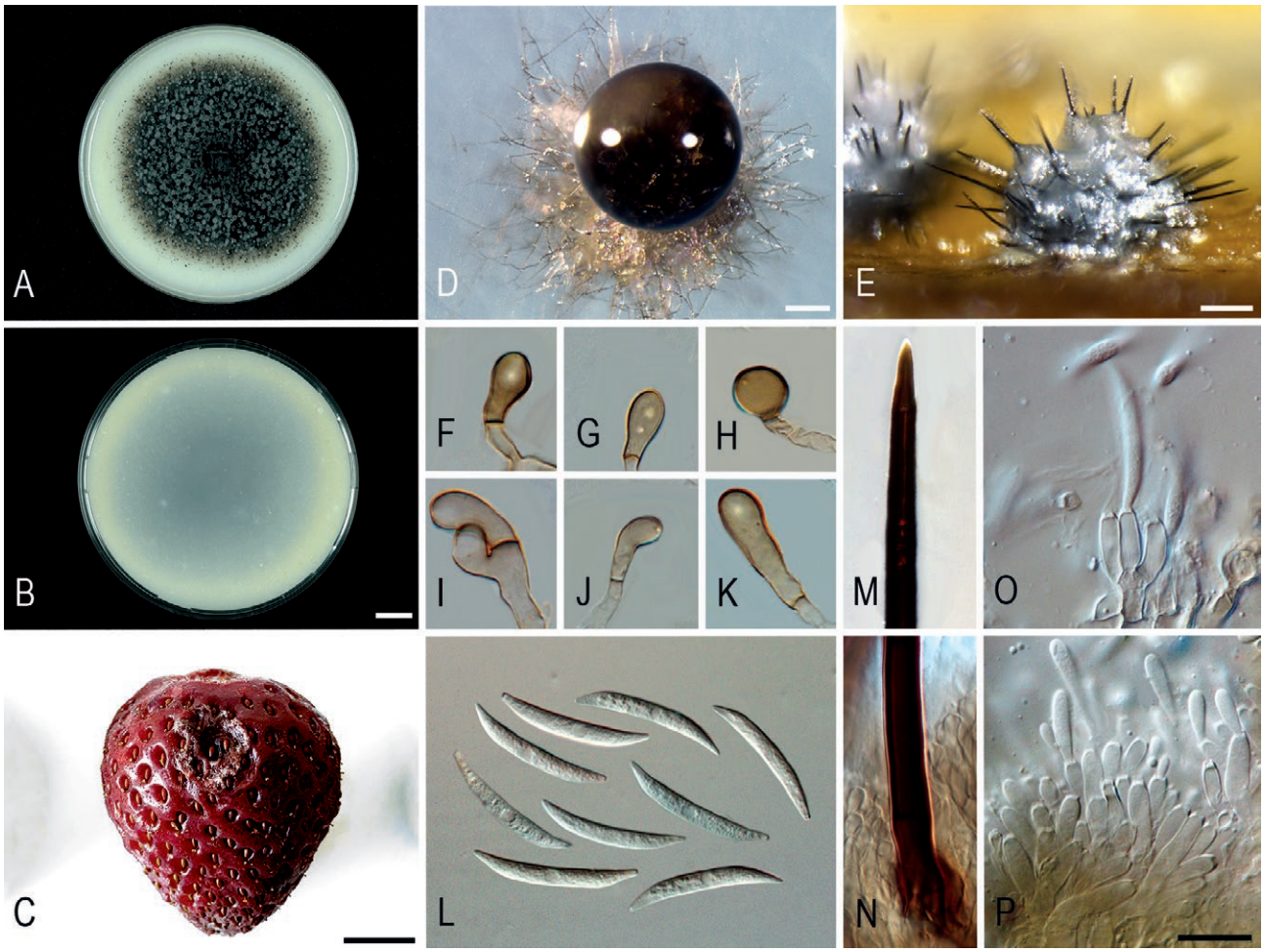

Figure 3. *Colletotrichum anthrisci* (strain GLMC 2616). A–B. Cultures on OA after 10 d. A. upper and B. reverse side. C. Symptom on fruit of *F.* × *ananassa* 'Asia' 10 dpi. D. Conidioma on SNA. E. Conidioma on *Anthriscus* stem. F–K. Appressoria. L. Conidia. M. Tip of a seta. N. Base of a seta. O–P. Conidiophores. F–P. from SNA. D–E. DM. F–P. DIC. Scale bars: B, C = 1 cm, D = 100 µm, E = 200 µm, P = 10 µm. Scale bar of B applies to A–B. Scale bar of P applies to F–P.

collarettes distinct, up to 2 µm long, periclinal thickening visible. *Conidia* hyaline, aseptate, smooth-walled, slightly curved, bases truncate, apices acute, (23.5–)25.5–27.5 × 2.5–3.5 µm, mean ± SD = 26.4 ± 1.0 × 3.0 ± 0.4 µm, L/W ratio = 8.8. *Appressoria* single, pale to medium brown, clavate to navicular, with entire edges, sometimes crenate, 5–22.5(–44) × (5–)5.5–8.5(–12) µm, mean ± SD = 13.7 ± 8.8 × 7.0 ± 1.6 µm, L/W ratio = 2.0. *Asexual morph on* Anthriscus *stems*. *Conidiomata* acervular, conidiophores and setae formed on pale brown angular cells. *Setae* dark brown, 122.5–155 µm long, bases conical to slightly inflated, 11.5–15.5 µm diam., tapering to acute apices. *Conidiophores* hyaline to pale brown, smooth-walled, septate. *Conidiogenous cells* hyaline to pale brown, smooth-walled, cylindrical to clavate, 12.5 × 3 µm, opening up to 2 µm diam., collarettes distinct, up to 2 µm long, periclinal thickening visible. *Conidia* hyaline, smooth-walled, aseptate, slightly curved, bases truncate, apices acute, (25–)26–27(–27.5) × 2.5–3.5 µm, mean ± SD = 26.5 ± 0.7 × 3.1 ± 0.4 µm, L/W ratio = 8.6.

Cultural characteristics. *Colonies on SNA* flat with entire margins, medium hyaline to pale cinnamon partly covered by whitish aerial mycelium, filter paper partly covered by olivaceous grey aerial mycelium, medium and *Anthriscus* stems partly with tiny dark grey spots, colony reverse sides same colours; 20–25 mm in 7 d (31–37 mm in 10 d). *Colonies on OA* flat with entire margins, olivaceous grey to iron grey, buff with iron grey spots towards the margins, colony reverse sides olivaceous grey, buff towards the margins; 18–26 mm in 7 d (30–35 mm in 10 d). Conidia in mass whitish to pale grey.

Material examined: Germany, Saxony, Markersdorf, forest, leaf spot of *Fragaria vesca*, 22 Sep. 2019, U. Damm, culture GLMC 2616 = DSM 115225.

Notes: Although the molecular data were identical, the conidia of the isolate from *F. vesca* formed on both media were slightly narrower, and appressoria were shorter (mean ± SD = 13.7 ± 8.8 × 7.0 ± 1.6 µm vs. 17.3 ± 6.1 × 7.0 ± 1.3 µm) than those in the original description of *C. anthrisci* (Damm *et al*., 2009).

Colletotrichum fioriniae (Marcelino & Gouli) Pennycook, *Mycotaxon* **132**(1): 150 (2017). (Figure 4)

Sexual morph not observed. *Asexual morph on SNA*. *Vegetative hyphae* 1.5–4 µm diam., hyaline, smooth-walled, septate, branched. *Conidiomata* acervular, conidiophores formed on pale brown, angular cells. *Setae* not observed. *Conidiophores* hyaline, smooth-walled, septate. *Conidiogenous cells* hyaline, smooth-walled, cylindrical, 11–14 × 3 µm, openings 1–1.5 µm diam., collarettes up to 1 µm long. *Conidia* hyaline, aseptate, smooth-walled, fusiform, both ends acute, (12–)13.5–16.5(–17.5) × 4–5.5 µm, mean ± SD = 15.0 ± 1.5 × 4.6 ± 0.5 µm, L/W ratio = 3.3. *Appressoria* single, pale brown, mostly clavate, with entire edges, (5.5–)7–11(–14.5) × (4.5–)5–6.5(–8) µm, mean ± SD = 8.9 ± 2.1 × 5.8 ± 0.7 µm, L/W ratio = 1.5. *Asexual morph on* Anthriscus *stems*. *Conidiomata* acervular, conidiophores formed on pale brown, angular cells. *Setae* not observed. *Conidiophores* hyaline, smooth-walled, septate. *Conidiogenous* cells hyaline, smooth-walled, cylindrical, 12–14 × 2.5–3 µm, openings up to 1.5 µm diam., collarettes distinct, up to 1 µm long, periclinal thickenings visible. *Conidia* hyaline, aseptate, smooth-walled, fusiform,

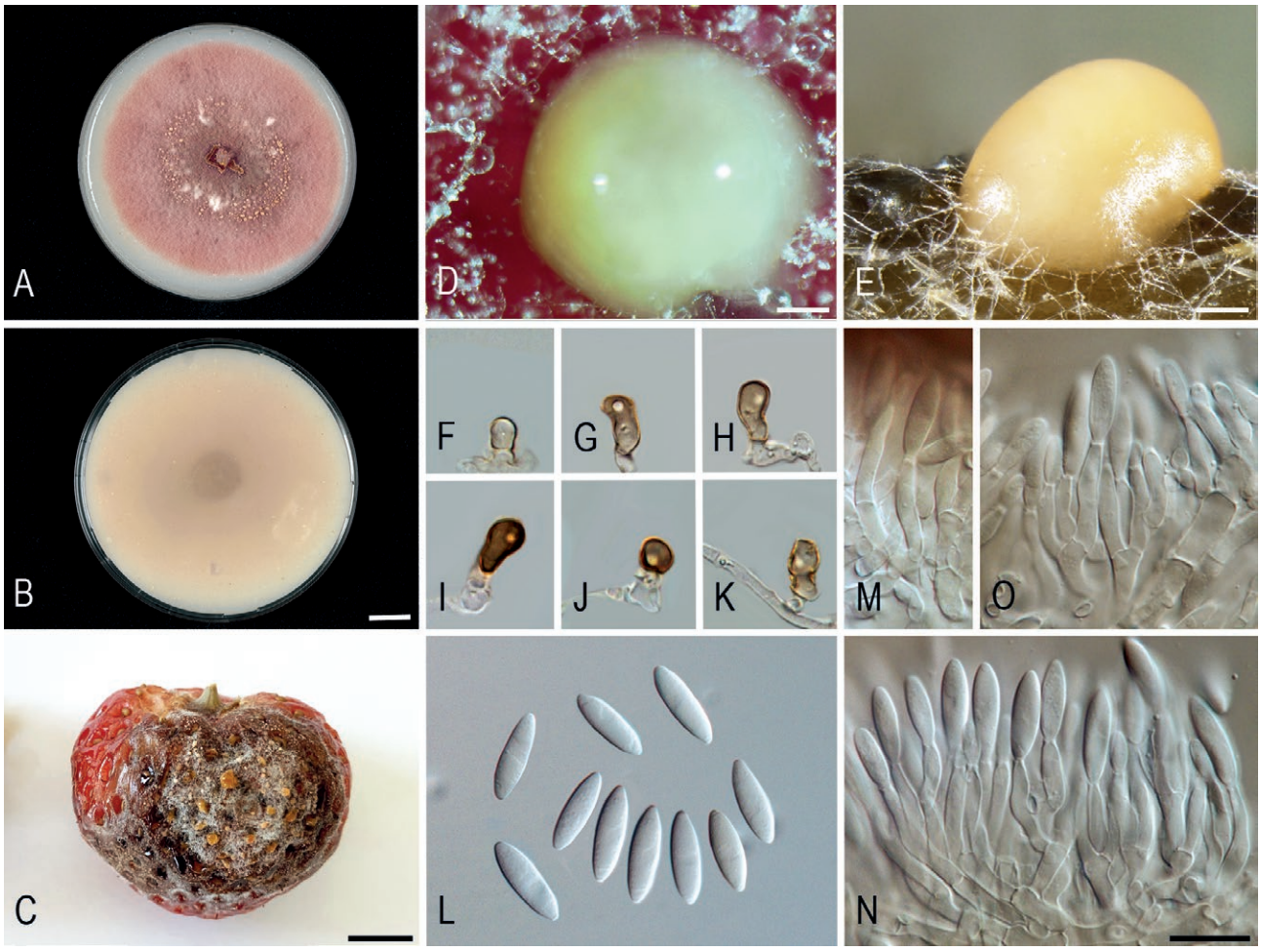

Figure 4. *Colletotrichum fioriniae* (strain GLMC 2660). A–B. Cultures on OA after 10 d. A. upper and B. reverse side. C. Symptom on fruit of *F.* × *ananassa* 'Asia' 7 dpi. D. Conidioma on SNA. E. Conidioma on *Anthriscus* stem. F–K. Appressoria. L. Conidia. M–O. Conidiophores. F–O. from SNA. D–E. DM. F–O. DIC. Scale bars: B, C = 1 cm, D–E = 100 µm, N = 10 µm. Scale bar of B applies to A–B. Scale bar of N applies to F–O.

both ends acute, (12.5–)14.5–16.5(–17.5) × 4–5.5 µm, mean ± SD = 15.4 ± 1.0 × 4.8 ± 0.4 µm, L/W ratio = 3.2.

Cultural characteristics. *Colonies on SNA* flat with entire margins, medium hyaline, pale cinnamon to pale peach, partly covered by whitish aerial mycelium, *Anthriscus* stems partly covered by saffron spore masses, colony reverse sides same colours; 21–26 mm in 7 d (30–38 mm in 10 d). *Colonies on OA* flat with undulate margins, surface coral to luteous, almost entirely covered by felty, flesh to rosy vinaceous aerial mycelium and saffron spore masses, colony reverse sides red, coral, brick to apricot; 9–18 mm in 7 d (14–30 mm in 10 d). Conidia in mass saffron.

Material examined: Germany, Saxony (Ore Mountains), from fruit anthracnose of *Fragaria* × *ananassa*, 18 Aug. 2021, C. Rose, culture GLMC 2660 = DSM 115228.

Notes: The morphology generally agreed with that of the ex-type strain on the same media. The isolate from strawberry studied here had very distinctly fusiform conidia, while other strains had fusiform to cylindrical conidia each with one round and one slightly acute end (Damm *et al*., 2012a).

Colletotrichum godetiae Neerg., *Friesia* **4**(1–2): 72 (1950). (Figure 5)

Sexual morph not observed. *Asexual morph on SNA*. *Vegetative hyphae* 2–4 µm diam., hyaline, smooth-walled, septate, branched. *Setae* not observed. *Conidiophores* hyaline, smooth-walled, septate. *Conidiogenous cells* hyaline, smooth-walled, cylindrical, 11–18 × 3.5 µm, opening 1 µm diam., collarette up to 1.5 µm long, periclinal thickenings visible. *Conidia* hyaline, asep-

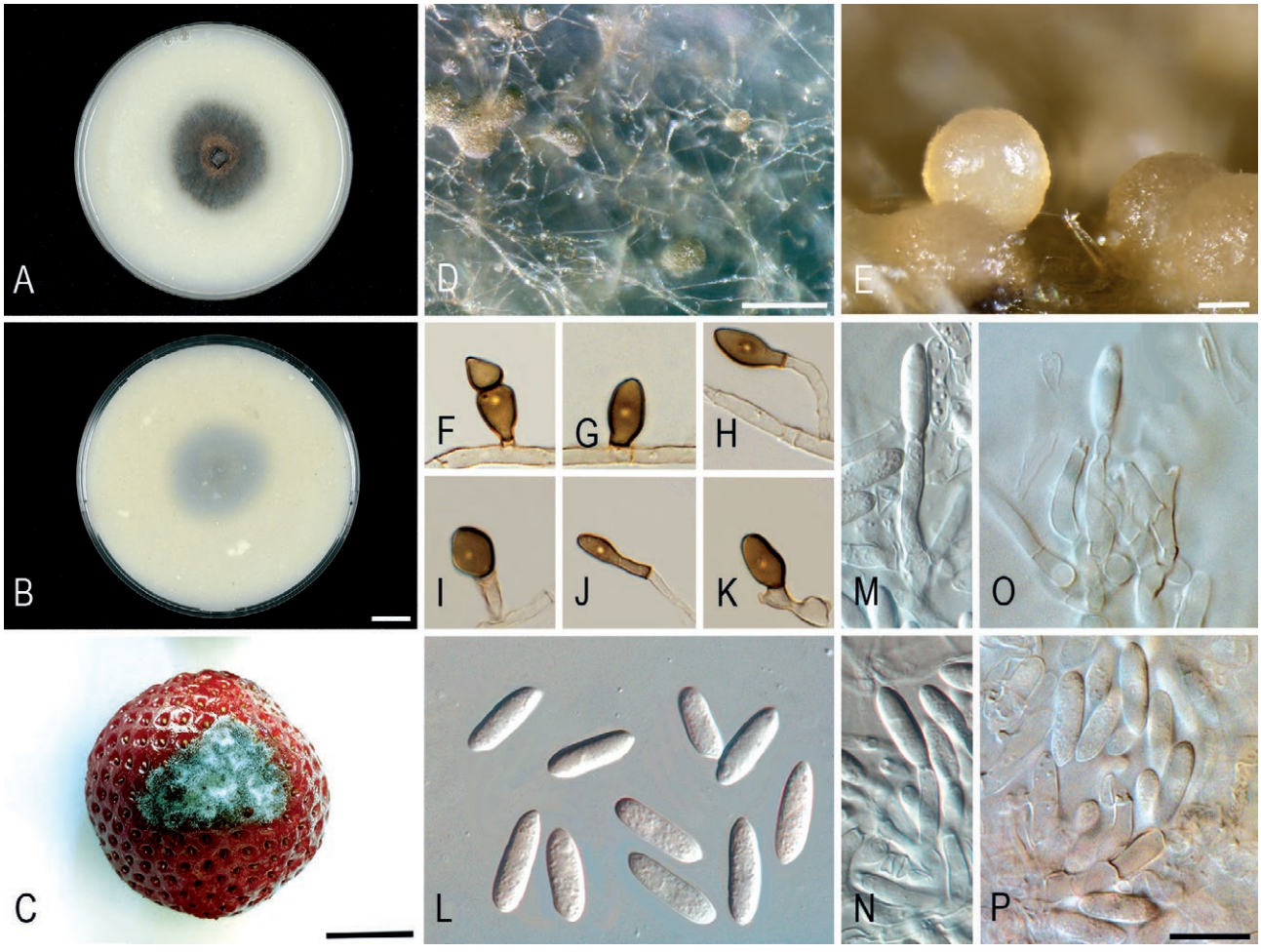

Figure 5. *Colletotrichum godetiae* (strain GLMC 2590). A–B. Cultures on OA after 10 d. A. upper and B. reverse side. C. Symptom on fruit of *F.* × *ananassa* 'Asia' 7 dpi. D. Conidiomata on SNA. E. Conidiomata on *Anthriscus* stem. F–K. Appressoria. L. Conidia. M–P. Conidiophores. F–P. from SNA. D–E. DM. F–P. DIC. Scale bars: B, C = 1 cm, D = 100 µm, E = 200 µm, P = 10 µm. Scale bar of B applies to A–B. Scale bar of P applies to F–P.

tate, smooth-walled, cylindrical, each one end round, the other end acute to round, (14.5–)15–16.5(–17.5) × (4–)4.5–5(–5.5) µm, mean ± SD = 15.9 ± 0.8 × 4.7 ± 0.3 µm, L/W ratio = 3.4. *Appressoria* medium brown, ellipsoidal to clavate, with entire to undulate edges, appressoria of strain GLMC 2590 measured (6–)7.5–13(–17.5) × (4–)4.5–6(–6.5) µm, mean ± SD = 10.3 ± 2.9 × 5.5 ± 0.7 µm, L/W ratio = 1.9, appressoria of GLMC 2589 broader, measuring (5–)7.5–13(–18) × (3.5–)5–7.5(–8.5) µm, mean ± SD = 10.0 ± 2.6 × 6.2 ± 1.2 µm, L/W ratio = 1.6. *Asexual morph on* Anthriscus *stems*. *Conidiomata* acervular, conidiophores on pale brown angular cells. *Setae* not observed. *Conidiophores* hyaline, smooth-walled, septate. *Conidiogenous cells* hyaline, smooth-walled, cylindrical, 9.5–21 × 3 µm, openings 1.5 µm diam., collarettes up to 2 µm long, periclinal thickenings visible. *Conidia* hyaline, aseptate, smooth-walled, cylindrical, each one end round, the other end acute to round, conidia of GLMC 2590 measured (15–)15.5–17(–17.5) × 4.5–5 µm, mean ± SD = 16.0 ± 0.8 × 4.7 ± 0.3 µm, L/W ratio = 3.4, conidia of GLMC 2589 shorter, measuring (12.5–)13.5–15.5(–17) × (4–)4.5–5 µm, mean ± SD = 14.7 ± 1.1 × 4.6 ± 0.2 µm, L/W ratio = 3.2.

Cultural characteristics. *Colonies on SNA* flat with entire margins, medium hyaline to pale cinnamon, partly covered by whitish to pale grey aerial mycelium, *Anthriscus* stems partly covered by saffron spore masses, filter papers partly pale olivaceous grey to olivaceous grey, colony reverse sides same colours; GLMC 2590: 18–24 mm in 7 d (29–35 mm in 10 d). *Colonies on OA* flat with entire margins, covered by woolly to felty, greyish sepia, pale smoke grey to white aerial mycelium, colony reverse sides pale purplish grey vinaceous grey to fuscous black; GLMC 2590: 6–19 mm in 7 d (15–28 mm in 10 d), GLMC 2589 faster growing: 16–22 mm in 7 d (25–32 mm in 10 d). Conidia in mass saffron.

Material examined: Germany, Mecklenburg-Western Pomerania, Rostock, vegetable farm, from a fruit of *Fragaria* × *ananassa*, 17 June 1999, P. Steinbach, culture GLMC 2590 = BBA 71234 = DSM 115223; Baden-Württemberg, from a necrotic runner of *Fragaria* × *ananassa*, unknown collection date (accessed by BBA 31 Oct. 1996), culture GLMC 2589 = BBA 70063 = DSM 115222.

Notes: Sequence data and morphology of *C. godetiae* are very variable, including the shape and size of the conidia that are studied and discussed in Damm *et al.* (2012a). While the ex-type strain and a strain from *Fragaria* in the Netherlands (CBS 125972) formed comparatively fusiform conidia, conidia of other strains, including those from *Fragaria* in Germany studied here, were rather cylindrical, and those of further strains were even clavate (Damm *et al.*, 2012a; this study, Figure 5L).

Colletotrichum lineola Corda, *Deutschlands Flora*, Abt. III. Die Pilze Deutschlands **3** (12): 41 (1831). (Figure 6)

Sexual morph not observed. *Asexual morph on SNA*. *Vegetative hyphae* 3.5–5 µm diam., hyaline, smooth-walled, septate, branched. *Conidiomata* acervular, conidiogenous cells and setae formed on bases of brown angular cells. *Setae* dark brown, 64–72.5 µm long, bases cylindrical to slightly inflated, 2.5–5 µm diam. *Conidiophores* pale brown, smooth-walled, septate. *Conidiogenous cells* pale brown, smooth-walled, cylindrical, 12–16.5 × 3.5 µm, openings 1–1.5 µm diam., collarettes visible. *Conidia* hyaline, aseptate, smooth-walled, slightly curved, bases truncate, apices acute, (21.5–)22.5–25.5(–26.5) × 2.5–3.5 µm, mean ± SD = 24.1 ± 1.4 × 3.1 ± 0.4 µm, L/W ratio = 7.7. *Appressoria* single, medium brown, obovoidal to clavate, sometimes crenate or lobed, (5–)6.5–16.5(–23) × 4.5–11(–16) µm, mean ± SD = 11.6 ± 4.9 × 7.9 ± 3.2 µm, L/W ratio = 1.5. *Asexual morph on* Anthriscus *stems*. *Conidiomata* acervular, conidiophores formed on brown angular cells. *Setae* dark brown, 64.5–68.5 µm long, base 2–4.5 µm diam. *Conidiophores* pale brown, smooth-walled, septate. *Conidiogenous cells* pale brown, smooth-walled, cylindrical, 13.5–16.5 × 3.5 µm, openings 1.5 µm diam. *Conidia* hyaline, aseptate, smooth-walled, slightly curved, bases truncate, apices acute, (22–)23–26(–26.5) × (2.5–)3–3.5 µm, mean ± SD = 24.4 ± 1.4 × 3.1 ± 0.3 µm, L/W ratio = 7.8.

Cultural characteristics. *Colonies on SNA* flat with entire margins, medium hyaline, pale cinnamon to pale ochreous, medium, filter papers and *Anthriscus* stems partly covered by tiny olivaceous black spots, aerial mycelium lacking, colony reverse sides same colours; 29–36 mm in 7 d (38–>40 mm in 10 d). *Colonies on OA* flat with entire margins, medium buff to honey, with tiny olivaceous grey to olivaceous black spots, aerial mycelium lacking, colony reverse sides honey to vinaceous buff; 21–26 mm in 7 d (36–>40 mm in 10 d). Conidia in mass whitish.

Material examined: Germany, Brandenburg, from fruit anthracnose of *Fragaria* × *ananassa*, 19 Jun. 2001, unknown collector, culture GLMC 2587 = BBA 71830 = DSM 115221.

Notes: The morphology of isolate GLMC 2587 agreed with the description in Damm *et al.* (2009) that based on material from *Apiaceae* hosts, except for the slightly longer conidia of the isolate from strawberry formed on *Anthriscus* stems.

Colletotrichum nymphaeae (Pass.) Aa, *Netherlands J. Plant Pathol.* **84**: 110 (1978). (Figure 7)

Sexual morph not observed. *Asexual morph on SNA*. *Vegetative hyphae* 2–3.5 µm diam., hyaline, smooth-

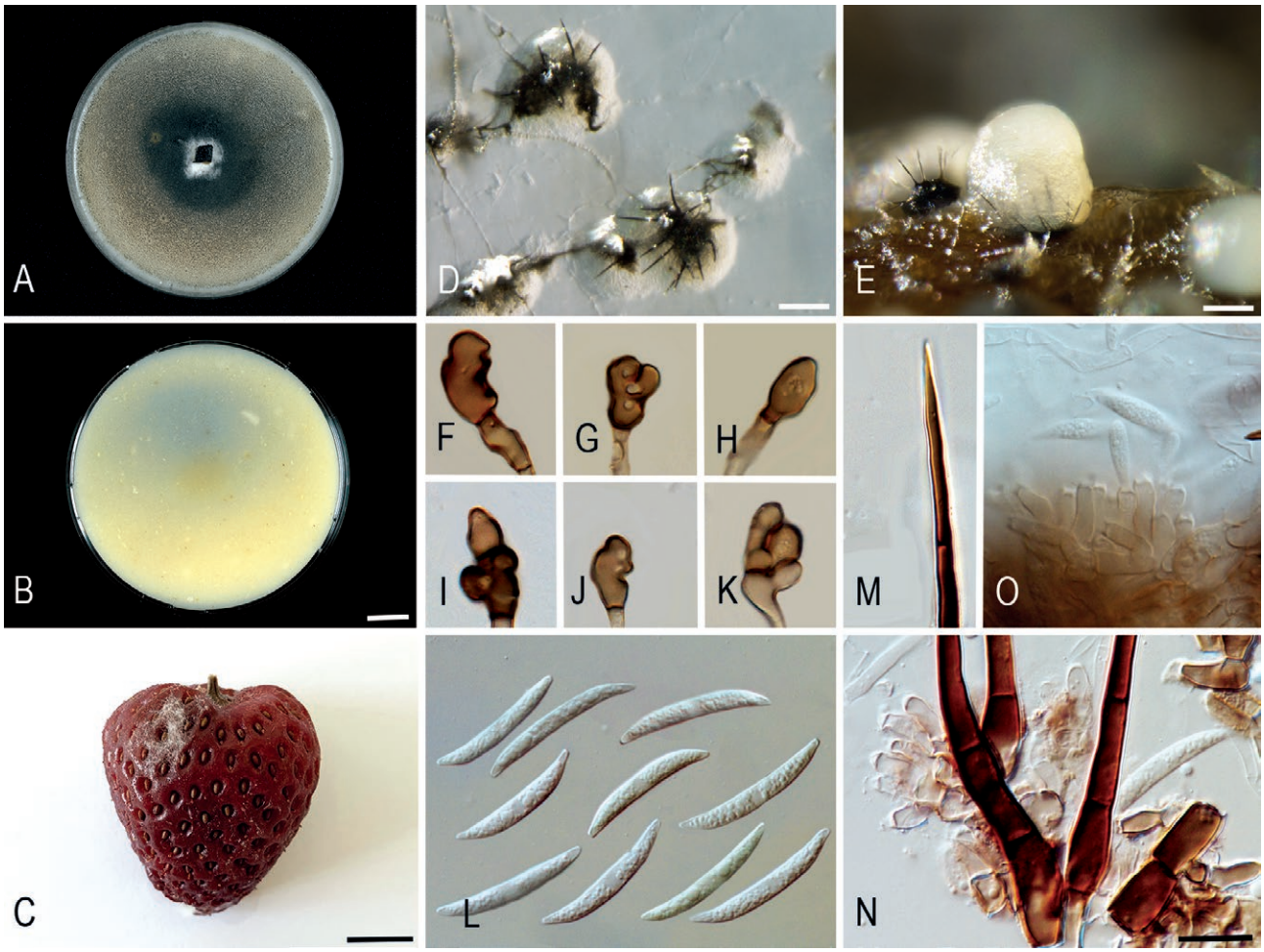

Figure 6. *Colletotrichum lineola* (strain GLMC 2587). A–B. Cultures on OA after 10 d. A. upper and B. reverse side. C. Symptom on fruit of *F.* × *ananassa* 'Asia' 10 dpi. D. Conidiomata on SNA. E. Conidiomata on *Anthriscus* stem. F–K. Appressoria. L. Conidia. M. Tip of a seta. N. Bases of setae. O. Conidiophores. F–O. from SNA. D–E. DM. F–O. DIC. Scale bars: B, C = 1 cm, D, E = 200 µm, N = 10 µm. Scale bar of B applies to A–B. Scale bar of N applies to F–O.

walled, septate, branched. *Setae* not observed. *Conidiophores* hyaline, smooth-walled, septate. *Conidiogenous cells* hyaline, smooth-walled, cylindrical, 14–15.5 × 2–3 µm, openings 1.5–2 µm diam., collarettes up to 2 µm long, periclinal thickenings distinct. *Conidia* hyaline, aseptate, smooth-walled, cylindrical to fusiform, ends acute to round, conidia of GLMC 2445 measured (8.5–)12–16(–17) × (2–)2.5–3.5(–4.5) µm, mean ± SD = 13.8 ± 1.9 × 3.1 ± 0.5 µm, L/W ratio = 4.5, conidia of GLMC 2653 shorter and wider, measuring (4.5–)9–15.5(–18) × (3–)3.5–4.5(–5) µm, mean ± SD = 12.4 ± 3.3 × 3.9 ± 0.5 µm, L/W ratio = 3.2, conidia of GLMC 2656 longer, measuring (8.5–)12–17(–22.5) × (2.5–)3.5–4(–4.5) µm, mean ± SD = 14.7 ± 2.5 × 3.7 ± 0.3 µm, L/W ratio = 4.2. *Appressoria* single, medium to pale brown, mostly clavate, with entire edges, appressoria of GLMC 2445 measured (6.5–)7–13(–20.5) × (5.5–)6–7.5(–9) µm, mean ± SD = 10.0 ± 3.2 × 6.8 ± 0.6 µm, L/W ratio = 1.5, appressoria of GLMC 2556 narrower, measuring (5–)6.5–13(–21) × (3.5–)5–7(–9) µm, mean ± SD = 10.0 ± 3.3 × 6.0 ± 1.1 µm, L/W ratio = 1.7. *Asexual morph on* Anthriscus *stems*. *Conidiomata* acervular, conidiophores formed on brown angular cells. *Setae* not observed. *Conidiophores* hyaline, smooth-walled, septate. *Conidiogenous cells* hyaline, smooth-walled, cylindrical, 14.5–18 × 2 µm, openings 1.5–2 µm diam., collarettes distinct, up to 2 µm long, periclinal thickenings visible. *Conidia* hyaline, aseptate, smooth-walled, fusiform to cylindrical, ends acute to round. (13.5–)14.5–17(–18.5) × 4–4.5 µm, mean ± SD = 15.7 ± 1.3 × 4.3 ± 0.2 µm, L/W ratio = 3.6, conidia of GLMC 2653 shorter, measuring (9.5–)12–14.5(–16) × (3–)4–4.5 µm, mean ± SD = 13.3 ± 1.3 × 4.3 ± 0.4 µm, L/W ratio = 3.1.

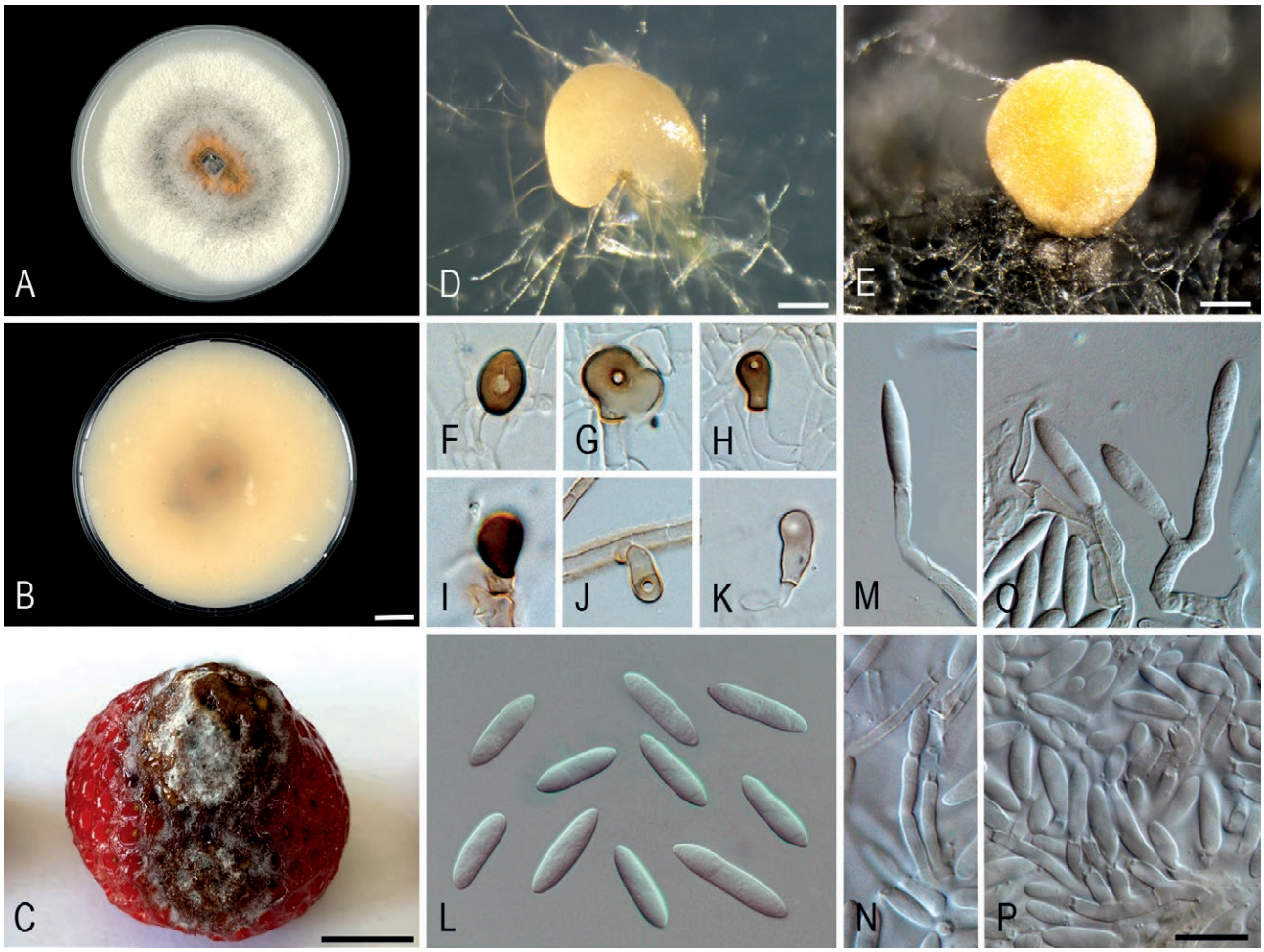

Figure 7. *Colletotrichum nymphaeae* (strain GLMC 2445). A–B. Cultures on OA after 10 d. A. upper and B. reverse side. C. Symptom on fruit of *F.* × *ananassa* 'Asia' 7 dpi. D. Conidioma on SNA. E. Conidioma on *Anthriscus* stem. F–K. Appressoria. L. Conidia. M–P. Conidiophores. F–P. from SNA. D–E. DM. F–P. DIC. Scale bars: B, C = 1 cm, D = 200 µm, E = 100 µm, P = 10 µm. Scale bar of B applies to A–B. Scale bar of P applies to F–P.

Cultural characteristics. Colonies on SNA flat with entire margins, medium hyaline to pale cinnamon, partly covered by whitish aerial mycelium and by saffron to orange spore masses, filter paper partly pale olivaceous grey, colony reverse sides hyaline to pale cinnamon, saffron to orange spore masses shining through, filter paper partly pale olivaceous grey to olivaceous black; 19–30 mm in 7 d (31–36 mm in 10 d). *Colonies on OA* flat with entire margins, entirely covered with woolly to felty, greyish sepia, pale mouse grey, rosy buff to white aerial mycelium, orange spore masses mainly in the centres, colony reverse sides olivaceous grey, saffron to pale luteous; GLMC 2445 16–25 mm in 7 d (29–39 mm in 10 d), GLMC 2656 slower growing: 16–22 mm in 7 d (25–32 mm in 10d). Conidia in mass saffron to orange.

Material examined: Germany, Saxony, Dresden, from fruit anthracnose of *F.* × *ananassa* 'Asia', 1 Jul. 2019, C. Rose, culture GLMC 2445 = DSM 115220; North Rhine Westphalia, near Münster, from brown spots on petiole of *F.* × *ananassa* 'Asia', 10 Sep. 2021, C. Rose, culture GLMC 2656; North Rhine Westphalia, near Münster, from brown spots on leaf of *F.* × *ananassa* 'Asia', 10 Sep. 2021, C. Rose, culture GLMC 2658; Brandenburg, Spreewald (bought on a market in Dresden), from fruit anthracnose of *F.* × *ananassa*, 16 Sep. 2021, C. Rose, culture GLMC 2653 = DSM 115226.

Notes: The ex-type strain of *C. nymphaeae* formed clavate conidia, while other strains studied by Damm *et al.* (2012a) including strains from *Fragaria* as well as the strains from *Fragaria* in Germany studied here form fusiform to cylindrical conidia.

Pathogenicity

Seven dpi, all tested isolates of the five *Colletotrichum* species caused symptoms on strawberry fruit *F.* × *ananassa* 'Asia'. However, for almost all isolates and species in both experiments, some fruit did not develop symptoms or showed symptoms that were very slight 7 dpi.

Colletotrichum anthrisci and *C. lineola* caused no or small lesions 7 dpi (GLMC 2616: 0.0–0.25 cm^2, GLMC 2587: 0.0–0.5 cm^2). Even 10 dpi the symptoms were small: after inoculations with *C. anthrisci*, circular, dry, sunken, black necroses developed that contained tiny dark grey spots, covered by whitish aerial mycelium and rosy vinaceous conidial masses (Figure 3C, 10 dpi). After inoculations with *C. lineola*, circular, dry, brown, sunken necroses developed, which were covered by sparse whitish aerial mycelium; rosy vinaceous conidial masses developed (Figure 6C, 10 dpi). The two strains of *C. godetiae* developed noticeable fruit symptoms 7 dpi. Variability of lesion sizes from the two strains was similar (GLMC 2589: 0.2–1.2 cm^2, GLMC 2590: 0.5–1.0 cm^2). Necroses formed that were nearly circular, brown, sunken and entirely covered by uniform woolly to felty, white to pale smoke grey aerial mycelium, without conidium formation (Figure 5C, 7 dpi).

Variability of strawberry lesion sizes was high after inoculations with the two isolates of *C. fioriniae*, and the nine isolates of *C. nymphaeae*. Both species caused large necrotic areas with abundant sporulation. The isolates of *C. fioriniae* formed circular, dry, dark brown, sunken necrotic areas, almost entirely covered by felty whitish to grey mycelium and saffron to brick conidial masses that were aggregated to large drops. There were also drops of discharged dark liquid in the lesions (Figure 4C, 7 dpi). The lesion sizes 7 dpi were 0.1–2.4 cm^2 with isolate GLMC 2660 and 0.0–0.6 cm^2 with isolate GLMC 2661. *Colletotrichum nymphaeae* formed brown, dry, sunken necrotic areas on inoculated strawberries that were entirely covered by woolly to felty, white to pale mouse grey aerial mycelium in concentric rings and small orange conidial masses, as well as drops of discharged liquid (Figure 7C, 7 dpi). The lesion sizes 7 dpi with different isolates were: GLMC 2445: 0.5–1.5 cm^2, GLMC 2552: 0.12–0.95 cm^2, GLMC 2588: 0.02–2.5 cm^2, GLMC 2595: 0.0–0.1 cm^2, GLMC 2600: 0.05–1.75 cm^2, GLMC 2610: 1.5–2.75 cm^2, GLMC 2653: 0.0–0.95 cm^2, GLMC 2656: 0.0–0.5 cm^2 and GLMC 2658: 0.0–0.25 cm^2.

Due to infection by other fungi or collapsing of individual strawberries, some were excluded from both experiments, and resulted in failures, especially after inoculations with *C. nymphaeae* isolates GLMC 2445, GLMC 2588, GLMC 2600, GLMC 2610, GLMC 2658, *C. lineola* isolate GLMC 2587 and *C. fioriniae* isolate 2661. However, all inoculated fruit in the experiments showed symptoms 10 dpi.

The species that were inoculated were respectively re-isolated from all symptoms developing on inoculated strawberries. No symptoms developed after control treatments with sterile, distilled water.

DISCUSSION

This study has demonstrated that *Colletotrichum* is widespread on strawberries in Germany, although neither the BBA collection nor recent sampling described here covered all regions of this country. The *Colletotrichum* collection of the BBA shows occurrence of *Colletotrichum* on strawberries around the year 2000 in up to seven federal states of Germany, including Brandenburg, Lower Saxony, Saxony, Mecklenburg-Western Pomerania, Baden-Württemberg, Hesse and (probably) Rhineland-Palatinate. The new collections (2019–2021) confirm this genus in Brandenburg, Lower Saxony, Saxony, Mecklenburg-Western Pomerania, and also include collections from North Rhine-Westphalia.

Most of the samples in these collections were of *C. nymphaeae*, which is the most common *Colletotrichum* species on strawberry in Germany. This species belongs to the *C. acutatum* species complex, occurs on several hosts and is common on strawberry in Europe, Iran and North America (Damm *et al*., 2012a; Baroncelli *et al*., 2015; Karimi *et al*., 2017; Grammen *et al*., 2019; Wang *et al*., 2019; Tsvetkova and Kuznetsova, 2022). Based on the present study, *C. nymphaeae* is present in all federal states of Germany for which data are available and occurs on *F.* × *ananassa* and *F. vesca* var. *semperflorens*, a cultivated variety of wild strawberry. *Colletotrichum nymphaeae* was mostly isolated from fruit of *F.* × *ananassa* in the field and from the market. Fruit bought from the marked in Görlitz originated from Poland, confirming a recent report of *C. nymphaeae* on strawberries in that country (Tsvetkova and Kuznetsova, 2022). This species was also isolated from symptoms on different green plant parts of *F.* × *ananassa*, both from established plants in the field and from purchased young plants from German propagation culture.

In a survey of the *C. acutatum* species complex on strawberry in the USA, *C. nymphaeae* dominated (97.7% of the isolates), and almost all isolates were of one clonal lineage regardless of the isolation source (Wang *et al*., 2019). One representative of these strains (isolate 16-320) was included in the phylogeny of the present study, and this isolate grouped with most of the isolates

from strawberry and with the majority of those examined by Damm *et al.* (2012a) and Baroncelli *et al.* (2015). Thus, this one clonal lineage is almost entirely restricted to strawberry, is distributed throughout Europe, also occurs in Israel and some African countries, and is demonstrated here to occur in Germany and Poland and to be the dominating lineage in Germany, both in historical and recent collections (Damm *et al*., 2012a; the present study). Wang *et al*. (2019) suggested that this clonal lineage had been distributed throughout the USA and Canada via quiescently infected strawberry transplants, which could also explain its widespread occurrence in European countries. In contrast, the dominating species on strawberry in China, Korea, Japan and Taiwan belong to the *C. gloeosporioides* complex. The species detected in Korea, Japan and Taiwan were completely different from those found in Europe, while in China *C. nymphaeae* is also present, but to a lesser extent (Nam *et al*., 2013; Han *et al*., 2016; Jayawardena *et al*., 2016; Gan *et al*., 2017; Chung *et al*., 2020).

The other two haplotypes of *C. nymphaeae* from strawberry in Germany detected in the present study were also identical to haplotypes from the USA, as described by Wang *et al.* (2019). This indicates three possibly independent introductions of this pathogen to German strawberries. One of these two haplotypes represented a clone that is closely related to the most common haplotype, which also includes some strains from strawberry from other European countries. The German isolates were part of the old collection. In contrast, the other haplotype has several nucleotide differences to the other haplotypes occurring on strawberry and included only three isolates, one from strawberry in the USA and two from a recent collection on strawberry in Brandenburg, Germany. This could represent a new lineage of *C. nymphaeae* which has restricted distribution and unknown impacts. Despite its dominating incidence on strawberries, there are few records of *C. nymphaeae* in Germany prior to the present study, including a collection from Freyburg, Saxony-Anhalt by H. Jage and one from a dried-up pond close to Flemsdorf, Brandenburg by J. Kruse (Dämmrich *et al*., 2023). Both collections are from *Nymphaea*, and both specimens are kept in the fungarium of the Senckenberg Museum of Natural History Görlitz (GLM-F127296, GLM-F129560). However, these identifications were not confirmed by DNA sequence data.

Colletotrichum godetiae also belongs to the *C. acutatum* species complex and occurs on several hosts including many woody plants as well as strawberry (Damm *et al*., 2012a). Although this fungus is probably common on strawberry in Europe (Damm *et al*., 2012a; Baroncelli *et al*., 2015; Tsvetkova and Kuznetsova, 2022), it was found only twice on strawberries from Germany in the present study and was not detected in the new collections. Despite proven infectivity of *C. godetiae* on *F.* × *ananassa* 'Asia' under laboratory conditions, there has been no invasive spread in German strawberry stocks within the last 20 years. In contrast to *C. nymphaeae* and *C. fioriniae*, *C. godetiae* is not known from strawberry in the USA and Canada (Baroncelli *et al*., 2015; Wang *et al*., 2019). The only North American strain of this species included in Damm *et al.* (2012a) was from a different host, and the haplotype represented by the strains from strawberry in the present study occurs both on strawberry and on other hosts. This suggests spread of this species on strawberries within Europe, rather than an introduction from the USA or occasional transmissions to strawberries by other hosts. This species was previously found in Germany, on leaf spots of *Mahonia aquifolium* and in necrotic wood of sour cherry (*Prunus cerasus*) (Damm *et al*., 2012a; Bien and Damm, 2020). However, the present report is the first from strawberry in Germany. A clade that was previously regarded as a subclade of *C. godetiae* and comprised exclusively strains from South America was recently described as new species, *C. americanum* (Zapata *et al*., 2024).

Colletotrichum fioriniae is another species belonging to the *C. acutatum* species complex. This pathogen occurs on several hosts, mainly crops, and is common on fruit of apple and strawberry as well as *Vaccinium* species in Europe, the USA and New Zealand and on *Persea* in Australia. In Germany, *C. fioriniae* has previously only been reported from an indoor collection of *Grevillea* sp. (*Proteaceae*) (Damm *et al*., 2012a), an exotic genus from Australia. However, the present report is the first of *C. fioriniae* from strawberry in Germany, and is also the first report from an outdoor cultivated crop in Germany. In contrast to *C. nymphaeae*, the haplotype of *C. fioriniae* detected in the present study, is not specialised to strawberry. There are several haplotypes of this species that occur both on strawberry and other hosts (Damm *et al*., 2012a; this study). This suggests a different transmission route of this pathogen to strawberries, possibly by host-jumps rather than in planting material of the same host. The high variability between isolates of *C. fioriniae* from the same hosts could also be related to recombination, as the formation of sexual morphs and of hybrids with *C. acutatum* (*sensu stricto*) are known (Marcelino *et al*., 2008; Damm *et al*., 2012a). In the USA, *C. fioriniae* was determined to be of low incidence on strawberries (five of 217 *Colletotrichum* isolates; Wang *et al*., 2019). In the present study, *C. fioriniae* was isolated

only twice from recently collected material from one strawberry field. However, since this fungus was able to infect *F.* × *ananassa* 'Asia' under laboratory conditions with development of large necrotic areas and abundant sporulation, there is a potential risk of the pathogen spreading to other strawberry stocks.

As the two subclades of *C. fioriniae* reported in the phylogeny of Damm *et al.* (2012a) were not supported and had similar hosts and distributions, they were treated as one species. The phylogeny of Chen *et al.* (2022) that included new strains from *Malus domestica* in China supported the two subclades, and the second subclade was described as *C. orientale* [actually as "orientalis"], but invalidly (Art. 40.8 Shenzhen), while Zhang *et al.* (2023a) described two further related strains from China as *C. radermacherae*. Since new strains from ornamental plants in China were intermediate between all three species, Zhang *et al.* (2023b) reduced both new species to synonymy with *C. fioriniae*. In the phylogeny of the present study that included one "*C. radermacherae*" strain (GZCC 21-0814) but not the intermediate strains of Zhang *et al.* (2023b), the two subclades were supported by one analysis (ML) that was not applied in Damm *et al.* (2012a). The strains from strawberry in Germany belong to the subclade containing the ex-type strain of *C. fioriniae*.

Colletotrichum lineola belongs to the *C. dematium* species complex and had been isolated from dead plant parts and diseases of several plants, mainly in Central Europe and North America. These hosts included *Fragaria* (petiole) in Canada (Damm *et al.*, 2009). Tsvetkova and Kuznetsova (2022) also isolated *C. lineola* from strawberries in Russia. In the present study, this fungus was found on strawberry fruit in Germany for the first time. In the pathogenicity tests, this species also caused very small symptoms on fruit, and it was not detected in the new collections. Therefore, *C. lineola* can be regarded as of minor importance for strawberry cultivation.

Another species of the *C. dematium* complex, *C. anthrisci*, was described from dead stems of *A. sylvestris* in the Netherlands (Damm *et al.*, 2009) and was recently classified as highly endangered (Talhinhas and Baroncelli, 2021). In contrast, this fungus was found to be ubiquitous in a forest in Japan, where it was isolated from seedlings of several trees, including *Prunus grayana*, *Fraxinus lanuginosa*, *Cornus controversa* and *Magnolia obovata* that had been killed by damping-off (Konno *et al.*, 2011). *Colletotrichum anthrisci* was also recorded on avocado fruit with anthracnose symptoms in Chile and was confirmed to cause this disease (Bustamente *et al.*, 2022). In the present study, *C. anthrisci* was isolated from leaf spots of *F. vesca* in a forest in Germany and was shown to cause fruit anthracnose of cultivated strawberry. Thus, this species is neither host-specific nor rare, and is known from three continents where it is at least locally very common. This is the first report of *C. anthrisci* both from Germany and from *Fragaria* worldwide and the first evidence of this species causing anthracnose on cultivated strawberry fruit under laboratory conditions. However, the symptoms caused on *F.* × *ananassa* 'Asia' were mild and *C. anthrisci* has to date not been collected from cultivated strawberry in the field.

Prior to the present study, most of the *Colletotrichum* strains from strawberry in Europe had been identified as *C. acutatum*. This also applies to the isolates from the BBA collection examined, one of which was the basis of the report by Nirenberg *et al.* (2002). In the present study, isolates previously identified as *C. acutatum* were re-identified as *C. nymphaeae*, except for the isolate originating from the Netherlands that was shown to be *C. godetiae*. None of the isolates were *C. acutatum* (*sensu stricto*). *Colletotrichum acutatum* (*sensu stricto*) has been found predominantly in the southern hemisphere (Damm *et al.*, 2012a) and is known to be associated with fruit rot of strawberry, but only in Australia (Sreenivasaprasad and Talhinhas, 2005; Damm *et al.*, 2012a). To date, there is no confirmed occurrence of *C. acutatum* (*sensu stricto*) on strawberries elsewhere in the world. Nearly all reports from strawberry prior to the treatment of the *C. acutatum* complex by Damm *et al.* (2012a) and some later reports, refer to other species within this complex, which was confirmed here for the pathogens causing strawberry anthracnose in Germany.

Other previously unreported *Colletotrichum* strains from the BBA collection had been identified as *C. truncatum*, *C. fragariae* and *C. gloeosporioides*, based on the original strain list. In the present study, *C. truncatum* was re-identified as *C. lineola*, and *C. fragariae* and *C. gloeosporioides* were re-identified as *C. godetiae*. *Colletotrichum truncatum* has not been reported from Germany (Farr and Rossman, 2024). This fungus forms curved conidia, but with different shape than *C. lineola* and belongs to the *C. truncatum* species complex, while *C. lineola* belongs to the *C. dematium* complex (Damm *et al.*, 2009). In contrast, *C. fragariae* and *C. gloeosporioides* form cylindrical conidia and belong to the *C. gloeosporioides* complex. However, no species of the *C. gloeosporioides* complex were found among the isolates from Germany that were examined here. However, the conidia of the *C. godetiae* isolates from strawberry studied here were more cylindrical than fusiform (Figure 5L). The cylindrical conidium shape of isolates of *C. godetiae*, like those from strawberries studied here, as well as of some other species of the *C. acutatum* species complex, is reminiscent of species of the *C. gloeosporioides* complex

(Damm *et al*., 2012a; Weir *et al*., 2012). This can cause confusion because identifications of isolates by morphology only are not reliable, even to species complex level. This also applies to species with curved conidia, as for the *C. lineola* isolate examined in this study. In contrast, *C. theobromicola* (syn. *C. fragariae*) has only been reported from strawberries from a few countries, of which only isolates from the USA have been confirmed by sequence data, while sequences of *C. fragariae* reported from the United Kingdom and Japan suggest also *C. godetiae* and a different species in the *C. gloeosporioides* complex, respectively (Nirenberg *et al*., 2002; Moriwaki *et al*., 2003; Weir *et al*., 2012; Farr and Rossman, 2024). The only reliable reports of *C. gloeosporioides* (*sensu stricto*) from strawberries are from China (e.g. Han *et al*., 2016). As the present study was the first molecular identification of *Colletotrichum* strains from strawberries in Germany after the revisions of the respective *Colletotrichum* species complexes based on multi-locus sequence data (Damm *et al*., 2009, 2012a; Weir *et al*., 2012), all species detected in this study are new reports on strawberries in Germany.

While symptoms caused by *C. eriobotryae* and *C. nymphaeae* on loquat fruit were indistinguishable (Damm *et al*., 2020), those caused by the species tested on strawberry fruit in the present study were very different from each other. This could be attributed to the high genetic distance of the species studied here that belong to different species complexes or at least different main clades within the *C. acutatum* complex. The two species from loquat both belonged to clade 2 of the *C. acutatum* complex. Although the symptoms caused by the five different species were typical for the individual species, it is unlikely that species can be identified based on host symptoms alone.

Colletotrichum nymphaeae and *C. fioriniae* were more aggressive than *C. godetiae* in strawberry fruit assays reported by Baroncelli *et al.* (2015). This can be tentatively confirmed by the present study, although our data could not be statistically analysed due to large variations and nil results. In pathogenicity tests, MacKenzie *et al.* (2009) showed that *Colletotrichum* isolates from strawberry and blueberry from Florida (USA) that were later identified as *C. nymphaeae* and *C. fioriniae*, respectively, based on ITS and *gapdh* sequences (Damm *et al*., 2012a), caused anthracnose on strawberry fruits; the lesions caused by *C. nymphaeae* isolates were larger than those caused by *C. fioriniae* isolates. This cannot be confirmed by the present study, because lesion sizes caused by one of the *C. fioriniae* isolates belonged to the largest in the tests. Because of variability in lesion sizes caused by these two species, no conclusions can be drawn about relative virulence of these species. Based on the number of isolates and virulence, *C. nymphaeae* is likely to be the most important strawberry anthracnose pathogen in Europe, representing the highest economic risk for commercial strawberry production. This was previously confirmed for the United Kingdom and Russia and in the present study also for Germany.

The present study has identified the pathogens causing anthracnose of cultivated strawberry in Germany, which provides the basis for application and development of targeted control measures for management of these pathogens in commercial strawberry cultivation. This will require assessments of fungicide effectiveness and pathogen resistance. Targeted strawberry breeding should be aimed at resistance to specific *Colletotrichum* pathogens defined at species and/or haplotype level. Monitoring of pathogens in the field and testing of acquired, especially imported planting material using molecular methods would help to detect possible new pathogen species and haplotypes, as the pathogen spectrum could change due to changes in prevailing climates.

ACKNOWLEDGEMENTS

The authors thank Dr Wolfgang Maier, curator of the JKI (previously BBA) culture collection, Julius Kühn-Institut, Bundesforschungsinstitut für Kulturpflanzen, Institut für Epidemiologie und Pathogendiagnostik, Braunschweig, Germany, for providing *Colletotrichum* strains, and Dr Alexandra Wichura, Landwirtschaftskammer Niedersachsen, Pflanzenschutzamt, Sachgebiet Obst- und Gemüsebau, Hannover, Germany, for providing diseased plant specimens. The authors also thank the other supporters who contributed material and data for this research. The research was financially supported by the Deutsche Bundesstiftung Umwelt, Osnabrück, Germany.

LITERATURE CITED

Anonymous, 2011. Amtsblatt der Europäischen Union 2011: Official Journal of the European Union. https://eur-lex.europa.eu/legal-content/DE/TXT/PDF/?uri=CELEX: 32011R0543&from=PT

Baroncelli R., Zapparata A., Sarrocco S., Sukno S.A., Lane C.R., … Sreenivasaprasad S., 2015. Molecular diversity of anthracnose pathogen populations associated with UK strawberry production suggests multiple introductions of three different *Colletotrichum* species. *PLoS ONE* 10(6): e0129140. https://doi.org/10.1371/journal.pone.0129140

Bien S., Damm U., 2020. *Prunus* trees in Germany – a hideout of unknown fungi? *Mycological Progress* 19: 667–690. https://doi.org/10.1007/s11557-020-01586-4

Bobev S.G., Zveibil A., Freeman S., 2002. First report of *Colletotrichum acutatum* on strawberry in Bulgaria. *Plant Disease* 86: 1178. https://doi.org/10.1094/PDIS.2002.86.10.1178A

Brooks A.N., 1931. Anthracnose of strawberry caused by *Colletotrichum fragariae*, n. sp. *Phytopathology* 21 (7): 739–744.

Bustamante M.I., Osorio-Navarro C., Fernández Y., Bourret T.B., Zamorano A., Henríquez-Sáez J.L., 2022. First record of *Colletotrichum anthrisci* causing anthracnose on avocado fruits in Chile. *Pathogens* 11: 1204. https://doi.org/10.3390/pathogens11101204

Carbone I., Kohn L.M., 1999. A method for designing primer sets for speciation studies in filamentous ascomycetes. *Mycologia* 91: 553–556. https://doi.org/10.1080/00275514.1999.12061051

Chen Y., Fu D., Wang W., Gleason M.L., Zhang R., … Sun G., 2022. Diversity of *Colletotrichum* species causing apple bitter rot and Glomerella leaf spot in China. *Journal of Fungi* 8, 740. https://doi.org/10.3390/jof8070740

Chung P.C., Wu H.Y., Wang Y.W., Ariyawansa H.A., Hu H.P., … Chung C.L., 2020. Diversity and pathogenicity of *Colletotrichum* species causing strawberry anthracnose in Taiwan and description of a new species, *Colletotrichum miaoliense* sp. nov. *Scientific Reports* 10: 14664. https://doi.org/10.1038/s41598-020-70878-2

Crous P.W., Groenewald J.Z., Risede J.M., Hywel-Jones N.L., 2004. *Calonectria* species and their *Cylindrocladium* anamorphs: species with sphaeropedunculate vesicles. *Studies in Mycology* 50: 415–430. https://doi.org/10.3114/sim.55.1.213

Crous P.W., Verkleij G.J.M., Groenewald J.Z., Houbraken J., 2019. Fungal biodiversity. *Westerdijk Laboratory Manual Series* 1. Westerdijk Fungal Biodiversity Institute, Utrecht, The Netherlands.

Damm U., Cannon P.F., Woudenberg J.H.C., Crous P.W., 2012a. The *Colletotrichum acutatum* species complex. *Studies in Mycology* 73: 37–113. https://doi.org/10.3114/sim0010

Damm U., Cannon P.F., Woudenberg J.H.C., Johnston P.R., Weir B., … Crous P.W., 2012b. The *Colletotrichum boninense* species complex. *Studies in Mycology* 73: 1–36. https://doi.org/10.3114/sim0002

Damm U., Crous P.W., Fourie P.H., 2007. Botryosphaeriaceae as potential pathogens of *Prunus* species in South Africa, with descriptions of *Diplodia africana* and *Lasiodiplodia plurivora* spp. nov. *Mycologia* 99: 664–680. https://doi.org/10.3852/mycologia.99.5.664

Damm U., Mostert L., Crous P.W., Fourie P.H., 2008. Novel *Phaeoacremonium* species associated with necrotic wood of *Prunus* trees. *Persoonia* 20: 87–102. https://doi.org/10.3767/003158508X324227

Damm U., O'Connell R.J., Crous P.W., Groenewald J.Z., 2014. The *Colletotrichum destructivum* species complex – hemibiotrophic pathogens of forage and field crops. *Studies in Mycology* 79: 49–84. https://doi.org/10.1016/j.simyco.2014.09.003

Damm U., Sato T., Alizadeh A., Groenewald J.Z., Crous P.W., 2019. The *Colletotrichum draecaenophilum*, *C. magnum* and *C. orchidearum* species complexes. *Studies in Mycology* 92: 1–46. https://doi.org/10.1016/j.simyco.2018.04.001

Damm U., Sun Y.C., Huang C.J., 2020. *Colletotrichum eriobotryae* sp. nov. and *C. nymphaeae*, the anthracnose pathogens of loquat fruit in central Taiwan, and their sensitivity to azoxystrobin. *Mycological Progress* 19: 367–380. https://doi.org/10.1007/s11557-020-01565-9

Damm U., Woudenberg J.H.C., Cannon P.F., Crous P.W., 2009. *Colletotrichum* species with curved conidia from herbaceous hosts. *Fungal Diversity* 39: 45–87. http://www.fungaldiversity.org /fdp/sfdp/FD39-3.pdf

Dämmrich F., Gminder A., Hardtke H.J., Karasch P., Schmidt M., Wehr K., 2023. Datenbank der Pilze Deutschlands, Deutsche Gesellschaft für Mykologie e. V. http://www.pilze-deutschland.de/. Retrieved December 27 2023.

Debode J., Van Hemelrijck W., Baeyen S., Creemers P., Heungens K., Maes M., 2009. Quantitative detection and monitoring of *Colletotrichum acutatum* in strawberry leaves using real-time PCR. *Plant Pathology* 58: 504–514. https://doi.org/10.1111/j.1365-3059.2008.01987.x

Denoyes B., Baudry A., 1995. Species identification and pathogenicity study of French *Colletotrichum* strains isolated from strawberry using morphological and cultural characteristics. *Phytopathology* 85: 53–57. https://doi.org/10.1094/Phyto-85-53

Farr D.F., Rossman A.Y., 2024. Fungal Databases, U.S. National Fungus Collections, ARS. USDA. http://nt.ars-grin.gov/fungaldatabases/. Retrieved April 23 2024.

Gan P., Nakata N., Suzuki T., Shirasu K., 2017. Markers to differentiate species of anthracnose fungi identify *Colletotrichum fructicola* as the predominant virulent species in strawberry plants in Chiba Prefecture of Japan. *Journal of General Plant Pathology* 83: 14–22. https://doi.org/10.1007/s10327-016-0689-0

Gardes M., Bruns T.D., 1993. ITS primers with enhanced specificity for basidiomycetes - application to the identification of mycorrhizae and rusts. *Molecular*

Ecology 2: 113–118. https://doi.org/10.1111/j.1365-294X.1993.tb00005.x

Garrido C., Carbú M., Fernández-Acero F.J., Budge G., Vallejo I., … Cantoral J. M., 2008. Isolation and pathogenicity of *Colletotrichum* spp. causing anthracnose of strawberry in south west Spain. *European Journal of Plant Pathology* 120: 409–415. https://doi.org/10.1007/s10658-007-9224-7

Glass N.L., Donaldson G., 1995. Development of primer sets designed for use with PCR to amplify conserved genes from filamentous ascomycetes. *Applied and Environmental Microbiology* 61: 1323–1330. https://doi.org/10.1128/aem.61.4.1323-1330.1995

Grammen A., Wenneker M., Van Campenhout J., Pham K.T.K., Van Hemelrijck W., … Keulemans W., 2019. Identification and pathogenicity assessment of *Colletotrichum* isolates causing bitter rot of apple fruit in Belgium. *European Journal of Plant Pathology* 153, 47–63. https://doi.org/10.1007/s10658-018-1539-z

Guerber J.C., Liu B., Correll J.C., Johnston P.R., 2003. Characterization of diversity in *Colletotrichum acutatum sensu lato* by sequence analysis of two gene introns, mtDNA and intron RFLPs, and mating compatibility. *Mycologia* 95: 872–895. https://doi.org/10.1080/15572536.2004.11833047

Guindon S., Dufayard J.-F., Lefort V., Anisimova M., Hordijk W., Gascuel O., 2010. New algorithms and methods to estimate Maximum-Likelihood phylogenies: assessing the performance of PhyML 3.0. *Systematic Biology* 59: 307–321. https://doi.org/10.1093/sysbio/ syq010

Han Y.C., Zeng X.G., Xiang F.Y., Ren L., Chen F.Y., Gu Y.C., 2016. Distribution and characteristics of *Colletotrichum* spp. associated with anthracnose of strawberry in Hubei, China. *Plant Disease* 100: 996–1006. https://doi.org/10.1094/PDIS-09-15-1016-RE

Hardigan M.A., Poorten T.J., Acharya C.B., Cole G.S., Hummer K.E., … Knapp S.J., 2018. Domestication of temperate and coastal hybrids with distinct ancestral gene selection in octoploid strawberry. *The Plant Genome* 11(3): 1–11. https://doi.org/10.3835/plantgenome2018.07.0049

Hillis D.M., Bull J.J., 1993. An empirical test of bootstrapping as a method for assessing confidence in phylogenetic analysis. *Systematic Biology* 42: 182–192. https://doi.org/10.1093/sysbio/42.2.182

Hoang D.T., Chernomor O., von Haeseler A., Minh B.Q., Vinh L.S., 2018. UFBoot2: improving the ultrafast bootstrap approximation. *Molecular Biology and Evolution* 35: 518–522. https://doi.org/10.1093/ molbev/msx281

Howard C.M., Maas J.L., Chandle C.K., Albregts E.E., 1992. Anthracnose of strawberry caused by the *Colletotrichum* complex in Florida. *Plant Disease* 76: 976–981. https://doi.org/10.1094/PD-76-0976

Jayawardena R.S., Huang J.K., Jin B.C., Yan J.Y., Li X., … Zhang G.Z., 2016. An account of *Colletotrichum* species associated with strawberry anthracnose in China based on morphology and molecular data. *Mycosphere* 7: 1147–1163. https://doi.org/10.5943/mycosphere/si/2c/6

Kalyaanamoorthy S., Minh B.Q., Wong T.K.F., von Haeseler A., Jermiin L.S., 2017. Fast model selection for accurate phyloge netic estimates. *Nature Methods* 14: 587–589. https://doi.org/10.1038/nmeth. 4285

Karimi K., Ahari A.B., Arzanlou M., Amini J., Pertot I., Rota-Stabelli O., 2017. Application of the consolidated species concept to identify the causal agent of strawberry anthracnose in Iran and initial molecular dating of the *Colletotrichum acutatum* species complex. *European Journal of Plant Pathology* 147: 375–387. https://doi.org/10.1007/s10658-016-1009-4

Konno M., Iwamoto S., Seiwa K., 2011. Specialization of a fungal pathogen on host tree species in a cross-inoculation experiment. *Journal of Ecology* 99: 1394–1401. https://doi.org/10.1111/ j.1365-2745.2011.01869.x

Laun N., Fried A., 1996. Anthraknose bei Erdbeeren - ein neues Pflanzenschutzproblem? *Rheinische Monatsschrift* 4/96: 232–235.

Lehari G., 2002. Erdbeeren. Sorten und Anbau, Fitness und Gesundheit, feine Rezepte. Stuttgart (Hohenheim): Ulmer (Garten-fit).

Liu F., Ma Z.Y., Hou L.W., Diao Y.Z., Wu W.P., … Cai L., 2022. Updating species diversity of *Colletotrichum*, with a phylogenomic overview. *Studies in Mycology* 101: 1–56. https://doi.org/10.3114/sim.2022.101.01

MacKenzie S.J., Peres N.A., Barquero M.P., Arauz L.F., Timmer L.W., 2009. Host range and genetic relatedness of *Colletotrichum acutatum* isolates from fruit crops and leatherleaf fern in Florida. *Phytopathology* 99: 620–631. https://doi.org/10.1094/PHYTO-99-5-0620

Marcelino J., Giordano R., Gouli S., Gouli V., Parker B.L., … Cesnik R., 2008. *Colletotrichum acutatum* var. *fiori-* (teleomorph: *Glomerella acutata* var. *fioriniae* var. nov.) infection of a scale insect. *Mycologia* 100: 353–374. doi: 10.3852/07-174R

Minh B.Q., Nguyen M.A.T., von Haeseler A., 2013. Ultrafast approximation for phylogenetic bootstrap. *Molecular Biology and Evolution* 30: 1188–1195. https://doi.org/10.1093/molbev/mst024

Moriwaki J., Sato T., Tsukiboshi T., 2003. Morphological and molecular characterization of *Colletotrichum boninense* sp. nov. from Japan. *Mycoscience* 44: 47–53. https://doi.org/10.1007/S10267-002-0079-7

Nam M.H., Park M.S., Lee H.D., Yu S.H., 2013. Taxonomic reevaluation of *Colletotrichum gloeosporioides* isolated from strawberry in Korea. *The Plant Pathology Journal* 29: 317–322. https://doi.org/10.5423/PPJ.NT.12.2012.0188

Nguyen L.-T., Schmidt H.A., von Haeseler A., Minh B.Q., 2015. IQ-TREE: A fast and effective stochastic algorithm for estimating maximum likelihood phylogenies. *Molecular Biology and Evolution* 32: 268–274. https://doi.org/10.1093/molbev/msu300

Nilsson U., Carlson-Nilsson U., Svedelius G., 2005. First report of anthracnose fruit rot caused by *Colletotrichum acutatum* on strawberry in Sweden. *Plant Disease* 89: 1242. https://doi.org/10.1094/PD-89-1242C

Nirenberg H.I., 1976. Untersuchungen über die morphologische und biologische Differenzierung in der *Fusarium*-Sektion Liseola. *Mitteilungen aus der Biologischen Bundesanstalt für Land- und Forstwirtschaft Berlin-Dahlem* 169: 1–117.

Nirenberg H.I., Feiler U., Hagedorn G., 2002. Description of *Colletotrichum lupini* comb. nov. in modern terms. *Mycologia* 94: 307–320. https://doi.org/10.2307/3761809

O'Donnell K., Cigelnik E., 1997. Two divergent intragenomic rDNA ITS2 types within a monophyletic lineage of the fungus *Fusarium* are nonorthologous. *Molecular Phylogenetics and Evolution* 7: 103–116. https://doi.org/10.1006/mpev.1996.0376

Rambaut A., 2002. Sequence Alignment Editor. Version 2.0. University of Oxford, Oxford, UK.

Rayner R.W., 1970. A mycological colour chart. Commonwealth Mycological Institute, Kew, UK. ISBN 0851980260

Smith B.J., Black L.L., 1986. First report of *Colletotrichum acutatum* on strawberry in the United States. *Plant Disease* 70: 1074.

Sreenivasaprasad S., Talhinhas P., 2005. Genotypic and phenotypic diversity in *Colletotrichum acutatum*, a cosmopolitan pathogen causing anthracnose on a wide range of hosts. *Molecular Plant Pathology* 6(4): 361–378 https://doi.org/10.1111/j.1364-3703.2005.00291.x

Statistisches Bundesamt, 2023. Obst, Gemüse und Gartenbau. Betriebe, Anbauflächen, Erträge und Erntemengen von Gemüse. Betriebe, Anbauflächen, Erträge und Erntemengen von Gemüse und Erdbeeren 2022. Statistisches Bundesamt.

Sundelin T., Schiller M., Lübeck M., Jensen D.F., Paaske K., Petersen B.D., 2005. First report of anthracnose fruit rot caused by *Colletotrichum acutatum* on strawberry in Denmark. *Plant Disease* 89: 432. https://doi.org/10.1094/PD-89-0432B

Swofford D.L., 2003. PAUP*. Phylogenetic analysis using parsimony (* and other methods). Version 4.0b 10. Sinauer Associates, Sunderland. https://doi.org/10.1111/j.0014-3820.2002.tb00191.x

Talhinhas P., Baroncelli R., 2021. *Colletotrichum* species and complexes: geographic distribution, host range and conservation status. *Fungal Diversity* 110: 109–198. https://doi.org/10.1007/s13225-021-00491-9

Talhinhas P., Baroncelli R., 2023. Hosts of *Colletotrichum*. *Mycosphere* 14: 158–261, https://doi.org/10.5943/mycosphere/14/si2/4

Trifinopoulos J., Nguyen L.T., von Haeseler A., Minh B.Q., 2016. W-IQ-TREE: a fast online phylogenetic tool for maximum likelihood analysis. *Nucleic Acids Research* 44(W1): W232–W235. https://doi.org/10.1093/nar/gkw256

Tsvetkova Y.V., Kuznetsova A.A., 2022. Detection of anthracnose in strawberry and methods of etiological diagnosis. *Doklady Biological Sciences* 507: 473–484. https://doi.org/10.1134/S0012496622060229

Wang N.Y., Forcelini B.B., Peres N.A., 2019. Anthracnose fruit and root necrosis of strawberry are caused by a dominant species within the *Colletotrichum acutatum* species complex in the United States. *Phytopathology* 109: 1293–1301. https://doi.org/10.1094/PHYTO-12-18-0454-R

Weir B., Damm U., Johnston P.R., 2012. The *Colletotrichum gloeosporioides* species complex. *Studies in Mycology* 73: 115–213. https://doi.org/10.3114/sim0011

White T.J., Bruns T., Lee S., Taylor J., 1990. Amplification and direct sequencing of fungal ribosomal RNA genes for phylogenetics. In: *PCR Protocols: a Guide to Methods and Applications* (Innis MA, Gelfand DH, Sninsky JJ, White TJ, ed). Academic Press, San Diego, USA. 315–322. http://doi.org/10.1016/B978-0-12-372180-8.50042-1

Woudenberg J.H.C., Aveskamp M.M., Gruyter J. de, Spiers A.G., Crous P.W., 2009. Multiple Didymella teleomorphs are linked to the *Phoma clematidina* morphotype. *Persoonia* 22: 56–62. https://doi.org/10.3767/003158509X427808

Zapata M., Rodríguez-Serrano E., Castro J.F., Santelices C., Carrasco-Fernández J., … Palfner G., 2024. Novel species and records of *Colletotrichum* associated with native woody plants in south-central Chile. *Mycological Progress* 23: 18. https://doi.org/10.1007/s11557-024-01956-2

Zhang Q., Nizamani M.M., Feng Y., Yang Y.Q., Jayawardena R.S., … Li C., 2023a. Genome-scale and multi-gene phylogenetic analyses of *Colletotrichum* spp. host preference and associated with medici-

nal plants. *Mycosphere* 14(2): 1–106. https://doi.org/10.5943/mycosphere/14/si2/1

Zhang YX, Chen JW, Manawasinghe IS, Lin YH, Jayawardena RS, … Xiang MM., 2023b. Identification and characterization of *Colletotrichum* species associated with ornamental plants in Southern China. *Mycosphere* 14(2): 262–302. https://doi.org/10.5943/mycosphere/14/si2/5

Phytopathologia Mediterranea
The international journal of the
Mediterranean Phytopathological Union

Firenze University Press
www.fupress.com/pm

Research Papers

Genetic variability of grapevine Pinot gris virus (GPGV) in an organically cultivated vineyard in Hungary

Réka SÁRAY[1], Erzsébet SZATHMÁRY[2], Dóra PINCZÉS[1], Asztéria ALMÁSI[1], Tamás DEÁK[3], László PALKOVICS[4,5], Katalin SALÁNKI[1,*]

[1] *Department of Plant Pathology, Plant Protection Institute, Centre for Agricultural Research, Eötvös Loránd Research Network, Budapest, Hungary*
[2] *Department of Plant Pathology, Institute of Plant Protection, Hungarian University of Agriculture and Life Sciences (MATE), Budapest, Hungary*
[3] *Department of Viticulture, Institute of Viticulture and Enology, Hungarian University of Agriculture and Life Sciences (MATE), Budapest, Hungary*
[4] *ELKH-SZE PhatoPlant-Lab, Széchenyi Isván University, Mosonmagyaróvár, Hungary*
[5] *Department of Plant Sciences, Albert Kázmér Faculty of Mosonmagyaróvár, Széchenyi István University, Mosonmagyaróvár, Hungary*
*Corresponding author. E-mail: salanki.katalin@atk.hu

Summary. *Grapevine Pinot gris virus* (GPGV) is a recently identified trichovirus infecting grapevines. Despite wide distribution, there is limited available information on epidemiology, transmission, and associated symptoms of grapevine leaf mottling and deformation. Occurrence and genetic diversity of GPGV variants were surveyed in an organically cultivated Hungarian vineyard that was planted between 1996 and 2014. Sequence analysis demonstrated the widespread presence and high variability of GPGV, and according to phylogenetic analyses, the Hungarian virus isolates were classified into three groups. Most of the identified variants clustered with the representative asymptomatic isolates, but all isolates from one grapevine cultivar grouped with representative isolates of clade B. Furthermore, one isolate clustered with representative isolates of clade C, and the identified clade C variant had previously undescribed polymorphisms.

Keywords. RT-PCR, phylogenetic analysis, sequence analysis.

Citation: Sáray, R., Szathmáry, E., Pinczés, D., Almási, A., Deák, T., Palkovics, L., & Salánki, K. (2024) Genetic variability of grapevine Pinot gris virus (GPGV) in an organically cultivated vineyard in Hungary. *Phytopathologia Mediterranea* 63(2): 179-190. doi: 10.36253/phyto-14492

Accepted: April 4, 2024

Published: July 17, 2024

Data Availability Statement: All relevant data are within the paper and its Supporting Information files.

Competing Interests: The Author(s) declare(s) no conflict of interest.

Editor: Nihal Buzkan, Kahramanmaraş Sütçü Imam University, Turkey.

ORCID:
RS: 0000-0003-1942-6004
ES: 0009-0000-0441-038X
DP: 0000-0003-3174-8460
AA: 0000-0003-2722-5800
TD: 0000-0001-8172-3259
LP: 0000-0002-1850-6750
KS: 0000-0002-0128-4338

INTRODUCTION

Grapevine Pinot gris virus (GPGV; *Betaflexiviridae*) is a newly emerging trichovirus. Since its discovery in Northeastern Italian grapevines in 2012 (Giampetruzzi *et al.*, 2012), GPGV has been identified in many grape-growing countries in Europe (Glasa *et al.*, 2014; Morelli *et al.*, 2014; Pleško *et al.*, 2014; Beuve *et al.*, 2015; Casati *et al.*, 2015; Bertazzon *et al.*, 2016, 2021a; Eichmeier *et al.*, 2016, 2017, 2018; Gazel *et al.*, 2016; Reynard *et al.*, 2016; Ruiz-García and Olmos, 2017; Czotter *et al.*, 2018; Silva *et al.*, 2018; Abou

Kubaa *et al*., 2019; Massart *et al*., 2020; Shvets and Vinogradova, 2022), the Middle East and Asia (Fan *et al*., 2016; Rasool *et al*., 2017; Abou Kubaa *et al*., 2020; Tokhmechi and Koolivand, 2020; Abe and Nabeshima, 2021), North and South America (Jo *et al*., 2015; Al Rwahnih *et al*., 2016; Poojari *et al*., 2016; Xiao *et al*., 2016; Fajardo *et al*., 2017; Zamorano *et al*., 2019; Debat *et al*., 2020), Africa (Eichmeier *et al*., 2020; Bertazzon *et al*., 2021b), and Australia (Wu and Habili, 2017).

Several studies have analyzed the incidence and evolutionary history of GPGV (Saldarelli *et al*., 2015; Bertazzon *et al*., 2017; Tarquini *et al*., 2019a; Hily *et al*., 2020, 2021a). Bertazzon *et al*. (2016) showed via comparative analyses that grapevine samples from Northeastern Italy collected in 2002 lacked GPGV infections, despite high incidence (79.4%) in samples from 2014. A similar conclusion was reached by Gentili *et al.* (2017), where no GPGV infection was detected in >10-year-old grapevines in southern and central Italian vineyards. This was also supported by the observation that local cultivars were less infected with GPGV than national and internationally well-known cultivars, implying a recent introduction of the virus from outside of Italy. A Brazilian survey also determined an increase in GPGV incidence in recently imported grapevine cuttings, compared with older samples or germplasm collections (Fajardo *et al*., 2017). PCR assays carried out on European grapevine samples from 2005 showed that GPGV was originally concentrated in Eastern Europe before it was detected in Southern and Western Europe (Bertazzon *et al*., 2016). These observations were further supported by Hily *et al.* (2020), who conducted phylogenetic and diversity analyses of new and already available high throughput sequencing data of GPGV. That survey indicated that Asia (and with high probability, China) was a possible source of origin for GPGV.

The means of natural transmission of GPGV remains a matter of speculation. No natural transmission and low prevalence of the virus were documented in the United States of America and Australia (Al Rwahnih *et al*., 2016; Wu and Habili, 2017), while other studies have recorded active vine-to-vine spread of the virus in vineyards during a 3-year-long monitoring period (Martelli, 2014; Bertazzon *et al*., 2017; Hily *et al*., 2021b). Furthermore, successful GPGV transmission was observed by grafting (Saldarelli *et al*., 2015). Distribution patterns of GPGV suggest the involvement of the eriophyid mite *Colomerus vitis* as a transmission vector, which was also shown to be the vector of another trichovirus, *Grapevine berry inner necrosis virus* (GINV). While *C. vitis* is a monophagous mite of grapevine, GPGV has been identified in other woody and herbaceous hosts, implying the contribution of other vectors in GPGV transmission (Gualandri *et al*., 2017; Demian *et al*., 2022). Herbaceous hosts could serve as reservoirs for GPGV, facilitating the dissemination of the virus. More information is required on the molecular and epidemiological aspects of the virus-vector interactions to provide guidance for the development of appropriate virus management decisions.

GPGV presence in grapevines is often connected with the appearance of grapevine leaf mottling and deformation (GLMD) symptoms (Tarquini *et al*., 2019b, 2021a). GLMD generally includes chlorotic mottling, leaf deformation, shortened internodes, as well as reduced yields (up to 50%) and berry quality (Bianchi *et al*., 2015; Saldarelli *et al*., 2015; Bertazzon *et al*., 2017). GPGV-infected grapevines show variable GLMD symptoms, ranging from mild to severe, or they can remain symptomless (Tarquini *et al*., 2023). This contrast in symptom expression remains to be explained. In some cases, the connection between GPGV presence and the severity of the symptoms was equivocal (Bianchi *et al*., 2015; Tarquini *et al*., 2018), while several studies have proposed a connection between molecular characteristics of GPGV variants and resulting host symptoms (Glasa *et al*., 2014; Saldarelli *et al*., 2015; Bertazzon *et al*., 2017; Tarquini *et al*., 2019a, 2021a). The ability of GPGV to trigger and suppress antiviral post-transcriptional gene silencing (PTGS) has also been demonstrated (Tarquini *et al*., 2021b), and boron deficiency, agronomic and abiotic factors may also contribute to GLMD symptom formation (Bertazzon *et al*., 2020; Kiss *et al*., 2021).

The GPGV genome consists of three overlapping open reading frames (ORFs), encoding the RNA-dependent RNA polymerase (RdRp) (ORF1), the movement protein (MP) (ORF2), and the coat protein (CP) (ORF3) (Giampetruzzi *et al*., 2012). Multiple classifications have been introduced based on phylogenetic analyses of partial sequence data of the movement protein and coat protein (MP/CP) regions of GPGV. Saldarelli *et al.* (2015) showed that MP/CP sequences partition into two groups, which was further supported by the asymptomatic and symptomatic phenotypes of these isolates. Bertazzon *et al.* (2017) classified three clusters, named clades A, B and C. Isolates derived from asymptomatic plants were classified as clade A; isolates with low (<1%) symptom incidence were clade B, and isolates with >1% symptom incidence were in clade C (Bertazzon *et al*., 2017). This three-cluster classification was further supported by full-genome phylogenetic analyses of GPGV, where the isolates were grouped into α-, β- and γ-clades (Tarquini *et al*., 2019a).

Although the symptom presence was not directly linked with the genetic variability of GPGV, distinctive molecular differences were identified in the MP/CP

and RdRp sequences (Tarquini *et al.*, 2019a). Tarquini *et al.* (2019a) demonstrated differentiating amino acid (aa) alterations between the clades, and suggested putative phosphorylation events which could play significant roles in symptom development. These single nucleotide polymorphisms (SNPs) were also shown to affect virus-derived siRNA production (Tarquini *et al.*, 2021a). Shvets and Vinogradova (2022) also investigated the putative role of detected SNPs in Russian grapevines.

Knowledge of the genetic variability of different GPGV strains has the potential to provide information on the evolutionary history of the virus. Research on GPGV is mainly focused on Western European countries with grape cultivation histories, and there is limited information available on vineyard GPGV spread in Eastern Europe. The present study aimed to verify the occurrence and diversity of GPGV isolates in one vineyard located in the southern wine region of Hungary.

MATERIALS AND METHODS

Plant material

The vineyard selected for this study is located in Szajk, in the Pécs wine region of southern Hungary. The vineyard was planted between 1996 and 2014 (Figure S1) and is maintained under organic cultivation. In the early summer of 2021, 20 different cultivars were sampled from the vineyard. The cultivars included the internationally well-known 'Cabernet sauvignon', 'Sauvignon blanc', and 'Traminer', traditional Hungarian cultivars such as 'Juhfark', 'Hárslevelű', and 'Olaszrizling', the recently bred Hungarian cultivars 'Pamerzs', 'Silver', and 'Jázmin', and experimental hybrid lines. Five plants were randomly selected and sampled from each grapevine cultivar, with a total of 100 samples collected and without distinction between the presence or absence of symptoms.

RNA extraction

Total RNA was extracted from the 100 samples, using a simplified version of the extraction method described by Xu *et al.* (2004). For each sample, 3 g of leaf tissue was ground in liquid nitrogen with a mortar and pestle, and 1 mL of lysis buffer (100 mM Tris-HCl pH 8.0, 50 mM EDTA, 1.5 M NaCl, 3% CTAB, 2% PVP, and 4% of β-mercaptoethanol added just before use) was added to the ground tissues. The mixture was then incubated at 65°C for 30 min, and the sample was vortexed every 10 min. An equal volume of chloroform:isoamyl alcohol (24:1 v/v) and 100 µL of 5 M potassium acetate were added to the sample, and gentle shaking was applied until homogenization. After a centrifuge step (6810 g for 5 min), the supernatant was transferred to a new microcentrifuge tube, and a new extraction step was performed by adding 800 µL of chloroform:isoamyl alcohol, followed by homogenization by inverting and centrifuging at 6810 g for 5 min. The supernatant was then transferred to a new microcentrifuge tube, and 750 µL isopropanol and 80 µL of 3 M sodium acetate were added and the sample was homogenized by inverting. The sample was then incubated at room temperature for 20–30 min and centrifuged (18 000 g for 8 min). The resulting pellet was washed twice with 70% ethanol, air-dried, and resuspended in 25 µL of sterile nuclease-free water. The DNase treatment was carried out as described by Oñate-Sánchez and Vicente-Carbajosa (2008). Three µL of 10× DNase buffer and 2 µL of DNase I (Thermo Fisher Scientific) were added and the mixture was incubated at 37°C for 30 min. Seventy µL of DEPC-treated water, 50 µL of 7.5 M sodium acetate, and 400 µL of ethanol were then added to the solution, which was thoroughly mixed, and then centrifuged at 4°C for 20 min. After a washing step with 70% ethanol and air-drying, the RNA was resuspended in 20 µL of sterile RNase-free water.

RT-PCR

Reverse transcription (RT) reaction was carried out using a RevertAid First Strand cDNA synthesis kit (Thermo Fisher Scientific) according to the manufacturer's instructions. RT-PCR was carried out using primer pairs for amplification of the MP/CP region of GPGV: DetF (5'-TGGTCTGCAGCCAGGGGACA-3') and DetR (5'-TCACGACCGGCAGGGAAGGA-3') (Morelli *et al.*, 2014). RT-PCR was carried out with a One-Step RT-PCR Kit (Qiagen), with the following conditions: an initial denaturation step of 94°C for 2 min; followed by 40 cycles each of 94°C for 30s, 58°C for 40 sec and 72°C for 45 sec, and a final extension of 72°C for 5 min. A control amplification of the *Vitis* 18S rRNA gene was carried out with primers 18S-H325 (5'-AAACGGCTAC-CACATCCAAG-3') and 18S-C997 (5'-GCGGAGTC-CTAAAAGCAACA-3') (Gambino and Gribaudo, 2006). The nucleotide sequence of the amplified products was determined either directly as a PCR product or cloned into pGEM®-T Easy vector (Promega).

Cloning procedure

Sequence analysis of isolate HU-27 showed multiple peaks in the chromatogram, indicating the pres-

ence of distinct isolates in the individual plant samples. For this reason, cloning of the amplified PCR products was carried out to clarify the exact nucleotide sequences. The PCR products were cloned into pGEM®-T Easy vector (Promega) and then transformed into *Esherichia coli* C53. After miniprep plasmid isolation, the nucleotide sequences of the amplified products were determined.

Phylogenetic studies and analyses of sequence diversity

For the phylogenetic and molecular analyses, one GPGV-positive sample was selected from each grapevine cultivar for nucleotide sequencing of the amplified MP/CP regions.

To investigate the diversity between the newly identified Hungarian sequences, an unrooted ML tree was also constructed, including the previously described sequences. The GenBank accession numbers of the these sequences are: KF134123, KF134124, KF134125, KF686810, KM491305, KT894101, KU194413, KU949328, KX522755, KY706085, LN606703, LN606705, LN606739, MH087439, MH087440, MH087441, MH087442, MH087443, MH087444, MH087445, MH087446, MH087447, and MH802023. The sequence diversity analysis was completed by using the Maximum likelihood method based on the JTT matrix-based model with MEGA6 (Tamura *et al*., 2013). The bootstrap consensus tree was inferred from 1000 replicates and branches corresponding to partitions reproduced in less than 40% of bootstrap replicates are collapsed. Detection of amino acid polymorphisms was carried out by multiple alignments of the protein sequence of MP/CP region, which were performed using JalView program (Waterhouse *et al*., 2009).

RESULTS

Virus detection via RT-PCR

Five samples per cultivar were assayed by RT-PCR to detect GPGV. In almost all cultivars (except 'Merlot'), all 5 out of 5 samples showed virus infection (100%), while in the case of 'Merlot', only 2 out of 5 samples were tested positive for GPGV (40%) (Table 1). All in all, the RT-PCR assays detected 97% GPGV infection among the sampled grapevines.

One isolate from each cultivar was selected for nucleotide sequence determination of the amplified PCR product. For isolate HU-27, two distinct sequences were identified, which are indicated as HU-27.1 and HU-27.2 (Figure 1, Table 2). The acquired nucleotide sequence data were deposited in the NCBI GenBank database (accession numbers OP56859 to OP56887).

Phylogenetic analyses

The sequence diversity analysis was carried out based on the nt sequences of the MP/CP region (564 nt), which includes the carboxyl-terminal region of the MP and the amino-terminal region of the CP (Figure 1). The analysis included the nt sequences of the Hungarian isolates identified in this study and 23 sequences available in the NCBI GenBank database (All acc. numbers are shown in Figure 1). The phylogenetic analysis demonstrated the diversity of the collected GPGV isolates and indicated their distribution between the three distinct clusters (clades A, B, and C) identified previously (Bertazzon *et al*., 2017).

The majority of the Hungarian sequences (from 18 of the 20 cultivars) clustered with "asymptomatic" GPGV isolates, belonging to clade A (according to the classifi-

Table 1. Detection of GPGV by RT-PCR from 100 grapevine samples collected from different grapevine cultivars in 2021.

Sample ID	Cultivar	GPGV	Sample ID	Cultivar	GPGV
HU-1 - HU-5	Pinot regina	5/5	HU-51 - HU-55	Cabernet sauvignon	5/5
HU-6 - HU-10	Castellum	5/5	HU-56 - HU-60	Traminer	5/5
HU-11 - HU-15	Jåzmin	5/5	HU-61 - HU-65	Hårslevelü	5/5
HU-16 - HU-20	Silver	5/5	HU-66 - HU-70	Olaszrizling SK	5/5
HU-21 - HU-25	Borsmenta	5/5	HU-71 - HU-75	Juhfark	5/5
HU-26 - HU-30	Olaszrizling BB20	5/5	HU-76 - HU-80	Sauvignon blanc	5/5
HU-31 - HUI-35	Pamerzs	5/5	HU-81 - HU-85	Hybrid #1	5/5
HU-36 - HU-40	Merlot	2/5	HU-86 - HU-90	Hybrid #2	5/5
HU-41 - HU-45	Blauer Portugieser	5/5	HU-91 - HU-95	Hybrid #3	5/5
HU-46 - HU-50	Cabernet franc	5/5	HU-96 - HU-100	Hybrid #4	5/5

The number of GPGV positive samples out of the total samples is reported for each cultivar.

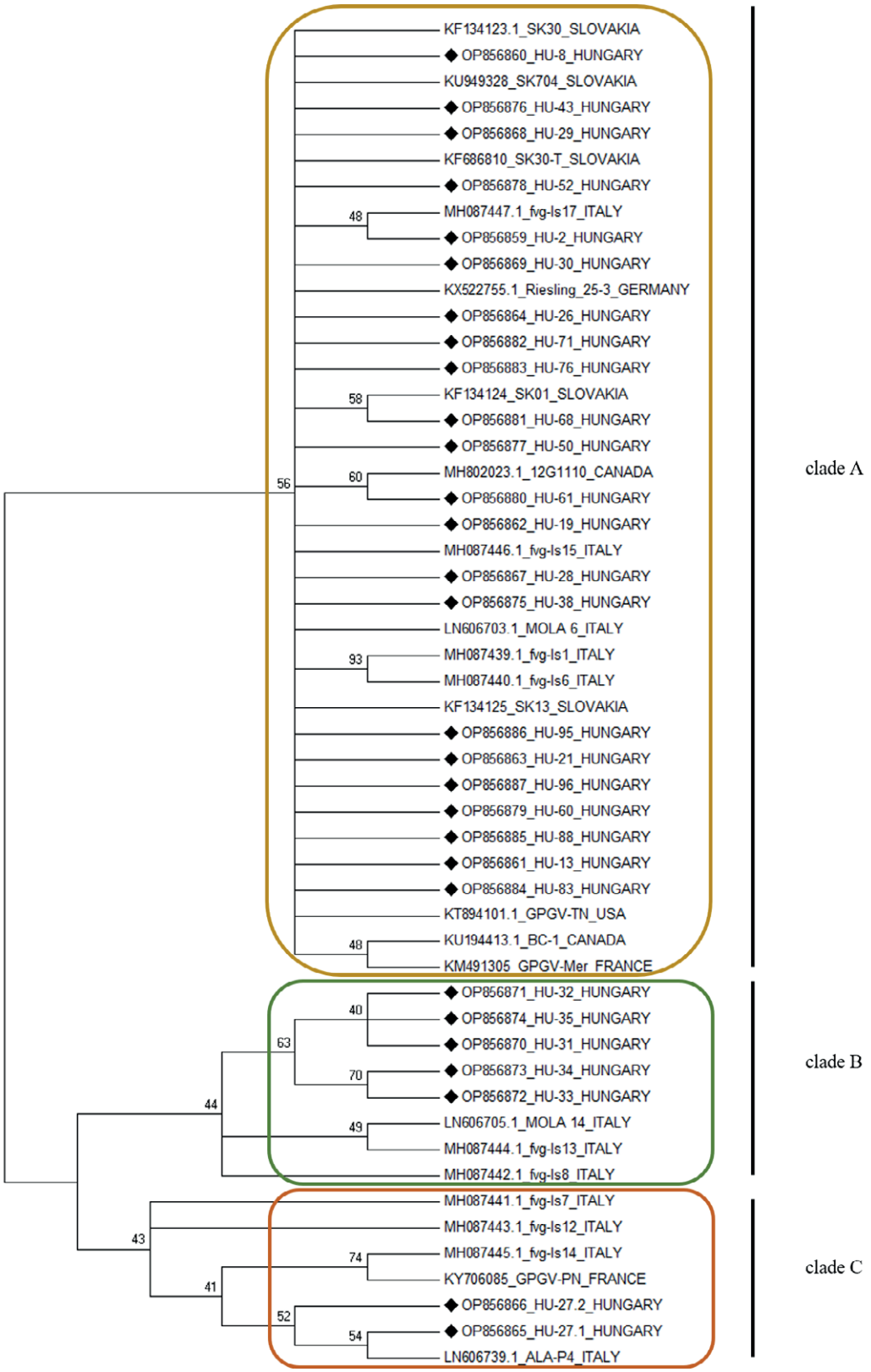

Figure 1. Unrooted ML tree of GPGV MP/CP sequences. The samples determined in the present study are marked with ♦. The sequences are available in the NCBI GenBank under the indicated accession numbers.

cation of Bertazzon *et al.* (2017). The nt sequence of the initially selected 'Pamerzs' sample (HU-31) clustered with Italian isolates classified as members of clade B. The HU-27.1 and HU-27.2 sequences (from 'Olaszrizling BB20') grouped in clade C with "symptomatic" isolates from Italy and France, showing close similarity between HU-27.1, HU-27.2 and the Italian ALA-P4 isolate, which is used as a representative isolate of clade C (Bertazzon *et al.*, 2017). Since only HU-31, HU-27.1 and HU-27.2 clustered into different clades than the majority of the identified sequences (which all grouped into clade A), the nt sequences of the rest of the PCR products (derived from the four different GPGV-positive, not yet sequenced plant samples of 'Pamerzs' and 'Olaszrizling BB20' cultivars) were also determined (included in Table 2).

After including the four additional sequences from the four different 'Pamerzs' vines in the sequence diversity analysis, all five isolates (HU-31, 32, 33, 34, 35) clustered in clade B, indicating close similarity between them. For the 'Olaszrizling BB20' samples, only the originally selected and analyzed isolates (HU-27.1 and HU-27.2) grouped in clade C, while all the other isolates (HU-26, 28, 29, 30) clustered in clade A.

Detection of amino acid polymorphisms in the MP/CP region of GPGV

The GPGV isolates differed in their MP/CP nucleotide sequences with sequence similarities between 90 and 99%. Multiple differences were identified in the examined 152 aa region of the 3'-end of the MP (Figure 2A). Based on Tarquini *et al.* (2019a), six aa alterations were proposed to distinguish between the three clades in

Table 2. The GPGV isolates analyzed in the present study, and their characteristics, showing the names of source grapevine cultivars, the year of planting and grafting, and the isolate GenBank accession numbers. The classification is based on Bertazzon *et al.* (2017), and the result of the sequence diversity analysis.

Sample ID	Cultivar	GenBank acc. number	Year planted/regrafted	Classification
HU-2	Pinot regina	OP56859	2014	clade A
HU-8	Castellum	OP56860	2003	clade A
HU-13	Bianka/Jåzmin	OP56861	2003/2018	clade A
HU-19	Silver	OP56862	2003	clade A
HU-21	V. vinifera hybrid#5/Borsmenta	OP56863	2003/2015	clade A
HU-26	Olaszrizling BB20	OP56864	2003	clade A
HU-27.1	Olaszrizling BB20	OP56865	2003	clade C
HU-27.2	Olaszrizling BB20	OP56866	2003	clade C
HU-28	Olaszrizling BB20	OP56867	2003	clade A
HU-29	Olaszrizling BB20	OP56868	2003	clade A
HU-30	Olaszrizling BB20	OP56869	2003	clade A
HU-31	Blauer Portugieser/Pamerzs	OP56870	2010/2017	clade B
HU-32	Blauer Portugieser/Pamerzs	OP56871	2010/2017	clade B
HU-33	Blauer Portugieser/Pamerzs	OP56872	2010/2017	clade B
HU-34	Blauer Portugieser/Pamerzs	OP56873	2010/2017	clade B
HU-35	Blauer Portugieser/Pamerzs	OP56874	2010/2017	clade B
HU-38	Merlot	OP56875	1997	clade A
HU-43	Blauer Portugieser	OP56876	2010	clade A
HU-50	Cabernet franc	OP56877	2008	clade A
HU-52	Cabernet sauvignon	OP56878	2000	clade A
HU-60	Traminer	OP56879	2008	clade A
HU-61	Hårslevelü	OP56880	2003	clade A
HU-68	Olaszrizling SK	OP56881	2008	clade A
HU-71	Juhfark	OP56882	2000	clade A
HU-76	Sauvignon blanc	OP56883	1996	clade A
HU-83	Pinot gris/Hybrid #1	OP56884	2005/2020	clade A
HU-88	Pinot gris/Hybrid #2	OP56885	2005/2020	clade A
HU-95	Pinot gris/Hybrid #3	OP56886	2005/2020	clade A
HU-96	Pinot gris/Hybrid #4	OP56887	2005/2020	clade A

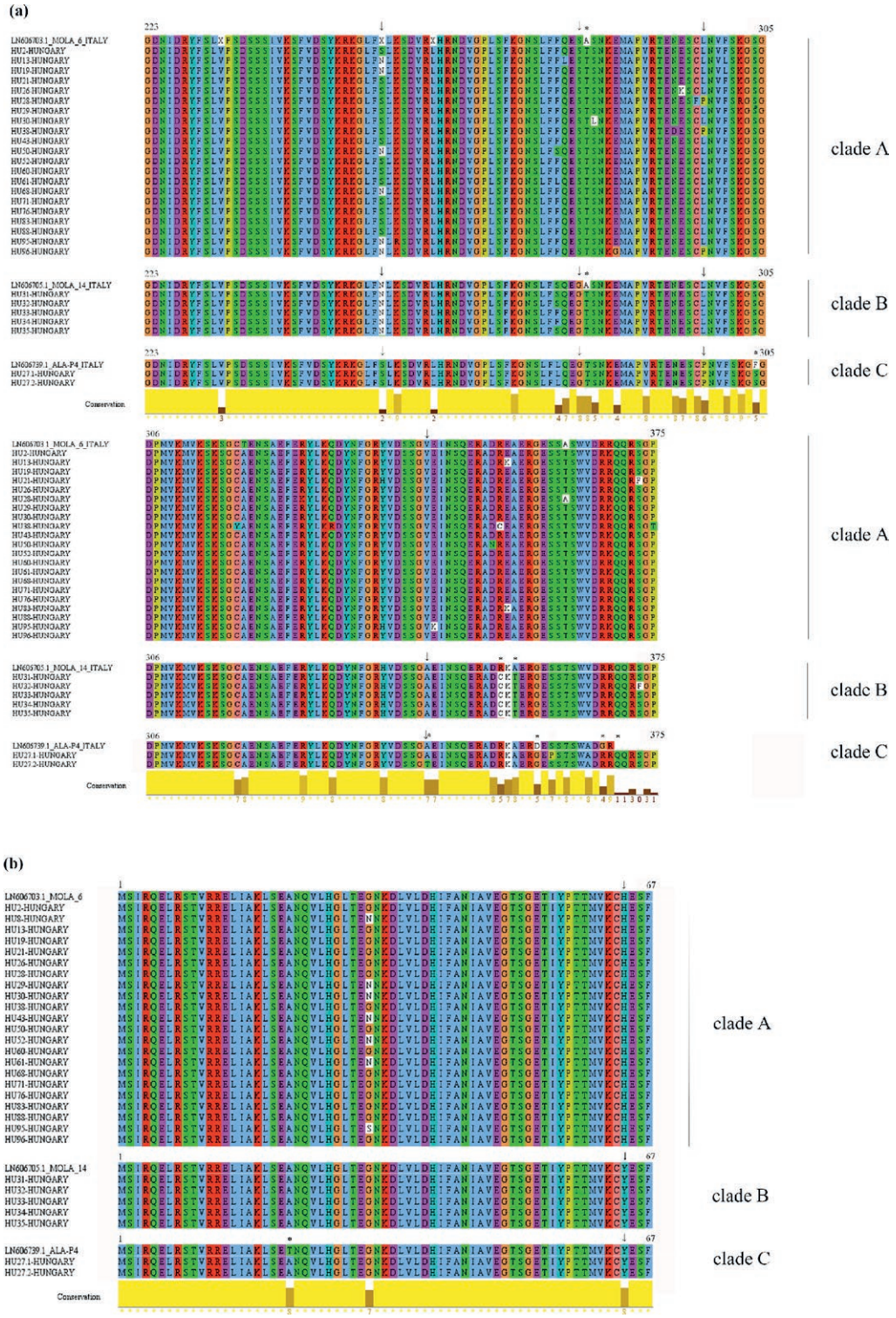

Figure 2. Amino acid alignments of the MP and the CP region of GPGV. (a) The multiple sequence alignment of the carboxyl-terminal region of GPGV MP, and (b) the amino-terminal region of the GPGV CP. The scale numbers indicate the aa positions according to the complete protein. The reference sequences for the classification were: MOLA 6 for clade A, MOLA 14 for clade B, and ALA-P4 for clade C (Saldarelli *et al.*, 2015). The corresponding GenBank accession are, respectively, LN606703, LN606705, and LN606739. The aa alterations of the isolates are indicated by asterisks, and the differentiating aa positions proposed by Tarquini *et al.* (2019a) are marked by arrowheads. The colours of the aa are according to the Clustal X Color Scheme. Conservation values quantify the similarity between the aa.

this region, five of which were detected in the Hungarian isolates as well: three in the MP and one in the CP.

At position 255 of GPGV MP, asparagine (N) was identified in isolates of clade B, but serine (S) in clade C. Both N and S were present in isolates belonging to clade A. Similar aa alteration was also observed in aa position 299; in clade A both leucine (L) and proline (P) were present, while clade B only contained L residue, and P was detected only in clade C. Moreover, discriminating aa changes between clade A and the 'symptomatic' clades (B and C) were present in two aa positions. Alterations were identified at position 282 serine-glycine (S-G), and at aa position 344 valine-alanine (V-A).

The aa alignment of the MP/CP region revealed multiple differences between the newly identified isolates and the three reference isolates, MOLA 6, MOLA 14, and ALA-P4, representing, respectively, clades A, B, and C (Bertazzon *et al.*, 2017). At three aa positions, all the Hungarian isolates of clade B showed differences from the MOLA 14 reference isolate. At positions 283, 354, and 356, threonine (T), cysteine (C), and another T residue were observed, instead of, respectively, aa alanine (A), arginine (R), and A. The two isolates belonging to clade C (HU-27.1 and HU-27.2) displayed significant alterations from the representative ALA-P4 isolate. HU-27.1 and HU-27.2 both lacked the SNPs at aa position 370, which resulted in a premature stop codon and a 6 amino acid short MP, which has been suggested as an important distinction between the clades and a putative determinant in severe symptom formation (Bertazzon *et al.*, 2017; Tarquini *et al.*, 2021a). Furthermore, HU-27.2 had a T residue instead of A at position 344, and HU-27.1 had a P residue at position 361, instead of S. Both these Hungarian isolates differed at positions 304, 359, and 368, where S, G, and R residues were present instead of, respectively, F, aspartic acid (D) and G. Both of these results indicate a wider variety in aa sequences within clade C than previously described.

Regarding the aa variance of the amplified CP region, a highly conservative 5'-end region was observed with only three aa alterations in the 67 aa long CP fragment (Figure 2B). A differentiating aa alteration was present at position 64, since in clade A only histidine (H) was present, while in the two other clades (B and C) tyrosine (Y) was detected. At position 22, both of the isolates HU-27.1 and HU-27.2 showed A residues instead of T. The diversity at position 32 was also only detected in isolates grouped within clade A (residues G, N, and S).

DISCUSSION

The internationally well-known and Hungarian grapevine cultivars included in this study were a mixture of young and older vines that were planted between 1996 and 2014. Later, in 2015-2020, some of the grapevines were regrafted onto the original cultivars (e.g., 'Pamerzs', 'Borsmenta', 'Jázmin') (Table 2). This study found that the surveyed vineyard is highly infected with GPGV (97% of the sampled grapevines). Because the identified GPGV variants displayed significant differences and showed similarity to all three GPGV clades, there is a high probability of multiple independent introduction events of GPGV into this vineyard. Previously, GPGV was reported in several Hungarian vineyards as shown by high-throughput sequencing methods, and the presence of the virus was also verified in rootstock cultivars (Czotter *et al.*, 2018), but no comprehensive evaluation of the GPGV isolates was carried out.

In the present study, 20 cultivars were evaluated for GPGV, and all but one was 100% infected by the virus. The exception was the 'Merlot' cultivar, for which two out of the five assayed plants were GPGV-positive (Table 1), which could be due to low virus titre. According to previous studies, 'Merlot' is one of the more GPGV-susceptible cultivars capable of displaying strong GLMD symptoms, compared with 'Pinot gris', 'Traminer', 'Sauvignon blanc', and others (Beuve *et al.*, 2015; Bianchi *et al.*, 2015; Gentili *et al.*, 2017).

Limited data are available on the dynamics of GPGV spread within vineyards. Two recent studies addressed the spatiotemporal spreading of GPGV in the major European wine-producing regions of Italy and France (Bertazzon *et al.*, 2020; Hily *et al.*, 2021b). During a 3-year monitoring period of two Italian vineyards, high disease occurrence and consistently increasing presence of GPGV (up to 76%) were observed. Patchy dissemination patterns of newly infected and symptom-bearing plantlets (clades B and C) were observed around the originally infected grapevines, while the asymptomatic plants (mainly clade A) occurred in a more scattered pattern throughout the vineyard. Over the monitoring period, only a small proportion of the newly infected plantlets showed GLMD symptoms, despite the drastic increase in the number of GPGV-positive samples (Bertazzon *et al.*, 2020). Hily *et al.* (2021b), who investigated GPGV spread in a vineyard in southern France, identified several major transmission events that increased the genetic diversity of GPGV by the end of an 8-year monitoring period. These studies raised questions about the mechanisms of GPGV transmission, and differences between transmission dynamics of symptomatic and

asymptomatic GPGV variants. In the present study, the correlation between symptoms and nucleotide sequence classifications was not addressed, because the observed symptoms (e.g., the strong GLMD of sample HU-27) may have been due to possible synergistic effects of multiple viruses.

Genetic determination of GLMD symptoms connected with some strains of GPGV is still unclear, despite the convincing results of other investigations (Tarquini *et al*., 2019a, 2021a). It has generally been observed that GPGV strains belonging to clade A do not induce severe symptoms, unlike isolates of clade C, which have been frequently shown to contribute to the presence of strong GLMD symptoms. Symptom formation was also suggested to be affected by virus titer. Studies have confirmed the hypothesis that increased GPGV concentration resulted in the elevated presence of severe GLMD symptoms (Bianchi *et al*., 2015; Bertazzon *et al*., 2017). To achieve high virus titer and overcome host defense mechanisms, the activation of PTGS was also demonstrated: Tarquini *et al*. (2021b) successfully identified GPGV CP as the viral suppressor of RNA silencing of GPGV. Furthermore, a putative role of the 3'-end of GPGV MP was also identified as a virulence determinant. The effect of the premature stop codon of the MP was first proposed by Saldarelli *et al*. (2015), when all the symptomatic variants of GPGV in clade C possessed the six aa shorter MP. Also, by replacing the 365 nt long 3'-end region of the MP gene in a symptomatic variant (previously linked with severe symptoms and inducing high virus titer) with the homologous region of a variant inducing milder symptoms, the chimeric construct elicited characteristics resembling the mild clone (Tarquini *et al*., 2021a).

In the present study, two GPGV isolates were identified which classified as clade C but lacked the SNP at the 3'-end of MP. New polymorphisms in the MP/CP region were previously described by Morán *et al.* (2018), but no clade C-member GPGV isolates were identified with six aa longer MPs before. This result is in accordance with the hypothesis that post-translational modifications (PTMs) could be the link between the genetic variability and symptom formation of GPGV (Tarquini *et al*., 2019a; Shvets and Vinogradova, 2022). There is, as yet, no direct proof of phosphorylation of GPGV MP, but it can be hypothesized that differences between elicited symptoms may originate from the presence or absence of phosphorylatable residues instead of the premature stop codon.

In the future, analysis of the sanitary status and the changes in the distribution of the different virus isolates in this vineyard could be worthwhile, since isolates from all three clades of GPGV were shown to be present. Further investigation of synergism/antagonism between different GPGV strains could also be important because of the possibilities of cross-protection from mixed virus infections.

ACKNOWLEDGMENTS

The authors thank Tibor Hárs for granting access to, and providing technical information about, the vineyard examined in this study.

LITERATURE CITED

Abe J., Nabeshima T., 2021. First report of grapevine Pinot gris virus in wild grapevines (Vitis coignetiae) in Japan. *Journal of Plant Pathology* 103: 725–725. https://doi.org/10.1007/s42161-021-00800-w

Abou Kubaa R., Lanotte P., Saldarelli P., 2019. First report of grapevine Pinot gris virus in grapevine in Moldavia. *Journal of Plant Pathology* 101: 441–441. https://doi.org/10.1007/s42161-018-00209-y

Abou Kubaa R., Choueiri E., Jreijiri F., El Khoury Y., Saldarelli P., 2020. First report of grapevine Pinot gris virus in Lebanon and the Middle East. *Journal of Plant Pathology* 102: 565–565. https://doi.org/10.1007/s42161-019-00453-w

Al Rwahnih M., Golino D., Rowhani A., 2016. First Report of Grapevine Pinot gris virus Infecting Grapevine in the United States. *Plant Disease* 100: 1030–1030. https://doi.org/10.1094/PDIS-10-15-1235-PDN

Bertazzon N., Filippin L., Forte V., Angelini E., 2016. Grapevine Pinot gris virus seems to have recently been introduced to vineyards in Veneto, Italy. *Archives of Virology* 161: 711–714. https://doi.org/10.1007/s00705-015-2718-2

Bertazzon N., Forte V., Filippin L., Causin R., Maixner M., Angelini E., 2017. Association between genetic variability and titre of Grapevine Pinot gris virus with disease symptoms. *Plant Pathology* 66: 949–959. https://doi.org/10.1111/ppa.12639

Bertazzon N., Forte V., Angelini E., 2020. Fast transmission of grapevine "Pinot gris" virus (GPGV) in vineyard. *VITIS - Journal of Grapevine Research* 29-34 Pages. https://doi.org/10.5073/VITIS.2020.59.29-34.

Bertazzon N., Angelini E., Signorotto M., Genov N., 2021a. First report of grapevine Pinot gris virus and grapevine leafroll-associated virus 2 in Bulgarian vineyards. *Journal of Plant Diseases and Protection* 128: 597–599. https://doi.org/10.1007/s41348-020-00415-w

Bertazzon N., Rahali M., Angelini E., Crespan M., Migliaro D., 2021b. First Report of Grapevine Pinot gris virus Infecting Grapevine in Algeria. *Plant Disease* 105: 234. https://doi.org/10.1094/PDIS-04-20-0723-PDN

Beuve M., Candresse T., Tannières M., Lemaire O., 2015. First Report of Grapevine Pinot gris virus (GPGV) in grapevine in France. *Plant Disease* 99: 293–293. https://doi.org/10.1094/PDIS-10-14-1008-PDN

Bianchi G.L., De Amicis F., De Sabbata L., Di Bernardo N., Governatori G., … Frausin C., 2015. Occurrence of Grapevine Pinot gris virus in Friuli Venezia Giulia (Italy): field monitoring and virus quantification by real-time RT-PCR. *EPPO Bulletin* 45: 22–32. https://doi.org/10.1111/epp.12196

Casati P., Maghradze D., Quaglino F., Ravasio A., Failla O., Bianco P.A., 2015. First report of grapevine pinot gris virus in Georgia. *Journal of Plant Pathology* 97, S67.

Czotter N., Molnar J., Szabó E., Demian E., Kontra L., … Varallyay E., 2018. NGS of Virus-Derived Small RNAs as a Diagnostic Method Used to Determine Viromes of Hungarian Vineyards. *Frontiers in Microbiology* 9. https://doi.org/10.3389/fmicb.2018.00122

Debat H., Luna F., Moyano S., Zavallo D., Asurmendi S., Gomez-Talquenca S., 2020. First report of grapevine Pinot gris virus infecting grapevine in Argentina. *Journal of Plant Pathology* 102: 1321–1321. https://doi.org/10.1007/s42161-020-00608-0

Demian E., Jaksa-Czotter N., Varallyay E., 2022. Grapevine Pinot Gris Virus Is Present in Different Non-Vitis Hosts. *Plants* 11(14): 1830. https://doi.org/10.3390/plants11141830

Eichmeier A., Peňázová E., Pavelková R., Mynarzová Z., Saldarelli P., 2016. Detection of Grapevine Pinot Gris Virus in Certified Grapevine Stocks in Moravia, Czech Republic. *Journal of Plant Pathology* 98: 155–157.

Eichmeier A., Pieczonka K., Peňázová E., Pečenka J., Gajewski Z., 2017. Occurrence of Grapevine Pinot gris virus in Poland and description of asymptomatic exhibitions in grapevines. *Journal of Plant Diseases and Protection* 124: 407–411. https://doi.org/10.1007/s41348-017-0076-x

Eichmeier A., Peňázová E., Muljukina N., 2018. Survey of Grapevine Pinot gris virus in certified grapevine stocks in Ukraine. *European Journal of Plant Pathology* 152: 555–560. https://doi.org/10.1007/s10658-018-1497-5

Eichmeier A., Peňázová E., Čechová J., Berraf-Tebbal A., 2020. Survey and Diversity of Grapevine Pinot gris virus in Algeria and Comprehensive High-Throughput Small RNA Sequencing Analysis of Two Isolates from Vitis vinifera cv. Sabel Revealing High Viral Diversity. *Genes* 11: 1110. https://doi.org/10.3390/genes11091110

Fajardo T.V.M., Eiras M., Nickel O., 2017. First report of Grapevine Pinot gris virus infecting grapevine in Brazil. *Australasian Plant Disease Notes* 12: 45. https://doi.org/10.1007/s13314-017-0270-5

Fan X.D., Dong Y.F., Zhang Z.P., Ren F., Hu G.J., … Zhou J., 2016. First Report of Grapevine Pinot gris virus in Grapevines in China. *Plant Disease* 100: 540–540. https://doi.org/10.1094/PDIS-08-15-0913-PDN

Gambino G., Gribaudo I., 2006. Simultaneous Detection of Nine Grapevine Viruses by Multiplex Reverse Transcription-Polymerase Chain Reaction with Coamplification of a Plant RNA as Internal Control. *Phytopathology* 96: 1223–1229. https://doi.org/10.1094/PHYTO-96-1223

Gazel M., Caglayan K., Elçi E., Öztürk L., 2016. First Report of Grapevine Pinot gris virus in Grapevine in Turkey. *Plant Disease* 100: 657–657. https://doi.org/10.1094/PDIS-05-15-0596-PDN

Gentili A., Prota V., Moro G., Schianchi N., Di Lucca E., … Faggioli F., 2017. Identification of Grapevine Pinot Gris Virus in Sardinia and Lazio (south and Central Italy). *Journal of Plant Pathology* 99: 527–530.

Giampetruzzi A., Roumi V., Roberto R., Malossini U., Yoshikawa N., … Saldarelli P., 2012. A new grapevine virus discovered by deep sequencing of virus- and viroid-derived small RNAs in Cv Pinot gris. *Virus Research* 163: 262–268. https://doi.org/10.1016/j.virusres.2011.10.010

Glasa M., Predajňa L., Komínek P., Nagyová A., Candresse T., Olmos A., 2014. Molecular characterization of divergent grapevine Pinot gris virus isolates and their detection in Slovak and Czech grapevines. *Archives of Virology* 159: 2103–2107. https://doi.org/10.1007/s00705-014-2031-5

Gualandri V., Asquini E., Bianchedi P., Covelli L., Brilli M., … Si-Ammour A., 2017. Identification of herbaceous hosts of the Grapevine Pinot gris virus (GPGV). *European Journal of Plant Pathology* 147: 21–25. https://doi.org/10.1007/s10658-016-0989-4

Hily J.-M., Poulicard N., Candresse T., Vigne E., Beuve M., … Lemaire O., 2020. Datamining, Genetic Diversity Analyses, and Phylogeographic Reconstructions Redefine the Worldwide Evolutionary History of Grapevine Pinot gris virus and Grapevine berry inner necrosis virus. *Phytobiomes Journal* 4: 165–177. https://doi.org/10.1094/PBIOMES-10-19-0061-R

Hily J.-M., Komar V., Poulicard N., Velt A., Renault L., … Lemaire O., 2021a. Evidence of differential spreading events of grapevine pinot Gris virus in Italy

using datamining as a tool. *European Journal of Plant Pathology* 161: 735–742. https://doi.org/10.1007/s10658-021-02343-3

Hily J.-M., Komar V., Poulicard N., Vigne E., Jacquet O., … Lemaire O., 2021b. Biological Evidence and Molecular Modeling of a Grapevine Pinot gris Virus Outbreak in a Vineyard. *Phytobiomes Journal* 5: 464–472. https://doi.org/10.1094/PBIOMES-11-20-0079-R.

Jo Y., Choi H., Kyong Cho J., Yoon J.-Y., Choi S.-K., Kyong Cho W., 2015. In silico approach to reveal viral populations in grapevine cultivar Tannat using transcriptome data. *Scientific Reports* 5: 15841. https://doi.org/10.1038/srep15841

Kiss T., Kocanová M., Vavříník A., Tekielska D., Pečenka J., … Eichmeier A., 2021. Incidence of GLMD-Like Symptoms on Grapevines Naturally Infected by Grapevine Pinot gris virus, Boron Content and Gene Expression Analysis of Boron Metabolism Genes. *Agronomy* 11: 1020. https://doi.org/10.3390/agronomy11061020

Martelli G.P., 2014. Directory of virus and virus-like diseases of the grapevine and their agents. *Journal of Plant Pathology* 96: 1–136.

Massart S., Vankerkoven L., Blouin A.G., Nourinejhad Zarghani S., Wetzel T., 2020. First Report of Grapevine Pinot Gris Virus and Grapevine Rupestris Stem Pitting-Associated Virus in Grapevine in Belgium. *Plant Disease* 104: 1879. https://doi.org/10.1094/PDIS-10-19-2071-PDN

Morán F., Olmos A., Lotos L., Predajňa L., Katis N., … Ruiz-García A.B., 2018. A novel specific duplex real-time RT-PCR method for absolute quantitation of Grapevine Pinot gris virus in plant material and single mites. *PLOS ONE* 13: e0197237. https://doi.org/10.1371/journal.pone.0197237

Morelli M., Catarino A. de M., Susca L., Saldarelli P., Gualandri V., Martelli G.P., 2014. First report of Grapevine pinot gris virus from table grapes in southern Italy. *Journal of Plant Pathology* 96.

Oñate-Sánchez L., Vicente-Carbajosa J., 2008. DNA-free RNA isolation protocols for Arabidopsis thaliana, including seeds and siliques. *BMC Research Notes* 1: 93. https://doi.org/10.1186/1756-0500-1-93

Pleško I.M., Marn M.V., Seljak G., Žežlina I., 2014. First Report of Grapevine Pinot gris virus Infecting Grapevine in Slovenia. *Plant Disease* 98: 1014–1014. https://doi.org/10.1094/PDIS-11-13-1137-PDN

Poojari S., Lowery T., Rott M., Schmidt A.-M., Úrbez-Torres J.R., 2016. First Report of Grapevine Pinot gris virus in British Columbia, Canada. *Plant Disease* 100: 1513–1513. https://doi.org/10.1094/PDIS-02-16-0178-PDN

Rasool S., Naz S., Rowhani A., Golino D.A., Westrick N.M., … Al Rwahnih M., 2017. First Report of Grapevine Pinot gris virus Infecting Grapevine in Pakistan. *Plant Disease* 101: 1958–1958. https://doi.org/10.1094/PDIS-04-17-0476-PDN

Reynard J.-S., Schumacher S., Menzel W., Fuchs J., Bohnert P., … Fuchs R., 2016. First Report of Grapevine Pinot gris virus in German Vineyards. *Plant Disease* 100: 2545–2545. https://doi.org/10.1094/PDIS-07-16-0966-PDN

Ruiz-García A.B., Olmos A., 2017. First Report of Grapevine Pinot gris virus in Grapevine in Spain. *Plant Disease* 101: 1070. https://doi.org/10.1094/PDIS-12-16-1858-PDN

Saldarelli P., Giampetruzzi A., Morelli M., Malossini U., Pirolo C., … Gualandri V., 2015. Genetic Variability of Grapevine Pinot gris virus and Its Association with Grapevine Leaf Mottling and Deformation. *Phytopathology* 105: 555–563. https://doi.org/10.1094/PHYTO-09-14-0241-R

Shvets D., Vinogradova S., 2022. Occurrence and Genetic Characterization of Grapevine Pinot Gris Virus in Russia. *Plants* 11: 1061. https://doi.org/10.3390/plants11081061.

Silva G., Lecourt J., Clover G.R.G., Seal S.E., 2018. First record of *Grapevine Pinot gris virus* infecting *Vitis vinifera* in the United Kingdom. *New Disease Reports* 38: 7. https://doi.org/10.5197/j.2044-0588.2018.038.007

Tamura K., Stecher G., Peterson D., Filipski A., Kumar S., 2013. MEGA6: Molecular Evolutionary Genetics Analysis Version 6.0. *Molecular Biology and Evolution* 30: 2725–2729. https://doi.org/10.1093/molbev/mst197

Tarquini G., Ermacora P., Bianchi G.L., De Amicis F., Pagliari L., … Musetti R., 2018. Localization and subcellular association of Grapevine Pinot Gris Virus in grapevine leaf tissues. *Protoplasma* 255: 923–935. https://doi.org/10.1007/s00709-017-1198-5

Tarquini G., De Amicis F., Martini M., Ermacora P., Loi N., … Firrao G., 2019a. Analysis of new grapevine Pinot gris virus (GPGV) isolates from Northeast Italy provides clues to track the evolution of a newly emerging clade. *Archives of Virology* 164: 1655–1660. https://doi.org/10.1007/s00705-019-04241-w

Tarquini G., Zaina G., Ermacora P., Amicis F.D., Franco-Orozco B., … Musetti R., 2019b. Agroinoculation of Grapevine Pinot Gris Virus in tobacco and grapevine provides insights on viral pathogenesis. *PLOS ONE* 14: e0214010. https://doi.org/10.1371/journal.pone.0214010

Tarquini G., Ermacora P., Firrao G., 2021a. Polymorphisms at the 3'end of the movement protein (MP)

gene of grapevine Pinot gris virus (GPGV) affect virus titre and small interfering RNA accumulation in GLMD disease. *Virus Research* 302: 198482. https://doi.org/10.1016/j.virusres.2021.198482

Tarquini G., Pagliari L., Ermacora P., Musetti R., Firrao G., 2021b. Trigger and Suppression of Antiviral Defenses by Grapevine Pinot Gris Virus (GPGV): Novel Insights into Virus-Host Interaction. *Molecular Plant-Microbe Interactions* 34: 1010–1023. https://doi.org/10.1094/MPMI-04-21-0078-R

Tarquini G., Ermacora P., Martini M., Firrao G., 2023. The Conundrum of the Connection of Grapevine Pinot Gris Virus with the Grapevine Leaf Mottling and Deformation Syndrome. *Plant Pathology* 72: 209–217. https://doi.org/10.1111/ppa.13667

Tokhmechi K., Koolivand D., 2020. First report of grapevine Pinot gris virus infecting grapevine in Iran. *Journal of Plant Pathology* 102: 549–549. https://doi.org/10.1007/s42161-019-00437-w

Waterhouse A.M., Procter J.B., Martin D.M.A., Clamp M., Barton G.J., 2009. Jalview Version 2—a multiple sequence alignment editor and analysis workbench. *Bioinformatics* 25: 1189–1191. https://doi.org/10.1093/bioinformatics/btp033

Wu Q., Habili N., 2017. The recent importation of Grapevine Pinot gris virus into Australia. *Virus Genes* 53: 935–938. https://doi.org/10.1007/s11262-017-1475-6.

Xiao H., Shabanian M., McFadden-Smith W., Meng B., 2016. First Report of Grapevine Pinot gris virus in Commercial Grapes in Canada. *Plant Disease* 100: 1030–1030. https://doi.org/10.1094/PDIS-12-15-1405-PDN

Xu Q., Wen X., Deng X., 2004. A simple protocol for isolating genomic DNA from chestnut rose (Rosa roxburghii tratt) for RFLP and PCR analyses. *Plant Molecular Biology Reporter* 22: 301–302. https://doi.org/10.1007/BF02773140

Zamorano A., Medina G., Fernández C., Cui W., Quiroga N., Fiore N., 2019. First Report of Grapevine Pinot gris virus in Grapevine in Chile. *Plant Disease* 103: 1438. https://doi.org/10.1094/PDIS-10-18-1855-PDN

Phytopathologia Mediterranea
The international journal of the
Mediterranean Phytopathological Union

Firenze University Press
www.fupress.com/pm

Research Papers

Enhancing epidemiological knowledge of *Botryosphaeriaceae* in Mexican vineyards

Edelweiss A. RANGEL-MONTOYA[1,2], Ofelia CANDOLFI-ARBALLO[3], José Abraham OBRADOR-SÁNCHEZ[4], Cesar VALENZUELA-SOLANO[5], Rufina HERNANDEZ-MARTINEZ[1,*]

[1] *Departamento de Microbiología, Centro de Investigación Científica y de Educación Superior de Ensenada (CICESE), Ensenada, Baja California, 22860, Mexico*
[2] *Facultad de Ciencias Químicas e Ingeniería campus Tijuana, Universidad Autónoma de Baja California. Tijuana, Baja California, 22390. Mexico*
[3] *Departamento de parasitología, Universidad Autónoma Agraria Antonio Narro Unidad Laguna (UAAAN-UL), Torreón, Coahuila, 27059, México*
[4] *Facultad de Ciencias de la Salud campus Valle Dorado. Universidad Autónoma de Baja California. Valle Dorado, 22890, Mexico*
[5] *Instituto Nacional de Investigaciones Forestales, Agrícolas y Pecuarias (INIFAP). Campo Experimental Costa de Ensenada, Ensenada, Baja California, 22880, Mexico*
*Corresponding author. E-mail: ruhernan@cicese.mx

Summary. Grapevine cultivation in Mexico is important, especially in the states of Baja California and Coahuila, which are the main wine production regions in the country. Grapevine trunk diseases (GTDs) impact productivity and cause substantial economic losses, with Botryosphaeria dieback being one of the most destructive. This disease is caused by fungi in the *Botryosphaeriaceae*, including species of *Botryosphaeria*, *Diplodia*, *Lasiodiplodia*, and *Neofusicoccum*. To date, *Lasiodiplodia* spp. are the primary *Botryosphaeriaceae* fungi reported in Mexico. The present study aimed to enhance the epidemiological knowledge of *Botryosphaeriaceae* in Mexican vineyards. Samples from grapevine plants exhibiting disease symptoms were collected from the states of Baja California and Coahuila. Of a total of 37 *Botryosphaeriaceae* isolates, six species were identified: *Neofusicoccum parvum*, *N. australe*, *N. vitifusiforme*, *Botryosphaeria dothidea*, *Diplodia corticola*, and *D. seriata*. *Neofusicoccum parvum* isolates were the most virulent, but were less virulent than previously reported *Lasiodiplodia* spp. The optimum growth temperatures for *N. parvum* and *B. dothidea* were from 28 to 30°C, but 25°C for *D. seriata, N. vitifusiforme, and N. australe* isolates. Only *D. seriata* isolates recovered growth when transferred to room temperature after exposure to 37°C or 40°C. This report is the first identification of *B. dothidea* and *N. parvum* as causative agents of Botryosphaeria dieback in the vine-growing regions of Mexico.

Keywords. Trunk disease fungi, Botryosphaeria canker, fungi.

OPEN ACCESS

Citation: Rangel-Montoya, E.A., Candolfi-Arballo, O., Obrador-Sánchez, J.A., Valenzuela-Solano, C., & Hernandez-Martinez, R. (2024). Enhancing epidemiological knowledge of *Botryosphaeriaceae* in Mexican vineyards. *Phytopathologia Mediterranea* 63(2): 191-206. doi: 10.36253/phyto-15292

Accepted: June 3, 2024

Published: July 17, 2024

Data Availability Statement: All relevant data are within the paper and its Supporting Information files.

Competing Interests: The Author(s) declare(s) no conflict of interest.

Editor: José R. Úrbez Torres, Agriculture and Agri-Food Canada, Summerland, British Columbia, Canada.

ORCID:
EAR-M: 0000-0002-2362-9229
OC-A: 0000-0001-8687-2915
JAO-S: 0000-0002-6531-2019
CV-S: 0000-0003-3030-6038
RH-M: 0000-0002-0914-3732

INTRODUCTION

In Mexico, the grapevine cultivation sector is economically important. In 2022, total grape production exceeded 450,000 tons, with Sonora, Zacatecas,

Baja California, Aguascalientes, and Coahuila being the foremost producers (SIAP, 2023). Despite regulations governing importation of grapevine planting materials, Mexico still relies on these imports, posing ongoing threats of introducing pathogens from foreign sources. Many factors may be involved in the emergence of these diseases, so that grapevine trunk diseases (GTDs) have emerged as an international problem with implications for productivity and significant economic losses (van Niekerk *et al*., 2006; Fontaine *et al*., 2016; Gramaje *et al*., 2018; Hrycan *et al*., 2020). Botryosphaeria dieback is one of the most destructive GTDs. This is a degenerative disease caused by fungi within the *Botryosphaeriaceae*. Botryosphaeria dieback has been linked to over 30 species in the genera *Botryosphaeria, Diplodia, Dothiorella, Lasiodiplodia, Neoscytalidium, Neofusicoccum, Phaeobotryosphaeria*, and *Spencermartinsia*. This extensive species range highlights the complexity of this disease, as has been documented in several studies (Úrbez-Torres, 2011; Rolshausen *et al*., 2013; Stempien *et al*., 2017; Gramaje *et al*., 2018).

Botryosphaeriaceae fungi cause necrotic lesions in grapevine vascular tissues, including xylem and phloem occlusions, as well as stunted growth, wedge-shaped cankers in woody trunks, dieback, and over time, plant death (Gramaje and Armengol, 2011; Úrbez-Torres, 2011; Bertsch *et al*., 2013; Hrycan *et al*., 2020). The primary source of inoculum for these pathogens is conidia, which are released and dispersed under conditions of high humidity, rainfall, and wind. Conidia enter plants through pruning wounds (Agustí-Brisach and Armengol, 2013; Gramaje *et al*., 2018; Waite *et al*., 2018). *Botryosphaeriaceae* spp. can exist as endophytes within asymptomatic plant tissues for extended periods, functioning as latent pathogens (Slippers and Wingfield, 2007). This characteristic is important, as infected plants can go undetected in nurseries or vineyards (Hrycan *et al*., 2020). The transition of *Botryosphaeriaceae* species from endophytic to pathogenic has been associated with environmental stress, particularly when host plant undergoes water or heat stresses (Slippers *et al*., 2007; Czemmel *et al*., 2015; Rathnayaka *et al*., 2023). Botryosphaeria dieback was previously primarily associated with older vineyards (Gubler *et al*., 2005), but this disease has also been found in young grapevines (Gramaje and Armengol, 2011; Bertsch *et al*., 2013). In the context of climate change, grapevines are likely to be subjected to consistent heat and water stresses, making them susceptible to trunk diseases (GTDs) (Fontaine *et al*., 2016; Mehl *et al*., 2017). Inadequate cultural practices, such as insufficient protection of pruning wounds and inadequate sanitary care of propagation material, can contribute to GTD proliferation (Graniti *et al*., 2000; Fontaine *et al*., 2016).

GTDs were first reported in Mexico in the late 1970s, when fungi linked to Eutypa dieback were identified in aged and neglected vineyards located in Coahuila, Durango and Aguascalientes (Téliz and Valle, 1979). Subsequently, Úrbez-Torres *et al*. (2008) identified the presence of *L. theobromae* and *D. seriata* associated with Botryosphaeria dieback in Baja California and Sonora. Following this, Candolfi-Arballo *et al*. (2010), found four *Botryosphaeriaceae* spp., *D. seriata*, *D. corticola*, *N. vitifusiforme*, and *N. australe*, in vineyards of Baja California. Later, Paolinelli-Alfonso *et al*. (2015) reported *Eutypella microtheca* associated with Eutypa dieback in Baja California. Most recently, Rangel Montoya *et al*. (2021) described species of *Lasiodiplodia* such as *L. crassispora*, *L. brasiliensis*, *L. exigua*, and *L. gilanensis* associated with Botryosphaeria dieback in Baja California and Sonora.

The status of GTDs is understudied in Mexico, so the present study aimed to broaden understanding of the fungi associated with Botryosphaeria canker present in Mexican vineyards, and compare their pathogenicity in grapevines.

MATERIALS AND METHODS

Isolation and morphological characterization of fungi

Samples of grapevine exhibiting Botryosphaeria dieback symptoms were collected from seventeen vineyards in the primary grape-producing regions of Baja California, and three vineyards from Coahuila. Trained personnel from the plant pathology laboratory of CICESE collected samples of wood pieces exhibiting wedge-shaped cankers. Approximately 100 samples were obtained and processed as follows. Small pieces of tissue were obtained, immersed in 95% ethanol, then quickly flamed, and placed onto potato dextrose agar (PDA, Difco Laboratories) supplemented with 25 $mg{\cdot}mL^{-1}$ chloramphenicol to prevent growth of bacteria. The PDA plates were incubated at 30°C until fungal growth was observed. Fungal colonies that showed fast growth with abundant aerial mycelium were sub-cultured onto PDA plates to obtain pure cultures, and these were preserved at -4°C in 20% glycerol.

Pure cultures were grown on PDA incubated at 30°C for 7 d to determine morphological characteristics of isolates, including their pigmentation and aerial mycelium. Pycnidium production was induced using liquid Minimal Medium 9 (MM9) (10.0 $g{\cdot}L^{-1}$ glucose (FagaLab), 1.0 $g{\cdot}L^{-1}$ NH_4Cl (Sigma), 0.5 $g{\cdot}L^{-1}$ NaCl (Fermont), 3.0 $g{\cdot}L^{-1}$ K_2HPO_4 (Jalmek), and 3.0 $g{\cdot}L^{-1}$ KH_2PO_4 (JT Baker), supplemented with sterile pine needles (5% w/v). Flasks containing medium were incubated for 15 d at room tem-

perature under a near ultraviolet electromagnetic radiation lamp, using 12 h in of light irradiation and 12h of darkness. Formed pycnidia were collected and suspended in 0.5% Tween 20 to obtain conidiospores, which were then observed under a light microscope (AxioVert200 Zeiss). Images of the conidia were captured with a Zeiss AxioCam HRc camera and analyzed using AxioVision 4.8.2. software, and the dimensions (length and width) of 30 conidia per isolate were measured. Statistical analyses of these data were performed using STATISTICA 8.0 to compare conidium spore sizes across species.

DNA extraction and PCR amplification of selected isolates

All *Botryosphaeriaceae* isolates were grown in potato dextrose broth (PDB, Difco Laboratories) at 30°C for 3 d, and the resulting mycelium was recovered by filtration. Total genomic DNA was extracted using the CTAB protocol (Wagner *et al*., 1987). To characterize *Botryosphaeriaceae* spp., the primers ITS1 and ITS4 were used to amplify the ITS region of the nuclear ribosomal DNA, including the 5.8S gene (White *et al*., 1990). In addition, EF1-728F and EF1-986R were used to amplify part of the translation elongation factor-1a (*tef*-1a) gene (Carbone and Kohn, 1999). These methods were carried out following the recommendations on TrunkDiseaseID.org (Lawrence *et al*., 2017), accessible at http://www.grapeipm.org/d.live/.

Each PCR reaction consisted of the following components: 2.5 µL of 10× PCR buffer with 15 mM $MgCl_2$, 0.5 µL of 20 mM dNTPs, 0.625 µL of 10 µM of each primer, 0.125 µL of Taq DNA polymerase (GoTaq® DNA polymerase, Promega) at 5 units·µL^{-1}, and 1 µL of template DNA at 30 ng·µL^{-1}, adjusted with purified water to reach a final volume of 25 µL. Amplification reactions were carried out in a Bio-Rad T-100 thermal cycler under the following conditions: for tef-1α, an initial cycle of 95°C for 3 min, followed by 35 cycles each of 95°C for 30 s, 55°C for 30 s, and 72°C for 1 min; for the ITS region, an initial cycle of 94°C for 2 min was followed by 35 cycles each of 94°C for 1 min, 58°C for 1 min, and 72°C for 1.5 min. Both programs concluded with a final cycle of 72°C for 10 min. After visualizing the amplicons by gel electrophoresis, they were purified using the GeneJet PCR purification kit (Thermo Scientific). The purified products were subsequently sequenced by Eton Bioscience Inc.

Phylogenetic analysis of Botryosphaeriaceae

Before the phylogenetic analysis, the sequence quality was evaluated, and noise was removed using BioEdit v.7.0.5.3 (Hall 1999), and a BLASTn analysis was conducted. Sequences with the greatest similarity were retrieved from GenBank (Table 1) and aligned using ClustalW. For pairwise alignment, the parameters used were a gap opening of 10 and a gap extension of 0.1. For multiple alignment, the parameters used were a gap opening of 10, a gap extension of 0.2, a transition weight of 0.5, and a delay for divergent sequences set to 25% (Thompson *et al*., 1994). The alignment was manually adjusted where necessary. The alignments of ITS and tef-1α were imported into BioEdit v.7.0.5.3 to create the concatenated matrix.

Maximum Likelihood (ML) analysis and Maximum Parsimony (MP) analysis were performed using MEGA-X (Kumar *et al*., 2018) based on the concatenated sequence alignment. The best model of nucleotide substitution was selected according to the Akaike Information Criterion (AIC). For the ML analysis, the K2+G+I model was used (Kimura, 1980). Parameters for Maximum Likelihood were set to Bootstrap method using 1000 replicates. Initial tree(s) for the heuristic search were obtained automatically by applying the Maximum Parsimony method. Gaps were treated as missing data. The tree was visualized in MX: Tree Explorer. New sequences were deposited in the GenBank (https://www.ncbi.nlm.nih.gov/genbank/).

Determination of optimal growth temperatures for Botryosphaeriaceae *spp.*

Optimal growth temperatures were assessed by selecting at least two isolates of each identified species, where possible. The isolates were grown on PDA plates by inoculating each plate with a 3-mm diam. plug of a 2-d-old colony on the edge of the plate. The plates were incubated at 20, 25, 28, 30, 35, 37, or 40°C. Resulting colony radii were measured every 24 h for 4 d. The optimal growth temperature at which maximum mycelial growth rate (mm d^{-1}) was determined following the method of Rangel-Montoya *et al*. (2021). This determination was made using the formula: $GR = R_f - R_i/T_f - T_i$ (where GR = growth rate; R_i, = initial radius (mm); R_f, = final colony radius (mm); T_i, = initial time (day 1), and T_f, = final time where fungal growth was measured. For each temperature, three replicate plates of each isolate were included. Statistical analyses of data obtained were carried out using STATISTICA 8.0, to compare the growth rates of each isolate.

Pathogenicity tests of selected isolates

One-year-old grapevine plants of the 'Merlot' cultivar were used to evaluate the pathogenicity of dif-

Table 1. List of GenBank and culture accession numbers of *Botryosphaeriaceae* spp. used for phylogenetic analyses in the present study.

Species	Isolate	Host	Origin	GenBank accession number	
				ITS	*tef*1-
Botryosphaeria agaves	MFLUCC11-0125	*Agave* sp.	Thailand	JX646791	JX646856
B. agaves	MFLUCC10-0051	*Agave* sp.	Thailand	JX646790	JX646855
B. dothidea	CMW8000	*Prunus* sp.	Switzerland	AY236949	AY236898
B. dothidea	CBS 110302	*Vitis vinifera*	Portugal	AY259092	AY573218
B. dothidea	**MXRJM2**	***V. vinifera***	**Mexico**	**MZ312534**	**MZ397922**
B. dothidea	**MXRJM9A**	***V. vinifera***	**Mexico**	**MZ312535**	**MZ397923**
B. dothidea	**MXRJM19**	***V. vinifera***	**Mexico**	**MZ312536**	**MZ397924**
B. dothidea	**MXRJM22**	***V. vinifera***	**Mexico**	**MZ312537**	**MZ397925**
B. dothidea	**MXRJM23**	***V. vinifera***	**Mexico**	**MZ312538**	**MZ397926**
B. dothidea	**MXRJM25**	***V. vinifera***	**Mexico**	**MZ312539**	**MZ397927**
Diplodia corticola	CBS 112549	*Quercus suber*	Potugal	AY259100	AY573227
D. corticola	CBS 112547	*Quercus. ilex*	Spain	AY259110	DQ458872
D. corticola	**MXSASI12-3**	***V. vinifera***	**Mexico**	**PP150458**	**PP377623**
D. mutila	CBS 112553	*V. vinifera*	Portugal	AY259093	AY573219
D. mutila	CBS230.30	*Phoenix dactylifera*	USA	DQ458886	DQ458869
D. sapinea	CBS393.8	*Pinus nigra*	Netherlands	DQ458895	DQ458880
D. sapinea	CBS109725	*Pinus patula*	South Africa	DQ458896	DQ458881
D. seriata	CBS 112555	*V. vinifera*	Portugal	AY259094	AY573220
D. seriata	CBS119049	*Vitis* sp.	Italy	DQ458889	DQ458874
D. seriata	**MXRF05**	***V. vinifera***	**Mexico**	**MZ312540**	**MZ397928**
D. seriata	**MXRF07**	***V. vinifera***	**Mexico**	**MZ312541**	**MZ397929**
D. seriata	**MXBY06**	***V. vinifera***	**Mexico**	**MZ312542**	**MZ397930**
D. seriata	**MXSASI19**	***V. vinifera***	**Mexico**	**MZ312543**	**MZ397931**
D. seriata	**MXER1**	***V. vinifera***	**Mexico**	**MZ312544**	**MZ397932**
D. seriata	**MX16P2**	***V. vinifera***	**Mexico**	**MZ312545**	**MZ397933**
D. seriata	**MXSASI15-01**	***V. vinifera***	**Mexico**	**PP150447**	**PP320328**
D. seriata	**MXSB01**	***V. vinifera***	**Mexico**	**PP150450**	**PP343114**
D. seriata	**MXSASI01**	***V. vinifera***	**Mexico**	**PP150448**	**PP377618**
D. seriata	**MXSASI08-01**	***V. vinifera***	**Mexico**	**PP150474**	**PP343113**
D. seriata	**MXCCBM09-2**	***V. vinifera***	**Mexico**	**PP150451**	**PP377620**
D. seriata	**MXR02-3**	***V. vinifera***	**Mexico**	**PP150452**	**PP377621**
D. seriata	**MXCCBM08-1**	***V. vinifera***	**Mexico**	**PP150453**	**PP343115**
D. seriata	**MXSACH29-2**	***V. vinifera***	**Mexico**	**PP150457**	**PP343118**
D. seriata	**MXSACH16**	***V. vinifera***	**Mexico**	**PP150456**	**PP343117**
D. seriata	**MXCT01**	***V. vinifera***	**Mexico**	**PP150455**	**PP343116**
D. seriata	**MXCT10**	***V. vinifera***	**Mexico**	**PP150454**	**PP377622**
D. seriata	**MXSACH19-1**	***V. vinifera***	**Mexico**	**PP150449**	**PP377619**
D. scrobiculata	CMW 189	*Pinus resinosa*	USA	AY253292	AY624253
D. scrobiculata	CBS109944	*Pinus greggii*	Mexico	DQ458899	DQ458884
Lasiodiplodia theobromae	CBS 164.96	Fruit along coral reef	PNG	AY640255	AY640258
L. theobromae	CBS111530	Unknown	Unknown	EF622074	EF622054
Neofusicoccum australe	CMW6837	*Acacia* sp.	Australia	AY339262	AY339270
N. australe	CMW6853	*Sequoiadendron giganteum*	Australia	AY339263	AY339271
N. australe	**MXBT10**	***V. vinifera***	**Mexico**	**MZ312546**	**MZ397934**
N. australe	**MXBT12**	***V. vinifera***	**Mexico**	**MZ312547**	**MZ397935**
N. australe	**MX5P5**	***V. vinifera***	**Mexico**	**MZ312548**	**MZ397936**
N. eucalypticola	CMW6539	*Eucalyptus grandis*	Australia	AY615141	AY615133

(Continued)

Table 1. (Continued).

Species	Isolate	Host	Origin	GenBank accession number	
				ITS	*tef*1-
N. eucalypticola	CMW6217	*E. rossi*	Australia	AY615143	AY615135
N. luteum	CBS110299	*V. vinifera*	Portugal	AY259091	AY573217
N. luteum	CBS 110497	*V. vinifera*	Portugal	EU673311	EU673277
N. mediterraneum	PD312	*Eucalyptus* sp.	Greece	GU251176	GU251308
N. mediterraneum	CBS121558	*V. vinifera*	USA	GU799463	GU799462
N. parvum	CMW9081	*P. nigra*	New Zealand	AY236943	AY236888
N. parvum	CBS 110301	*V. vinifera*	Portugal	AY259098	AY573221
N. parvum	**MX14P4**	***V. vinifera***	**Mexico**	**MZ312549**	**MZ397937**
N. parvum	**MX24P4**	***V. vinifera***	**Mexico**	**MZ312550**	**MZ397938**
N. parvum	**MXRJM6**	***V. vinifera***	**Mexico**	**MZ312551**	**MZ397939**
N. parvum	**MXRJM15**	***V. vinifera***	**Mexico**	**MZ312552**	**MZ397940**
N. parvum	**MXRJM16**	***V. vinifera***	**Mexico**	**MZ312553**	**MZ397941**
N. parvum	**MXCHP08E**	***V. vinifera***	**Mexico**	**MZ312554**	**MZ397942**
N. viticlavatum	STE-U 5044	*V. vinifera*	South Africa	AY343381	AY343342
N. viticlavatum	STE-U 5041	*V. vinifera*	South Africa	AY343380	AY343341
N. vitifusiforme	STE-U 5252	*V. vinifera*	South Africa	AY343383	AY343343
N. vitifusiforme	STE-U 5050	*V. vinifera*	South Africa	AY343382	AY343344
N. vitifusiforme	**MXSACH23**	***V. vinifera***	**Mexico**	**MZ312555**	**MZ397943**
N. vitifusiforme	**MXSACH24**	***V. vinifera***	**Mexico**	**MZ312556**	**MZ397944**
N. vitifusiforme	**MXCNA1**	***V. vinifera***	**Mexico**	**MZ312557**	**MZ397945**
Mycosphaerella pini	CMW14822	*Pinus ponderosa*	USA	AY808300	AY808265

Isolates from the present study are highlighted in bold text.

ferent *Botryosphaeriaceae* isolates in green and woody host tissues. Green shoots were each inoculated by inserting a mycelial plug of the respective fungal isolate into a 2 mm diameter wound created with a drill. The plants were then kept in a greenhouse for 15 d, The woody tissue was inoculated in a similar manner, but the plants were left in a greenhouse for 2 months. Two isolates previously reported as strains of *Lasiodiplodia*, namely *L. brasiliensis* MXBCL28 and *L. gilanensis* MXCS01 (Rangel-Montoya *et al*., 2021), were used for comparisons. Each selected isolate was inoculated into five plants for the green and woody tissue assessments, while sterile PDA plugs were used for experimental inoculation control plants. All wounds were covered with Parafilm® to prevent desiccation. Samples were collected after the respective times to measure lengths of the resulting necrotic lesions caused by the *Botryosphaeriaceae* isolates. To determine fulfillment of Koch's postulates, tissues from all inoculated plants was retrieved, flamed, inoculated onto PDA, and incubated at 30°C. The experiments with the plants were carried out twice. The virulence of each fungus was compared through statistical analyses carried out using STATISTICA 8.0.

RESULTS

Molecular and morphological characterization of Botryosphaeriaceae *isolates*

From plants displaying wedge-shaped cankers and necrotic lesions in the vascular tissues, a total of 37 fungal isolates of similar phenotype to *Botryosphaeriaceae* spp. were obtained. Out of these, 31 isolates were collected from Baja California, and six were from Coahuila. The isolate colonies were whitish to gray or olivaceous, with moderate aerial mycelium. Some of the isolates exhibited yellow pigmentation at the colony centre within the first 24 h of incubation, a characteristic associated with particular *Neofusicoccum* species (Phillips *et al*., 2013). Based on their morphological characteristics, these isolates belonged to the genera *Botryosphaeria*, *Diplodia*, or *Neofusicoccum*. Seven strains of *Lasiodiplodia* were found in Baja California, but none in Coahuila. These *Lasiodiplodia* spp. were reported separately (Rangel-Montoya et al., 2021).

Statistically significant differences in conidium size were observed among the analyzed species (Table 2 and Figure 1). Isolates identified as *Botryosphaeria dothidea*

had narrow hyaline conidia with fusiform bases and granular contents. Some of these conidia had a single septum and were larger compared to conidia of other *Botryosphaeriaceae* species, with average size of 26.6 × 5.0 µm. Isolates of *D. seriata* had dark brown, aseptate and septate, ovoid and wide conidia, averaging 23.3 × 10.05 µm. Some isolates had smaller conidia 17.2 ± 2.8 × 9.3 ±1.1 µm. The *D. corticola* isolate had oblong to cylindrical hyaline and aseptate conidia with granular contents and thick walls, as well as brown and septate conidia. The conidia were of average size 25.3 × 14.1 µm. There were no discernible differences in sizes compared to *D. seriata*, although Phillips *et al*. (2013) suggested that *D. corticola* generally had larger conidia than other *Diplodia* species. Isolates of *N. australe* had hyaline conidia with fusiform bases and granular contents, which lacked septa, and had average size of 19.4 × 5.7 µm. Isolates identified as *N. parvum* had ellipsoidal conidia with flat apices and bases, most of which were hyaline, with an average size of 21.3 × 5.2 µm. Some older conidia of *N. parvum* were light brown and had 1 to 2 septa, with the middle cells being darker coloured. *Neofusicoccum vitifusiforme* isolates had hyaline, ellipsoid conidia with wide apices and subtruncate bases, with average size of 20.7 × 5.5 µm.

Sequences obtained from the ITS regions and *tef*1-α loci were, respectively, approx. 550 and 300 bp. The concatenated dataset comprised 924 characters, including gaps after alignment (578 corresponding to ITS gene and 346 corresponding to *tef*1-α gene), and 68 taxa. *Mycosphaerella pini* (CMW14822) was used as the outgroup taxon. The maximum likelihood analysis using Kimura 2-parameter model resulted in a tree with a log likelihood value of -2038.86, and estimated base frequencies were as follows: A = 0.20968, T = 0.23324, C = 0.29582, and G = 0.26139. A discrete Gamma distribution was used to model evolutionary rate differences among sites [five categories (+G, parameter = 0.4676)]. The rate variation model allowed for some sites to be evolutionarily invariable ([+I], 32.28% of sites). The maximum parsimony analysis yielded one most parsimonious tree of length = 269, CI = 0.691943, RI = 0.946765, and RC = 0.655107 for parsimony-informative sites.

Based on the phylogenetic analysis, the Mexican isolates were categorized into six species (Figure 2). Eighteen isolates belonged to *D. seriata*, six belonged to *B. dothidea*, six belonged to *N. parvum*, three to *N. australe*, three were *N. vitifusiforme*, and one isolate belonged to *D. corticola*. *Botryosphaeria dothidea* and

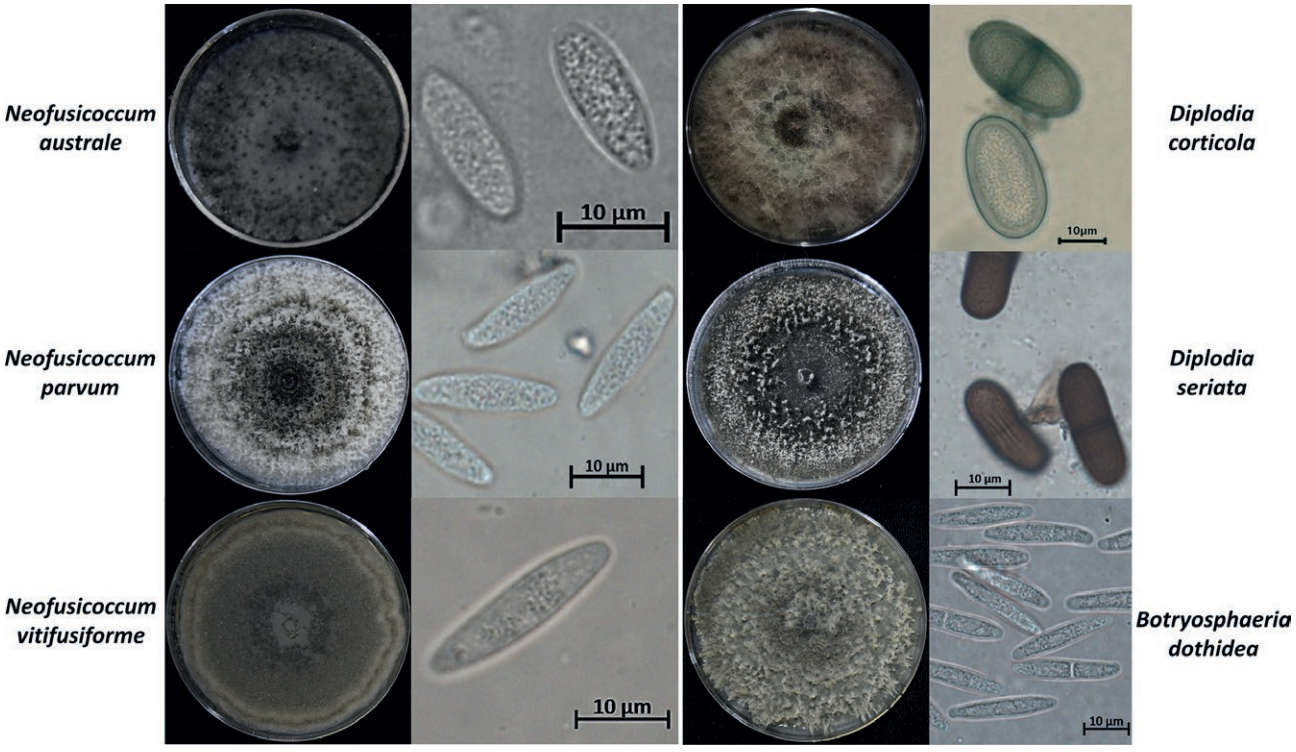

Figure 1. Macroscopic and microscopic characteristics of *Botryosphaeriaceae* spp. isolated from grapevine tissues and grown on PDA at 30°C for 7 d. *Neofusicoccum australe* MX5P5, *Neofusicoccum parvum* MX14P4, *Neofusicoccum vitifusiforme* MXSACH24, *Diplodia corticola* MXSASI12-3, *Diplodia seriata* MXBY06, and *Botryosphaeria dothidea* MXRJM25. Left panel, colony, right panel, conidia.

Table 2. Conidium dimensions of the isolated *Botryosphaeriaceae* spp. from this study.

Isolate	Origin	Conidium size (µm)*	Mean ± SD**
Neofusicoccum australe[a]			
MXBT10	Baja California	(17.8-)18.7-20.1 × (5.7-)6.3-7.2	18.9±1.3 × 5.6 ±1.6
MXBT12	Baja California	(17.9-)18.5-20.3 × (6.8-)6.4-7.5	18.6±1.2 × 6.7±0.6
MX5P5	Coahuila	(17.1-)21.1-24.0 × (4.3-)5.0-6.4	20.9±1.9 × 5.0±0.5
Neofusicoccum parvum[b]			
MX14P4	Coahuila	(19.5-)20.3-24.0 × (4.5-)5.1-5.5	21.9±1.3 × 5.0±0.2
MX24P4	Coahuila	(19.0-)21.9-23.9 × (4.9-)5.2-6.3	21.4±1.4 × 5.5±0.4
MXRJM6	Baja California	(17.9-)21.7-23.8 × (4.4-)5.3-5.8	21.8±1.3 × 5.0±0.4
MXRJM15	Baja California	(18.5-)20.3-22.9 × (4.8-)5.3-5.8	21.0±1.3 × 5.3±0.2
MXRJM16	Baja California	(16.9-)19.6-23.6 × (4.4-)5.8-7.1	20.3±1.9 × 5.6±0.8
MXCHP08E	Coahuila	(18.1-)21.1-24.4 × (4.4-)5.1-6.2	21.7±1.6 × 5.2±0.5
Neofusicoccum vitifusiforme[a]			
MXSACH23	Baja California	(19.4-)21.2-23.9 × (5.2-)5.9-6.8	21.5±1.2 × 5.8±0.5
MXSACH24	Baja California	(16.7-)20.5-23.0 × (5.1-)5.3-6.5	21.0±1.5 × 5.6±0.4
MXCNA1	Coahuila	(16.8-)19.2-23.6 × (4.7-)5.1-5.8	19.7±1.4 × 5.3±0.3
Diplodia seriata[c]			
MXRF05	Baja California	(21.0-)23.9-27.5 × (8.4-)9.6-10.0	23.6±1.4 × 9.5±0.6
MXRF07	Baja California	(21.3-)23.4-25.7 × (8.6-)10.3-10.9	23.4±1.1 × 10.0±0.5
MXER1	Baja California	(20.1-)22.9-28.9 × (8.0-)8.9-11.2	24.1±2.0 × 9.2±0.8
MXBY06	Baja California	(21.9-)24.9-27.2 × (9.3-)11.7-13.4	24.7±1.2 × 11.8±1.0
MXSASI19	Baja California	(19.0-)20.0-22.8 × (8.0-)9.3-11.2	20.3±1.1 × 9.7±0.9
MXSASI15-01	Baja California	(14.0-)27.0-33.0 × (0.5-)10.0-13.0	26.4±3.0 × 9.0±1.5
MXSB01	Baja California	(16.0-)22.0-24.0 × (7.0-)8.0-10.0	20.6±2.2 × 8.2±0.8
MXSASI01	Baja California	(21.0-)27.5-32.0 × (8.0-)10.0-13.5	27.0±2.0 × 9.9±1.0
MXSASI08-01	Baja California	(20.9-)27.7-32.0 × (8.9-)9.0-16.0	26.5±2.3 × 11.4±1.6
MXCCBM09-2	Baja California	(10.8-)22.6-27.0 × (7.9-)10.0-13.0	21.1±2.1 × 9.7±0.8
MXR02-3	Baja California	(13.1-)23.0-27.6 × (5.3-)8.5-12.0	22.1±2.8 × 8.3±1.2
MXCCBM08-1	Baja California	(18.4-)22.8-32.0 × (8.7-)11.0-13.0	22.8±2.3 × 10.7±0.7
MXSACH29-2	Baja California	(16.6-)21.2-27.6 × (8.0-)9.4-20.0	21.4±2.6 × 10.9±2.9
MXSACH16	Baja California	(24.0-)27.8-34.0 × (9.0-)9.0-17.0	28.2±1.8 × 12.0±1.5
MXCT01	Baja California	(20.0-)22.3-26.0 × (7.9)8.0-11.0	22.2±1.3 × 8.8±0.8
MXCT10	Baja California	(19.0-)23.7-29.0 × (8.0-)10.0-15.0	23.6±2.0 × 10.9±1.3
MXSACH19-1	Baja California	(11.0-)16.0-25.0 × (7.0)10.0-14.5	17.2±2.8 × 9.3±1.1
MX16P2	Coahuila	(20.5-)23.2-28.6 × (8.2-)9.8-12.1	23.7±2.2 × 10.1±0.9
D. corticola[c]			
MXSASI12-3	Baja California	(24.0-)17.5-37.0 × (11.0-)14.0-17.5	25.3±3.9 × 14.1±1.3
Botryosphaeria dothidea[d]			
MXRJM2	Baja California	(24.0-)26.3-31.2 × (4.2-)5.6-6.4	26.3±1.9 × 5.5±0.5
MXRJM9A	Baja California	(24.7-)26.1-31.1 × (4.1-)5.3-6.0	26.8±1.6 × 5.0±0.5
MXRJM19	Baja California	(23.5-)26.1-32.4 × (4.1-)4.8-5.5	27.0±2.1 × 4.7±0.3
MXRJM22	Baja California	(24.3-)28.1-30.0 × (4.1-)5.1-6.1	26.9±1.6 × 5.1±0.5
MXRJM23	Baja California	(24.1-)24.6-27.4 × (4.1-)4.8-5.4	25.7±1.1 × 4.6±0.4
MXRJM25	Baja California	(24.2-)27.8-31.9 × (4.3-)5.5-6.1	27.1±1.5 × 5.3±0.4

* Minimum size, most repetitive value and maximum size for length and width of 30 selected conidia.
** SD = standard deviation.
[a,b,c,d] Indicate differences between fungi in conidium size. Species accompanied by the same letters are not significantly different ($\alpha < 0.05$).

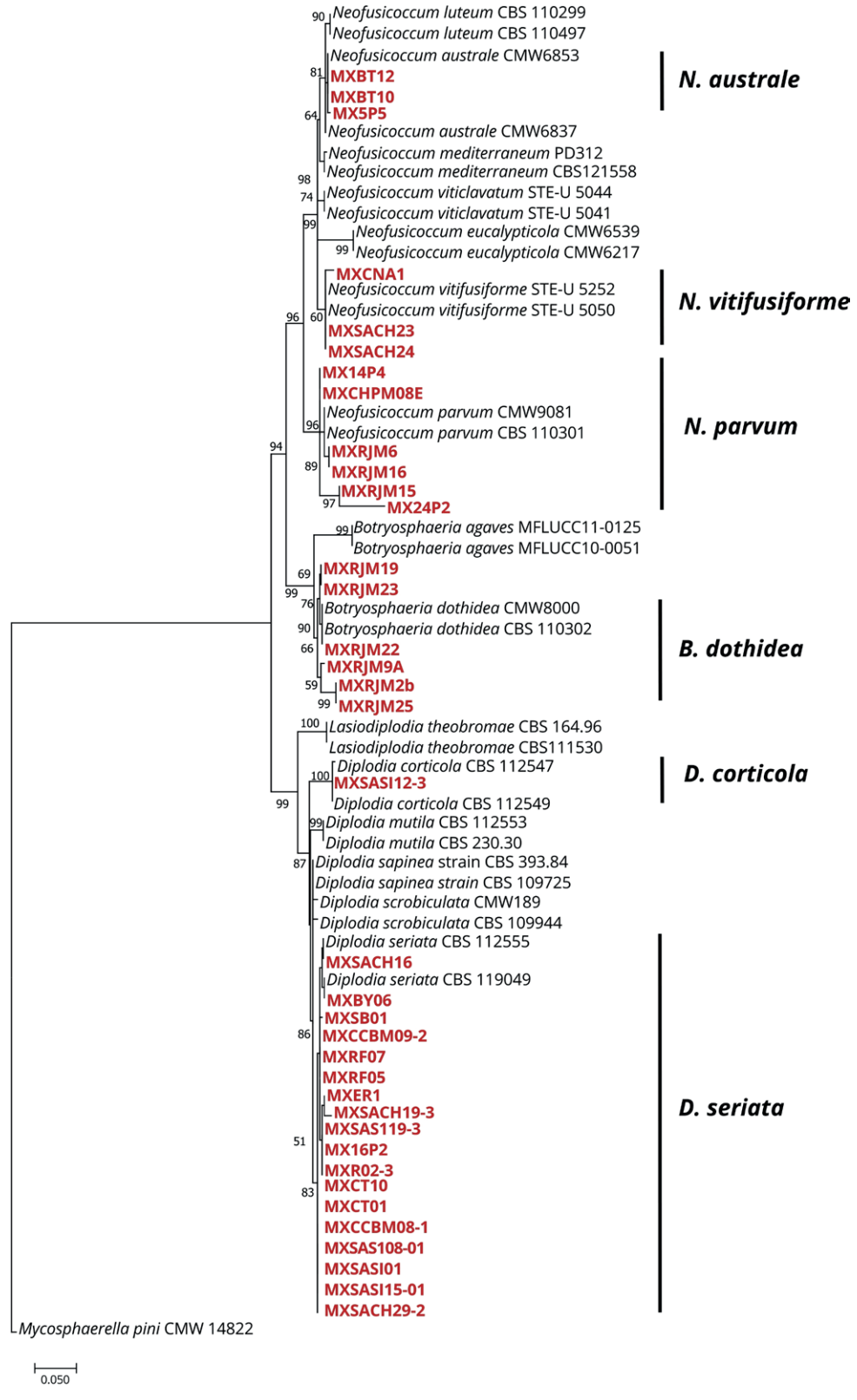

Figure 2. Phylogenetic analyses of *Botryosphaeriaceae* species. Maximum likelihood tree with the greatest log likelihood (-2038.86) obtained from the ITS and tef-1α concatenated dataset. The tree is rooted with *Mycosphaerella pini* (CMW 14822). The isolates from the present study are indicated in bold red font. Bootstrap values from 1000 replicates greater than 50 are indicated at the nodes.

D. corticola were only isolated from samples from Baja California, while *N. australe, N. vitifusiforme, N. parvum* and *D. seriata*, were isolated from samples from Baja California and Coahuila.

Optimum growth temperatures of selected Botryosphaeriaceae *spp.*

Among the selected isolates, *N. parvum* MXRJM6, *N. parvum* MXRJM16, and *B. dothidea* MXRJM22 had optimum growth temperatures within the range of 25 to 30°C (Table 3). Specifically, *N. parvum* MX14P4 grew optimally in the range of 28 to 30°C, while *B. dothidea* MXRJM25 showed optimum growth in the range of 28 to 35°C. *Diplodia seriata*, *D. corticola* and *N. australe* isolates had greatest growth rates at 25°C. *Neofusicoccum vitifusiforme* MXSACH23 had optimum growth at 30°C, while *N. vitifusiforme* MXSACH24 grew best at 25°C. *Botryosphaeria dothidea* RJ22MX had the greatest growth rate, reaching 16.4 ± 1.7 mm d^{-1} at 28°C. For *D. seriata*, isolates MXSASI101 and MXSASI15-01, obtained from Baja California vineyards, showed minimal growth at 37°C, while the remaining isolates did not grow at 37 or 40°C. Nevertheless, all the *D. seriata* isolates were capable of recovering growth when cultures exposed to 37 or 40°C for 4 d were transferred to room temperature.

Pathogenicity assays

In green tissues, plants that were inoculated with *N. parvum* MX14P4, MX24P4, MXRJM6, or MXRJM16, or *B. dothidea* MXRJM22, developed large necrotic lesions 15 d post inoculation (Figure 3A). *Diplodia corticola* did not produce lesions in green tissues (0.4 ± 0.1 cm), so this fungus was not included in the next experiment. The isolates of *B. dothidea*, *N. australe*, *N. vitifusiforme,* and *D. seriata* had mean necrotic lesion lengths that were not significantly different ($\alpha > 0.05$).

Table 3. Mean mycelium growth rates (mm d^{-1}) for Mexican *Botryosphaeriaceae* isolates at different temperatures.

Isolate	Temperature					
	25°C	28°C	30°C	35°C	37°C	40°C
N. parvum						
MX14P4	11.8 ± 0.3 e	12.2 ± 0.4 d	12.7 ± 1.6 cd	3.8 ± 0.2 j	NG*	NG
MX24P4	7.1 ± 1.5 h	10.0 ± 1.3 f	5.9 ± 0.6 i	2.6 ± 0.1 k	NG	NG
MXRJM6	15.8 ± 2.1 a	15.3 ± 2.3 a	15.1 ± 2.2 a	3.1 ± 0.1 k	NG	NG
MXRJM16	15.1 ± 1.5 ab	15.9 ± 0.8 a	15.4 ± 1.0 a	3.3 ± 0.01 jk	NG	NG
N. vitifusiforme						
MXSACH24	15.0 ± 2.5 ab	13.2 ± 3.7 c	13.3 ± 4.4 c	2.2 ± 1.1 kl	NG	NG
MXSACH23	9.3 ± 0.5 g	9.7 ± 0.5 fg	10.0 ± 0.01 f	2.8 ± 0.8 k	NG	NG
N. australe						
MXBT12	9.6 ± 1.8 fg	7.4 ± 1.2 h	4.6 ± 1.0 ij	2.8 ± 0.5 k	NG	NG
MXBT10	14.4 ± 0.3 ab	9.3 ± 0.2 g	4.3 ± 0.3 j	0.9 ± 0.2 l	NG	NG
D. seriata						
MXBY06	14.1 ± 0.6 b	12.8 ± 0.9 cd	11.4 ± 1.0 e	8.9 ± 0.7 g	NG	NG
MXRF05	12.8 ± 0.4 cd	7.1 ± 1.2 h	6.7 ± 0.7 h	3.8 ± 0.3 j	NG	NG
MXSASI101	13.9 ± 0.4 b	12.6 ± 1.2 cd	10.0 ± 0.9 f	5.2 ± 0.5 i	1.7±0.1 l	*NG*
MXSASI15-01	13.7 ± 0.3 b	13.2 ± 1.0 c	8.3 ± 1.4 gh	6.5 ± 1.1 hi	1.2±0.1 l	*NG*
MX16P2	13.6 ± 0.1 bc	13.0 ± 0.4 c	12.4 ± 0.8 d	9.0 ± 0.9 g	NG	NG
D. corticola						
MXSASI12-3	14.0 ± 0.4 b	9.0 ± 2.2 g	4.8 ± 0.8 ij	3.5 ± 0.3 j	NG	NG
B. dothidea						
MXRJM9A	5.5 ± 1.1 i	5.8 ±1.1 i	5.3 ± 1.1 i	5.0 ± 0.6 i	NG	NG
MXRJ22	15.3 ± 2.2 a	16.4 ± 1.7 a	15.6 ± 0.9 a	9.3 ± 0.5 g	NG	NG
MXRJM25	7.3 ± 0.3 h	7.9 ± 0.7 h	8.2 ± 1.5 gh	8.6 ± 0.2 g	NG	NG

NG = no mycelial growth. Means accompanied by the same letters indicate there are not statistically different ($\alpha < 0.05$) based on Fisher's analysis.

Figure 3. Examples of grapevine shoots cv. 'Merlot' inoculated with *Botryosphaeriaceae* spp., showing dark-brown lesions at A) 15 d post inoculation in green tissues, and B) 2-months post inoculation in woody tissues.

In woody tissues, 2 months post inoculation, *N. parvum* isolates MX14P4, MX24P4, MXRJM6, and MXRJM16 were the most virulent (Figure 3B). These plants developed lesions longer than 4 cm, although virulence of these isolates was less than that of the *Lasiodiplodia* isolates used for comparison (Figure 4). *Botryosphaeria*

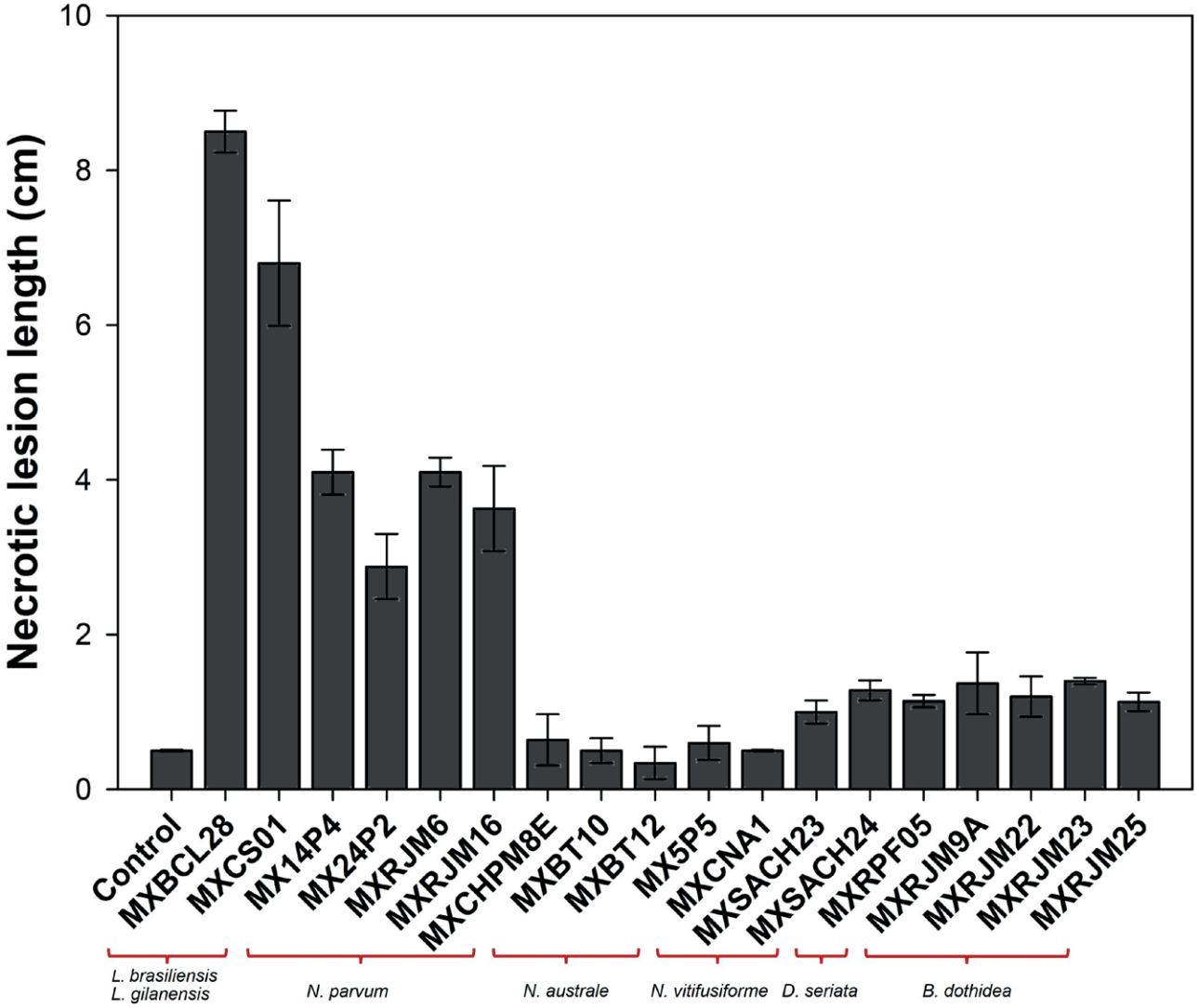

Figure 4. Mean lengths of lesions caused by different *Botryosphaeriaceae* isolates in grapevine plants 'Merlot' observed 2 months post inoculation in woody tissue. letters accompanying the means were assigned based on Fisher's analysis ($P < 0.05$). The bars accompanying each mean represent standard deviations, and means accompanied by the same letters are not significantly different ($\alpha < 0.05$).

dothidea, D. seriata, N. australe, and *N. vitifusiforme* caused lesions shorter than 2 cm. None of the control plants developed necrotic lesions. Koch's postulates were confirmed, as the inoculated fungi were re-isolated from the inoculated plants.

DISCUSSION

This study has identified six *Botryosphaeriaceae* species associated with Botryosphaeria dieback and isolated from vineyards in Baja California and Coahuila. The identified species include *N. parvum*, *B. dothidea*, *D. seriata, N. australe*, *N. vitifusiforme*, and *D. corticola*. Previously, *D. seriata*, *L. theobromae* (Úrbez-Torres *et al*., 2008), *D. corticola*, *N. australe*, *N. vitifusiforme* (Candolfi-Arballo *et al*., 2010), *L. gilaniensis, L. crassispora, L. brasiliensis*, and *L. exigua* (Rangel-Montoya *et al*., 2021) have been reported in Baja California and Sonora. Thus, the isolations *N. parvum* and *B. dothidea* reported in the present study are the first records of these two fungi in vineyards of Mexico.

While this study did not focus on the distribution or abundance of *Botryosphaeriaceae* fungi, among the identified species, *D. seriata* was the most common. This species has previously been documented in Mexico (Úrbez-

Torres *et al*., 2008; Candolfi-Arballo *et al*., 2010). It is a cosmopolitan and plurivorous fungus, broadly prevalent among *Botryosphaeriaceae* species and affecting grapevines in most countries where these plants are cultivated, and causing Botryosphaeria canker (Larignon *et al*., 2001; Úrbez-Torres, 2011). Strains reported from other countries exhibit varying conidium morphologies and dimensions, ranging from 21.5 – 28 × 11 – 15.5 µm, and never exceeding 30 µm in length. Initially hyaline, the conidia darken with time, typically remaining aseptate and ovoid, with smooth external walls that become roughened on the inner surfaces. However, some isolates may develop septa upon germination (Phillips *et al*., 2013). Among the 18 isolates examined, the majority had septate conidia, while for particular isolates (e.g. MXSACH19-1), conidia were smaller (average = 17.2 × 9.3 µm) than the average size. This indicates intraspecific variation, as has been previously highlighted (Elena *et al*., 2015).

Differences in conidium dimensions were observed among species, providing a basis for differentiation. For example, while the conidia of *N. parvum* and *B. dothidea* had similar characteristics, those of *B. dothidea* were longer and narrower; *N. vitifusiforme* (average = 20.7 × 5.5 µm) and *N. australe* (average = 19.4 × 5.7 µm) had similarly sized conidia, but *N. vitifusiforme* had fusoid to ellipsoid conidia widest in the upper thirds, with an obtuse apices and flattened, subtruncate bases. In contrast, the conidia of *N. australe* were non-septate and fusiform, with subtruncate to bluntly rounded bases (Phillips *et al*., 2013). *Diplodia corticola* isolates mainly had hyaline and aseptate conidia, which were oblong to cylindrical with both ends broadly rounded, and gradually became brown and septate with time. This species has the largest conidia of the genus *Diplodia* (average = 29.9 × 13.6 µm) (Phillips *et al*., 2013). However, differentiating among species solely based on their conidium morphology is challenging due to their striking similarities.

Botryosphaeriaceae fungi have cosmopolitan distributions (Úrbez-Torres, 2011), but particular genera within this family tend to prevail in specific climatic regions. For example, *Diplodia* spp. are often found in temperate regions (Burgess and Wingfield, 2002), while species of *Lasiodiplodia* are commonly found in tropical and subtropical regions (Mohali *et al*., 2005; Burgess *et al*., 2006). The optimum growth temperatures for *Neofusicoccum*, *Diplodia*, and *Botryosphaeria* spp. is typically within the range of 25 to 30°C (Phillips *et al*., 2013; Dardani *et al*., 2023). Results from the present study agree with those reports, although two isolates of *D. seriata* (MX16P2 from Coahuila and MXBY06 from Baja California) showed slight growth at 37°C. Furthermore, all the *D. seriata* isolates exposed to 37 or 40°C recovered their growth when cultures were transferred to room temperature. Similarly, Mexican *Lasiodiplodia* spp. did not grow at 40°C but resumed growth once returned to room temperature (Rangel-Montoya *et al*., 2021). Plasticity in temperature tolerance may be linked to broad international distribution of *D. seriata*. On the other hand, the climate of Valle de Guadalupe, where most of the isolates were obtained, is usually warm. Over the course of each year, the temperature varies from 4°C (at night) to 33°C, and is rarely less than 2°C or greater than 34°C (CONAGUA, 2023). This indicates that the Valle de Guadalupe favours occurrence and distribution of *D. seriata*.

Neofusicoccum parvum was initially reported in grapevines in 2002 as *Botryosphaeria parva* (Phillips, 2002). Since then, this fungus has emerged as one of the most frequently isolated species and among the most virulent pathogens affecting grapevines, alongside several species of *Lasiodiplodia* (Úrbez-Torres *et al*., 2006). The isolates of *N. parvum*, specifically MX14P4, MX24P4, MXRJM6, and MXRJM16, exhibited greater virulence in both green and woody tissues. However, previously reported *Lasiodiplodia* isolates from Baja California and Sonora displayed higher levels of virulence than those of *N. parvum* (Rangel-Montoya *et al*., 2021). In contrast, the isolate MXCHP08E, also *N. parvum*, demonstrated weak virulence. As previously indicated, isolates within the same species can vary in virulence (Billones-Baaijens *et al*., 2013; Rangel-Montoya *et al*., 2021). Further investigation is required to determine the reasons for these variations.

Neofusicoccum parvum strains obtained in this study had optimal growth temperatures of 28 to 30°C. This temperature range favours the virulence of *N. parvum*, as it the fungus causes greatest damage at temperatures between 25 and 30°C (Ploetz *et al*., 2009). The isolates of *N. parvum* from Baja California were obtained from a recently planted vineyard, while in older plants, the most isolated species were *D. seriata* and *Lasiodiplodia* spp. It is therefore likely that in regions with low rainfall and high temperatures such as Sonora and Baja California in Mexico, this fungus is not commonly found. Furthermore, conidium germination is also affected by high relative humidity (Amponsah *et al*., 2010), and the optimum conidium germination temperature for this fungus is 30°C (Úrbez-Torres *et al*., 2010b).

Neofusicoccum australe was originally described as *Botryosphaeria australis* and isolated from native Acacia species in Australia (Slippers *et al*., 2004). Presence of this fungus in grapevines was first confirmed in 2004 in South Africa, where it caused lesions in green shoots and mature canes of 'Periquita' plants (van Niekerk *et al*., 2004). In the present study, however, plants inocu-

lated with *N. australe* did not show damage; instead, tissue regeneration was observed at the sites of the mechanical wounds. These differences could be due to the different cultivars used in the tests, as cultivars can exhibit varying levels of susceptibility to this pathogen. Nevertheless, *N. australe* is generally considered a weak pathogen with narrow distribution (Úrbez-Torres *et al*., 2006; Pitt *et al*., 2010).

The isolates of *N. vitifusiforme* used in the present study caused lesions ranging from 0.5-1.2 cm in length, which were not significantly different from those on the control plants. *Neofusicoccum vitifusiforme* was first reported in grapevine in 2004 as a weak pathogen (van Niekerk *et al*., 2004). Initially, this fungus was believed be restricted to *Vitis* spp. (Phillips *et al*., 2013), until it was isolated in Italy from *Olea europaea*, where it was reported to be an aggressive pathogen (Lazzizera *et al*., 2008). Cross-inoculations followed by histological or transcriptomic analyses using isolates from grapevine and *O. europaea* would help to clarify reasons for this different behaviour.

Botryosphaeria dothidea was initially found as an endophyte in the bark of white cedar (Xiao *et al*., 2014). More recently, this fugus has gained recognition as a latent pathogen of widespread significance in woody plants. This is attributed to its ability to undergo a prolonged endophytic phases before causing decay symptoms in host plants (Marsberg *et al*., 2017). The pathogenicity of *B. dothidea* isolates evaluated in the present study resulted in lesions that were larger than experimental controls. The *B. dothidea* isolates MXRJM9A and MXRJM25 did not have differences in growth within the range of 25 to 35°C, while isolate MXRJM22 exhibited greatest growth at 25 to 30°C and also grew at 35°C. This pathogenicity and ability to grow at different temperatures indicates that *B. dothidea* poses potential challenges for vineyards in Mexico.

Diplodia corticola was first reported as associated with oak (*Quercus suber* L.) dieback in Portugal (Alves *et al*., 2004), establishing this fungus as one of the most important pathogens affecting these trees (Muñoz-Adalia and Colinas, 2021; Muñoz-Adalia *et al*., 2023). In grapevines, *D. corticola* has been isolated in Texas (Úrbez-Torres *et al*., 2009), California (Úrbez-Torres *et al*., 2010a), Spain (Pintos Varela *et al*., 2011), and Italy (Carlucci *et al*., 2015), where it has been assessed to be a moderately virulent pathogen. The isolate obtained from Baja California exhibited no virulence to grapevine and displayed optimal growth at 25°C. The isolate was obtained from an approx. 30-year-old plant growing in a temperate climate. This suggests that *D. corticola* may not be well adapted to the climate conditions of Baja California, but could potentially exist as an endophyte within that region.

The diversity, distribution, wide host range, and the several factors that favour conidium distribution (e.g. wind, rain, and insects), make *Botryosphaeriaceae* important plant pathogens (Slippers and Wingfield 2007; Mehl *et al*., 2017). Reports of the distribution and pathogenicity of *Botryosphaeriaceae* in different countries provide helpful information on the frequency and diversity of hosts of these fungi (Batista *et al*., 2021). The present study has broadened knowledge on the incidence of *Botryosphaeriaceae*, and provides a benchmark for future research on GTD epidemiology and disease management in Mexico.

ACKNOWLEDGMENTS

Edelweiss Airam Rangel-Montoya was supported for the postdoctoral program of El Consejo Nacional de Humanidades, Ciencias y Tecnologías (CONAHCYT-México). The authors thank the grape growers of Baja California and Coahuila for allowing sampling in their vineyards, and SADER-Baja California, La Junta Local de Sanidad Vegetal de Hermosillo, and CONAHCYT for their support for this research.

LITERATURED CITED

Agusti-Brisach C., Armengol J., 2013. Black-foot disease of grapevine: an update on taxonomy, epidemiology and management strategies. *Phytopathologia Mediterranea* 52: 245–261.

Alves A., Correia A., Luque J., Phillips A., 2004. *Botryosphaeria corticola*, sp. nov. on *Quercus* species, with notes and description of *Botryosphaeria stevensii* and its anamorph, *Diplodia mutila*. *Mycologia* 96: 598–613. https://doi.org/10.1080/15572536.2005.11832956.

Amponsah N.T., Jones E.E., Ridgway H.J., Jaspers M.V., 2010. Effects of solar radiation and relative humidity on germination of *Botryosphaeriaceae* species conidia. *New Zealand Plant Protection* 63: 28–32. https://doi.org/10.30843/nzpp.2010.63.6610

Batista E., Lopes A., Alves A., 2021., What do we know about *Botryosphaeriaceae*? An overview of a worldwide cured dataset. *Forests* 12: 313. https://doi.org/10.3390/f12030313

Bertsch C., Ramírez-Suero M., Magnin-Robert M., Larignon P., Chong J., … Fontaine F., 2013. Grapevine trunk diseases: complex and still poorly understood. *Plant Pathology* 62: 243–265. https://doi.org/10.1111/j.1365-3059.2012.02674.x

Billones-Baaijens R., Jones E.E., Ridgway H.J., Jaspers M.V., 2013. Virulence affected by assay parameters during grapevine pathogenicity studies with *Botryosphaeriaceae* nursery isolates. *Plant Pathology* 62: 1214–1225. https://doi.org/10.1111/ppa.12051

Burgess T., Wingfield M.J., 2002. Impact of fungal pathogens in natural forest ecosystems: a focus on eucalypts. In: *Microorganisms in plant conservation and biodiversity* (K. Sivasithamparama, K.W. Dixon, R.L. Barrett, ed.), Dordrecht: Springer Netherlands, 285–306.

Burgess T.I., Barber P.A., Mohali S., Pegg G., de Beer W., Wingfield M.J., 2006. Three new *Lasiodiplodia* spp. from the tropics, recognized based on DNA sequence comparisons and morphology. *Mycologia* 98: 423–435. https://doi.org/10.1080/15572536.2006.11832677

Candolfi-Arballo O., Valenzuela-Solano C., Gubler W.D., Hernández-Martínez R., 2010. *Botryosphaeriaceae* species associated with grapevine decline in Mexico. In: *7th International Workshop on Grapevine Trunk Diseases, Santa Cruz, Chile, 2010*. *Phytopathologia Mediterranea* 49: 103–133 (abstract).

Carbone I., Kohn L., 1999. A method for designing primer sets for speciation studies in filamentous Ascomycetes. *Mycologia* 91: 553–556. https://doi.org/10.1080/00275514.1999.12061051

Carlucci A., Cibelli F., Lops F., Raimondo M.L., 2015. Characterization of *Botryosphaeriaceae* species as causal agents of trunk diseases on grapevines. *Plant Disease* 99: 1678–1688. https://doi.org/10.1094/PDIS-03-15-0286-RE

CONAGUA Comisión Nacional del Agua (2023) Red de estaciones climatológicas, Ciudad de México México: Servicio Meteorológico Nacional. https://smn.conagua.gob.mx/

Czemmel S., Galarneau E.R., Travadon R., McElrone A.J., Cramer G.R., Baumgartner K., 2015. Genes expressed in grapevine leaves reveal latent wood infection by the fungal pathogen *Neofusicoccum parvum*. *PloS One* 10: e0121828. https://doi.org/10.1371/journal.pone.0121828

Dardani G., Mugnai L., Bussotti S., Gullino M.L., Guarnaccia V., 2023. Grapevine dieback caused by *Botryosphaeriaceae* species, *Paraconiothyrium brasiliense*, *Seimatosporium vitis-viniferae* and *Truncatella angustata* in Piedmont: characterization and pathogenicity. *Phytopathologia Mediterranea* 60: 283–306. https://doi.org/10.36253/phyto-14154

Elena G., Garcia-Figueres F., Reigada S., Luque J., 2015. Intraspecific variation in *Diplodia seriata* isolates occurring on grapevines in Spain. *Plant Pathology* 64: 680–689. https://doi.org/10.1111/ppa.12296

Fontaine F., Pinto C., Vallet J., Clément C., Gomes A.C., Spagnolo A., 2016. The effects of grapevine trunk diseases (GTDs) on vine physiology. *European Journal of Plant Pathology* 144: 707–721. https://doi.org/10.1007/s10658-015-0770-0

Gramaje D., Armengol J., 2011. Fungal trunk pathogens in the grapevine propagation process potencial inoculum sources, detection, identification, and management strategies. *Plant Disease* 95: 1040–1055. https://doi.org/10.1094/PDIS-01-11-0025

Gramaje D., Úrbez-Torres J.R., Sosnowski M.R., 2018. Managing grapevine trunk diseases with respect to etiology and epidemiology: current strategies and future prospects. *Plant Disease* 102: 12–39. https://doi.org/10.1094/PDIS-04-17-0512-FE

Graniti A., Mugnai L., Surico G. 2000. Esca of grapevine: a disease complex or a complex of diseases. *Phytopathologia Mediterranea* 39: 1000–1005. https://doi.org/10.14601/Phytopathol_Mediterr-1539

Gubler W.D., Rolshausen P.E., Trouillase F.P., Úrbez J.R., Voegel T., 2005. Grapevine trunk diseases in California. *Practical Winery & Vineyard* Jan/Feb: 6–25.

Hall T.A., 1999. BioEdit: a user-friendly biological sequence alignment editor and analysis program for Windows 95/98/NT. *Nucleic Acids Symposium series* 41: 95–98.

Hrycan J., Hart M., Bowen P., Forge T., Úrbez-Torres J.R., 2020. Grapevine trunk disease fungi: their roles as latent pathogens and stress factors that favour disease development and symptom expression. *Phytopathologia Mediterranea* 59: 395–424. https://doi.org/10.14601/Phyto-11275

Kimura M., 1980. A simple method for estimating evolutionary rates of base substitutions through comparative studies of nucleotide sequences. *Journal of Molecular Evolution* 16: 111–120. https://doi.org/10.1007/BF01731581

Kumar S., Stecher G., Li M., Knyaz C., Tamura K., 2018. MEGA X: Molecular Evolutionary Genetics Analysis across computing platforms. *Molecular Biology and Evolution* 35: 1547–1549. https://doi.org/10.1093/molbev/msy096

Larignon P., Fulchic R., Cere L., Dubos B., 2001. Observation on black dead arm in French vineyards. *Phytopathologia Mediterranea* 40: 336–342. https://doi.org/10.14601/Phytopathol_Mediterr-1629

Lawrence D.P., Travadon R., Nita M., Baumgartner K., 2017. TrunkDiseaseID. org: A molecular database for fast and accurate identification of fungi commonly isolated from grapevine wood. *Crop Protection* 102: 110–117. https://doi.org/10.1016/j.cropro.2017.08.017

Lazzizera C., Frisullo S., Alves A., Phillips A.J.L., 2008. Morphology, phylogeny and pathogenicity of *Botryosphaeria* and *Neofusicoccum* species associated with drupe rot of olives in southern Italy. *Plant Pathology* 57: 48–956. https://doi.org/10.1111/j.1365-3059.2008.01842.x

Marsberg A., Kemler M., Jami F., Nagel J. H., Postma-Smidt A., … Slippers B., 2017. *Botryosphaeria dothidea*: a latent pathogen of global importance to woody plant health. *Molecular Plant Pathology* 18: 477–488. https://doi.org/10.1111/mpp.12495

Mehl J., Wingfield M.J., Roux J., Slippers B., 2017. Invasive everywhere? Phylogeographic analysis of the globally distributed tree pathogen *Lasiodiplodia theobromae*. *Forests* 8: 1–22. https://doi.org/10.3390/f8050145

Mohali S., Burgess T.I., Wingfield M.J., 2005. Diversity and host association of the tropical tree endophyte *Lasiodiplodia theobromae* revealed using simple sequence repeat markers. *Forest Pathology* 35: 385–396. https://doi.org/10.1111/j.1439-0329.2005.00418.x

Muñoz-Adalia E.J., Colinas C., 2021. Susceptibility of cork oak (*Quercus suber*) to canker disease caused by *Diplodia corticola*: when time is of the essence. *New Forests* 52: 863–873. https://doi.org/10.1007/s11056-020-09829-8

Muñoz-Adalia E.J., Uppara A.B., Albó D., Meijer A., Colinas C., 2023. Cork harvest planning and climate: high air humidity favors availability of airborne inoculum of *Diplodia corticola*. *Forest Ecology and Management* 536: 120935. https://doi.org/10.1016/j.foreco.2023.120935

Paolinelli-Alfonso M., Serrano-Gomez C., Hernandez-Martinez R., 2015. Occurrence of *Eutypella microtheca* in grapevine cankers in Mexico. *Phytopathologia Mediterranea* 54: 86–93. https://doi.org/10.14601/Phytopathol_Mediterr-14998

Phillips A.J.L. 2002. *Botryosphaeria* species associated with diseases of grapevines in Portugal. *Phytopathologia Mediterranea* 4:3–18.

Phillips A.J.L., Alves A., Abdollahzadeh J., Slippers B., Wingfield, M.J., … Crous P.W., 2013. The *Botryosphaeriaceae* : genera and species known from culture. *Studies in Mycology* 76: 51–167. https://doi.org/10.3114/sim0021

Pintos Varela C., Fernández V.R., Casal O.A., Vázquez J.M., 2011. First report of cankers and dieback caused by *Neofusicoccum mediterraneum* and *Diplodia corticola* on grapevine in Spain. *Plant Disease* 95: 1315–1315. https://doi.org/10.1094/PDIS-05-11-0429

Pitt W.M., Huang R., Steel C.C., Savocchia S., 2010. Identification, distribution and current taxonomy of *Botryosphaeriaceae* species associated with grapevine decline in New South Wales and South Australia. *Australian Journal of Grape and Wine Research* 16: 258–271. https://doi.org/10.1111/j.1755-0238.2009.00087.x

Ploetz R.C., Pérez-Martínez J.M., Palmateer A.J., Tarnowski T.L., 2009. Influence of temperature, light intensity, and isolate on the development of *Neofusicoccum parvum*–induced dieback of Eugenia, *Syzygium paniculatum*. *Plant Disease* 93: 804–808. https://doi.org/10.1094/PDIS-93-8-0804

Rangel-Montoya E.A., Paolinelli M., Rolshausen P.E., Valenzuela-Solano, C., Hernandez-Martinez R., 2021. Characterization of *Lasiodiplodia* species associated with grapevines in Mexico. *Phytopathologia Mediterranea* 60: 237–251. https://doi.org/10.36253/phyto-12576

Rathnayaka A.R., Chethana K.T., Phillips A.J., Liu J.K., Samarakoon M.C., … Zhao C.L., 2023. Re-evaluating Botryosphaeriales: ancestral state reconstructions of selected characters and evolution of nutritional modes. *Journal of Fungi* 9: 184. https://doi.org/10.3390/jof9020184

Rolshausen P.E., Akgül D.S., Perez R., Eskalen A., Gispert C., 2013. First report of wood canker caused by *Neoscytalidium dimidiatum* on grapevine in California. *Plant Disease* 97: 1511–1511. https://doi.org/10.1094/PDIS-04-13-0451-PDN

SIAP Servicio de Información y Estadística Agroalimentaria y Pesquera, 2023. Ministerio de Agricultura de Mexico, Secretaría de Agricultura, Ganadería, Desarrollo Rural, Pesca y Alimentación (SAGARPA).

Slippers B., Fourie G., Crous P.W., Coutinho T.A., Wingfield B.D., Wingfield M.J., 2004. Multiple gene sequences delimit *Botryosphaeria australis* sp. nov. from *B. lutea*. *Mycologia* 96: 1030–1041. https://doi.org/10.1080/15572536.2005.11832903

Slippers B., Wingfield M., 2007. *Botryosphaeriaceae* as endophytes and latent pathogens of woody plants: diversity, ecology and impact. *Fungal Biology Reviews* 21: 90–106. https://doi.org/10.1016/j.fbr.2007.06.002

Slippers B., Smit W.A., Crous P.W., Coutinho T.A., Wingfield B.D., Wingfield M.J., 2007. Taxonomy, phylogeny and identification of *Botryosphaeriaceae* associated with pome and stone fruit trees in South Africa and other regions of the world. *Plant Pathology* 56: 128–139. https://doi.org/10.1111/j.1365-3059.2006.01486.x

Stempien E., Goddard M.L., Wilhelm K., Tarnus C., Bertsch C., Chong, J., 2017. Grapevine Botryosphaeria dieback fungi have specific aggressiveness factor repertory involved in wood decay and stilbene metabolization. *PloS One* 12: e0188766. https://doi.org/10.1371/journal.pone.0188766

Téliz D., Valle P., 1979. Eutypa dieback in Mexican vineyards. *Plant Disease Reporter* 63: 312–314.

Thompson J.D., Higgins D.G., Gibson T.J., 1994. CLUSTAL W: improving the sensitivity of progressive multiple sequence alignment through sequence weighting, position-specific gap penalties and weight matrix choice. *Nucleic Acids Research* 22: 4673–4680.

Úrbez-Torres J.R., Leavitt G.M., Voegel T.M., Gubler W.D., 2006. Identification and distribution of *Botryosphaeria* spp. associated with grapevine cankers in California. *Plant Disease* 90: 1490–1503. https://doi.org/10.1094/PD-90-1490

Úrbez-Torres J.R., Leavitt G.M., Guerrero J.C., Guevara J., Gubler W.D., 2008. Identification and pathogenicity of *Lasiodiplodia theobromae* and *Diplodia seriata*, the causal agents of bot canker disease of grapevines in Mexico. *Plant Disease* 92: 519–529. https://doi.org/10.1094/PDIS-92-4-0519

Úrbez-Torres J.R., Adams P., Kamas J., Gubler W.D., 2009. Identification, incidence, and pathogenicity of fungal species associated with grapevine dieback in Texas. *American Journal of Enology and Viticulture* 60: 497–507. https://doi.org/10.5344/ajev.2009.60.4.497

Úrbez-Torres J.R., Peduto F., Rooney-Latham S., Gubler W.D., 2010a. First report of *Diplodia corticola* causing grapevine (*Vitis vinifera*) cankers and trunk cankers and dieback of canyon live oak (*Quercus chrysolepis*) in California. *Plant Disease* 94: 785–785. https://doi.org/10.1094/PDIS-94-6-0785A

Úrbez-Torres J.R., Bruez E., Hurtado J., Gubler W.D., 2010b. Effect of temperature on conidial germination of *Botryosphaeriaceae* species infecting grapevines. *Plant Disease*, 94: 1476–1484. https://doi.org/10.1094/PDIS-06-10-0423

Úrbez-Torres J.R., 2011. The status of *Botryosphaeriaceae* species infecting grapevines. *Phytopathologia Mediterranea* 50: S5–S45.

van Niekerk J.M., Crous P.W., Groenewald J.Z., Fourie P.H., Halleen F., 2004. DNA phylogeny, morphology and pathogenicity of *Botryosphaeria* species on grapevines. *Mycologia* 96: 781–798. https://doi.org/10.1080/15572536.2005.11832926

van Niekerk J.M., Fourie P.H., Halleen F., Crous P.W., 2006. *Botryosphaeria* spp. as grapevine trunk disease pathogens. *Phytopathologia Mediterranea* 45: 43–54.

Wagner D.B., Furnier G.R., Saghai-Maroof M.A., Williams SM, Dancik B.P., Allard R.W., 1987. Chloroplast DNA polymorphisms in lodgepole and jack pines and their hybrids. *PNAS* 84: 2097–2100.

Waite H., Armengol J., Billones-Baaijens R., Gramaje D., Hallen F., … Smart R., 2018. A protocol for the management of grapevine rootstock mother vines to reduce latent infections by grapevine trunk pathogens in cuttings. *Phytopathologia Mediterranea* 57: 384–398. https://doi.org/10.14601/Phytopathol_Mediterr-22772

White T.J., Bruns T., Lee S.J.W.T., Taylor J. 1990. Amplification and direct sequencing of fungal ribosomal RNA genes for phylogenetics. *PCR protocols: a Guide to Methods and Applications* 18: 315–322.

Xiao J., Zhang Q., Gao Y.Q., Tang J.J., Zhang A.L., Gao J.M., 2014. Secondary metabolites from the endophytic *Botryosphaeria dothidea* of *Melia azedarach* and their antifungal, antibacterial, antioxidant, and cytotoxic activities. *Journal of Agricultural and Food Chemistry* 62: 3584–3590. https://doi.org/10.1021/jf500054f

Phytopathologia Mediterranea
The international journal of the
Mediterranean Phytopathological Union

Firenze University Press
www.fupress.com/pm

Research Papers

Fusarium wilt caused by *Fusarium oxysporum* f. sp. *cubense* tropical race 4 in banana plantations in Türkiye

Mümine ÖZARSLANDAN[1], Davut Soner AKGÜL[2,*]

[1] *Biological Control Research Institute, Ministry of Agriculture and Forestry, 01321, Yüreğir, Adana, Türkiye*
[2] *Department of Plant Protection, Agriculture Faculty, University of Çukurova, 01330, Balcalı, Adana, Türkiye*
*Corresponding author. E-mail: sakgul@cu.edu.tr

OPEN ACCESS

Citation: Özarslandan, M., & Akgül, D.S. (2024). Fusarium wilt caused by *Fusarium oxysporum* f. sp. *cubense* tropical race 4 in banana plantations in Türkiye. *Phytopathologia Mediterranea* 63(2): 207-221. doi: 10.36253/phyto-15133

Accepted: June 21, 2024

Published: July 17, 2024

Data Availability Statement: All relevant data are within the paper and its Supporting Information files.

Competing Interests: The Author(s) declare(s) no conflict of interest.

Editor: Akif Eskalen, University of California, Davis, CA, United States.

ORCID:
MO: 0000-0003-4125-1028
DSA: 0000-0002-9990-4194

Summary. Fusarium wilt, caused by *Fusarium oxysporum* f. sp. *cubense* tropical race 4 (*Foc*TR4), is an important disease for banana production. Presence and prevalence of *Foc*TR4 in banana plantations on the Mediterranean coast of Türkiye were assessed during 2018 to 2020 in a total of 117 banana plantations in open fields and protected plastic greenhouses. Rhizome, pseudostem, and root samples were taken from plants showing typical symptoms associated to the disease and from suspected affected plants. Fungi were isolated from the plant internal tissues, and *Fusarium oxysporum*-like colonies were sub-cultured for further analyses. Phylogenetic analyses of 36 isolates showed that they belonged to four different *Fusarium* species: *F. musae, F. oxysporum, F. sacchari*, and *F. solani*. Eight representative *F. oxysporum* isolates were identified as *Foc*TR4 by specific PCR and qPCR tests. Pathogenicity tests were carried out on tissue-cultured 'Cavendish' type banana seedlings ('Grand Naine') for 36 *Fusarium* isolates, and their virulence was assessed based on the internal necrosis observed in the rhizomes. Approx. 40 to 65 d after inoculations, *Foc*TR4, *F. oxysporum*, and *F. sacchari* isolates caused severe to mild necroses in the seedling rhizomes. This is the first report of *F. sacchari* associated with root and collar rot of bananas in Türkiye. This study showed that Fusarium wilt caused by *Foc*TR4 is present, but at low incidence (6.8%) in Turkish banana plantations.

Keywords. Collar rot, Grand Naine, *Fusarium sacchari,* identification.

INTRODUCTION

Bananas and plantains (*Musa* spp.) are important agricultural products in tropical and subtropical regions. Banana plantations are located on the coastline of the Mediterranean Region of Türkiye, and 883,455 tons of sweet bananas are produced annually from approx. 11,000 ha (Anonymous, 2022). This production does not meet the domestic consumption, and 20% of domestic consumption is imported from other banana-producing countries, including Costa Rica and Ecuador (Anonymous, 2021).

Fusarium wilt, caused by *Fusarium oxysporum* Schlecht. f. sp. *cubense* (E.F. Smith) Snyder and Hansen (*Foc*), is the most important fungal disease in banana-producing countries, due to the lack of practical management methods and the severe economic losses this disease can cause. *Foc* first infects banana plants via root hairs, then develops in the internal corm tissues, progressing to the xylem vessels and activating xylem-secreted genes that trigger initial symptoms (Dong *et al*., 2016; Czislowski *et al*., 2021). Water transport in the xylem is disrupted due to the conidial and mycelial mats produced by the pathogen, and by host substances such as gums, and mechanical barriers produced to prevent systemic spread of the fungus. Enzymes and toxins produced by *Foc* cause the host leaves to turn yellow and the lower leaves to droop (Stover, 1962).

Fusarium wilt of banana was first reported in Brisbane, Australia, in 1874 but reached severe levels in Panama and Costa Rica in the 1890s (Pegg *et al*., 2019). Destruction of the Gros Michel cultivar (susceptible to race 1 of *Foc*) by the fungus in Latin America and the Caribbean has made it one of the most important fungal pathogens wherever bananas are grown. Since the early 1960s, Fusarium wilt was not of concern due to adoption of the *Foc* resistant banana cultivar 'Cavendish'. However, despite the use of resistant 'Cavendish'-related cultivars, the disease re-appeared in the 1990s in Taiwan, Indonesia and Malaysia, caused by the new physiological race, Tropical Race 4 (*Foc*TR4) (Ploetz, 2006). To date, four physiological races of *Foc* have been described to cause Fusarium wilt, including Race 1 in 'Gros Michel' and 'Silk'; Race 2 in 'Bluggoe'; Race 3 in *Heliconia* spp., and Race 4 in all commercial banana cultivars. In addition, the subtropical race of the pathogen (*Foc*STR4) was found to be ineffective in the tropics or in areas where optimum banana growth conditions occur.

*Foc*TR4 has also caused Fusarium wilt in commercially grown banana cultivars regardless of environmental conditions (Ploetz, 2015). This race was first reported in 1990 in Taiwan; in 1992 in Indonesia and Malaysia (Ploetz and Pegg, 1997); in 1997 in Northern Australia (Conde and Pitkethley, 2001); in 1998 in China (Qi *et al*., 2008); in 2005 in the Philippines; in 2012 in the Sultanate of Oman; in 2013 in Mozambique and Jordan (García-Bastidas *et al*., 2014; Perez-Vicente *et al*., 2014; Viljoen *et al*., 2020); in 2015 in Lebanon and Pakistan (Ordonez *et al*., 2016); in 2018 in Vietnam (Hung *et al*., 2018); in Laos (Chittarath *et al*., 2018), Myanmar (Zheng *et al*., 2018) and Israel (Maymon *et al.,* 2018); in 2019 in India (Thangavelu *et al.,* 2019), Thailand and Colombia (García-Bastidas *et al*., 2020); in 2020 in Türkiye (Özarslandan and Akgül, 2020); in 2021 in Mayotte (Aguayo *et al*., 2021), and Peru (Acuna *et al*., 2022); and in 2022 in Venezuela (Mejias Herrera *et al*., 2023).

As with other soil-borne plant pathogenic fungi, managing *Foc*TR4 is challenging, and practical control has not yet been found for eradicating the pathogen from soil. *Foc* has long persistence in the soil (more than 20 years), due to its ability to survive as a saprophyte in plant residues and to produce chlamydospores. As these inocula are pushed deeper into the soil with tillage, eliminating the pathogen from infested areas becomes almost impossible (Stover, 1962). Solarization is ineffective in eradicating this pathogen when applied alone, because of its inability to penetrate deep into the soil (Herbert and Marx, 1990). In addition, using this method in large areas is difficult and costly. Breeding for resistance is ongoing, but a banana cultivar with high commercial potential and complete resistance has not yet been produced, as was previously the case for the *Foc*1 and *Foc*2 resistant 'Cavendish' (Dita *et al*., 2018).

Fusarium oxysporum is a large species complex including saprophytes, endophytes, plant and human pathogens; it also has 143 *formae speciales* (106 of them are well-documented) and 25 physiological races (including *Foc*TR4) from monocotyledon and dicotyledon host plants (Edel-Hermann and Lecomte, 2019). Formerly, *Fusarium* species have been identified based on their morphological characteristics, which primarily include asexual reproductive structures (chlamydospores, conidiophores, macro- and microconidia, and phialides) and colony morphology (Fourie *et al.,* 2009). However, molecular tools and phylogenetic analyses supported by DNA gene sequencing, as well as pathogenicity tests, have shown that these features are insufficient for species identification. Since it is not possible to discriminate pathogenic isolates (or physiological races) using morphology and microscopy, precise diagnostic procedures (e.g. PCR, gene sequencing, VCG tests) and pathogenicity tests must be used for accurate identification. In the last 15 years, commercial diagnostic kits and PCR primers that amplify specific regions in genomic DNA of these races have been designed for molecular identifications. Lin *et al.* (2009) followed the RAPD marker technique to design specific primers for identifying tropical race 4 using 96 *Foc*TR4 isolates from Taiwan. Their primer (*Foc*1/*Foc*2) amplifies a specific 242-bp gene product in *Foc* genomic DNA. Dita *et al.* (2010) designed *Foc*TR4-F/*Foc*TR4-R primers to identify *Foc*TR4 strains using single nucleotide polymorphism in the IGS region. These primers have been widely used for monitoring the disease and in pathogen identification studies. Some commercial diagnostic kits containing pathogen-positive DNA have also been developed for qPCR ampli-

fication, and have been used in studies aimed at disease monitoring in banana-producing countries (Dale *et al*., 2017; García-Bastidas *et al.,* 2019).

If the pathogen has not appeared in a country, the most effective control measure is to exclude the pathogen by implementing strict quarantine measures. When the pathogen is detected in a limited area, it is necessary to contain and eradicate it before becoming widespread. Pathogen tracing and disease monitoring with regular surveys, and accurate identification procedures, are essential. Fusarium wilt of banana was first reported in Türkiye was in 2018. *Foc*TR4 was detected in three protected plastic covered greenhouses after identification using specific PCR primers and pathogenicity tests (Özarslandan and Akgül, 2020). However, a more comprehensive study is required to determine prevalence of Fusarium wilt in Türkiye.

The aim of the present study was to determine the prevalence of Fusarium wilt caused by *Foc*TR4 in open-field and plastic-covered-greenhouse banana plantations in Türkiye. Knowledge of *Foc*TR4 prevalence in these areas would provide a basis for appropriate quarantine measurements, and for further investigations on disease management and screening of local banana cultivars for resistance breeding.

MATERIALS AND METHODS

Survey, sample collection and isolation of fungi

A survey was carried out in protected plastic, greenhouses (n = 72) and open field banana plantations (n = 45) located in Seyhan, Yüreğir (Adana province), Alanya, Gazipaşa (Antalya province), Arsuz (Hatay), and Anamur, Bozyazı, Erdemli, Silifke, Tarsus districts (Mersin province), in the Mediterranean Region of Türkiye (Figure 1). A total of 117 plantations (approx. total area 76 ha) were inspected, from March 2018 to December 2020. Individual banana the plants were examined for general appearance, and rhizome, pseudostem, and root samples were collected from those with typical disease symptoms (Figure 2). These samples were placed in paper bags and then in an ice box, and transported to a laboratory for further processing.

Small sections (5 to 8 cm each) of symptomatic pseudostem, corm, and root tissues were dissected from each sample, and then surface sterilized with 2.5% sodium hypochlorite solution (>5% active chlorine) for 3 min, then rinsed twice in sterile distilled water. The internal tissues (4 to 6 mm) from each section were aseptically placed onto ¼ strength Potato Dextrose Agar (PDA; CondaLab) amended with streptomycin sulfate (250 µg mL^{-1}), and the culture were incubated at 25°C for 4-5 d. Twenty Petri dishes were used isolations from tissues from each banana plantation. After morphological and microscopic examinations, *Fusarium oxysporum*-like colonies were transferred by single-conidium isolation techniques onto fresh PDA plates, backed up on sterile green banana leaf cultures, and were stored at -20°C (Seifert, 1996). Among the *F. oxysporum*-like fungi, a representative sample of 36 isolates was selected for further pathogenicity testing and gene sequencing. These isolates were tentatively identified using cultural and microscopical characteristics (fluffy mycelia, simple short phialides, and pale violet or pinkish colony colour), as described by Nelson (1983) and Leslie and Summerell (2006). *Foc*TR4 prevalence (%) was calculat-

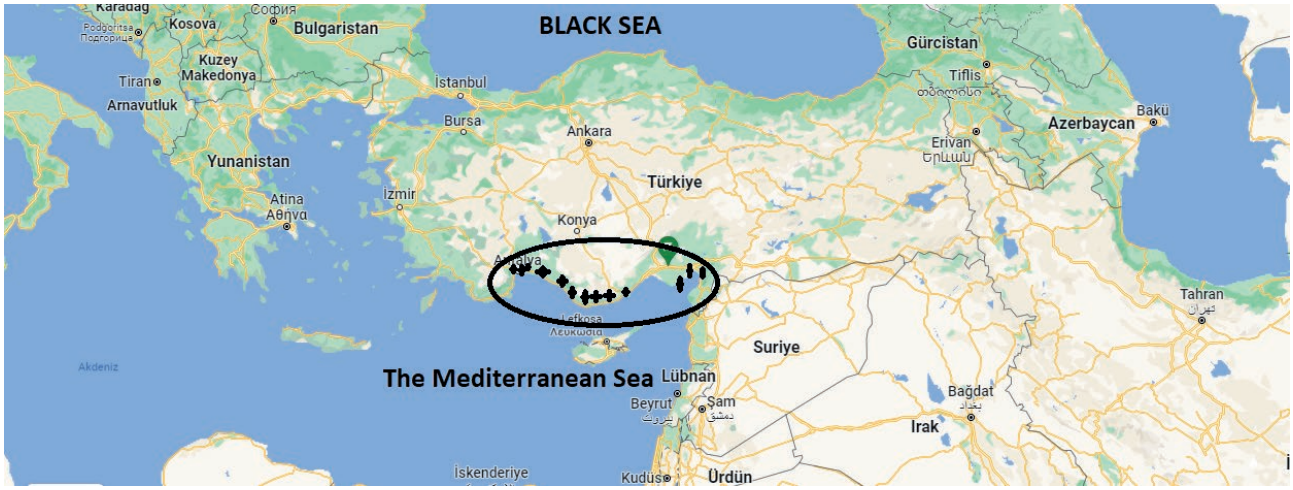

Figure 1. The location of surveyed banana plantations in the Mediterranean Region of Türkiye.

Figure 2. A protected banana greenhouse with wilt symptomatic plants, and vascular necrosis in an affected pseudostem.

ed based on the number of greenhouse or banana fields (where *Foc*TR4 detected and the total number of banana plantations (surveyed). The isolation frequency (%) of all fungi in each plantation was estimated using 140 tissue pieces plated (20 Petri plates, seven tissue fragments each) from symptomatic plants.

Molecular identification of Fusarium *isolates*

Thirty-six *F. oxysporum*-like isolates (tentatively identified based on their simple short phialides on hyphae, salmon or pale violet colony colour after 3 weeks incubation on PDA at 24°C in the dark) were selected for further molecular identification. Isolates were grown on PDA at 24°C for 8-10 d in the dark. Fresh aerial mycelia were collected by scraping the colonies with a sterile scalpel, and the mycelia were placed in sterile Eppendorf tubes containing 2% CTAB buffer. The following extraction steps were then followed, as described by O'Donnell *et al*. (1998). For gene sequencing, translation elongation factor 1α (TEF-1α) and intergenic spacer (IGS) region (nuclear ribosomal operon) genes were amplified using PCR using, respectively, the EF1/EF2 primer (O'Donnell *et al*., 1998) and *Foc*TR4F/*Foc*TR4R primer (Dita *et al*., 2010). Each PCR reaction mixture contained 5 µL of buffer (10× Green Buffer, DreamTaq Green DNA Polymerase, Thermo Scientific™), 2 µL of the dNTPs mixture (10 mM each, Thermo Scientific™), 0.5 µL of forward and reverse primers (stock concentration: 10 pmol·µL^{-1}), 0.25 µL of Taq polymerase (DreamTaq Green DNA Polymerase, Thermo Scientific™), 39.75 µL of PCR grade water and 1 µL of genomic DNA (approx. 100 ng·µL^{-1}). PCR amplifications were carried out in a thermocycler (Simpli-Amp A24811™ Thermal Cycler, Applied Biosystems), using the conditions specified in Table 1. PCR products were separated by gel electrophoresis in 1.5% agarose

Table 1. PCR conditions used in this study to amplify partial genomic DNA of *Fusarium* isolates.

Amplification stages	EF1/EF2			*Foc*TR4/*Foc*TR4R			Clear Detections Kit™		
	Temp. (°C)	Duration (min)	No. of cycles	Temp. (°C)	Duration (min)	No. of cycles	Temp. (°C)	Duration (sec)	No. of cycles
Initial denaturation	95	3	1	95	5	1	95	3	1
Denaturation	95	1	35	95	1	30	95	10	40
Annealing	52	1		60	1		63	60	
Extension	72	1.5		72	3		72	30	
Final extension	72	10	1	72	10	1	70	60	1

(Sigma) gels in 1× Tris-Acetic acid-EDTA (TAE) buffer, to check DNA band size and quality. These products were then sequenced by Macrogen Co. (South Korea), and the sequences were compared with those deposited in the NCBI GenBank database using the BLAST tool (version 2.0; National Center for Biotechnology Information, US National Institutes of Health). TEF-1α and IGS sequences obtained were deposited to the NCBI GenBank.

FocTR4 identification was also confirmed by Real-Time PCR using SYBR® Green technology (Clear Detections TR4 Kit™). For each isolate, 5 µL of genomic DNA was added to 200 µL capacity thermocycler tubes each containing 15 µL of Clear Detections qPCR master mix, then vortexed for 20 sec. of PCR-grade water (5 µL) and *Foc*TR4 genomic DNA (provided by the manufacturer) were then added to other PCR tubes to confirm negative and positive amplifications as controls. The thermal cycler (Roche Light Cycler 480™) was set according to the conditions outlined in Table 1, and whether the isolates were *Foc*TR4 was determined according to the obtained cycle thresholds (Ct). To avoid missing weak positive amplifications due to DNA quality and other factors, melting-curve analysis was also carried out, and amplifications around 75°C were considered primer dimers. The molecular identification tests were each repeated once.

The phylogenetic analysis was carried out using data from the translation elongation factor-1α gene. The data set was constructed using reference sequences (Table 2) from relevant publications (Maryani *et al*., 2019a; Crous *et al*., 2021; Tava *et al*., 2021). The sequences were aligned using the algorithm in Muscle, and a maximum likelihood tree was constructed using MEGA-X software with the Hasegawa-Kishino-Yano model (Hasegawa *et al*., 1985). *Geejayessia zealandica* (= *F. zealandicum*) CBS isolate 111.93 was used as a root taxon, and node support was estimated by bootstrap analysis on 1000 random trees.

Table 2. GenBank accession numbers of partial sequence of TEF 1-α of reference species used in the phylogenetic analyses.

Species	Isolate	GenBank Accession No.
Fusarium grosmichelii	InaCC F820	LS479810
Fusarium musae	F31	MW916961
Fusarium oxysporum	CAV794	FJ664922
Fusarium oxysporum	CAV189	FJ664956
Fusarium oxysporum	NRRL26029	AF008493
Fusarium oxysporum f. sp. *cubense* TR4	FocII5 NRRL36104	LS479644
Fusarium oxysporum f. sp. *cubense* TR4	InaCC F816	LS479677
Fusarium *oxysporum* f. sp. cubense TR4	InaCC F817	LS479753
Fusarium philaophorum	FocIndo25	LS479650
Fusarium proliferatum	NRRL62905	KU171727
Fusarium purpurascens	InaCC F823	LS479838
Fusarium sacchari	NRRL13999	AF160278
Fusarium solani	CBS 102429	KM231936
Fusarium solani	KARE233	MK077039
Fusarium tardichlamydosporum	FocCNPMF-R2	LS479643

Pathogenicity tests

The 36 selected *Fusarium* isolates were used in pathogenicity tests on banana seedlings, as described by Thangavelu *et al*. (2019). The isolates were grown on PDA for 7-8 d at 25°C in the dark. The mature cultures were then flooded with sterile distilled water, and mycelia were scraped with a sterile plastic needle to dislodge macro and microconidia. The conidium suspensions were each filtered through two layers of sterilized cheesecloth, and the concentration of resulting conidium suspension was adjusted to 10^6 conidia mL^{-1}, after enumeration with a Thoma® slide under a light microscope. Banana seedlings ('Grand Naine' at 4 to 6 leaf stage, produced by tissue culture), were uprooted

from trays; their roots were slightly trimmed and then dipped into the conidium suspensions of respective isolates for 10 min. The seedlings were then planted in plastic pots (15 cm diam.) containing sterile peat moss, sand and perlite mixture (1:1:1 v/v/v), and were placed in climate controlled greenhouses (at 27°C, 85% relative humidity, 12 h illumination). The inoculated plants were grown for 65 d, and the pathogenicity of the isolates was assessed using a 0 to 3 severity scale, based on the discolouration of the each plant rhizome and whole plant wilting, as described by Li *et al*. (2015). Disease severity was calculated using the formula of Towsend and Heuberger (1943): (∑ (number of plants in a disease scale category × disease scale category) / (total number of plants × maximum disease scale category)) ×100). Eight plants (one plant per pot and four replicates with two plants per replicate) were inoculated with each *Fusarium* isolate. Inoculation control plants were treated with sterile distilled water. Pathogenicity was confirmed by re-isolating inoculated isolates from roots and necrotic internal tissues of plants. The pathogenicity tests were each repeated once.

Statistical analyses

Analysis of variance (ANOVA) were carried out on disease severity data (mean lesion lengths in two experiments), and the data were checked for normality. Means were compared using Fisher's least significant difference (LSD) test at $P \leq 0.05$ (Gomez and Gomez, 1984).

RESULTS

Fungal isolations, identification of Foc*TR4, and disease severity assessments*

In the surveyed banana plantations, 12 fungal genera, including *Alternaria, Aspergillus, Cladosporium, Epicoccum, Fusarium, Macrophomina, Nigrospora, Penicillium, Pythium, Phytophthora, Rhizoctonia,* and *Trichoderma* (based on ITS sequencing and simple BLAST searches), were obtained from symptomatic and asymptomatic banana plants. Among these fungi, *Fusarium* was the most commonly isolated genus, obtained from 96% (112 of 117 plantations) of the total plantations assessed. According to cultural morphological characteristics of isolates (fluffy mycelia, simple short phialides, and pale violet or pinkish colonies) and microscopic features (short or long simple phialides, macro- and microconidium shapes, chlamydospore production), 36 *Fusarium* isolates were selected for further identification studies.

A nucleotide BLAST search using the translation elongation factor 1-α gene revealed four different *Fusarium* species; *F. musae*, *F. oxysporum*, *F. sacchari*, and *F. solani* (Table 3). Of the 36 selected *Fusarium* isolates, most belonged to *F. oxysporum* (25 isolates), followed by *F. sacchari* (eight isolates), *F. solani* (two isolates), and *F. musae* (one isolate).

The BLAST results were confirmed by the clustering of the isolates with respective reference sequences of *F. musae* (F31), *F. oxysporum* (CAV794, NRRL_26029), *F. sacchari* (NRRL_13999), and *F. solani* (CBS 102429) in the phylogenetic tree. However, these methods could not differentiate *Foc*TR4 from the closely related *Fusarium oxysporum* isolates.

The conventional PCR tests showed that eight of the *F. oxysporum* isolates belonged to the tropical race four, so 463 bp DNA bands were observed with agarose gel electrophoresis (Figure 4). However, genomic DNAs from the remaining 28 isolates could not be amplified using these specific primers.

The real-time PCR tests using a *Foc*TR4-specific diagnostic kit agreed with the conventional PCR results. On average, while the CT value average for the reference DNA provided by the Clear Detection™ commercial kit was 21.59, these values varied between 24.97 and 31.63 in eight isolates suspected to be *Foc*TR4 (Figure 5). No amplification was recorded for DNA of the other *Fusarium* isolates (including the water control), and their Ct values were greater than 36 (Table 3).

Pathogenicity tests

Approx. 40 d after inoculating 'Grand Naine' banana seedlings with the *Fusarium* isolates, some plants showed yellowing of the lower leaves (Figure 6, a and b). Plants inoculated with two *Fusarium solani* isolates (BMAE41 and BMAE43), *F. musae* (BMAE3MM), or the non-inoculated control plants, did not develop disease symptoms (Figure 6 j). Approx. 50 d post inoculation, yellowing symptoms progressed to the upper leaves, while the lower leaves wilted and dried thoroughly. Two weeks after these symptoms appeared, plants inoculated with isolates identified as *Foc*TR4 wilted and died, while plants inoculated with the other isolates continued to live for approx. 20 d. Rhizome necroses started from the pith tissues in *Foc*TR4 inoculated plants (Figure 6 c to f), this progressed from the cortex to the centres in *F. oxysporum* and *F. sacchari* inoculated plants (Figure 6 g and h). According to the evaluation scale of

Table 3. *Fusarium* species, isolate identification numbers, source banana plantation locations, and cultivars, isolate translation elongation factor (TEF 1-α) and 28S-18S intergenic spacer (IGS) GenBank accession numbers, and cycle threshold (Ct) values from Real-Rime PCR.

Fungal Species	Isolate	Location	Cultivar	GenBank Accession Numbers		Ct Values at
				TEF 1-α	IGS	Real_Time PCR
Fusarium musae	BMAE3MM	Erdemli, Mersin	Grand Naine	OM350374	-	NA
Fusarium sacchari	BMAE4MM	Erdemli, Mersin	Azman	OM350339	-	"
	BMAE5MM	Erdemli, Mersin	Azman	OM350340	-	"
	BMAE8MM	Silifke, Mersin	Grand Naine	OM350375	-	"
	BMAE11MM	Silifke, Mersin	Grand Naine	OM350343	-	"
	BMAE44MM	Bozyazı, Mersin	Azman	OM350348	-	"
	BMAE101MM	Anamur, Mersin	Grand Naine	OM350379	-	"
	BMAE103MM	Bozyazı, Mersin	Grand Naine	OM350364	-	"
	BMAE107MM	Arsuz, Hatay	Grand Naine	OM350368	-	"
F. oxysporum f. sp. *cubense* TR4	BMAE9MM	Silifke, Mersin	Grand Naine	OM350342	OM350369	27.92
	BMAE36MM	Anamur, Mersin	Grand Naine	OM350345	OM350370	24.97
	BMAE49MM	Bozyazı, Mersin	Bodur Azman	OM350350	OM350371	26.88
	BMAE70MM	Gazipaşa, Antalya	Bodur Cavendish	OM350354	MN419031	28.92
	BMAE83MM	Alanya, Antalya	Bodur Cavendish	OM350356	OM350372	31.63
	BMAE87MM	Alanya, Antalya	Bodur Cavendish	OM350357	MN419032	26.73
	BMAE102MM	Anamur, Mersin	Bodur Azman	OM350363	OM350373	26.30
	BMAE104MM	Anamur, Mersin	Azman	OM350365	MN419033	26.00
F. oxysporum	BMAE7MM	Silifke, Mersin	Grand Naine	OM350341	-	NA
	BMAE20MM	Arsuz, Hatay	Grand Naine	OM350376	-	"
	BMAE35MM	Anamur, Mersin	Bodur Azman	OM350344	-	"
	BMAE46MM	Bozyazı, Mersin	Şimşek	OM350349	-	"
	BMAE61MM	Alanya, Antalya	Bodur Cavendish	OM350351	-	"
	BMAE62MM	Alanya, Antalya	Bodur Cavendish	OM350377	-	"
	BMAE63MM	Alanya, Antalya	Bodur Cavendish	OM350352	-	"
	BMAE69MM	Alanya, Antalya	Bodur Cavendish	OM350353	-	"
	BMAE79MM	Alanya, Antalya	Bodur Cavendish	OM350355	-	"
	BMAE93MM	Alanya, Antalya	Bodur Cavendish	OM350358	-	"
	BMAE96MM	Alanya, Antalya	Bodur Cavendish	OM350359	-	"
	BMAE97MM	Alanya, Antalya	Bodur Cavendish	OM350360	-	"
	BMAE98MM	Alanya, Antalya	Bodur Cavendish	OM350361	-	"
	BMAE99MM	Alanya, Antalya	Bodur Cavendish	OM350362	-	"
	BMAE100MM	Alanya, Antalya	Bodur Cavendish	OM350378	-	"
	BMAE105MM	Silifke, Mersin	Grand Naine	OM350366	-	"
	BMAE106MM	Silifke, Mersin	Grand Naine	OM350367	-	"
F. solani	BMAE41MM	Bozyazı, Mersin	Azman	OM350346	-	"
	BMAE43MM	Bozyazı, Mersin	Azman	OM350347	-	"

Li *et al*., (2015), *F. sacchari* and *F. oxysporum* caused rhizome necrosis and seedling death at rates from 33.3% to 83.3%, while no symptoms were observed from *F. solani* (BMAE41MM and BMAE43MM) or *F. musae* (BMAE-3MM) isolates and the sterile water inoculated controls (Figure 6 j). Disease severity was greater (66.7-91.7%) in plants inoculated with *Foc*TR4 isolates (Figure 7). *Fusarium* isolates were re-isolated from internal rhizome tissues of these plants. *Fusarium solani* isolates were re-isolated only from the hairy roots (not rhizomes), while no *Fusarium* colonies were obtained from the rhizomes of the non-inoculated control plants. Based on the overall averages of all isolates from each species, *F. oxysporum* f. sp. *cubense* TR4 caused the most severe rhizome necrosis (74.0%), followed by *F. sacchari* (61.5%) and *F. oxysporum* (58.3%).

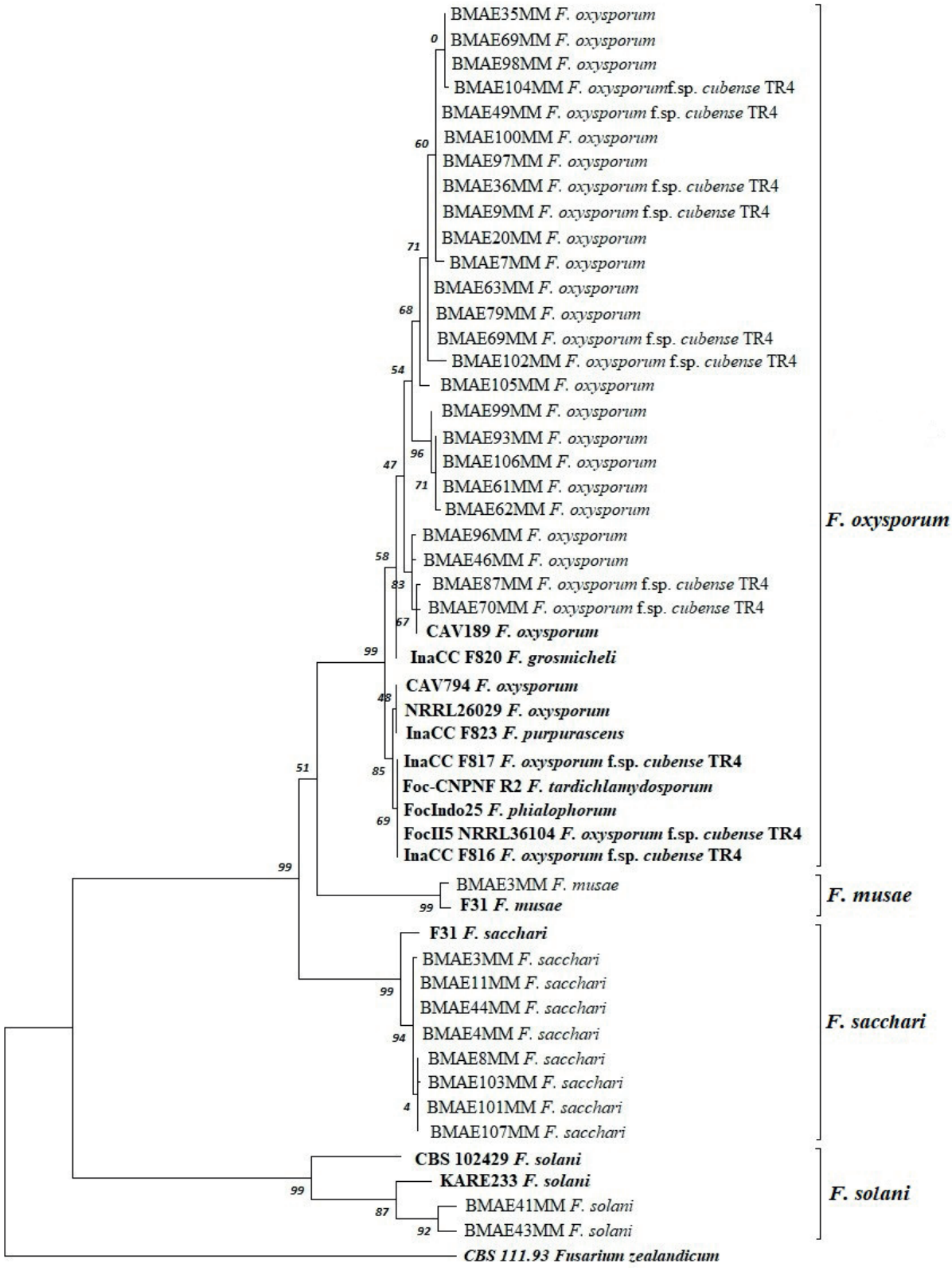

Figure 3. Maximum likelihood analysis of *Fusarium* species isolates, based on TEF-1α gene sequences. Numbers above the branch nodes represent bootstrap values from 1,000 replications. The sequence of the TEF-1α gene from *F. zealandicum* isolate CBS 111.93 was the outgroup used to root the tree.

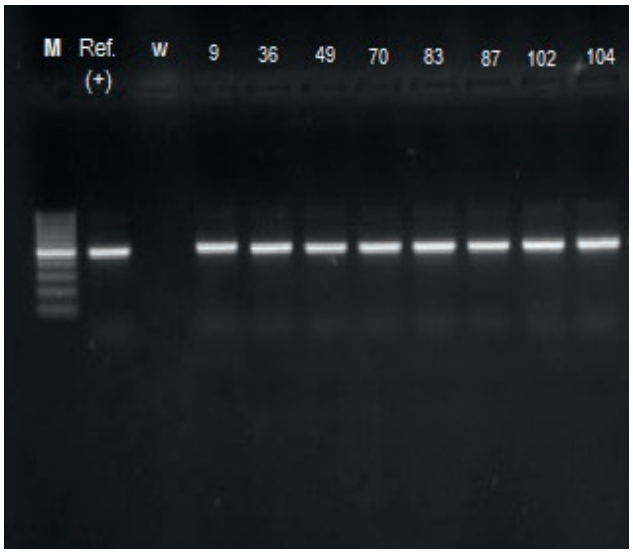

Figure 4. Electrophoretic separation of DNA bands (463 bp) of *Foc*TR4 isolates obtained from *Foc*TR4F/*Foc*TR4R primer pairs. Lane M, DNA ladder (Thermo Scientific); lane 1, Reference *Foc*-TR4 (Jordan); lane 2: PCR-grade water; lane 3, BMAE9MM; lane 4, BMAE36MM; lane 5, BMAE49MM;, lane 6, BMAE70MM; lane 7, BMAE83MM; lane 8, BMAE87MM; lane 9, BMAE102MM; lane 10,: BMAE104MM.

DISCUSSION

Fusarium wilt of banana is a severe disease affecting banana plantations, and is ranked among the top ten most important fungal diseases (Dean *et al*., 2012). The physiological races of *F. oxysporum* f. sp. *cubense* were unable to infect resistant banana cultivars until the 1990s, but the new race (Tropical Race 4) overcame this resistance in 1992 in Southeast Asia, and rapidly spread across banana producing areas. *Foc*TR4 has since been reported in more than 20 countries (Bregard *et al.,* 2022). The present study detected *Foc*TR4 in eight of 117 plantations (6.8%) in Türkiye, and all eight were in protected plastic greenhouses. No plants showing typical disease symptoms were found in open field plantations, and the pathogen was not detected in suspected plants. The limited detection of the pathogen in Türkiye is probably because bananas are mostly grown in protected greenhouses, with limited access and under drip irrigation systems, limiting the spread and proliferation of the pathogen. Growing conditions in other banana-growing countries are different, with most banana plantations located in open fields exposed to tropical climates (high precipitation and warm tem-

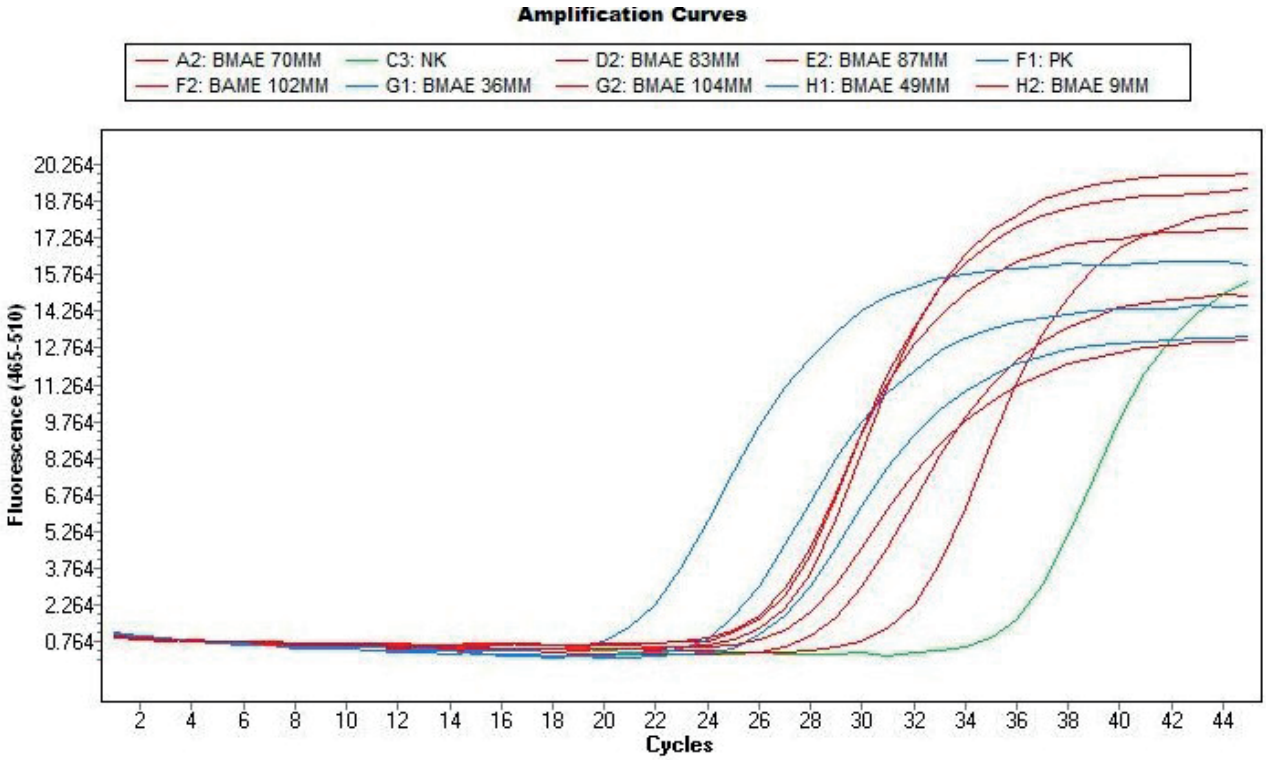

Figure 5. Real-time PCR amplification curves for *Foc*TR4 isolates (curves A2, D2, E2, F2, G1, G2, H1, and H2), and the reference positive control (curve F1) and water control (curve C3).

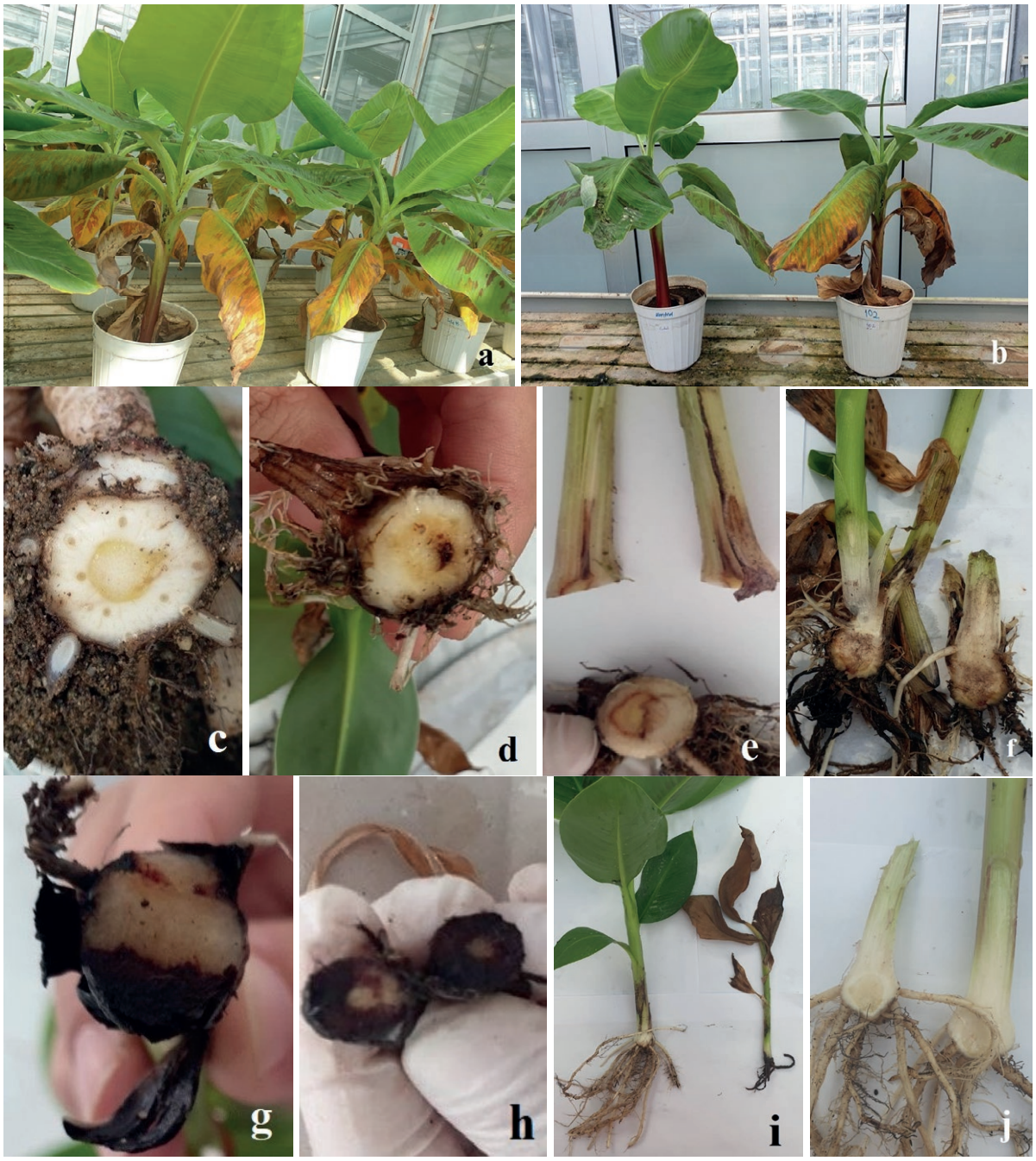

Figure 6. Leaf yellowing (a), wilt (b and i), and rhizome necrosis, caused by isolates of *Fusarium oxysporum* f. sp. *cubense* TR4 (c to f), *F. oxysporum* (g) and *F. sacchari* (h), and non-inoculated controls or *F. musae* or *F. solani* inoculated plants (j), 65 d after inoculations in greenhouse conditions.

peratures). This is probably why the disease is more prevalent in other countries.

Karangwa *et al.* (2016) assessed the distribution and incidence of Fusarium wilt in Burundi, the Democratic Republic of Congo, Rwanda, and Tanzania. They reported that 54.1% of the banana plantations had disease incidences greater than 40%, and the greatest incidence (63.6%) was in Tanzania. Zheng *et al.* (2018) surveyed banana fields in Laos, Myanmar, Vietnam, and Yunnan Province of China, to determine presence of *Foc*TR4. *Fusarium oxysporum*-like isolates were recovered from symptomatic plants from 25 banana fields, and 81.3% of

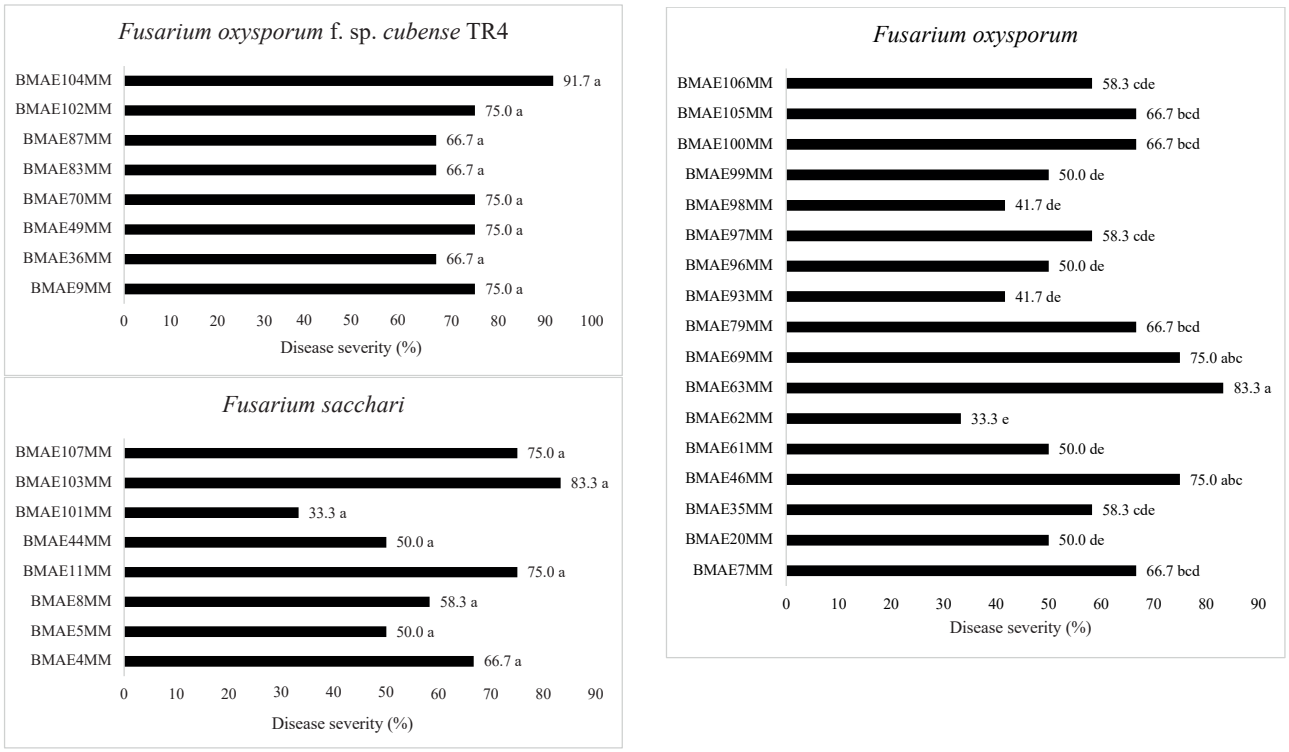

Figure 7. Mean disease severity percentages in corm tissues of 'Grand Naine' banana seedlings (inoculated at the 4 to 6 leaf stage) caused by the *Fusarium oxysporum* f. sp. *cubense* TR4, *F. sacchari* and *F. oxysporum* isolates in greenhouse conditions.

these were identified as *Foc*TR4. In a survey by Thi *et al.* (2022) in Vietnam, Fusarium wilt associated with *Foc*-TR4 was not widespread in Vietnam. Using molecular tools, these authors analyzed 19 *Fusarium* isolates from three different geographical regions, and found that only 10% were *Foc*TR4.

In the present study, *Fusarium* isolates were obtained from banana roots, rhizomes, and internal pseudostem tissues, and this was the most frequently isolated genus (96% of isolates). In addition to *Fusarium*, soilborne phytopathogenic fungi and fungus-like organisms (including *Macrophomina, Pythium, Phytophthora,* and *Rhizoctonia*) associated with root and rhizome rot, and common endophytes of bananas (*Alternaria, Aspergillus, Cladosporium, Epicoccum, Nigrospora, Penicillium, Trichoderma*), were also isolated from these tissues. More than 100 *Fusarium* isolates were obtained, from which 36 that were morphologically similar to *Fusarium oxysporum* were selected and taken to the next stages of identification. Phylogenetic analysis showed that nine of these isolates were in the *F. fujikuroi* species complex, 25 were in *F. oxysporum*, and two in the *F. solani* species complex. Among these complexes, four different *Fusarium* species (*F. musae, F. oxysporum, F. sacchari,* and *F. solani*) were identified.

Maryani *et al.* (2019a) obtained many *Fusarium* isolates from 34 geographically and environmentally different locations in Indonesia, and identified 200 of them using detailed phylogenetic analyses. The pathogen community included 14 *Fusarium* species within four species complexes, and 180 isolates were within *F. oxysporum* species complex (FOSC). Ujat *et al.* (2021) studied *Fusarium* species diversity in 17 regions of Malaysia, and found that most of the 38 isolates (86.8%) obtained were in the FOSC. Within this complex, *F. oxysporum* f. sp. *cubense* was the most frequently isolated species (71.1%), followed by *F. oxysporum* (10.5%) and *F. grosmicheli* (5.3%). Similarly, Karangwa *et al.,* (2018) discriminated *Fusarium* isolates obtained from East and Central African countries using phylogenetic analysis and VCG tests, and identified *F. sacchari* and *F. semitectum* as well as *Fusarium oxysporum* f. sp. *cubense*. Although some of these *F. oxysporum* isolates were confirmed to be pathogenic to banana seedlings, these isolates could not be discriminated using VCG tests. Czislowski *et al.* (2021) obtained 105 isolates from plantations in Australia, from symptomatic and asymptomatic banana plants, recovering fungi belonging to the *F. fujikuroi* and *F. oxysporum* species complexes more frequently than those of *F. solani and F. incarnatum-equiseti* complexes. *Fusarium*

solani and *F. fujikuroi* were found to predominate in the other species complexes. Results from these studies indicate that Fusarium wilt may have different prevalence in different countries, and that banana decline can be caused by non-*Foc*TR4 species.

The TEF 1-α gene was amplified by PCR and sequenced in the present study to make robust distinction between morphologically similar *Fusarium* isolates. While this approach identified species within species complexes, it was insufficient to distinguish between *formae speciales* and physiological races within the *F. oxysporum* species complex. To make robust phylogenetic discrimination between *Fusarium* species, O'Donnell *et al.* (2022) suggested that the RPB1 or RPB2 genes should be studied together with the TEF 1-α gene, but noted that TEF 1-α sequencing results would also be valuable in cases of limited resources. Ujat *et al.* (2021) performed phylogenetic differentiation of *Fusarium* isolates in bananas by sequencing the TEF or Histone-H3 genes, and suggested that working with the TEF 1-α gene revealed more consistent results than those from Histone-H3. Maryani *et al.* (2019a) carried out phylogenetic analyses by combining RPB1, RPB2, and TEF 1-α genes, and made detailed identification of *Fusarium* species complexes from bananas and the species in these complexes. Greatest phylogenetic support was obtained in their study by combining RPB1 and TEF 1 genes. Phylogenetic analyses using the sequences of gene regions proposed by Maryani *et al.* (2019a) could be used to identify *F. oxysporum* f. sp. *cubense*, and assess relationships among isolates. However, since the presence of *Foc*TR4 was to be investigated in the present study by other methods (*Foc*TR4-specific primers and a commercial identification kit), phylogenetic analyses with only the TEF 1-α gene was used as a first stage to confirm sequencing results.

The *Foc*TR4-specific primers (*Foc*TR4F/*Foc*TR4R) identified eight out of the 36 selected isolates, and results were validated with a commercially available diagnostic real-time PCR kit (Clear Detections™) designed for *Foc*TR4 detection. These two detection methods were used to detect first incursions of the pathogen in Colombia (in 2020) and Peru (in 2022). García-Bastidas *et al.* (2020) first tested the *Fusarium* isolates with *Foc*TR4-specific primers to detect the presence of *Foc*TR4 in banana plantations in Colombia. They also confirmed the presence of *Foc*TR4 using the Clear Detection Kit™, loop-mediated isothermal amplification, and whole genome analyses. Acuna *et al.* (2022) examined *Fusarium* isolates from a suspected *Foc*TR4 infested banana plantation in Querecotillo, Peru, and detected this race in that country by conventional PCR (Dita *et al*., 2010; Li *et al*., 2015) and qPCR tests using the Clear Detection Kit™. The studies cited above, which have used various molecular identification methods, indicate that the *Foc*TR4 can be accurately identified based on resources available in most countries.

Regarding pathogenicity, except for *F. solani*, the *Fusarium* species included in the pathogenicity tests of the present study (*F. oxysporum, F. oxysporum* f. sp. *cubense*, and *F. sacchari*) caused mild to severe necroses in the rhizomes of inoculated plants 40 d after inoculation. Discolouration in rhizome cores confirmed the pathogenicity of *Fusarium* isolates identified as *Foc*TR4 and its association with wilt, while the other isolates were associated with root and collar rot. This study is the first to report *F. oxysporum* and *F. sacchari* causing root necrosis, collar and rhizome rots in Türkiye. Maryani *et al.* (2019b) examined *Fusarium* diversity in banana plants in small holder fields in Indonesia, and 90% of the *Fusarium* species isolated from pseudostems were in the *F. oxysporum* species complex, but members of the *F. incarnatum-equiseti*, *F. fujikuroi* and *F. sambucinum* species complexes were also recovered. In their pathogenicity tests, none of the Indonesian *Fusarium* species belonging to these species complexes (including *F. sacchari*) were found to be associated with Fusarium wilt in 'Cavendish' banana plants. The present study results agree with the pathogenicity results of Maryani *et al.* (2019b), but the present study *F. sacchari* isolates caused root collar and rhizome rots. Therefore, *F. sacchari* should not be overlooked in banana plantations. In addition, Cui *et al.* (2021) highlighted horizontal gene transfer between *Fusarium* species, indicating that the potential of *F. sacchari* to cause wilt in bananas should be carefully monitored.

Fusarium oxysporum isolates caused severe symptoms, although not as severe as those caused by *Foc*TR4 isolates. Rhizome necroses started from outside and progressed towards the plant cores, suggesting that *F. oxysporum* isolates also cause root and root collar rot, but not wilt. *Fusarium oxysporum* is an important species, with numerous *formae speciales* and physiological races, now associated with wilt, root/crown rot, damping-off, head blight, and seed/fruit rots in many plants (Edel-Hermann and Lecomte, 2019). The host specificity of *F. oxysporum*, and the fact that some isolates have endophytic or pathogenic characteristics, indicate that the fungus has a complex genetic diversity (Lombard *et al.,* 2019). Alteration of pathogenic characteristics by horizontal gene transfer between isolates has also been reported in *F. oxysporum* (Vlaardingerbroek *et al*., 2016). In pathogenicity tests by Wu *et al.,* (2019), using the 'Cavendish' (AAA) cultivar, only *Foc*TR4 isolates

induced rhizome pith necroses, whereas this symptom was not observed in plants inoculated with *Foc*1 isolates.

The present study has revealed that Fusarium wilt caused by *Foc*TR4 was present but had low prevalence (6.8%) in Turkish banana plantations. Since this race was detected in bananas in closed plastic protected greenhouses, legal and technical requirements have been fulfilled to eradicate the disease in these areas. In addition to wilt caused by *Foc*TR4, some *F. oxysporum* and *F. sacchari* isolates used in this study were found to cause root and collar rots, and, eventually, death of banana seedlings. This is the first report of *F. sacchari* associated with root and collar rot of banana in Türkiye. More research is required to enable rapid and accurate pathogen detection, and to restrain the re-emergence and spread of these diseases in this country.

ACKNOWLEDGEMENTS

The authors thank the Turkish Ministry of Agriculture and Forestry, the General Directorate of Agricultural Research and Policies, Dr Suat Kaymak, Mr Ahmet Yasin Gökçe (Ankara Plant Protection Central Research Institute), Dr Şefika Yavuz (Adana Biological Control Research Institute), The Rectorate of Cukurova University, and the Mersin Banana Farmers Association, for their valuable contributions to this research. The study was financially supported by the Turkish Ministry of Agriculture and Forestry, in project TAGEM/BSAD/A/19/A2/P1/1032, and the Cukurova University Scientific Research Projects Department, in project FDK-2019-11497.

LITERATURE CITED

Acuna R., Rouard M., Leiva A.M., Marquez C., Olortegui J.A., … Dita M., 2022. First report of *Fusarium oxysporum* f. sp. *cubense* tropical race 4 causing Fusarium wilt in Cavendish bananas in Peru. *Plant Disease* 106 (8): 2268. https://doi.org/10.1094/PDIS-09-21-1951-PDN

Aguayo J., Cerf-Wendling I., Folscher A.B., Fourrier-Jeandel C., Ioos R., … Viljoen A., 2021. First report of *Fusarium oxysporum* f. sp. *cubense* tropical race 4 (TR4) causing banana wilt in the Island of Mayotte. *Plant Disease* 105 (1): 219. https://doi.org/10.1094/PDIS-06-20-1196-PDN

Anonymous, 2021. Tarım ürünleri piyasaları; muz (in Turkish). Tarım ve Orman Bakanlığı, Tarımsal Ekonomi ve Politika Geliştirme Enstitüsü resmi internet sitesi, https://arastirma.tarimorman.gov.tr/tepge Accession Date 21.01.2024

Anonymous, 2022. Crop production statistics, Turkish Statistical Institute, https://www.data.tuik.gov.tr/Kategori/GetKategori?p=Tarim-111 Accession Date 31.01.2024.

Bregard C., Baptista P., Chatzivassiliou E., Di Serio F., Gonthier P., … Reignault P.L., 2022. Pest categorisation of *Fusarium oxysporum* f. sp. *cubense* Tropical Race 4. *EFSA Journal* 20 (1): 7092. https://doi.org/10.2903/j.efsa.2022.7092

Chittaraht K., Mostert D., Crew K.S., Viljoen A., Kong G., … Thomas J.E., 2018. First report of *Fusarium oxysporum* f. sp. *cubense* tropical race 4 (VCG 01213/16) associated with Cavendish bananas in Laos. *Plant Disease* 102 (2): 449. https://doi.org/10.1094/PDIS-08-17-1197-PDN

Conde B.D., Pitkethley R.N., 2001. The discovery, identification and management of banana Fusarium wilt outbreaks in the Northern Territory of Australia. In: *Banana Fusarium wilt management: towards sustainable cultivation* (A.B., Molina, N.H., Nik Masdek K.W., Liew, ed.) *Proceedings of the International workshop on the banana Fusarium wilt disease*, Genting Highlands Resort, Malaysia, 18–20 October 1999. INIBAP, Montpellier. pp. 260–265.

Crous P.W., Lombard L., Sondoval-Denis M., Seifert K.A., Schroers H.J., … Thines M., 2021. Fusarium: more than a node or a foot-shaped basal cell. *Studies in Mycology* 98: 100116. https://doi.org/10.1016%2Fj.simyco.2021.100116

Czislowski E., Zeil-Rolfe I., Aitken E.A.B., 2021. Effector profiles of endophytic *Fusarium* associated with asymptomatic banana (*Musa* sp.) Hosts. *International Journal of Molecular Sciences* 22: 2508. https://doi.org/10.3390/ijms22052508

Cui Y., Wu B., Peng A., Song X., Chen X., 2021. The genome of banana leaf blight pathogen *Fusarium sacchari* str. FS66 harbors widespread gene transfer from *Fusarium oxysporum*. *Frontiers in Plant Science* 12: 629859. https://doi.org/10.3389/fpls.2021.629859

Dale J., James A., Paul J.Y., Khanna H., Smith M., … Harding R., 2017. Transgenic Cavendish bananas with resistance to Fusarium wilt tropical race 4. *Nature Communications* 8: 1496. https://doi.org/10.1038/s41467-017-01670-6

Dean R.D., Van Kan J.A.L., Pretorius Z.A., Hammond-Kosack K.E., Di Pietro A., Foster G.D., 2012. The top 10 fungal pathogens in molecular plant pathology. *Molecular Plant Pathology* 13 (4): 414–430. https://doi.org/10.1111/j.1364-3703.2011.00783.x

Dita M.A., Waalwick C., Buddenhagen I.W., Souza M.T., Kema G.H.J., 2010. A molecular diagnostic for tropi-

cal race 4 of the banana fusarium wilt pathogen. *Plant Pathology* 59: 348–357. https://doi.org/10.1111/j.1365-3059.2009.02221.x

Dita M., Barquero M., Heck D., Muzubuti E.S.G., Staver C.P., 2018. Fusarium wilt of banana: current knowledge on epidemiology and research needs toward sustainable disease management. *Frontiers in Plant Sciemce* 9: 1468. https://doi.org/10.3389/fpls.2018.01468

Dong X., Wang M., Ling N., Shen Q., and Guo S., 2016. Potential role of photosynthesis-related factors in banana metabolism and defense against *Fusarium oxysporum* f. sp. *cubense*. *Environmental and Experimental Botany* 129: 4–12. https://doi.org/10.1016/j.envexpbot.2016.01.005

Edel-Hermann V., Lecomte C., 2019. Current status of *Fusarium oxysporum Formae Speciales* and Races. *Phytopathology* 109: 512–530. https://doi.org/10.1094/PHYTO-08-18-0320-RVW

Fourie G., Steenkamp E.T., Gordon T.R., Viljoen A., 2009. Evolutionary relationships among the *Fusarium oxysporum* f.sp. *cubense* vegetative compatibility groups. *Applied and Environmental Biology* 75: 4770–4781. https://doi.org/10.1128/AEM.00370-09

García-Bastidas F.A., Ordonez N., Konkol J., Al-Qasim M., Naser Z., … Kema G.H.J., 2014. First report of *Fusarium oxysporum* f. sp. *cubense* tropical race 4 associated with Panama disease of banana outside Southeast Asia. *Plant Disease* 98(5): 694. https://doi.org/10.1094/pdis-09-13-0954-pdn

García-Bastidas F.A., van der Veen A.J.T., Nakasato-Tagami G., Meijer H.J.G., Arango-Isaza R.E., Kema G.H.J., 2019. An improved phenotyping protocol for Panama disease in banana. *Frontiers in Plant Science* 10: 1006. https://doi.org/10.3389/fpls.2019.01006

García-Bastidas F.A., Quintero-Vargas J.C., Ayala-Vasquez M., Schermer T., Seidl M.F., … Kema G.H.J., 2020. First report of Fusarium wilt tropical race 4 in Cavendish bananas caused by *Fusarium odoratissimum* in Colombia. *Plant Disease* 104 (3): 994. https://doi.org/10.1094/PDIS-09-19-1922-PDN

Gomez K.A., Gomez, A.A., 1984. Statistical procedures for agricultural research (2nd ed.). Wiley 680 pp.

Hasegawa M., Kishino H., Yano T., 1985. Dating of the human-ape splitting by a molecular clock of mitochondrial DNA. *Journal of Molecular Evolution* 22(2): 160–174. https://doi.org/10.1007/BF02101694

Herbert J.A., Marx D., 1990. Short-term control of Panama disease of bananas in South Africa. *Phytoparasitica* 22: 339–340. https://journals.co.za/doi/pdf/10.10520/AJA03701263_1354

Hung N.T., Hung N.Q., Mostert D., Viljoen A., Chao C.P., … Molina A.B., 2018. First report of Fusarium wilt on Cavendish bananas, caused by *Fusarium oxysporum* f. sp. *cubense* tropical race 4 (VCG 01213/16), in Vietnam. *Plant Disease* 102 (2): 448. https://doi.org/10.1094/PDIS-08-17-1140-PDN

Karangwa P., Blomme G., Beed F., Niyongere C., Viljoen A., 2016. The distribution and incidence of banana Fusarium wilt in subsistence farming systems in east and central Africa. *Crop Protection* 84: 132–140. https://doi.org/10.1016/j.cropro.2016.03.003

Karangwa P., Mostert D., Ndayihanzamaso P., Dubois T., Niere B., … Viljoen A., 2018. Genetic Diversity of *Fusarium oxysporum* f. sp. *cubense* in East and Central Africa. *Plant Disease* 102: 552–560. https://doi.org/10.1094/PDIS-02-17-0282-RE

Leslie F.J, Summerell A.B., 2006. *The Fusarium Laboratory Manual*. Blackwell Publishing, London, UK. pp 220.

Li W.M., Dita M., Wu W., Hu G.B., Xie J.H., … Ge X.J., 2015. Resistance sources to *Fusarium oxysporum* f. sp. *cubense* tropical race 4 in banana wild relatives. *Plant Pathology* 64: 1061–1067. https://doi.org/10.1111/ppa.12340

Lin Y.H., Chang J.Y., Liu E.T., Chao C.P., Huang J.W., … Chang P.F.L., 2009. Development of a molecular marker for specific detection of *Fusarium oxysporum* f. sp. *cubense* race 4. *European Journal of Plant Pathology* 123: 353–365. https://doi.org/10.1007/s10658-008-9372-4

Lombard L., Sandoval-Denis M., Cai L., Crous P.W., 2019. Changing the game: resolving systematic issues in key *Fusarium* species complexes. *Persoonia* 43: 1–2. https://doi.org/10.3767/persoonia.2019.43.00

Maryani N., Lombard L., Poerba Y.S., Subandiyah S., Crous P., … Kema H.J.G. 2019a. Phylogeny and genetic diversity of the banana Fusarium wilt pathogen *Fusarium oxysporum* f. sp. *cubense* in the Indonesian centre of origin. *Studies in Mycology* 92: 155–194. https://doi.org/10.1016/j.simyco.2018.06.003

Maryani N., Sandoval-Denis M., Lombard L., Crous P.W., Kema G.H.J., 2019b. New endemic *Fusarium* species hitch-hiking with pathogenic *Fusarium* strains causing Panama disease in small-holder banana plots in Indonesia. *Persoonia* 43: 48–69. https://doi.org/10.3767/persoonia.2019.43.02

Maymon M., Shpatz U., Harel Y.M., Levy E., Elkind G., … Freeman S., 2018. First report of *Fusarium oxysporum* f. sp. *cubense* tropical race 4 causing Fusarium Wilt of Cavendish bananas in Israel. *Plant Disease* 102 (12): 2655. https://doi.org/10.1094/PDIS-05-18-0822-PDN

Mejias Herrera R., Hernandez Y., Magdama F., Mostert D., Bothma S., … Maryse E.E. 2023. First report of Fusarium wilt of Cavendish bananas caused by

Fusarium oxysporum f. sp. *cubense* tropical race 4 in Venezuela. *Plant Disease* 107 (10) 3297. https://doi.org/10.1094/PDIS-04-23-0781-PDN

Nelson P.E., Tousson T.A., Marassas W.F.O., 1983. *Fusarium species*: *An Illustrated Manual for Identification*. The Pennsylvania State University Press, University Park and London. pp. 193.

O'Donnell K., Cigelnik E., Nirenberg H.I., 1998. Molecular systematics and phylogeography of the *Gibberella fujikuroi* species complex. *Mycologia* 90 (3): 465–493. https://doi.org/10.1080/00275514.1998.12026933

O'Donnell K., Whitaker B.K., Laraba I., Proctor R.H., Brown D.W., … Geiser D.M., 2022. DNA sequence-based ıdentification of *Fusarium*: a work in progress. *Plant Disease* 106: 1597–1609. https://doi.org/10.1094/PDIS-09-21-2035-SR

Ordóñez N., García-Bastidas F., Laghari H.B., Akkary M.Y., Harfouche E.N., … Kema G.H.J., 2016. First report of *Fusarium oxysporum* f.sp. *cubense* tropical race 4 causing Panama disease in Cavendish bananas in Pakistan and Lebanon. *Plant Disease*, 100(1): 209. https://doi.org/10.1094/PDIS-12-14-1356-PDN

Özarslandan M., Akgül D.S., 2020. First report of *Fusarium oxysporum* f. sp. *cubense* race 4 causing Fusarium wilt disease of banana in Turkey. *Plant Disease* 104(3): 974. https://doi.org/10.1094/PDIS-09-19-1881-PDN

Pegg K.G., Coates L.M., O'Neill W.T.O., Turner D.W., 2019. The epidemiology of Fusarium wilt of banana. *Frontiers in Plant Science* 10: 1395. https://doi.org/10.3389/fpls.2019.01395

Perez-Vicente L., Dita M.A., 2014. Fusarıum wilt of banana or Panama disease by *Fusarium oxysporum* f. sp. *cubense*: A review on history, symptoms, biology, epidemıology and management. In: *FAO Technical Manual, Prevention and Diagnostic of Fusarium wilt (Panama disease) of Banana Caused by Fusarium oxysporum f. sp. cubense Tropical Race 4* (L., Perez-Vicente, M., Dita., E., Martínez- de la Parte ed.), 6–30.

Ploetz R.C., 2006. Fusarium wilt of banana is caused by several pathogens referred to as *Fusarium oxysporum* f. sp. *cubense*. *Phytopathology* 96: 653–656. https://doi/pdf/10.1094/PHYTO-96-0653

Ploetz R.C., 2015. Fusarium wilt of banana. *Phytopathology* 12: 1512–1521. http://dx.doi.org/10.1094/PHYTO-04-15-0101-RVW

Ploetz R.C., Pegg K., 1997. Fusarium wilt of banana and Wallace's line: was the disease originally restricted to his Indo-Malayan region? *Australasian Plant Pathology* 26: 239–249. https://doi.org/10.1071/AP97039

Qi Y.X., Zhang X., Pu J.J., Xie Y.X., Zhang H.Q., … Huang S.L., 2008. Race 4 identification of *Fusarium oxysporum* f. sp. *cubense* from Cavendish cultivars in Hainan province, China. *Australasian Plant Disease Notes* 3 (1): 46–47. https://doi.org/10.1007/BF03211234

Seifert K.A., 1996. *Fusarium interactive key*. Agriculture and Agri-Food Canada. 65 pp.

Stover R.H., 1962. *Fusarial wilt (Panama disease) of bananas and other Musa species.* UK: Commonwealth Mycological Institute. 117 pp.

Tava V., Prigitano A., Cortesi P., Espoto M.A., Pasquali M., 2021. *Fusarium musae* from diseased bananas and human patients: susceptibility to fungicides used in clinical and agricultural settings. *Journal of Fungi* 7: 784. https://doi.org/10.3390/jof7090784

Thangavelu R., Mostert D., Gopi M., Ganga Devi P., Padmanaban M., Viljoen A., 2019. First detection of *Fusarium oxysporum* f. sp. *cubense* tropical race 4 (TR4) on Cavendish banana in India. *European Journal of Plant Pathology* 154: 777–786. https://doi.org/10.1007/s10658-019-01701-6

Thi L.L., Mertens A., Vu D.T., Vu T.D., Anh Minh P.L., … Janssens S.B., 2022. Diversity of *Fusarium* associated banana wilt in northern Viet Nam. *MycoKeys* 87: 53–76. https://doi.org/10.3897/mycokeys.87.72941

Townsend G.R., Heuberger J.W., 1943. Methods for estimating losses caused by diseases in fungicide experiments. *The Plant Disease Reporter* 27: 340–343.

Ujat A.H., Vadamalai G., Hattori Y., Nakashima C., Wong C.K.F., … Zulperi D., 2021. Current classification and diversity of *Fusarium* species complex, the causal pathogen of Fusarium wilt disease of banana in Malaysia. *Agronomy* 11: 955. https://doi.org/10.3390/agronomy11101955

Viljoen A. 2020. *Emerging Plant Diseases and Global Food Security*. American Phytopathological Society, St. Paul, MN, United States of America. 159 pp.

Vlaardingerbroek I., Beerens B., Rose L., Fokkens L., Cornelissen B.J., … Rep M., 2016. Exchange of core chromosomes and horizontal transfer of lineage-specific chromosomes in *Fusarium oxysporum*. *Environmental Microbiology* 18: 3702–3713. https://doi.org/10.1111/1462-2920.13281

Wu K., Chen W., Yang S., Wen Y., Zheng Y., … Wang Z., 2019. Isolation and identification of *Fusarium oxysporum* f. sp. *cubense* in Fujian Province, *China. Journal of Integrative Agriculture* 18(8): 1905–1913. https://doi.org/10.1016/S2095-3119(18)62149-5

Zheng S.J., Garcia-Bastidas F.A., Li X., Zeng L., Bai T., … Kema G.H.J., 2018. New geographical insights of the latest expansion of *Fusarium oxysporum* f.sp. *cubense* tropical race 4 Into the Greater Mekong Subregion. *Frontiers in Plant Science* 9: 457. https://doi.org/10.3389/fpls.2018.00457

Phytopathologia Mediterranea
The international journal of the
Mediterranean Phytopathological Union

Firenze University Press
www.fupress.com/pm

Research Papers

Plant extracts to manage the parasitic weed branched broomrape (*Phelipanche ramosa*)

Ezzudeen EISAWI[1,2,*], Generosa Jenny CALABRESE[1], Angela BOARI[3], Maurizio VURRO[3]

[1] *International Center for Advanced Mediterranean Agronomic Studies, Mediterranean Agronomic Institute of Bari (CIHEAM Bari), via Ceglie 9, 70010 Valenzano, Italy*
[2] *Cairo University; Faculty of Agriculture, Field crops and weed science department, El-Gamaa Street/Orman - Giza, 12613 Cairo, Egypt*
[3] *Institute of Sciences of Food Production (ISPA), National Research Council (CNR), via Amendola 122/O, 70125 Bari, Italy*
*Corresponding author. Email: ezzudeen.eisawi@cu.edu.eg

Summary. Some weeds have parasitic lifestyles, causing severe problems in agriculture. These plants include *Phelipanche ramosa* (L.) Pomel (branched broomrape). Greenhouse and nursery trials were carried out to assess control of *P. ramosa* using organic extracts from 14 plant species. The parameters recorded were counts of living and dead tubercles of *P. ramosa* and fresh weights of living tubercles. Organic extract of *Olea europea* reduced lengths of germ tubes during *P. ramosa* seed germination, and extracts of *Bidens bipinnata* and *Dittrichia viscosa* reduced production and development of the parasite's tubercles, with very encouraging results in reducing seed germination rates. This research provides knowledge insights on the potential use of plant secondary metabolites to limit spread of *P. ramosa*, addressing an increasing challenge for organic crop production.

Keywords. Parasitic weeds, organic farming, allelopathy, agricultural sustainability.

Citation: Eisawi, E., Calabrese, G.J., Boari, A., & Vurro, M. (2024). Plant extracts to manage the parasitic weed branched broomrape (*Phelipanche ramosa*). *Phytopathologia Mediterranea* 63(2):223-232. doi:10.36253/phyto-15164

Accepted: June 25, 2024

Published: September 15, 2024

Data Availability Statement: All relevant data are within the paper and its Supporting Information files.

Competing Interests: The Author(s) declare(s) no conflict of interest.

Editor: Diego Rubiales, Institute for Sustainable Agriculture, (CSIC), Cordoba, Spain.

ORCID:
EE: 0009-0003-9555-6123
GJC: 0000-0002-9540-5339
AB: 0000-0003-1444-019X
MV: 0000-0001-6875-4093

INTRODUCTION

Root parasitic weeds pose serious problems in agriculture, causing severe crop losses in yield and quality. These weeds rely on neighbouring host plants for their whole life cycles, depleting water and nutrients, and severely reducing host plant growth. Their life cycles are spent mostly underground, and when they emerge, most of the damage they cause has already been accomplished. These parasitic weeds also produce large numbers of long-lived seeds that determine the formation of persistent seedbanks, making the soil infestation, after occurring, almost impossible to remove (Fernández-Aparicio *et al.*, 2020).

The most damaging root parasitic weeds, including broomrapes (*Orobanche* and *Phelipanche* spp.) and witchweeds (*Striga* spp.), are widespread in Europe, Africa, and Asia, while other parasitic weeds (*Alec-*

tra, *Aeginetia*, *Buchnera*, and *Rhamphicarpa*) are also becoming increasingly important. Due to their characteristics, traditional control strategies based on herbicides, agronomic practices, and resistant varieties, are only partially effective, particularly in low-input crops (Parker, 2021; Rubiales, 2023), or cannot be fully applied in organic farming and other agriculture systems. To effectively manage parasitic weeds, it is important to understand the physiological and molecular mechanisms of their germination, haustorium development, as well as crop resistance, and to discover new herbicides and bioherbicides and their applications for control of parasitic weeds (Kebede and Ayana, 2018).

Phelipanche ramosa (L.) Pomel., commonly known as branched broomrape, has a broad host range, primarily including *Solanaceae* hosts such as tomato, potato, and tobacco. This parasitic weed also infects other plant including *Brassicaceae*, *Cannabaceae*, *Fabaceae*, *Apiaceae*, and *Asteraceae* (Musselman and Parker, 1982). *P. ramosa* is native in Europe, Africa, and Asia, and has high adaptability and evolution to expand presence and host range. Furthermore, with the high dispersal capabilities, new areas are being infested by *P. ramosa* (Rubiales, 2020). The detrimental impacts of this parasitic weed on host plants surpasses the anticipated consequences based on the parasite's dry weight. This could be due to arid conditions or imbalanced effects on the fruiting capacity of host plants compared to their vegetative biomass. Documented yield losses due to broomrape in tomato and tobacco crops are likely to range from 30% to 50% (Parker, 2013).

The present study aimed to assess the potential of plant extracts as natural herbicides against *P. ramosa*. The focus was to assess their effects during the most vulnerable stages of *P. ramosa* growth cycle: seed germination, tubule elongation, haustorium attachment, and tubercle development. By targeting these stages, the aim was to develop an effective and precise strategy for controlling *P. ramosa*. This approach utilizes the unique properties of selected plant compounds to disrupt specific growth processes, offering an avenue for eco-friendly and sustainable weed management. The plants assessed in this study are from families known for producing secondary metabolites or phytotoxic substances, enhancing the likelihood of identifying potent natural herbicides. Additionally, the selected plants are prevalent throughout the Mediterranean region, and are easily propagated and multiplied, providing practical advantages for further experimentation and application of their metabolites. Except for *Dittrichia viscosa* (L.) Greuter, these plant species assessed here have not been previously assessed against *P. ramosa*. This study was a preliminary screening of the plant species with potential bioactive organic compounds, and the aim was to find novel extracts, to purify them, and obtain compounds with potential as broomrapes bioherbicides.

MATERIALS AND METHODS

Extraction

Plant materials (leaves and green twigs) were harvested during November 2022 to March 2023 from 14 plant species. These included; *Ailanthus altissima* (Mill.) Swingle, *Amaranthus retroflexus* (L.), *Avena fatua* (L.), *Bidens bipinnata* (L.), *Brassica nigra* (L.), *Cirsium arvense* (L.) Scop., *Diplotaxis erucoides* (L.), *Dittrichia viscosa* (L.) Greuter, *Ecballium elaterium* (L.) A.Rich., *Juglans regia* (L.), *Olea europaea* (L.), *Oxalis pes-caprae* (L.), *Solanum nigrum* (L.), and *Sorghum halepense* (L.). The plants were harvested from the experimental field at the Mediterranean Agronomic Institute of Bari (CIHEAM Bari), Valenzano, southern Italy.

The harvested plant materials were cleaned and dried in a fan oven at 45°C for 3 d. They were then ground until to powder and kept in air-sealed plastic bags at 8°C, until further processing and extraction.

Dried plant material (100 g of each plant) was added to a glass flask, and 500 mL of methanol solution (H_2O: MeOH, 1:1, v:v) was added. The flasks were then kept in stirred conditions at room temperature (25°C) for 24 h, to separate the aqueous extracts (Fernández-Aparicio *et al.*, 2021). The obtained solutions were then filtered from solid plant material using gauze cloth, and centrifuged at 7000 rpm at 5°C for 10 min. Supernatants were separated from the solid phases after centrifugation. Dichloromethane (CH_2Cl_2; 600 mL) was then added (three times, each of 200 mL CH_2Cl_2) as organic solvent to the supernatants, to obtain the organic extracts. Separating funnels were then used to separate the aqueous extracts from organic extracts. The organic extracts were then dehydrated and filtered with cotton wool, and evaporated using a rotavapor (Dor and Hershenhorn, 2012). The concentrated organic extracts were purified from any methanol traces by nitrogen evaporator, and were then kept in freezer at -12°C.

Seed germination test

The aim of this test was to measure effects of the plant extracts on the germination of *P. ramosa*. The test was conducted using the design described by Boari and Vurro (2004), to verify which organic extracts of the

harvested plants had potential to suppress or inhibit germination of *P. ramosa* seeds. After selecting and collecting the 14 adventitious plants, the 14 organic extracts were compared with experimental controls containing water, GR_{24}[1] and MeOH. For each individual test, a triangular piece of filter paper was placed into a Petri dish (total of 45 dishes), and 1 mL of water solution containing organic extract (0.5 mg mL^{-1}). Conditioned *P. ramosa* seeds (approx. 100 seeds) were added to each Petri dish, and the dishes were then wrapped in plastic wrap and covered with aluminum foil. The dishes were then placed in the incubator. After 72 h, germination percentages were observed using a binocular microscope. Seeds with emerged radicles were classified as germinated. The design used for this experiment was a completely random block with three replicates. Treatments that reduced *P. ramosa* seed germination were considered effective.

Assessment of infectivity of tomato by Phelipanche ramosa *in plastic file bags*

Tomato seeds (*Solanum lycopersicum* cv. Marmande) were sown into vermiculite in Styrofoam trays and were irrigated frequently as needed. The resulting seedlings were fertilized once each week with Hoagland solution (Chen *et al.*, 1961).

Modified plastic file bags were prepared for this test (Amsellem *et al.*, 2001; Vurro *et al.*, 2006). An A4 plastic files were sealed at the edges with a heat sealer and were each cut in the middle to form a window-like flipper with the same dimensions as a fiberglass sheet held inside the plastic file. A plastic tube (20 cm length) was also inserted into each file. The fiberglass sheet was moistened with 12 mL of sterilized tap water. Seven plastic crates were prepared to host 70 of these plastic file bags assessments of *P. ramosa* infection of tomato seedlings. Dry *P. ramosa* seeds (30 mg) were then sprinkled evenly distributed on the fiberglass sheet. These plastic file bags were then placed inside a plastic crate modified for the purpose. The experimental design was a completely randomized design with ten replicates. One day later, tomato seedlings (24 d old, two to three true leaves) were removed from the trays. Their roots were washed and cleaned from vermiculite and the plants were inserted into each plastic bag, positioned on the fiberglass paper, and fixed in place by scotch tape. These plants were irrigated and fertilized with Hoagland solution periodically. Organic extracts (500 mL each; 0.5 mg mL^{-1}) were prepared from *A. altissima*, *B. bipinnata*, *C. arvense*, *D. viscosa*, *J. regia*, and *O. europaea*, so that each tomato plant received 10 mL of treatment solution. The treatments were applied 26 d after the plants were transplanted. The trial lasted about 2 months.

At the end of the trial, living and dead tubercles were counted, and fresh weights of living tubercles were measured. The tubercles were divided into three categories, A (small), B (medium), or C (large), based on their surface areas (visible from outside the bag) as A, <0.3 cm^2, B, 0.3–0.6 cm^2, or C, >0.6 cm^2. Measurement of surface areas and counting of the tubercles were done using ImageJ version 1.54d, free software for image analysis (Schneider *et al.*, 2012).

Pot experiment

This experiment aimed to evaluate effectiveness of treatments under greenhouse and nursery conditions. Tomato seeds (cv. Marmande) were sowed into seedling trays containing peatmoss. The trays were kept in a growth chamber under optimal conditions and irrigated as needed. Seventy pots (each 1 L capacity) were prepared, each containing a layer of tissue paper at the bottom to block the drainage holes and prevent soil escape. A layer (2–3 cm thick) of peatmoss mixed with soil was added, followed by a layer of soil inoculated with *P. ramosa* seeds (approx. 0.85 L of soil mixed with 24 mg of *P. ramosa* seeds). Tomato plants (23 d old, 3 to 4 true leaves) were then transplanted into the pots, and another 2–3 cm layer of peatmoss was added to each pot. The pots were irrigated periodically from above with water, and Hoagland solution was added for fertilization. The experiment was a completely randomized design with ten replicates.

Each pot received 50 mL (conc. 0.5 mg mL^{-1}) of extracts from either *A. altissima*, *B. bipinnata*, *C. arvense*, *D. viscosa*, *J. regia*, and *O. europaea*. Final evaluations were carried out 20 d after treatment. The trial lasted 2 months. At the end of the trial, numbers of living *P. ramosa* tubercles were counted, and fresh weights of tubercles were measured. The tubercles were divided into three categories, as A (small, <0.3 cm^2), B (medium, 0.3–0.6 cm^2), or C (large, >0.6 cm^2).

Statistical analyses

RStudio IDE of the R programming language (RStudio Team, 2020) was used to analyze the results obtained and determine statistical significance of mean differences, using core packages (R Core Team, 2023),

[1] A synthetic germination stimulant for broomrape seeds (Lechat *et al.*, 2012).

as well as the "tidyverse", "knitr", "car", "haven", "TukeyC", "ggpubr", "dunn.test", "reshape2", "superb", and "ggplot2" metapackage (John Fox and Sanford Weisberg, 2019; Wickham *et al*., 2019; Jose *et al*., 2023; Smith, 2023; Yihui Xie, 2023).All the variables were first tested for normal distributions using the Shapiro-Wilk normality test, and variables that followed normal distributions ($P > 0.05$) were subjected to Analysis of Variance (2-way ANOVA) tests, followed by Tukey's HSD post-hoc tests at $P = 0.05$. Means were then visualized using boxplots. Variables that did not follow normal distributions (Shapiro-Wilk; $P > 0.05$) were analyzed using analysis of variance (Kruskal–Wallis, non-parametric) of independent samples, followed by Dunn's post-hoc test at $P = 0.05$, then visualization using Boxplots.

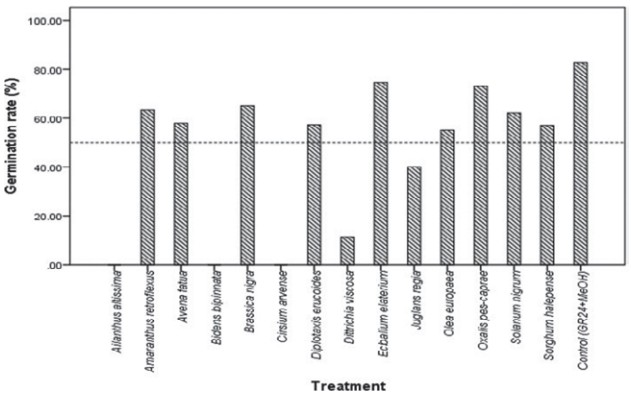

Figure 1. Germination (%) of preconditioned *Phelipanche ramosa* seeds treated with different plant extracts (0.5 mg mL^{-1}), and synthetic germination stimulant (Control; see materials and methods for the details of the bioassay).

RESULTS

Seed germination assays

The organic extracts of three plants, *A. altissima*, *B. bipinnata*, and *C. arvense*, applied at 0.5 mg mL^{-1} to preconditioned seeds of *P. ramosa* caused complete inhibition of germination. (from 81% to 0%); the extract of *D. viscosa* was also active, reducing germination rate by 68.5% (from 81% to 12.5%), and the extract from *J. regia* gave germination of 44% (Figure 1). All the other extracts reduced *P. ramosa* seed germination to a lesser extent in comparison with the control. The extracts which reduced germination to less than 50% were selected for further assessments in plastic bag bioassays (below) for the *P. ramosa* infection phase. The extracts from *A. altissima*, *B. bipinnata*, *C. arvense*, *D. viscosa* and *J. regia* were selected for the tomato plant assay (below), together with that from *O. europaea*. that, although reduced germination by only 26% (from 81 to 55%), induced an unusual deformation to the germ tube of the *P. ramosa* seed (Figure 2).

Tomato infectivity test in plastic file bags

This test aimed to evaluate effects of the selected organic extracts applied to tomato plants during the *P. ramosa* infection phase.

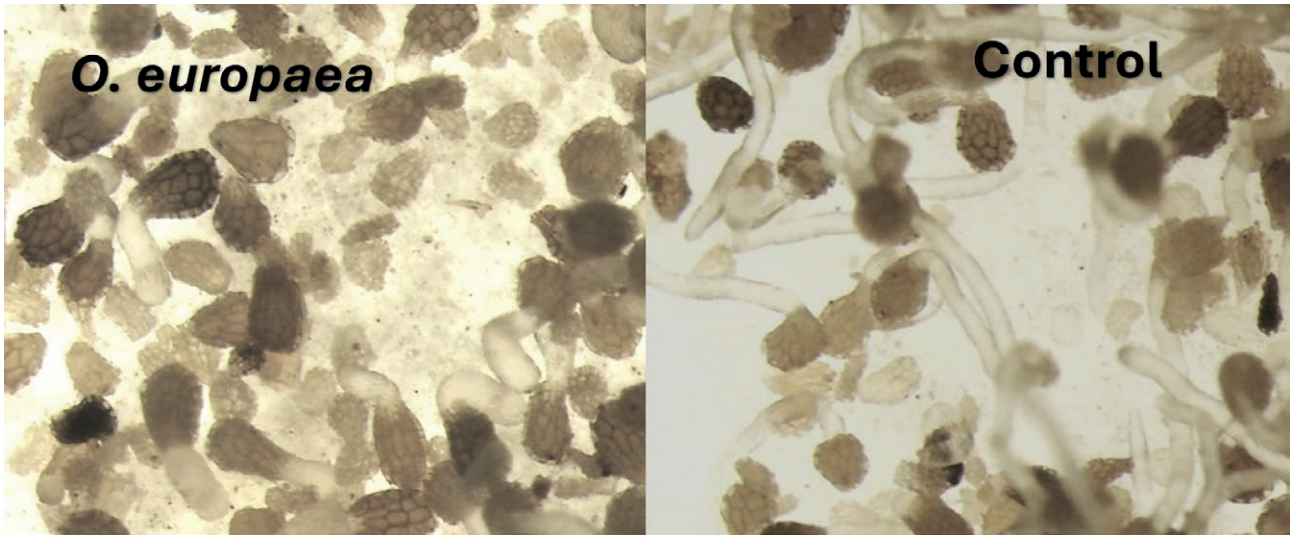

Figure 2. Binocular microscope images showing deformed germ tubes of *Phelipanche ramosa* seeds after treatment with organic extract from *Olea europaea* (left image), compared to the control treatment (right image).

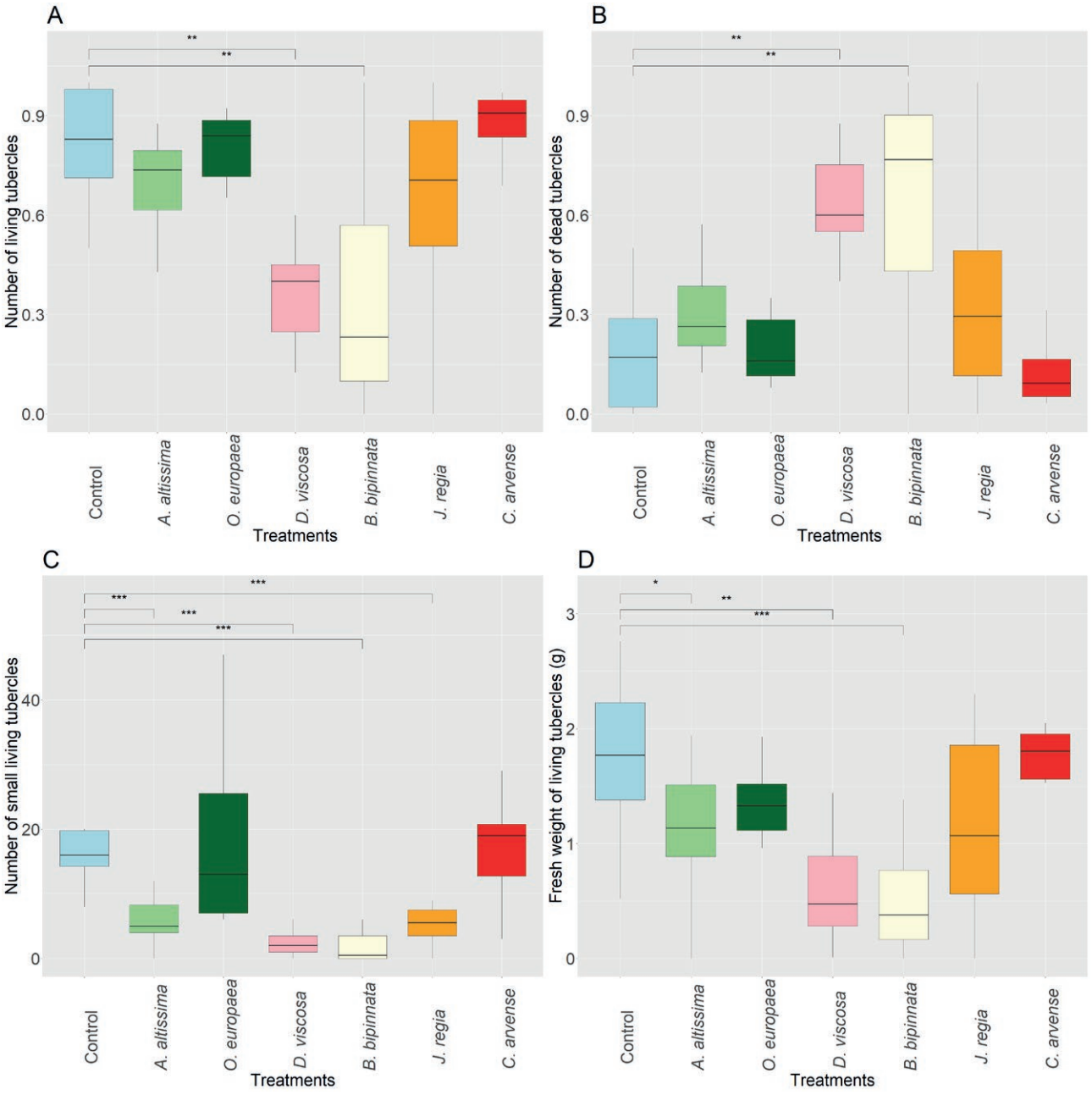

Figure 3. Boxplots of parameters for *Phelipanche ramosa* tubercles after exposure to organic extracts from different plants ("Treatments") in the tomato infectivity test. A, numbers of living *P. ramosa* tubercles; B, numbers of dead tubercles; C, numbers of small living tubercles; D, fresh weights of living tubercles.

After 30 d from the treatment application, the numbers of live *P. ramosa* tubercles was reduced by organic extracts from *B. bipinnata*, *D. viscosa*, *J. regia* and *A. altissima* to be 0.2, 0.4, 0.7, and 0.75, respectively, compared to the control (0.85) (Figure 3 A).

The numbers of dead *P. ramosa* tubercles treated with organic extracts of *B. bipinnata* was the greatest (mean = 0.8), followed by *D. viscosa* (0.6), both of which were greater ($P < 0.05$) than the control (mean = 0.17) (Figure 3 B).

The numbers of small (<0.3 cm^2) *P. ramosa* tubercles were reduced from the treatments of organic extracts from *B. bipinnata* (mean = 2.2), *D. viscosa* (2.7), *J. regia* (5.1), and *A. altissima* (mean =

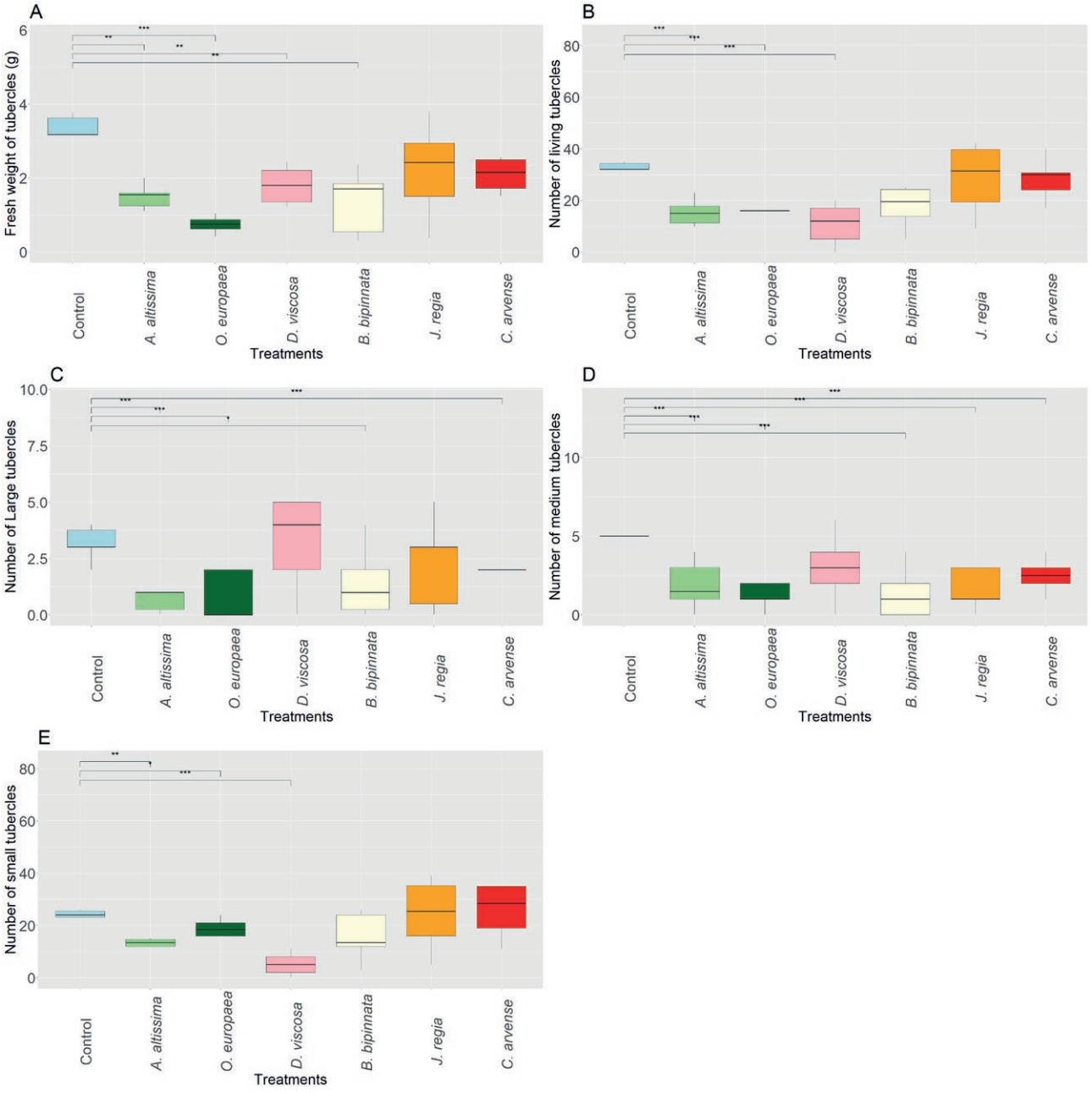

Figure 4. Boxplots regarding the pot experiment carried out by using the organic extracts of the plants. A: fresh weight of living *P. ramosa* tubercles; B: number of living tubercles; C: number of large-size tubercles; D: number of medium-size tubercles; E: the number of small-size tubercles.

5.7), compared with the control (mean = 17.9) (Figure 3 C).

Application of organic extracts reduced mean fresh weights of *P. ramosa* living tubercles to 0.51 g for *B. bipinnata*, 0.56 g for *D. viscosa*, 1.0 g for *A. altissima*, 1.1 g for *J. regia*, and 1.3 g for *O. europaea*, compared to 1.8 g for the control treatment (Figure 3 D).

Pot experiment

Twenty d after application of treatments, fresh weights of *P. ramosa* living tubercles treated with the organic extracts of *O. europaea* (mean = 0.7 g) were less compared to the controls (3.1 g). All the other treatments with *B. bipinnata* (mean = 1.3 g), *A. altissima*

(1.5 g), *D. viscosa* (1.6 g), *C. arvense* (2.0 g), and *J. regia* (mean = 2.2 g) also reduced tubercule fresh weights (Figure 4 A).

Numbers of living tubercles were reduced by applying organic extracts of *D. viscosa* (mean = 11.2), *A. altissima* (14.2), *O. europaea* (14.4) and *B. bipinnata* (24.6), compared with the control (mean = 31.9) (Figure 4 B).

The numbers of tubercles with sizes >0.6 cm^2 were less from the treatments with organic extracts of *A. altissima* (mean = 0.7), *O. europaea* (0.8), and *B. bipinnata* (mean = 1.5), compared to the control (mean = 3.2; Figure 4 C).

Numbers of tubercles with medium size (0.3-0.6 cm^2) were less from all the treatments of organic extracts of *O. europaea* (mean = 1.2), *B. bipinnata* (1.3), *J. regia* (2.6), *A. altissima* (1.8), *C. arvense* (2.4), and *D. viscosa* (mean = 3.1), compared to the control (mean = 5.4; Figure 4 D).

The numbers of small (<0.3 cm^2) *P. ramosa* tubercles were less from all of the treatments with organic extracts of *D. viscosa* (mean = 5.2), *A. altissima* (11.6), and *O. europaea* (mean = 16.3), compared with the control (mean = 23.1; Figure 4 E).

DISCUSSION

This study included bioassays to assess the effectiveness of plant organic extracts for inhibiting seed germination and tubercle development of *P. ramosa*. In the initial germination bioassay, three extracts, those from *A. altissima*, *B. bipinnata*, and *C. arvense*, completely inhibited seed germination at the assessed concentrations. Two other extracts, from *D. viscosa* and *J. regia*, had comparatively lower activity. In the tomato infectivity assessments, *B. bipinnata* and *A. altissima* were consistently toxic to *P. ramosa*, but *C. arvense* had reduced effectiveness compared to the initial seed germination bioassay. This variation indicates a need to explore potential factors contributing to the observed assay differences. In contrast, the *D. viscosa* extract gave stronger inhibition of *P. ramosa* in the tomato infectivity bioassay than in the germination assay.

In the assessment of *O. europaea* and *D. viscosa* extracts in the tomato infectivity assay, *O. europaea* gave less inhibition but longer phytotoxicity, while *D. viscosa* had stronger toxicity but for shorter periods. This possibly explains why the numbers of medium-sized living tubercles were greater from *O. europaea* than *D. viscosa* treatments. The most effective organic extracts against *P. ramosa* in tomato infectivity assay were from *B. bipinnata* and *D. viscosa*, with both extracts giving the least numbers of living tubercles, lowest fresh weights of living tubercles, and greatest numbers of dead tubercles.

In the pot experiment, most of the extracts behaved differently compared to the tomato infectivity assay. This could have been due to the different substrates used in the two assays. In soil, there can be interactions with microorganisms and soil physical and chemical complexes that lead to the decomposition and alteration of biochemicals in organic extracts. This could lead to different effects and functions (positive or negative) of the compounds at the whole system level. In the pot experiment, the host plants were in conditions similar to those of normal growth, and the plants would behave as in field conditions. The extract that showed greatest contrast in effects from the tomato infectivity assay to the pot bioassay was *O. europaea*, having greater activity the pot bioassay than the tomato infectivity assay.

The most effective treatments for reducing numbers of living *P. ramosa* tubercles were *D. viscosa*, *O. europaea*, *A. altissima*, and *B. bipinnata*, although *D. viscosa* and *A. altissima* were less effective in case of the living tubercule fresh weight. The overall performance of these extracts ranged from very inhibitory to mildly inhibitory compared to the experimental control.

Treatment with *D. viscosa* resulted in more large tubercles and fewer small tubercules than from the other treatments. This treatment was probably more effective on small than on large tubercles, and possibly because the active compound was unstable and rapidly degraded in the soil, it could not affect growth of, already well-developed, tubercles that are more dependent on the host plant, and more resistant to the treatment in the surrounding environment. Number of large tubercles also influenced fresh weights of the living tubercles. For example, *O. europaea* and *B. bipinnata* gave lower fresh weights of tubercles than *D. viscosa* and *D. viscosa* gave greater numbers of large tubercles than *O. europaea* and *B. bipinnata*. Extracts from *O. europaea* and *B. bipinnata* gave greater numbers of small tubercles than that from *D. viscosa*.

Activity of extracts from *B. bipinnata* have not been previously investigated for effects species of broomrapes, and allelopathic effects of *B. bipinnata* have been rarely noted. The plant genus *Bidens* is well known for its strong allelopathic activity, which probably arises from a variety of secondary metabolites, including phenolics, saponins, flavonoids, glycosides of flavones, polyacetylenes, terpenes, chalcone glucosides, phenylpropanoid glucosides, and terpenoids (Brandão *et al.*, 1997). The invasive relative from the same genus, *B. pilosa* has been widely studied, and produces many secondary metabo-

lites and allelochemicals active against other plant species. Khanh *et al.* (2009) reported that application of *B. pilosa* biomass suppressed weeds, but this has not been assessed against *P. ramosa*.

Organic extracts of *D. viscosa* were assessed for effects on germination of *P. ramosa* seeds by Serino *et al.* (2021), and our findings agree to the results found by them regarding the germination bioassay of *P. ramosa*, despite that they used biodegradable polymer to preserve release of the extract over long periods to improve the efficacy of the extract. Furthermore, many Other studies have reported inhibitory effects of organic extracts from *D. viscosa* on *P. ramosa* seed germination and tubercle development (Moeini *et al*., 2019; Boari *et al*., 2021). Laboratory investigation showed that *D. viscosa* produced several secondary metabolites, including sesquiterpenoids, flavonoids, and caffeic acids, although in varying concentrations across different plant parts (Grauso *et al*., 2020).

Olea europaea was studied against *P. ramosa* in tomato crops by Qasem (2020), who reported that olive mill wastewater and olive cakes reduced dry weight of *P. ramosa*, with wastewater being most active. Those results indicate possible presence of secondary metabolites able to reduce *P. ramosa* seed germination. However, those results from wastewater and olive cake by-products from olive fruits, while the present study assessed organic extracts from the leaves. Olive fruits and leaves have different secondary metabolite profiles, so the present study results provide expanded knowledge on *O. europaea* phytotoxicity. Research by Di Donna *et al.* (2010) and Kabbash *et al.* (2023) analyzed metabolites produced in *O. europaea* leaves using high performance liquid chromatography and electrospray ionization tandem mass spectrometry. This showed the presence of twelve phenolic compounds in the leaves.

The present study results for *A. altissima* agree with those of Scavo and Mauromicale (2020), who reported that extract from this plant can completely inhibit germination of *P. ramosa*. Strong allelopathic activity lead those authors to extract canthin-6-one (CO) alkaloids and ailanthone which have strong allelopathic activity (Cho *et al*., 2018).

In plastic bags, extracts from *A. altissima*, *C. arvense*, and *J. regia* did not show strong activity as in Petri dish tests. This could be due to the instability of the phytotoxic compounds active against *P. ramosa*. The active compound must be present in appropriate concentrations when *P. ramosa* seeds (already conditioned) are germinating to be effective. If the time of application is too early, the compounds could degrade without affecting *P. ramosa* seed germination. The active compounds must be present during germination, but not after attachment, since the tubercles become more isolated from the environment and are completely dependent on the host plants (Vurro *et al*., 2019).

In conclusion, this study has provided valuable insights into the potential of organic extracts from several spontaneous plants for control of *P. ramosa*. Organic extracts of *B. bipinnata* and *D. viscosa* should be further investigated because of their demonstrated inhibitory effects on *P. ramosa* seed germination and tubercule development. The organic extract of *O. europaea* also reduced *P. ramosa* tubercule fresh weights. Different extraction procedures, without solvents, could be assessed in future experiments, which could be utilized for chemical-free extraction. It would be also advisable to identify the chemical compounds active in suppressing P. ramosa seed germination and tubercle development to better understand the mechanism of action to improve the effectiveness of *P. ramosa* control. Effective plant species should be also tested in field conditions, where they could be directly cultivated and incorporated into soil prior to tomato cultivation. Appropriate application times should be investigated so that the decomposition of these plant materials would timely release the secondary bioactive metabolites into the soil and provides effective broomrape control. This would be an innovative and sustainable approach and could provide intensive solution for combating parasitic weeds.

ACKNOWLEDGMENTS

The authors of this paper thank the Faculty of Agriculture, Cairo University, for allowing the first author of this paper to conduct Master of Science studies at CIHEAM Bari.

AUTHOR CONTRIBUTIONS

Conceptualization, MV, GJC and AB; methodology, MV, AB and GJC; validation, MV, GJC and AB; formal analysis, EE; investigation, EE; resources, GJC, MV and AB; data curation, EE and GJC; writing of original draft, EE; writing after review and editing, MV and GJC; visualization, EE; supervision, GJC, MV and AB; project administration, GJC.

LITERATURE CITED

Amsellem Z., Kleifeld Y., Kerenyi Z., Hornok L., Goldwasser Y., Gressel J., 2001. Isolation, identification, and activity of mycoherbicidal pathogens from juve-

nile broomrape plants. *Biological Control* 21: 274–284. DOI: 10.1006/bcon.2001.0934.

Boari A., Vurro M., 2004. Evaluation of *Fusarium spp*. and other fungi as biological control agents of broomrape (*Orobanche ramosa*). *Biological Control* 30: 212–219. DOI: https://doi.org/10.1016/j.biocontrol.2003.12.003.

Boari A., Vurro M., Calabrese G.J., Mahmoud M.N.Z., Cazzato E., Fracchiolla M., 2021. Evaluation of *Dittrichia viscosa* (L.) greuter dried biomass for weed management. *Plants* 10: 147. DOI: https://doi.org/10.3390/plants10010147.

Brandão M.G.L., Krettli A.U., Soares L.S.R., Nery C.G.C., Marinuzzi H.C., 1997. Antimalarial activity of extracts and fractions from *Bidens pilosa* and other Bidens species (Asteraceae) correlated with the presence of acetylene and flavonoid compounds. *Journal of Ethnopharmacology* 57: 131–138. DOI: https://doi.org/10.1016/S0378-8741(97)00060-3.

Chen T.-A., Kilpatrick R.A., Rich A.E., 1961. Sterile culture techniques as tools in plant nematology research. *Phytopathology* 51: 799 - 800.

Cho S.-K., Jeong M., Jang D.S., Choi J.-H., 2018. Anti-inflammatory Effects of Canthin-6-one Alkaloids from *Ailanthus altissima*. *Planta Medica* 50: 527–535. DOI: 10.1055/s-0043-123349.

Di Donna L., Mazzotti F., Naccarato A., Salerno R., Tagarelli A., … Sindona G., 2010. Secondary metabolites of *Olea europaea* leaves as markers for the discrimination of cultivars and cultivation zones by multivariate analysis. *Food Chemistry* 121: 492–496. DOI: https://doi.org/10.1016/j.foodchem.2009.12.070.

Dor E., Hershenhorn J., 2012. Allelopathic effects of *Inula viscosa* leaf extracts on weeds. *Allelopathy Journal* 30: 281–289.

Fernández-Aparicio M., Cimmino A., Soriano G., Masi M., Vilariño S., Evidente A., 2021. Assessment of weed root extracts for allelopathic activity against *Orobanche* and *Phelipanche* species. *Phytopathologia Mediterranea* 60: 455–466.

Fernández-Aparicio M., Delavault P., Timko M.P., 2020. Management of Infection by Parasitic Weeds: A Review. *Plants* 9: 1184. DOI: 10.3390/plants9091184.

Grauso L., Cesarano G., Zotti M., Ranesi M., Sun W., … Lanzotti V., 2020. Exploring *Dittrichia viscosa* (L.) Greuter phytochemical diversity to explain its antimicrobial, nematicidal and insecticidal activity. *Phytochemistry Reviews* 19: 659–689. DOI: https://doi.org/10.1007/s11101-019-09607-1.

John Fox and Sanford Weisberg, 2019. *An {R} Companion to Applied Regression*. Thousand Oaks, CA, USA, Sage.

Jose F., Enio G. J., Ivan A., 2023. Conventional Tukey Test. Ilheus, Bahia, Brasil, Universidade Estadual de Santa Cruz - UESC.

Kabbash E.M., Abdel-Shakour Z.T., El-Ahmady S.H., Wink M., Ayoub I.M., 2023. Comparative metabolic profiling of olive leaf extracts from twelve different cultivars collected in both fruiting and flowering seasons. *Scientific Reports* 13: 612. DOI: https://doi.org/10.1038/s41598-022-27119-5.

Kebede M., Ayana B., 2018. Economically important parasitic weeds and their management practices in crops. *Journal of Environment and Earth Science* 8: 104–115.

Khanh T.D., Cong L.C., Xuan T.D., Uezato Y., Deba F., … Tawata S., 2009. Allelopathic plants: 20. Hairy beggarticks (*Bidens pilosa* L.). *Allelopathy Journal* 24: 243–259.

Lechat M.-M., Pouvreau J.-B., Péron T., Gauthier M., Montiel G., … Macherel D., 2012. PrCYP707A1, an ABA catabolic gene, is a key component of *Phelipanche ramosa* seed germination in response to the strigolactone analogue GR24. *Journal of Experimental Botany* 63: 5311–5322.

Moeini A., Masi M., Zonno M.C., Boari A., Cimmino A., … Evidente A., 2019. Encapsulation of inuloxin A, a plant germacrane sesquiterpene with potential herbicidal activity, in β-cyclodextrins. *Organic & Biomolecular Chemistry* 17: 2508–2515.

Musselman L.J., Parker C., 1982. Preliminary host ranges of some strains of economically important broomrapes (*Orobanche*). *Economic Botany* 36: 270–273.

Parker C., 2013. *The Parasitic Orobanchaceae: Parasitic Mechanisms and Control Strategies,* Berlin, Heidelberg, Germany PP: 313–344. Available at: https://link.springer.com/chapter/10.1007/978-3-642-38146-1_18

Parker C., 2021. A Personal History in Parasitic Weeds and Their Control. *Plants* 10: 2249. DOI: 10.3390/plants10112249.

Qasem J.R., 2020. Control of branched broomrape (*Orobanche ramosa* L.) in tomato (*Lycopersicon esculentum* Mill.) by olive cake and olive mill waste water. *Crop Protection* 129: 105021. DOI: https://doi.org/10.1016/j.cropro.2019.105021

R Core Team, 2023. A language and environment for statistical computing. Vienna, Austria., R Foundation for Statistical Computing.

RStudio Team, 2020. RStudio: *Integrated Development Environment for R*. Boston, MA, RStudio, PBC.

Rubiales D., 2020. Broomrape threat to agriculture. *Outlooks on Pest Management* 31: 141–145.

Rubiales D., 2023. Managing Root Parasitic Weeds to Facilitate Legume Reintroduction into Mediterranean Rain-Fed Farming Systems. *Soil Systems* 7: 99.

Scavo A., Mauromicale G., 2020. Integrated weed management in herbaceous field crops. *Agronomy* 10: 466.

Schneider C.A., Rasband W.S., Eliceiri K.W., 2012. NIH Image to ImageJ: 25 years of image analysis. *Nature Methods* 9: 671–675. DOI: https://doi.org/10.1038/nmeth.2089.

Serino N., Boari A., Santagata G., Masi M., Malinconico M., … Vurro M., 2021. Biodegradable polymers as carriers for tuning the release and improve the herbicidal effectiveness of *Dittrichia viscosa* plant organic extracts. *Pest Management Science* 77: 646–658.

Smith H.W. and E.M. and D., 2023. haven: Import and Export "SPSS", "Stata" and "SAS" Files.

Vurro M., Boari A., Pilgeram A.L., Sands D.C., 2006. Exogenous amino acids inhibit seed germination and tubercle formation by *Orobanche ramosa* (Broomrape): Potential application for management of parasitic weeds. *Biological Control* 36: 258–265. DOI: https://doi.org/10.1016/j.biocontrol.2005.09.017.

Vurro M., Boari A., Thiombiano B., Bouwmeester H., 2019. Strigolactones and parasitic plants. *Strigolactones-Biology and Applications* 89–120. DOI: https://doi.org/10.1007/978-3-030-12153-2_3.

Wickham H., Averick M., Bryan J., Chang W., McGowan L.D., … Hester J., 2019. Welcome to the Tidyverse. *Journal of Open Source Software* 4: 1686.

Yihui Xie, 2023. knitr: *A General-Purpose Package for Dynamic Report Generation in R Markdown.*Available at: https://bookdown.org/yihui/bookdown/bookdown.pdf

Phytopathologia Mediterranea
The international journal of the
Mediterranean Phytopathological Union

Firenze University Press
www.fupress.com/pm

Research Papers

Fusarium species and assessments of mycotoxin (deoxynivalenol), in wheat seeds from different regions of Türkiye

Kubra SARACOGLU[1,2], Greice Amaral CARNEIRO[1,*], Eleonora CAPPELLETTI[1], Fatma Sara DOLAR[2], Antonio PRODI[1]

[1] *Department of Agricultural and Food Sciences (DISTAL), University of Bologna, 40126 Bologna, Italy*
[2] *Ankara University, Faculty of Agriculture, Department of Plant Protection, 06120 Ankara, Türkiye*
*Corresponding author. Email: greice.amaral2@unibo.it

Summary. Wheat cultivation is important in Turkish agriculture, which ranks 10th among international wheat producers, and is an important wheat exporter, particularly to Europe. *Fusarium*-related threats, such as Fusarium Head Blight (FHB) and Fusarium Crown and Root Rots (FCR, FRR), and related mycotoxin seed contamination, jeopardize product quality. This study analysed 65 wheat seed samples for presence of *Fusarium* species, from cultivars of *Triticum aestivum* (bread wheat) and *T. durum* (durum wheat) collected from seven regions of Türkiye. PCR with specific primers, and phylogenetic analyses of TEF1-*α* segments, discriminated *Fusarium* species. Levels of the mycotoxin deoxynivalenol (DON) in flour samples were also evaluated. Out of 195 *Fusarium* isolates, the prominent species included *F. graminearum* (32% of isolates), *F. proliferatum* (16%), *F. avenaceum* (11%), *F. clavum* (11%), and *F. verticillioides* (7%). Less frequently isolated species were *F. oxysporum* (6%), *F. acuminatum* (3%), *F. ramigenum* (3%), *F. culmorum* (3%), *F. poae* (2%), *F. sambucinum* (2%), *F. tricinctum* (2%), *Fusarium* sp. FTSC12 (2%), *F. andiyazi* (1%), and *F. equiseti*, *F. incarnatum*, and *F. fasciculatum* (each 0.5%). Five of the 65 samples tested positive for DON, with two exceeding the European Commission threshold for mycotoxin contamination; one bread wheat from the Black Sea region, known for its annual rainfall, and a durum wheat sample from southeastern Anatolia, which had the highest detected DON level of 1730 μg kg^{-1}. Among these samples *F. graminearum* was the predominant species. As *F. andiyazi* and *F. ramigenum* are not normally associated with wheat plants, a pathogenicity test was conducted with two isolates of each of these species, revealing no pathogenicity on the durum wheat cultivar 'San Carlo'. These results provide a basis for managing fungal threats and mycotoxin contamination, safeguarding the quality of wheat grain as an essential agricultural product.

Keywords. Species complex, DON, wheat kernels, molecular characterisation, phylogenetic analyses.

OPEN ACCESS

Citation: Saracoglu, K., Carneiro, G.A., Cappelletti, E., Dolar, F.S., & Prodi, A. (2024). *Fusarium* species and assessments of mycotoxin (deoxynivalenol), in wheat seeds from different regions of Türkiye. *Phytopathologia Mediterranea* 63(2): 233-253. doi: 10.36253/phyto-15152

Accepted: June 4, 2024

Published: September 15, 2024

Data Availability Statement: All relevant data are within the paper and its Supporting Information files.

Competing Interests: The Author(s) declare(s) no conflict of interest.

Editor: Mario Masiello, National Research Council, (CNR), Bari, Italy.

ORCID:
KS: 0009-0001-5235-1860
GAC: 0000-0003-4115-5677
EC: 0000-0003-3931-9249
FSD: 0000-0003-1634-4046
AP: 0000-0002-7221-7271

INTRODUCTION

The wheat species *Triticum aestivum* L. and *Triticum durum* Desf. are important cereals produced in Türkiye, where wheat production in 2021 was 17,650,000 tonnes from 6,623,061 ha, placing the country as 10th among world producers (FAOSTAT, 2021). Wheat production in Türkiye is 80% for food, 11% for feed, and 6% for seed, and wheat is produced across all regions of Türkiye, with most in Central Anatolia, Marmara, and Southeastern Anatolia regions (TÜİK, 2021). In this country, 82% of wheat production is from 495 varieties of bread wheat, and 128 high-quality durum wheat varieties are registered or approved for cultivation (BÜGEM, 2021; TÜİK, 2021).

The diseases Fusarium Head Blight (FHB) and Fusarium Crown/Root Rots (FCR, FRR), caused by different *Fusarium* species, are among major contributors to large international economic losses in wheat production (Savary *et al*., 2019). FCR and FRR cause pre- and post-emergence death of wheat seedlings, particularly in areas with dry weather and minimal tillage. In contrast, FHB reduces grain yield and quality by generating small, weak, and poor-quality seeds, and hollow, white spikes that occur during anthesis under humid conditions (Smiley *et al*., 2005; Scherm *et al*., 2013). Seeds obtained from diseased plants have reduced viability, are smaller than those from healthy plants, are wrinkled and pale, and occasionally have black spots on the surfaces (Busman *et al*., 2012; Shah *et al*., 2018; Hassani *et al*., 2019).

FHB, FCR and FRR are usually caused by multiple *Fusarium* species complex groups. *Fusarium graminearum*, *F. pseudograminearum* and *F. culmorum* are the predominant species in wheat production areas (Shikur Gebremariam, 2015; Zhou *et al*., 2019; Abdallah-Nekache *et al*., 2019; Dehghanpour-Farashah *et al*., 2019; Rigorth *et al*., 2021; Leyva-Mir *et al*., 2022). *Fusarium acuminatum*, *F. avenaceum*, and *F. tricinctum*, in the *Fusarium tricinctum* species complex (FTSC), are emerging as wheat pathogens in Europe, especially related to FHB (Senatore *et al*., 2021). These species are difficult to distinguish morphologically, and require use of molecular identification techniques for discrimination. *Fusarium* sp. FTSC 1 to FTSC 11, *F. flocciferum*, *F. torolosum*, *F. iranicum* and *F. gamsii* are often reported on wheat, although they have minor impacts on production (O'Donnell *et al*., 2018; Summerell, 2019; Torbati *et al*., 2019).

Fusarium species can occur singly or coexist in the different organs of wheat plants, varying from year to year as different pathogens dominate. Identification of *Fusarium* species in wheat seeds is important, as these pathogens can disseminate across regions or countries. This is facilitated by use of seeds for crop establishment, and can cause diseases with far-reaching consequences.

Fusarium species are also responsible for production and accumulation of mycotoxins in wheat grains (Isebaert *et al*., 2009). The most important mycotoxins in wheat are trichothecenes and zearalenone, including deoxynivalenol (DON), in the trichothecenes B group and which is synthesized by several *Fusarium* species (Xu and Nicholson, 2009; Mishra *et al*., 2019; Wang *et al*., 2019; Mousavi Khaneghah *et al*., 2020). DON has harmful effects on human and animal health, including oxidative and endoplasmic reticulum stress, ribosomal toxicity, hepatotoxicity, immunotoxicity, gastrointestinal toxicity, and neurotoxicity (Tian *et al*., 2022). This mycotoxin is stable and heat-resistant, making it difficult to prevent DON contamination in food products for humans and animals (Guo *et al*., 2020). European Commission Regulation (EU) 2024/1022 of 8th April 2024, amending Regulation (EU) 2023/915 on maximum levels of deoxynivalenol (DON) in foodstuffs, stipulates that the maximum limits for DON in unprocessed wheat as 1000 μg kg^{-1} for bread wheat and 1500 μg kg^{-1} for durum wheat. Considering the prevalence of DON-producing *F. graminearum* and *F. culmorum* in European wheat crops, DON has emerged as the dominant mycotoxin associated with FHB in European food and feed wheat (Waalwijk *et al*., 2003; Gruber-Dorninger *et al*., 2019; Eskola *et al*., 2020). Species such as *F. pseudograminearum* and *F. cerealis* (syn. *F. crookwellence*) have also been reported on wheat as DON producers (Ji *et al*., 2019; Haidukowski *et al*., 2022). In Türkiye, changes in climatic conditions between regions have promoted the spread of several foodborne mycotoxins, especially in cereal crops and cereal products; based on a literature review, Ünüsan (2019) showed that mycotoxin levels exceeding EU limits had been found in 2% of cereals and their derivatives.

In recent years, global climate changes have been altering the profiles of typical *Fusarium* species on wheat, which may also cause variability of associated mycotoxins. Vigilant monitoring and differentiation of *Fusarium* species, along with the associated mycotoxins in wheat, are therefore important. This proactive approach is required for early-stage assessment of mycotoxin risks, enabling formulation and implementation of effective control strategies (Tunali *et al*., 2008; Haidukowski *et al*., 2022). In Türkiye, which is a leading bread and durum wheat producing country, identification of *Fusarium* species in wheat seeds may affect production quality and sanitation.

The main purpose of the present study was to collect samples of bread and durum wheat seed cultivars from

across the Turkish regions, to assess by molecular characterization the contaminating *Fusarium* species, and to determine their DON production. This information would provide a starting point for implementing management strategies for wheat diseases and mycotoxin contamination caused by *Fusarium* in Türkiye, and for regulating DON through increased understanding of *Fusarium* populations in wheat seeds grown in Türkiye.

MATERIALS AND METHODS

Investigation areas, wheat sampling and fungal isolation

In 2020, 2021, and 2022 a total of 65 samples of wheat seeds (250 g each) were obtained of which 45 were of bread wheat and 20 of durum wheat. The samples represented the different wheat production in Türkiye (Figure 1). One hundred seeds from each sample, randomly selected out of the 250 g, were disinfected in a sodium hypochlorite solution for 4 min and then rinsed twice in sterile water. For each sample, ten Petri plates containing Potato Dextrose Agar (PDA, Biolife Italiana) supplemented with streptomycin sulfate (0.16 g L^{-1}; Sigma Aldrich) were prepared with ten seeds added to each plate. The cultures were then incubated at 24°C in the dark, and fungal growth was observed from the 5th day of incubation. Colonies resembling *Fusarium* species, according to morphological characteristics on PDA (Leslie and Summerell, 2006), were selected and each transferred to a new PDA plate and then incubated for 7 d at 22°C in darkness. A single conidium procedure (Leslie and Summerell, 2006) was used to ensure reliable isolate characterization. Incidence of *Fusarium* colonies was determined by calculating the percentage relative to the total number of seeds from which the isolations were made. Morphologically identified isolates of *F. graminearum*, *F. culmorum*, *F. proliferatum*, *F. verticillioides* and *F. poae* were subjected to molecular analyses with species-specific primers, while colonies belonging to the *Fusarium tricinctum* species complex (FTSC) and *Fusarium incarnatum-equiseti* species complex (FIESC) were subjected to phylogenetic analyses with the TEF1-α gene.

PCR-based diagnoses with specific primers, and phylogenetic analyses of FIESC and FTSC groups

Pure cultures of representative colonies displaying morphological characteristics of *F. graminearum*, *F. culmorum*, *F. proliferatum*, *F. verticillioides* or *F. poae* were transferred onto fresh PDA and were then incubated at 22°C for 1 week to obtain enough mycelium for genomic DNA isolation using the protocol described by Prodi *et*

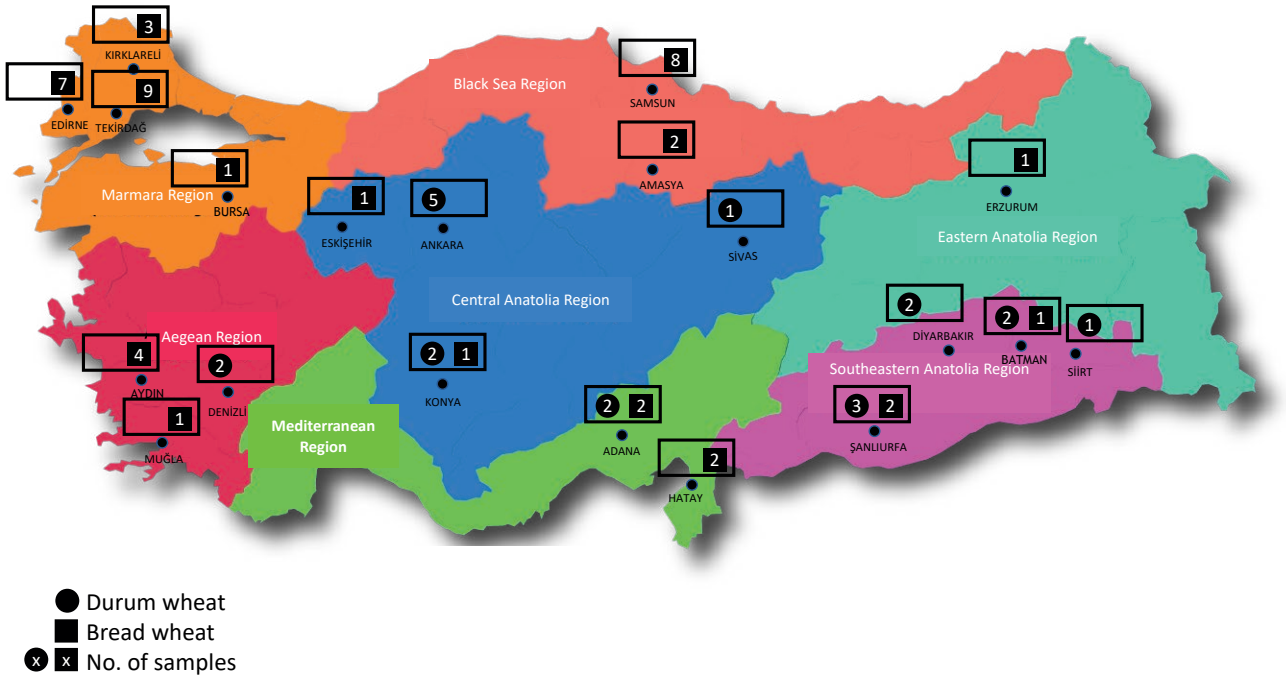

Figure 1. Map of Türkiye showing the regions from which samples were collected for this study.

Table 1. Data on the *Fusarium* isolates obtained from wheat seed samples in 2020, 2021, and 2022, and the corresponding quantities of DON mycotoxin detected in each sample.

Sample No.	Wheat cultivar	Wheat type	Turkish provinces	Region	Year	Isolate code	*Fusarium* species	DON (μg kg^{-1})
1	Kızıltan-91	Durum wheat	Denizli	Aegean	2022	1311a	*F. ramigenum*	20
						1312a	*F. culmorum*	<LOD
						1312b	*F. culmorum*	
						1312c	*F. graminearum*	
						1312d	*F. graminearum*	
2	Çeşit-1252	Durum wheat	Denizli	Aegean	2022	-	-	0
3	Cumhuriyet-75	Bread wheat	Muğla	Aegean	2020	281	*F. proliferatum*	0
						277a	*F. oxysporum*	
						277b	*F. oxysporum*	
						278	*F. oxysporum*	
4	Masaccio	Bread wheat	Aydın	Aegean	2021	982a**	*F. incarnatum*	0
5	Sagittario	Bread wheat	Aydın	Aegean	2021	995	*F. proliferatum*	10
								<LOD
6	Adana 99	Bread wheat	Aydın	Aegean	2021	112	*F. proliferatum*	10
						115	*F. proliferatum*	<LOD
						116 (a=b)	*F. acuminatum**	
						116 (a=b)	*F. acuminatum**	
						119	*F. clavum*	
7	Negev	Bread wheat	Aydın	Aegean	2021	-	-	0
8	Kate-A1	Bread wheat	Amasya	Black Sea	2020	-	-	0
9	Flamura-85	Bread wheat	Amasya	Black Sea	2020	-	-	0
10	Sakin	Bread wheat	Samsun	Black Sea	2021	1230b	*F. graminearum*	1150
						1230c	*F. graminearum*	
						1230d	*F. graminearum*	
						1232c	*F. graminearum*	
						1232d	*F. graminearum*	
						1233b	*F. graminearum*	
						1234b	*F. avenaceum*	
						1235B	*F. avenaceum**	
						1236A	*F. avenaceum**	
						1236c	*F. graminearum*	
						1236d	*F. graminearum*	
						1237a	*F. graminearum*	
						1237b	*F. graminearum*	
						1237BmonoA	*F. avenaceum**	
						1237c	*F. graminearum*	
11	Pandas	Bread wheat	Samsun	Black Sea	2021	328a	*F. graminearum*	40
						328b	*F. graminearum*	<LOD
						328c	*F. graminearum*	
						330B	*F. avenaceum**	
						331	*F. poae*	
						332a	*F. clavum*	
						332B	*F. avenaceum**	
						335	*F. clavum*	
						336a	*F. graminearum*	
						336b	*F. graminearum*	
						336c	*F. graminearum*	
						337	*F. clavum*	

(Continued)

Table 1. (Continued).

Sample No.	Wheat cultivar	Wheat type	Turkish provinces	Region	Year	Isolate code	*Fusarium* species	DON (μg kg^{-1})
12	Canik	Bread wheat	Samsun	Black Sea	2021	81	*F. graminearum*	110
						82	*F. graminearum*	<LOD
						86A	*F. acuminatum**	
						86e	*F. graminearum*	
13	Altındane	Bread wheat	Samsun	Black Sea	2021	169a	*F. clavum*	320
						169B	*F. ramigenum*	
						171a	*F. oxysporum*	
						171b	*F. proliferatum*	
						173a	*F. proliferatum*	
						173B	*F. avenaceum**	
						174a	*F. proliferatum*	
						174B	*F. acuminatum**	
						175a	*F. verticillioides*	
						175b	*F. oxysporum*	
						176A	*F. avenaceum**	
						176b	*F. ramigenum*	
						177a	*F. oxysporum*	
						177b	*F. verticillioides*	
						177c	*F. verticillioides*	
						177d	*F. ramigenum*	
						178B	*F. andiyazi*	
						178a	*F. graminearum*	
						178c	*F. graminearum*	
						178d	*F. graminearum*	
14	Bafra	Bread wheat	Samsun	Black Sea	2021	91A**	*F. fasciculatum*	110
						91B	*F. avenaceum**	<LOD
						92a	*F. ramigenum*	
						92B	*F. ramigenum*	
						93A	*F. avenaceum**	
						95A**	*F. clavum*	
						95b	*F. clavum*	
						95C	*F. avenaceum**	
						95D	*F. avenaceum**	
						95x	*F. proliferatum*	
						95Z	*F. andiyazi*	
						98a	*F. graminearum*	
						98b	*F. graminearum*	
						98c	*F. graminearum*	
						98d	*F. graminearum*	
						98e	*F. proliferatum*	
						99	*F. verticillioides*	
						100C	*F. acuminatum*	
15	Nevzatbey	Bread wheat	Samsun	Black Sea	2021	190a	*F. poae*	710
						190b	*F. poae*	
						191	*F. poae*	
						195	*F. avenaceum*	
						197A	*F. avenaceum*	
						198A	*F. avenaceum**	
						198B	*F. avenaceum**	

(Continued)

Table 1. (Continued).

Sample No.	Wheat cultivar	Wheat type	Turkish provinces	Region	Year	Isolate code	*Fusarium* species	DON (μg kg^{-1})
16	Kirve	Bread wheat	Samsun	Black Sea	2021	102a	*F. proliferatum*	170
						102b	*F. sambucinum*	<LOD
						105B	*F. avenaceum**	
						105C	*F. avenaceum**	
						107a	*F. sambucinum*	
						107b	*F. sambucinum*	
						109a	*F. oxysporum*	
						109b	*F. graminearum*	
						110a	*F. graminearum*	
						110b	*F. graminearum*	
						110c	*F. graminearum*	
						110d	*F. graminearum*	
						117C	*F. avenaceum**	
17	Efe	Bread wheat	Samsun	Black Sea	2021	179a	*F. proliferatum*	380
						179b	*F. graminearum*	
						180C	*F. avenaceum**	
						182	*F. graminearum*	
						183a	*F. graminearum*	
						183b	*F. proliferatum*	
						186	*F. avenaceum*	
						187a	*F. proliferatum*	
						187b	*F. graminearum*	
18	Kızıltan-91	Durum wheat	Konya	Central Anatolia	2022	1265a	*F. clavum*	0
						1266a	*F. culmorum*	
						1266b	*F. culmorum*	
						1266d	*F. culmorum*	
						1272a	*F. graminearum*	
						1272b	*F. graminearum*	
19	Vehbibey	Durum wheat	Ankara	Central Anatolia	2022	-		0
20	Ankara98	Durum wheat	Ankara	Central Anatolia	2022	1324a	*F. clavum*	0
						1324b	*F. clavum*	
						1329a	*F. clavum*	
						1329b	*F. clavum*	
21	Mirzabey	Durum wheat	Ankara	Central Anatolia	2022	-		0
22	Eminbey	Durum wheat	Ankara	Central Anatolia	2022	1354a	*F. graminearum*	40
						1354b	*F. clavum*	<LOD
						1356	*F. avenaceum*	
						1356a	*F. proliferatum*	
						1360	*F. proliferatum*	
23	Kızıltan-91	Durum wheat	Sivas	Central Anatolia	2022	1364	*F. clavum*	0
24	Kızıltan-91	Durum wheat	Konya	Central Anatolia	2022	-		0
25	İmren	Durum wheat	Ankara	Central Anatolia	2022	-		0
26	Albachiara	Bread wheat	Konya	Central Anatolia	2020	215	*F. verticillioides*	0
						217	*F. verticillioides*	
						219	*F. verticillioides*	
27	Flamura-85	Bread wheat	Eskişehir	Central Anatolia	2020	-		0
28	Flamura-85	Bread wheat	Kırklareli	Marmara	2020	-		10
								<LOD

(Continued)

Table 1. (Continued).

Sample No.	Wheat cultivar	Wheat type	Turkish provinces	Region	Year	Isolate code	*Fusarium* species	DON (μg kg^{-1})
29	Rumeli	Bread wheat	Tekirdağ	Marmara	2020	-		10 <LOD
30	Kağan	Bread wheat	Tekirdağ	Marmara	2020	1689	*F. proliferatum*	0
						1691a	*F. proliferatum*	
						1691b	*F. proliferatum*	
						1696	*F. proliferatum*	
						1697	*F. proliferatum*	
31	Kobra-59	Bread wheat	Tekirdağ	Marmara	2020	-		0
32	Turkuaz	Bread wheat	Tekirdağ	Marmara	2020	919	*F. verticillioides*	0
						927	*Fusarium* sp. FTSC12*	
33	Akmira	Bread wheat	Tekirdağ	Marmara	2020	-		0
34	Maden	Bread wheat	Tekirdağ	Marmara	2020	1315	*F. acuminatum*	0
						1318a	*F. verticillioides*	
						1318b	*F. verticillioides*	
						1319a	*F. proliferatum*	
						1319b	*F. verticillioides*	
						1320	*F. proliferatum*	
						1321	*Fusarium* sp. FTSC12*	
35	Hakan	Bread wheat	Tekirdağ	Marmara	2020	931	*Fusarium* sp. FTSC12*	0
						933	*F. proliferatum*	
36	Tekir	Bread wheat	Tekirdağ	Marmara	2020	-		0
37	TT601	Bread wheat	Tekirdağ	Marmara	2020	1334	*F. verticillioides*	0
						1335	*F. proliferatum*	
						1337**	*F. clavum*	
						1338	*F. proliferatum*	
38	Kayra	Bread wheat	Bursa	Marmara	2020	-		220 <LOQ
39	Tekirdağ	Bread wheat	Kırklareli	Marmara	2020	-		0
40	Yüksel	Bread wheat	Kırklareli	Marmara	2020	-		0
41	Kate A-1	Bread wheat	Edirne	Marmara	2020	-		0
42	Esperia	Bread wheat	Edirne	Marmara	2020	131	*F. clavum*	0
						134	*F. clavum*	
						2030	*F. proliferatum*	
43	Rumeli	Bread wheat	Edirne	Marmara	2020	144a	*F. oxysporum*	10 <LOD
						144b	*F. oxysporum*	
						148	*F. clavum*	
						2042	*F. graminearum*	
44	Eylül	Bread wheat	Edirne	Marmara	2020	1142a**	*F. clavum*	10
						1145	*F. oxysporum*	
						1147	*F. oxysporum*	
45	Saraybosna	Bread wheat	Edirne	Marmara	2020	-		0
46	Dropia	Bread wheat	Edirne	Marmara	2020	959	*F. clavum*	0
47	Glosa	Bread wheat	Edirne	Marmara	2020	1346	*F. proliferatum*	10 <LOD
						1352**	*F. clavum*	
48	Masaccio	Bread wheat	Hatay	Mediterranea	2021	-		10
49	Sarıbaşak	Durum wheat	Adana	Mediterranea	2022	-		0

(Continued)

Table 1. (Continued).

Sample No.	Wheat cultivar	Wheat type	Turkish provinces	Region	Year	Isolate code	*Fusarium* species	DON (μg kg^{-1})
50	Ayzer	Durum wheat	Adana	Mediterranea	2022	-		0
51	Adana-99	Bread wheat	Adana	Mediterranea	2021	-		0
52	Tekira	Bread wheat	Adana	Mediterranea	2021	-		0
53	Sagittario	Bread wheat	Hatay	Mediterranea	2021	-		0
54	Kızıltan-91	Durum wheat	Şanlıurfa	Southeast Anatolia	2021	-		0
55	Ağabey	Durum wheat	Şanlıurfa	Southeast Anatolia	2020	-		0
56	Fırat-93	Durum wheat	Şanlıurfa	Southeast Anatolia	2020	-		0
57	Fırat-93	Durum wheat	Siirt	Southeast Anatolia	2021	1019	*F. proliferatum*	0
						1024	*F. graminearum*	
						1025	*F. proliferatum*	
58	Svevo (Zivago)	Durum wheat	Diyarbakır	Southeast Anatolia	2021	-		0
59	Burgos	Durum wheat	Batman	Southeast Anatolia	2021	1363a	*F. graminearum*	10
						1363b	*F. graminearum*	<LOD
						1363c	*F. graminearum*	
						1363d	*F. verticillioides*	
						1365a	*F. graminearum*	
						1365b	*F. graminearum*	
						1365c	*F. graminearum*	
						1365d	*F. graminearum*	
						1370	*F. verticillioides*	
60	Tosunbey	Bread wheat	Batman	Southeast Anatolia	2021	-		0
61	Fırat-93	Durum wheat	Diyarbakır	Southeast Anatolia	2021	1164a	*F. graminearum*	1730
						1164b	*F. graminearum*	
						1165a	*F. graminearum*	
						1165b	*F. graminearum*	
						1166a	*F. graminearum*	
						1166b	*F. graminearum*	
						1169	*F. graminearum*	
						1170a	*F. proliferatum*	
						1170b	*F. proliferatum*	
						1171a**	*F. equiseti*	
						1172a	*F. graminearum*	
						1172b	*F. graminearum*	
						1172c	*F. graminearum*	
						1173a	*F. graminearum*	
						1173b	*F. graminearum*	
						1173c	*F. graminearum*	
62	Bayraktar2000	Bread wheat	Şanlıurfa	Southeast Anatolia	2021	-		0
63	Çeşit-1252	Durum wheat	Şanlıurfa	Southeast Anatolia	2021	213	*F. proliferatum*	10
								<LOD
64	Ceyhan-99	Bread wheat	Batman	Southeast Anatolia	2021	-		0
65	Nota	Bread wheat	Erzurum	East Anatolia	2022	-		0

#Isolates marked * and **, belonging, respectively, to FTSC and FIESC groups, were selected for phylogenetic analysis.

al. (2011). The quality and quantities of extracted DNA were evaluated using a Qubit 3.0 fluorometer (ThermoFisher Scientific) and a NanoDrop-2000 (ThermoFisher Scientific). In addition, DNA samples were analysed by 0.7% agarose gel electrophoresis to assess molecular integrity, size, concentrations, and to detect any traces of RNA contamination. PCR with specific primers was carried out with GoTaq® 5× green reaction buffer, sup-

plied with GoTaq® DNA Polymerase ($MgCl_2$ concentration 7.5 mM, for a final concentration of 1.5 mM in the 1× reaction; Promega Corporation). Each PCR reaction contained 7 µL of buffer, 0.7 µL of dNTPS, 0.2 µL of Taq DNA Polymerase, 1.4 µL of each forward and reverse primer (10 µM), and 17.5 µL of sterile water. The final volume of the PCR reaction, 30 µL, was obtained by adding 2 µL of DNA template. The specific primer names, sequences, amplicon sizes and reference sources are listed in Table 2. Each PCR analysis included a well-characterised DNA sample (positive controls) of *F. graminearum*, *F. culmorum*, *F. proliferatum*, *F. verticillioides* and *F. poae* from the in-house collection of the plant pathology group of the Department of Food Science and Technology, University of Bologna (Italy). PCR products were separated and visualised on 1× Tris-borate-EDTA buffer agarose (1%) gels, stained with ethidium bromide. Amplicons showing defined bands of expected sizes were purified using the Wizard® SV Gel and PCR Clean-Up System (Promega Corporation), and were sent for Sanger sequencing with forward primers to an external molecular diagnostics laboratory (Eurofin Genomics, Ebersberg, Germany). Raw ABI sequence files were controlled and edited using Geneious Prime ® v2023.1.1 (Biomatters Ltd., Auckland, New Zealand). All FASTA sequences were then subjected to nucleotide basic local alignment search tool (BLASTn) analyses (National Center for Biotechnology Information, Bethesda, Maryland, United States of America) (Boratyn *et al*., 2013) and the *Fusarium* MLST database to confirm identifications.

Identification and discrimination of species belonging to the FTSC and FIESC groups were carried out by amplifying partial portions of the TEF1-*α* gene. The standard EF-1 and EF-2 primers (O'Donnell *et al*., 1998) gave suboptimal amplification results, characterized by nonspecific outcomes when applied to the majority of the FTSC isolates. To address this limitation, novel primers TEF1-F (5'-ATGGGTAAGGAGAAGAC-3') and TEF1-R (5'-GGAAGTACCAGTRATCATG-3') were designed by leveraging the genomic sequences of *F. acuminatum* strain F829, *F. avenaceum* strain S18/60, and *F. tricinctum* strain T6. These genomes were previously employed as references for phylogenetic and comparative analyses of species within the *Fusarium tricinctum* species complex by Turco *et al.* (2021). This strategic redesign aimed to enhance the efficiency of amplification for increased analysis accuracy of FTSC isolates. The PCR reaction, purification and sequencing protocols used were as described above. The PCR conditions were as follows: an initial denaturation phase of 2 min at 95°C, followed by 35 cycles each of 94°C for 30 s, 53 C for 30 s and 72°C for 45 s, and a final extension phase of 5 min at 72°C. Each forward DNA sequence was assembled with the corresponding reverse to generate a single consensus sequence, defined as the calculated order of the most frequent nucleotides found at each position in a sequence assembly. TEF1-*α* sequences of species in the FTSC group were submitted to GenBank (see Table S1 for accession numbers). The partial TEF1-*α* sequences obtained in the present study were aligned with those of 94 isolates from the reference FIESC group and 139 isolates from the reference FTSC group, in the FUSARIUM-ID v.3.0 database (https://github.com/fusariumid/fusariumid; Torres-Cruz *et al*., 2022), to perform phylogenetic analyses. The sequences were edited in Geneious Prime® v2023.1.1, and were aligned with MAFFT v7.450 (Katoh and Standley, 2013). Once the best fit molecular evolution model was determined (K2 + G) using MEGA 11 (Tamura *et al*., 2021) based on Bayesian information criterion (BIC) scores (Chernomor *et al*., 2016), the Markov chain Monte Carlo (MCMC) algorithm was used to generate phylogenetic trees with Bayesian posterior probabilities for alignment. Four MCMC chains were run simultaneously for random trees for 5,000,000 generations and were sampled every 500 generations (obtained with MrBayes 3.2.6; Ronquist *et al*., 2012). The

Table 2. Species-specific primers used to identify *Fusarium* species.

Species	Primer name	Primer sequence (5'-3')	Product size	Reference
F. proliferatum	PRO1 PRO2	CTTTCCGCCAAGTTTCTTC TGTCAGTAACTCGACGTTGTTG	585 bp	Mulè *et al.* (2004)
F. verticillioides	VER1 VER2	CTTCCTGCGATGTTTCTCC AATTGGCCATTGGTATTATATATCTA	578 bp	Mulè *et al.* (2004)
F. graminearum	Fg16F Fg16R	CTCCGGATATGTTGCGTCAA GGTAGGTATCCGACATGGCAA	410 bp	Nicholson *et al.* (1998)
F. poae	Fp82F Fp82R	CAAGCAAACAGGCTCTTCACC TGTTCCACCTCAGTGACAGGTT	220 bp	Parry and Nicholson (1996)
F. culmorum	Fc01F Fc01R	ATGGTGAACTCGTCGTGGC CCCTTCTTACGCCAATCTCG	570 bp	Nicholson *et al.* (1998)

sequences of *Fusarium nurragi* NRRL 36452 (lineages most closely related to the FTSC), and *Fusarium camptoceras* CBS 193.65 (most closely related to FIESC), were used as outgroups.

Pathogenicity assay

Pathogenicity tests were carried out using two isolates each of *F. andiyazi* (isolates 95Z and 178B) and *F. ramigenum* (isolates 92B and 169B), the identities of which were confirmed by TEF1-*α* portion sequencing. The inoculum for each isolate was prepared by placing three pieces of 7-d-old culture from PDA in liquid V8 juice (Campbell) medium according to the protocol described by Singleton *et al.* (1992). The medium was then placed in an orbital shaker (Thermo Scientific) under 120 rpm at 25 ± 1°C for approx. 7 d. Conidia concentrations were estimated by haemocytometer and adjusted to 10^6 mL^{-1}. In a greenhouse, pots each containing 600 g of plant growth medium (1:2:2:4 (v/v/v/v) ratio of sand, perlite, vermiculite and soil) were prepared, and 120 mL of isolate inoculum was added and mixed with the medium, with 120 mL of sterile water poured into medium as a negative experimental control. Three pots with the inoculated soil per isolate were each planted with 30 seeds per pot of the *Fusarium*-susceptible durum wheat cultivar 'San Carlo'. Seedling emergence was first observed at 7 d post-inoculation, and was recorded again at 21 d post-inoculation. Plants were removed at the 21st day, were rinsed with water and then cut with a scalpel to inspect for symptoms attributable to diseases caused by *Fusarium* (FCR and FRR). Symptom severity was assessed according to Parry *et al.* (1985) (Table 3), based on the number of plants grown and calculated using the formula (McKinney's, 1923): [Infection rating = (sum of all numerical ratings × number of plants examined) ÷ (total number of observation × maximum disease rating) × 100], and these data were statistically analyzed using the software Statgraphics 18 (Statpoint Technologies, Inc.).

Table 3. Categories of symptoms (Parry *et al.*, 1985), used in this study to assess disease severity on wheat plantlets.

Category	Plantlet symptoms
0	healthy, symptom-free with normal development
1	symptom-free, but underdeveloped or slightly necrotic at neck level
2	neck necrosis
3	obvious neck necrosis, or death following necrosis

DON detection in wheat flour

Analyses were conducted by grinding 50 g of wheat seeds from each assessed sample. From each resulting flour, 20 g was weighed into a clean Erlenmeyer flask and 100 mL of distilled water was added. The flasks were then shaken for 5 min with a mechanical stirrer 5 min (ThermoFisher Scientific). The resulting liquid fractions were each transferred to a 50 mL capacity falcon tube, and then centrifuged at 4000 rpm for 4 min. Subsequently, 500 µL of solution was aliquoted and diluted to 1:4 with distilled water. Quantification of DON was accomplished on a total of 65 samples, using the AgraQuant® Deoxynivalenol Plus kit (0.25 - 5.0 ppm), following the manufacturer's instructions. Optical densities of samples and standard curves were read at 450 nm wavelength using a spectrophotometer (OpsysMR, Dynex Technologies), assisted by Agraquant Assay Spreadsheet software (Romer Labs Division Holding GmbH).

RESULTS

Fusarium *species distributions*

In the years 2020, 2021 and 2022, a total of 195 *Fusarium* isolates were obtained from 32 of 65 wheat seed bag samples collected in the seven regions of Türkiye. All the isolates characterized in the present study are shown in Table 1. Samples from the Black Sea region were those with the most (50.2%) *Fusarium* isolates obtained, and these isolates included 11 different *Fusarium* species. The 16.9% of isolates were from samples from the Marmara region, 14.8% were from Southeastern Anatolia, 9.7% were from Central Anatolia, and 8.2% were Aegean, No *Fusarium* isolates were identified in samples from the East Anatolia and Mediterranean regions.

Fusarium graminearum was the dominant species isolated, accounting for 32.3% of the isolates obtained, followed by *F. proliferatum* (16.4%), *F. avenaceum* (11.2%), *F. clavum* (FIESC 5) (10.7%) and *F. verticillioides* (7.1%). Less frequently isolates were *F. oxysporum* (5.6%), *F. acuminatum* (3%), *F. ramigenum* (3%), *F. culmorum* (2.5%), *F. poae* (2%), *F. sambucinum* (1.5%), *F. tricinctum* (1.5%), *Fusarium* sp. FTSC12 (1.5%), *F. andiyazi* (1%), and one isolate (0.5%) each of *F. equiseti*, *F. incarnatum* and *F. fasciculatum*.

A total of 50 *Fusarium* isolates were obtained from durum wheat seed samples, of which 26 (52%) were identified as *F. graminearum*. In comparison from bread wheat, this species accounted for 25.5% of the 145 *Fusarium* isolates (Figure 2). Seven representative isolates of the *Fusarium incarnatum-equiseti* species complex

(FIESC), selected according to morphological characteristics, were discriminated by partial sequence analysis of the TEF1-α gene. The sequences generated in this study (final length ≈ 600 bp) were aligned with those of 94 reference isolates. The phylogenetic tree based on maximum likelihood and Bayesian posterior probability (BPP) analyses showed that *F. clavum* was the most abundant species (21 of 24) within the FIESC group (Figure 3). For *F. clavum*, *F. equiseti*, *F. incarnatum* and *F. fasciculatum* as FIESC members, these accounted for 16.0% (eight of 50) of the isolates in durum wheat and 11.0% (16 of 145) in bread wheat seeds. *Fusarium proliferatum* was detected in 25 (17%) of the 145 bread wheat samples, while *F. verticillioides* was present in 12 (8%) of these samples. In durum wheat, seven (14%) of 50 isolates were *F. proliferatum* and 4% (two of 50 samples) were *F. verticillioides*. Similarly, five isolates (3.4%) of *F. ramigenum* were detected in bread wheat and one isolate (2%) was obtained from durum wheat. *Fusarium culmorum* was only isolated from durum wheat, with 5 isolates (10%) detected out of the 50 samples. *Fusarium poae* (2.7% of isolates), *F. sambucinum* (2.1%), and *F. andiya-*

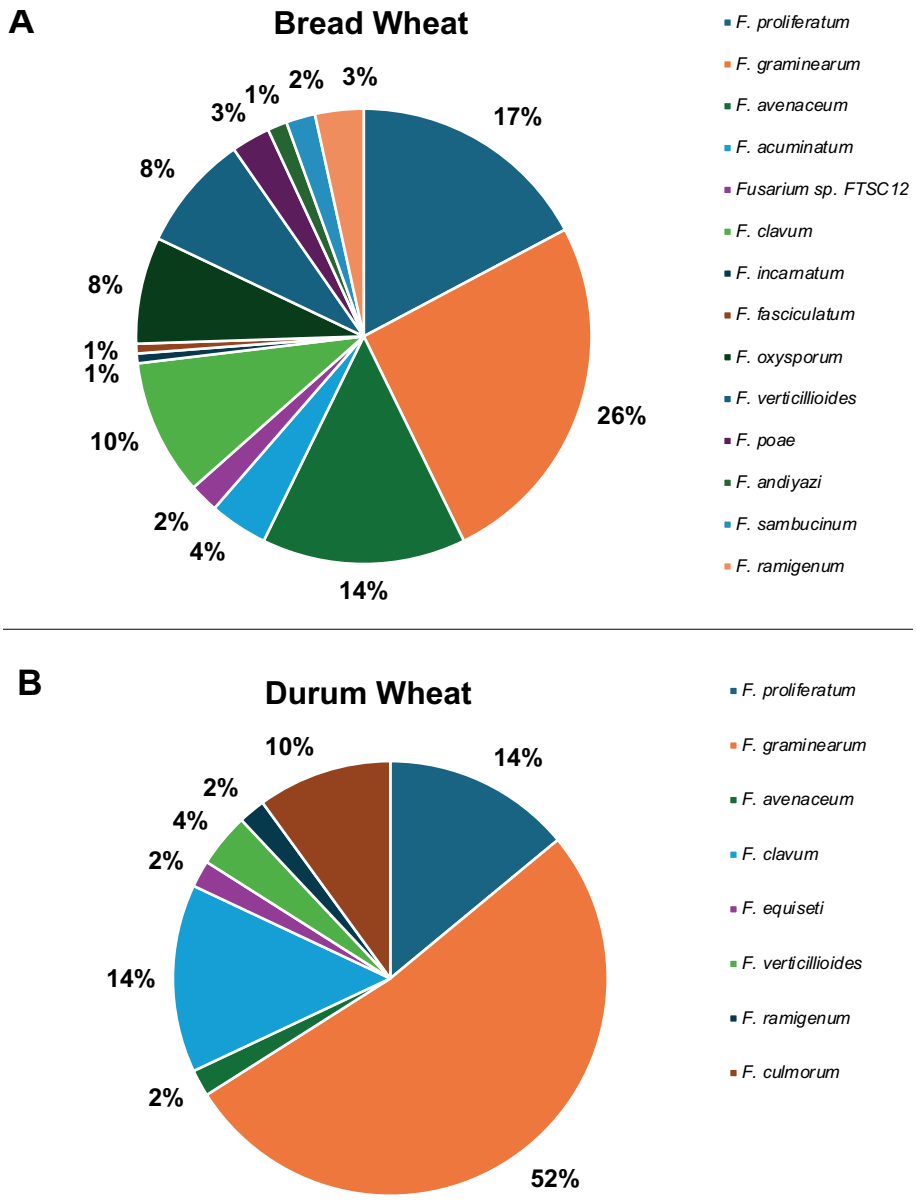

Figure 2. Occurrence (% of total) of different *Fusarium* species isolated from 45 bread wheat seed samples (A) and 20 durum wheat seed samples (B) seeds samples from Türkiye in 2020, 2021 and 2022.

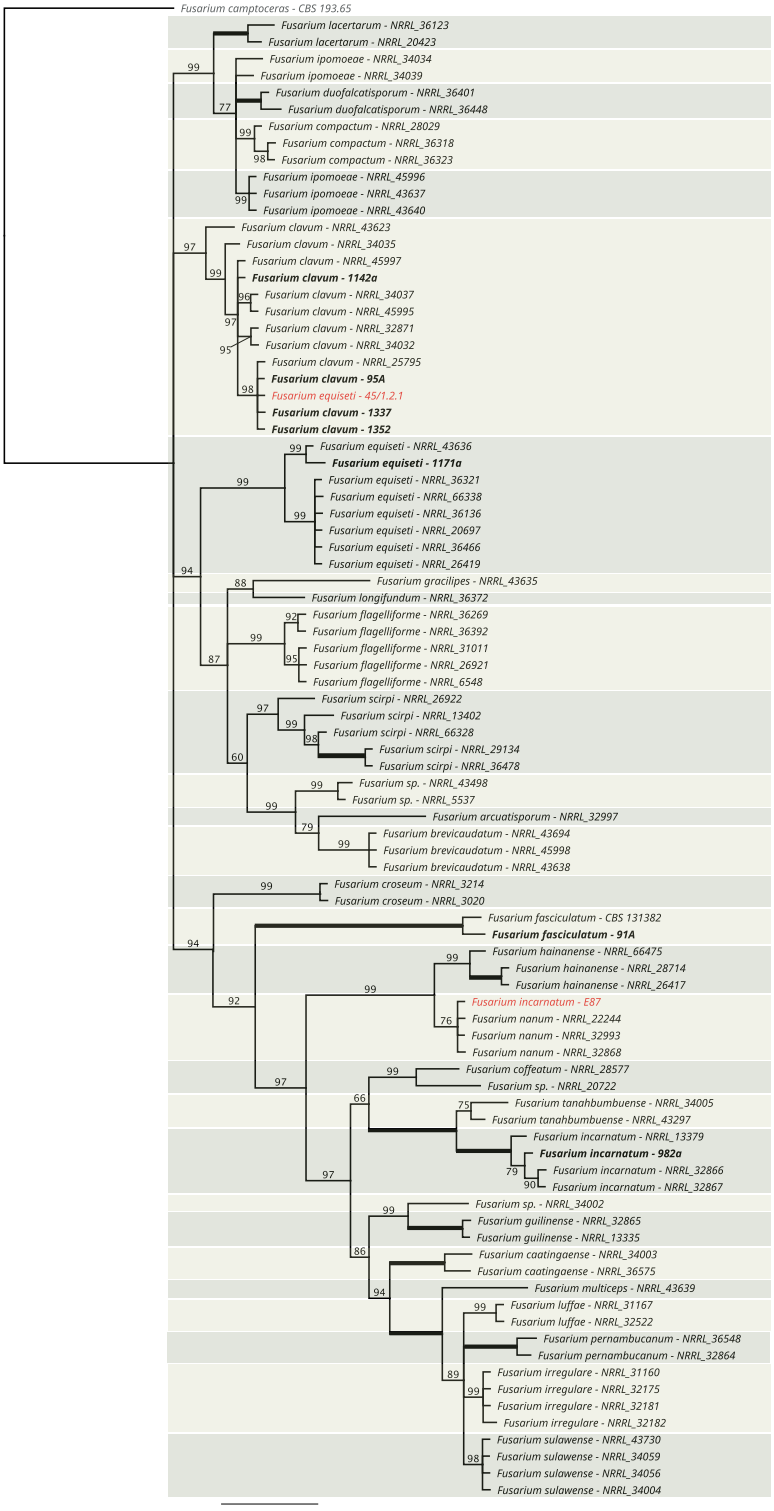

Figure 3. Bayesian inference phylogenetic tree of the *Fusarium incarnatum-equiseti* species complex (FIESC), which was constructed by aligning the sequences of the partial region of the TEF1-*α* gene produced in this study with those of the reference isolates available in the FUSARIUM ID database. The isolates obtained in this study are highlighted in bold font. *Fusarium camptoceras* CBS 193.65 was used as the outgroup. Bayesian posterior probabilities (BPP) are shown next to the nodes. The scale bar represents the number of expected changes per site. The isolate labelled "45/1.2.1" are taxonomic references for *F. equiseti*, and those labelled "E87," are taxonomic references for *F. incarnatum* (Shikur Gebremariam *et al.*, 2018). These isolates clustered with, respectively, *F. clavum* and *F. nanum*.

zi (1.3% of isolates) were only identified from the bread wheat samples.

The 23 isolates of the FTSC group were obtained only from bread wheat samples (16%), and theses isolates were further identified at species level based on partial sequence analyses of the TEF1-α gene. The sequences generated were aligned with those of 139 reference isolates, and were trimmed to final length of approx. 600 bp. The phylogenetic tree based on maximum likelihood and BPP analyses (Figure 4) showed that most of the FTSC group isolated in Türkiye from bread wheat seeds (16 of 23 samples) clustered with *F. avenaceum*. Fewer isolates (four of 23) clustered in the monophyletic group of *F. acuminatum*. Three of the 23 were assigned to FTSC group 12, which has not yet been described at species level. All clades comprising distinct isolates of the three species *F. avenaceum*, *F. acuminatum* and *Fusarium* sp. FTSC12 identified on wheat seeds from Türkiye were supported by bootstrap proportions close to 100% and had BPP values ranging from 0.91 to 0.97.

Pathogenicity assays

Pathogenicity evaluation of isolates 95Z and 178B (*F. andiyazi*) and 92B and 169B (*F. ramigenum*) on 30 seeds of the cultivar 'San Carlo' gave germination of 80% for 95Z, 76% for 178B, 72% for 92B, and 85% for 169B, at the 7 d for inoculated plants. Mean germination was similar (82%) for seeds treated with sterile water (Table 4). Disease severity, calculated at 21 d post-inoculation, was 5.9% from isolate 95Z and 3.4% from and 178B (both *F. andiyazi* isolates), and 4.4% isolate 92B and 3.3% from isolate 169B (both *F. ramigenum* isolates). No statically significant differences ($P > 0.05$) were found among the tests; germination of inoculated plants and disease severity were comparable to the negative experimental controls.

DON contamination in Turkish wheat grain

Based on the results of ELISA tests for DON in grain samples, numbers of wheat samples positive for the mycotoxin were: ten samples of 'Sakin' (mean DON concentration = 1150 µg kg^{-1}), 13 of 'Altındane' (mean = 320 µg kg^{-1}), 15 of 'Nevzatbey' (mean = 710 µg kg^{-1}), 17 of 'Efe' (mean = 380 mg kg^{-1}), and 61 samples of 'Fırat-93' (mean = 1730 mg kg^{-1}). Four of the five positive samples are bread wheats from the Black Sea region (see Table 1) among which sample No. 10 'Sakin' exceed the maximum limits for DON in unprocessed bread wheat. In sample No. 61 ('Fırat-93', from Southeastern Anatolia), DON concentration (1730 µg kg^{-1}) was the greatest amount detected, up to the European Commission threshold for mycotoxin contamination in durum wheat. The greatest amount of *F. graminerarum* was isolated from this sample (13 isolates from 100 seeds plated. Similarly, for sample No. 10, with 1150 µg kg^{-1} of DON, ten *F. graminearum* isolates were found from 100 seeds plated. In contrast, 710 µg kg^{-1} of DON were detected from sample No. 15, from which *F. avenaceum* and *F. poae* were the only isolated species.

DISCUSSION

The present study research is first to provide an overview of *Fusarium* species obtained from wheat seeds sampled in the Aegean, Black Sea, Central Anatolia, Eastern Anatolia, Marmara, Mediterranean and South-Eastern Anatolia regions of Türkiye. Although this country is a major wheat producer (FAOSTAT, 2021), detailed information is lacking on the *Fusarium* species associated with wheat seeds produced and harvested in Türkiye. Bentley *et al*. (2006) investigated the presence of *Fusarium* species obtained from diseased plants with crown and sub-crown rot symptoms in the Black Sea, Central Anatolia, and Marmara regions. They isolated 36 *Fusarium* colonies from 160 wheat plants based on morphological identifications, of which 13 isolates (36%) were identified as *F. culmorum*. In contrast, Shikur Gebremariam *et al.* (2018) identified 339 isolates of *Fusarium* from crown rot-affected plants from the Aegean, Black Sea, Central Anatolia and South-Eastern Anatolia regions of Türkiye, and, based on translation elongation factor 1-alpha (TEF1-α) segment sequencing, determined that *F. equiseti* was the predominant species. Both of these studies evaluated diseased wheat plants with crown or sub-crown rot symptoms and conducted pathogenicity tests on wheat plants, showing that *F. culmorum*, *F. graminearum* and *F. pseudograminearum* were the most pathogenic, but *F. equiseti* isolates were not pathogenic.

In the present study, 195 *Fusarium* strains isolated from wheat seeds were molecularly identified as *F. culmorum*, *F. graminearum*, *F. poae*, *F. proliferatum,* or belonging to FTSC or FIESC. In 2009 and 2010, in the neighboring country Syria, Alkadri *et al*., (2013) carried out mycological analyses on 48 wheat grain samples from diverse areas with different climates. The predominant *Fusarium* species detected were *F. tricinctum* (30%), *F. culmorum* (18%), *F. equiseti* (14%), and *F. graminearum* (13%). In Iran, which also borders Türkiye, prevalent species in pre-base wheat seeds collected in 2016 and 2017 in northern regions were *F. graminearum*, *F. cul-*

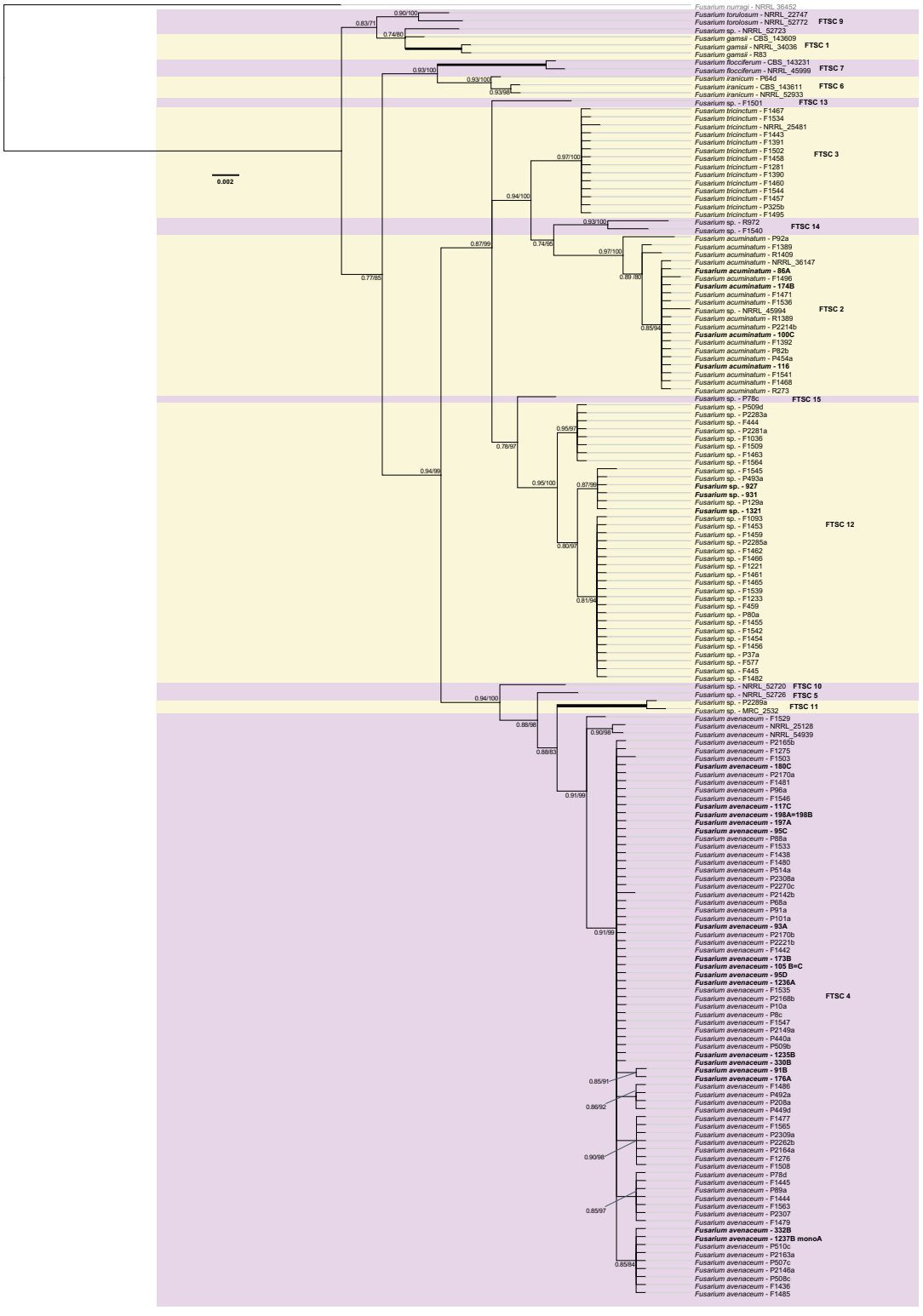

Figure 4. Bayesian inference phylogenetic tree of the *Fusarium tricinctum* species complex (FTSC), which was constructed by aligning the sequences of the partial region of the TEF1-*α* gene produced in this study with those of the reference isolates available in the FUSARIUM ID database. The isolates obtained in this study are highlighted in bold font. *Fusarium nurragi* (NLR 135819) was used as the outgroup. Bayesian posterior probabilities (BPP) are shown next to the nodes. The scale bar represents the number of expected changes per site. The different FTSC groups are highlighted by light violet and yellow boxes and are named on the right.

Table 4. Average germination rates and disease severities at the 7 and 21 d after inoculation of seeds of wheat 'San Carlo' with isolates of *F. andiyazi* or *F. ramigenum*.

Isolate code	Average germination (%)		Mean disease severity (%)	Tukey/Duncan test ($P < 0.05$)
	7th day	21st day		
169B, *F. ramigenum*	85	91.1	3.3	a
92B, *F. ramigenum*	72	80.0	4.4	a
95Z, *F. andiyazi*	80	85.6	5.9	a
178B, *F. andiyazi*	76	81.1	3.4	a
Control	82	78.9	0.7	a

morum, *F. avenaceum*, and *F. poae* (Hassani *et al*., 2019). However, in 2023, only *F. graminearum* and *F. culmorum* were detected in samples collected from northern and southwestern regions of the same country (Khaledi *et al*., 2023).

In the different geographical context of Western Australia, which is characterized by climates ranging from arid, semi-arid, Mediterranean, to tropical, Wright *et al*. (2010) found that *F. graminearum* was the predominant species in wheat grains, while *F. avenaceum*, *F. acuminatum*, and *F. culmorum* were identified in four grain samples. In Italy, Senatore *et al*. (2023) assessed fungal on durum wheat seeds across 13 regions. They identified *F. avenaceum* and *F. graminearum* as predominant species using culturing and TEF1-α assessments, and *F. proliferatum* using deep-freezing blotter (DFB) and morphological traits. In Norway, which has severe winters and high precipitation, Kosiak *et al*. (2003) surveyed wheat grain samples from different regions for *Fusarium* species. They ranked the most common species in order of *F. avenaceum*, *F. poae*, *F. tricinctum*, *F. culmorum,* and *F. graminearum*.

Across several studies in different countries and over different years, there is uniformity in the predominant *Fusarium* species that have been associated with wheat grains. However, there has been variability in the relative abundance of particular *Fusarium* species recorded across different countries and survey periods.

Fusarium graminearum, acknowledged internationally as a major contributor to FHB (Pecoraro *et al*., 2018), was shown to prevail in Türkiye in the present study. The absence of statistically significant differences in the *t*-test analyses of incidence of *F. graminearum* isolates in the bread and durum wheat samples is noteworthy. These results indicate the broad genetic differences for FHB resistance in bread wheat, while durum wheat, acknowledged as highly susceptible to this disease, lacks identified resistance sources (Haile *et al*., 2019). *Fusarium graminearum* was prevalent in bread wheat samples from the Black Sea region, where no durum wheat samples were obtained. This region, characterized by high and consistent rainfall and mild temperatures, provides optimal conditions for FHB development (Tunali *et al*., 2008). The Black Sea region has substantial maize production, which also applies in southeastern Anatolia, from which the second greatest numbers of *F. graminearum* isolates were detected. This indicates that increased susceptibility to FHB infection and mycotoxin contamination in wheat and barley crops could result from previous maize cultivation, and the adoption of diminished or nil tillage techniques (Drakopoulos *et al*., 2020).

Fusarium culmorum, which can cause FHB and FCR (Pecoraro *et al*., 2018), was identified in 2.5% of seed samples examined in this study. This contrasts with results from 2006 and 2018 in Türkiye (Bentley *et al*., 2006; Shikur Gebremariam *et al*., 2018), where *F. culmorum* predominated on wheat plants affected by crown rot, and *F. graminearum* was absent or negligible. Similar prevalence was observed for *F. poae*, detected in only 2% of the samples in the present study. Despite being categorized as a weak pathogen, monitoring for *F. poae* is important, due to its association with FHB and its capability to produce trichothecenes, which are regulated by EU Commission limits (Nazari *et al*., 2018). *Fusarium sambucinum* is closely related to *F. graminearum*, *F. culmorum* and *F. poae*. In this study, it was found in 1.5% of samples assessed. Therefore, this fungus probably does not pose threats to wheat cultivation (Kosiak *et al*., 2003; Pereyra and Dill-Macky, 2021).

The frequency of isolation of *F. avenaceum* in this study is noteworthy, as this fungus accounted for 11.2% of the isolates obtained. During the last two decades, *F. avenaceaum* has become a major contributor to FHB in cereals grown in Europe, including Denmark (Nielsen *et al*., 2011), France (Ioos *et al*., 2004), Italy (Beccari *et al*., 2018; Senatore *et al*., 2021), Norway (Kosiak *et al*., 2003), and Poland (Golinsky *et al*., 1996). *F. avenaceum* isolates were mainly obtained in the present study from bread wheat (21 of 22 isolates compared to one of 22 isolates from durum wheat), although durum wheat has been

reported as highly susceptible to this fungus (Beccari *et al*., 2018; Senatore *et al*., 2021). Two additional species of the FTSC group were found in the present study: *F. acuminatum* (3% of isolates) and the unnamed taxon *Fusarium* sp. FTSC12 (1.5% of the isolates). *F. acuminatum* has been reported as a minor contaminant in wheat crops in Spain and Canada (Marín *et al*., 2012; Grafenhan *et al*., 2013), while in North Carolina, United States of America, incidence of this fungus was approx. 49%, suggesting that it could become a significant contaminant under favourable conditions (Cowger *et al*., 2020). *Fusarium* sp. FTSC 12, in contrast, was the second most common FTSC species recovered from Italian wheat and barley by Senatore *et al*. (2021). They suggested that this species could contribute to mycotoxin contamination of Italian cereals, given its ability to produce mycotoxins such as enniatins (ENNs) and moniliformin (MON).

Incidence of FIESC was high (12.3%) in the present study. In 2018, *F. equiseti* was the predominant species from wheat plants with crown rot symptoms, constituting 36% of the isolates, while Tunali *et al*. (2006) reported lower incidence of this fungus (two isolates out of 32). In both studies, however, the isolates tested for pathogenicity gave no disease-causing effects on cultivars 'Pehlivan' and 'Kızıltan 91' (durum wheat) (Tunali *et al*., 2006; Shikur Gebremariam *et al*., 2018). In the present study, *F. clavum* was the most prevalent within the FIESC group. The phylogenetic analysis of Jedidi *et al*. (2021), examining TEF1-*α* sequences of three FIESC isolates from barley and wheat in Tunisia in comparison with isolates from northern and southern Europe, showed that the Tunisian southern European isolates were grouped in *F. clavum*, whereas isolates from northern Europe were assigned to *F. equiseti*.

Shikur Gebremariam *et al*. (2018) identified *F. equiseti* using sequencing of TEF1-*α* (amplicon sizes 243 to 655) for 123 isolates, but the sequences have not been deposited in databases, which prevents comparative analyses. The sequence comparisons performed by Shikur Gebremariam *et al*. (2018) using the BLASTn algorithm on NCBI demonstrated 97% to 100% similarity with accession number DQ854855. This refers to '*Fusarium equiseti* isolates 45/1.2.1', deposited in the GenBank database in 2006, from fungi isolated from *Lygeum spartum* in the Mediterranean region. However, a phylogenetic analysis carried out in the present study indicated that isolate '45/1.2.1', previously identified as *F. equiseti*, is closely related to isolates 95A, 1337 and 1352 of *F. clavum* obtained in the present study, as well as to the reference isolate *F. clavum* - NRRL_25795 from the FUSARIUM-ID database v.3.0 (Torres-Cruz *et al*., 2022). *F. clavum* represented the phylo-species FIESC 5 (O'Donnell *et al*., 2009), to which the Latin binomials were attributed in the 2019 taxonomic revision of this group by Xia *et al*. (2019). Three additional FIESC species were found in the present study: *F. equiseti*, *F. incarnatum* and *F. fasciculatum*. The first two were previously reported on wheat (Tunali *et al*., 2006; Shikur Gebremariam *et al*., 2018), and *F. incarnatum* was shown to be pathogenic causing foot rot in wheat plants (Er and Akgül, 2021). For *F. fasciculatum*, however, the only currently available report is for three isolates from a wild rice species (*Oryza australiensis*) cultivated in Australia, so it is uncertain whether *F. fasciculatum* species is a pathogen or an endophyte (Xia *et al*., 2019). Species belonging to the *Fusarium fujikuroi* species complex (FFSC) were relevant in this the present study: *F. proliferatum* was the second most frequently isolated (16.4%), while *F. verticillioides* was found at 7.1% incidence. These two species have been mainly associated with severe maize kernel rot (Desjardins *et al*., 2007; Amato *et al*., 2015). In wheat, *F. proliferatum* can cause the disease kernel black point, characterised by dark discolouration of the embryonic faces of grains. This disease can reduce germination of wheat seeds and alter seedling development (Busman *et al*., 2012), which can contribute to reductions in wheat crop yields and grain quality (El-Gremi *et al*., 2017; Busman *et al*., 2012; Stanković *et al*., 2012). *F. verticillioides* is a minor threat for wheat, and was found at low frequency on wheat plants with root rot in Türkiye in surveys by Arıcı *et al*. (2013) and Ünal *et al*. (2017). However, *F. proliferatum* and *F. verticillioides* should continue to be monitored, as these two species have potential to produce fumonisin, leading to economic losses in for maize and wheat cultivation (Leslie and Summerell, 2006; Niehaus *et al*., 2014). This also applies in Türkiye, where wheat is a primary crop and maize is secondary (Demirdogen *et al*., 2023).

Fusarium andiyazi and *F. ramigenum,* both members of the FFSC, were observed at incidence of 1% and 3%, respectively. These two species were reported as part of the *Fusarium* community associated with the 'Bakanae' disease of rice in Türkiye (Eğerci, 2019). The two fungi have also been reported in Italy: *F. andiyazi* as a pathogen causing 'Bakanae' (Dal Prà *et al*., 2010), and *F. ramigenum* responsible for endosepsis of fig (Moretti *et al*., 2010). The present study is the first to report *F. andiyazi* and *F. ramigenum* in association with wheat plants but, based on the pathogenicity tests, both fungi were non-pathogenic on the durum wheat 'San Carlo'.

DON mycotoxin detection was carried out for all 65 wheat seed samples examined, with four DON-positive bread wheat samples (from Samsun province in the central Black Sea area) out of five positive samples.

This region is in the northern transition zone with high annual rainfall (Morgounov *et al*., 2016). The presence of *F. graminearum* was detected in three of the four samples from the Black Sea region, with the highest amount in sample No. 10, which reached a DON concentration of 1150 μg kg^{-1}, surpassing the latest European Commission threshold for mycotoxin contamination. In contrast sample No. 15, in which only *F. avenaceum* and *F. poae* were isolated showed DON quantities of 710 μg kg^{-1}. These fungi are not renowned for producing DON, but DON-producing *Fusarium* species could be present in this sample, which were not detected during the isolation procedures. The greatest DON concentration (1730 μg kg^{-1}) was detected in sample No. 61 from Diyarbakır, exceed the maximum limits for DON in unprocessed durum wheat, where greatest contamination by *F. graminearum* was also observed. This area of Türkiye is characterized by hot and dry Mediterranean summers and mild and rainy winters (Tunali *et al*., 2008; Morgounov *et al*., 2016). Investigations are few on *Fusarium* species and their genetic variability in wheat seeds collected from different regions of Türkiye. The present study survey, identified the predominant species responsible for FHB, FCR and FRR. Notable findings include detection of *F. andiyazi*, *F. ramigenum*, and *F. fasciculatum*, heretofore unreported in wheat seeds. Research is required to assess the pathogenicity of these species; continued monitoring of the *Fusarium* community is necessary. This will be important for evaluating potential shifts in the *Fusarium* community associated with wheat, which may change, with species defined as weak pathogens becoming more dominant and destructive. The outcomes of the present study suggest that, although only two samples exceed the most recently updated European Union thresholds for DON content in unprocessed cereal grains, the Black Sea and southeastern Anatolia regions should be monitored, and because of the important export of wheat from all parts of Türkiye (FAOSTAT, 2021). Monitoring the presence of mycotoxins, including DON, ENN, MON and others, is important, as these compounds can be virulence factors for *Fusarium* species. This surveillance is important for understanding qualitative damage to wheat production and for implementing measures to mitigate these emerging threats to human health.

ACKNOWLEDGEMENTS

The authors acknowledge the Turkish farmers and agronomist colleagues for their provision of seed samples from the wheat species analyzed in this study. Without these contributions, this study could not have been completed.

LITERATURE CITED

Abdallah-Nekache N., Laraba I., Ducos C., Barreau C., Bouznad Z., Boureghda H., 2019. Occurrence of Fusarium head blight and Fusarium crown rot in Algerian wheat: identification of associated species and assessment of aggressiveness. *European Journal of Plant Pathology* 154(3): 499–512. https://doi.org/10.1007/s10658-019-01673-7.

Alkadri D., Nipoti P., Döll K., Karlovsky P., Prodi A., Pisi A., 2013. Study of fungal colonization of wheat kernels in Syria with a focus on *Fusarium* species. *International Journal of Molecular Sciences* 14(3): 5938–5951. https://doi:10.3390/ijms14035938.

Amato B., Pfohl, K., Tonti S., Nipoti P., Dastjerdi R., … Prodi A., 2015. *Fusarium proliferatum* and fumonisin B1 co-occur with *Fusarium* species causing Fusarium head blight in durum wheat in Italy. *Journal of Applied Botany and Food Quality* 88: 228–233. https://doi.org/10.5073/JABFQ.2015.088.033.

Arıcı Ş. E., Arap Ü., Yatağan F. B., 2013. Isparta ve Burdur İlleri Buğday Ekim Alanlarındaki Kök ve Kök Boğazı Fungal Hastalık Etmenlerinin Belirlenmesi (in Turkish). *Journal of Natural and Applied Science* 17(2): 26–30.

Beccari G., Senatore M. T., Tini F., Sulyok M., Covarelli L., 2018. Fungal community, Fusarium head blight complex and secondary metabolites associated with malting barley grains harvested in Umbria, central Italy. *International Journal of Food Microbiology* 273: 33–42. https://doi.org/10.1016/j.ijfoodmicro.2018.03.005.

Bentley A., Tunali B., Nicol J., Burgess L., Summerell B., 2006., A survey of *Fusarium* species associated with wheat and grass stem bases in northern Turkey. *Sydowia* 58(2): 163–177.

Boratyn G. M., Camacho C., Cooper P. S., Coulouris G., Fong A., … Zaretskaya I., 2013. BLAST: a more efficient report with usability improvements. *Nucleic Acids Research* 41: 29–33. https://doi.org/10.1093/nar/gkt282.

Busman M., Desjardins A. E., Proctor R. H., 2012. Analysis of fumonisin contamination and the presence of *Fusarium* in wheat with kernel black point disease in the United States. *Food Additives and Contaminants* 29(7): 1092–1100. https://doi.org/10.1080/19440049.2012.671787.

BÜGEM, 2021. Bitkisel Üretim Genel Müdürlüğü Available at: https://www.tarimorman.gov.tr/BUGEM/

TTSM/Sayfalar/Detay.aspx?SayfaId=158 Acession Date: 01.05.2023.

Chernomor O., Von Haeseler A., Minh B. Q., 2016. Terrace aware data structure for phylogenomic inference from supermatrices. *Systematic Biology* 65(6): 997–1008. https://doi.org/10.1093/sysbio/syw037.

Cowger C., Ward T. J., Nilsson K., Arellano C., McCormick S. P., Busman M., 2020. Regional and field-specific differences in *Fusarium* species and mycotoxins associated with blighted North Carolina wheat. *International Journal of Food Microbiology* 323. https://doi.org/10.1016/j.ijfoodmicro.2020.108594.

Dal Prà M., Tonti S., Pancaldi D., Nipoti P., Alberti I., 2010. First report of *Fusarium andiyazi* associated with rice bakanae in Italy. *Plant Disease* 94(8): 1070. https://doi.org/10.1094/PDIS-94-8-1070A.

Dehghanpour-Farashah S., Taheri P., Falahati-Rastegar M., 2019. Virulence factors of *Fusarium* spp., causing wheat crown and root rot in Iran. *Phytopathologia Mediterranea* 58(1): 115–125. https://doi.org/10.13128/Phytopathol_Mediterr-23860.

Demirdogen A., Guldal H. T., Sanli H., 2023. Monoculture, crop rotation policy, and fire. *Ecological Economics* 203. https://doi.org/10.1016/j.ecolecon.2022.107611.

Desjardins A. E., Busman M., Proctor R. H., Stessman R., 2007. Wheat kernel black point and fumonisin contamination by *Fusarium proliferatum*. *Food Additives and Contaminants* 24(10): 1131–1137. https://doi.org/10.1080/02652030701513834.

Drakopoulos D., Kägi A., Gimeno A., Six J., Jenny E., … Vogelgsang S., 2020. Prevention of Fusarium head blight infection and mycotoxins in wheat with cut-and-carry biofumigation and botanicals. *Field Crops Research* 246. https://doi.org/10.1016/j.fcr.2019.107681.

Eğerci Y., 2019. *Balikesir ve Çanakkale Illerinde çeltik kök çürüklüğüne Neden Olan Fusarium Türlerinin Saptanmasi, Yayginlik Oranlarinin Belirlenmesi ve Mücadelesine Yönelik Araştirmalar*. PhD Thesis, Ege University, Türkiye, 160 pp.

El-Gremi S. M., Draz I. S., Youssef W. A. E., 2017. Biological control of pathogens associated with kernel black point disease of wheat. *Crop Protection* 91: 13–19. https://doi.org/10.1016/j.cropro.2016.08.034.

Er Ö., Akgül D. S., 2021. Osmaniye ili buğday ekim alanlarında sap çürüklüğü hastalığıyla ilişkili *Fusarium* türleri. *Mustafa Kemal Üniversitesi Tarım Bilimleri Dergisi* 26(2): 292–305. https://doi.org/10.37908/mkutbd.884544.

Eskola M. Kos G., Elliot C.T., Hajšlová J., Mayar S., Krska R., 2020. Worldwide contamination of food-crops with mycotoxins: validity of the widely cited 'FAO estimate' of 25%. *Critical Reviews in Food Science Nutrition* 60(16): 2773–2789. doi: 10.1080/10408398.2019.1658570.

FAOSTAT, 2021. Food and Agriculture Organization of the United Nations (FAO). FAOSTAT Database. Available at https://www.fao.org/faostat/en/#home Accessed March 1, 2023.

Golinsky, P., Kostecki, M., Lasocka, I., Wisniewska, H., Chelkowsky, J., Kaczmarek, Z., 1996. Moniliformin accumulation and other effects of *Fusarium avenaceum* (Fr.) Sacc. on kernels of winter wheat cultivars. *Journal of Phytopathology* 144(9–10): 459–499. https://doi.org/10.1111/j.1439-0434.1996.tb00331.x.

Gräfenhan T., Patrick S. K., Roscoe M., Trelka R., Gaba D., … Tittlemier S. A., 2013. *Fusarium* damage in cereal grains from Western Canada. 1. Phylogenetic analysis of moniliformin-producing *Fusarium* species and their natural occurrence in mycotoxin-contaminated wheat, oats, and rye. *Journal of Agricultural and Food Chemistry* 61(23): 5425–5437. https://doi.org/10.1021/jf400651p.

Gruber-Dorninger C., Jenkins T., Schatzmayr G., 2019. Global mycotoxin occurrence in feed: a ten-year survey. *Toxins* 11(7): 375. https://doi.org/10.3390/toxins11070375.

Guo H., Ji J., Wang J.S., Sun X., 2020. Deoxynivalenol: Masked forms, fate during food processing, and potential biological remedies. *Comprehensive Reviews in Food Science and Food Safety* 19(2): 895–926. https://doi.org/10.1111/1541-4337.12545.

Haidukowski M., Somma S., Ghionna V., Cimmarusti M. T., Masiello M., … Moretti A., 2022. Deoxynivalenol and T-2 toxin as major concerns in durum wheat from Italy. *Toxins* 14(9): 627. https://doi.org/10.3390/toxins14090627.

Haile J.K., N'Diaye A., Walkowiak S., Nilsen K.T., Clarke J.M., … Pozniak C.J., 2019. Fusarium head blight in durum wheat: recent status, breeding directions, and future research prospects. *Journal Phytopathology* 109(10): 1664–1675. https://doi.org/10.1094/PHYTO-03-19-0095-RVW.

Hassani F., Zare L., Khaledi N., 2019. Evaluation of germination and vigor indices associated with *Fusarium*-infected seeds in pre-basic seeds wheat fields. *Journal of Plant Protection Research* 59(1): 69–85. https://doi.org/10.24425/jppr.2019.126037.

Ioos R., Belhadj A., Menez M., 2004. Occurrence and distribution of *Microdochium nivale* and *Fusarium* species isolated from barley, durum and soft wheat grains in France from 2000 to 2002. *Mycopathologia* 158: 351–362. https://doi.org/10.1007/s11046-004-2228-3.

Isebaert S., de Saeger S., Devreese R., Verhoeven R., Maene P., … Haesaert G., 2009. Mycotoxin-producing *Fusarium* species occurring in winter wheat in Belgium (Flanders) during 2022–2005. *Journal Phytopathology* 157(2): 108–116. https://doi.org/10.1111/j.1439-0434.2008.01443.x.

Jedidi I., Jurado M., Cruz A., Trabelsi M. M., Said S., González-Jaén M. T., 2021. Phylogenetic analysis and growth profiles of *Fusarium incarnatum-equiseti* species complex strains isolated from Tunisian cereals. *International Journal of Food Microbiology* 353. https://doi.org/10.1016/j.ijfoodmicro.2021.109297.

Ji F., He D., Olaniran A.O., Mokoena M.P., Xu J. Shi J., 2019. Occurrence, toxicity, production and detection of *Fusarium* mycotoxin: a review. *Food Production, Processing and Nutrition* 1(6). https://doi.org/10.1186/s43014-019-0007-2.

Katoh K., Standley D. M., 2013. MAFFT multiple sequence alignment software version 7: improvements in performance and usability. *Molecular Biology and Evolution* 30(4): 772–780. https://doi.org/10.1093/molbev/mst010.

Khaledi N., Zare L., Hashemi Fesharaki S., 2023. Effect of Fusarium head blight disease on the quality indicators of germination of wheat (*Triticum aestivum* L.). *Journal of Applied Research in Plant Protection* 12 (3): 303–321. https://doi.org/10.22034/ARPP.2023.16370.

Kosiak B., Torp M., Skjerve E., Thrane, U., 2003. The prevalence and distribution of *Fusarium* species in Norwegian cereals: A survey. *Acta Agriculturae Scandinavica Section B: Soil and Plant Science* 53 (4): 168–176. https://doi.org/10.1080/09064710310018118.

Leslie J.F., Summerell B.A., 2006. *The* Fusarium *Laboratory Manual*. Blackwell Publishing, Hoboken, 1-2. https://doi.org/10.1002/9780470278376

Leyva-Mir S. G., Garc Ia-Le E., Camacho-Tapia M., Villase~ Nor-Mir H. E., Leyva-Madrigal K. Y., … Tovar-Pedraza J. M., 2022. Occurrence of the *Fusarium incarnatum-equiseti* species complex causing Fusarium head blight of wheat in Mexico. *Plant Disease* 106(10): 2755. https://doi.org/10.1094/PDIS-11-21-2467-PDN.

Marín P., Moretti A., Ritieni A., Jurado M., Vázquez C., González-Jaén M.T., 2012. Phylogenetic analyses and toxigenic profiles of *Fusarium equiseti* and *Fusarium acuminatum* isolated from cereals from Southern Europe. *Food Microbiology* 31(2): 229–37. https://doi.org/10.1016/j.fm.2012.03.014.

McKinney H.H, 1923. Influence of soil temperature and moisture on infection of wheat seedling by *Helminthosporium sativum*. *Journal of Agricultural Research* 26: 195–217.

Mishra S., Dewangan J., Divakar A., Rath S.K., 2019. Global occurrence of deoxynivalenol in food commodities and exposure risk assessment in humans in the last decade: a survey. *Critical Reviews in Food Science and Nutrition* 60(8): 1346–1374. doi: 10.1080/10408398.2019.1571479.

Moretti A., Ferracane L., Somma S., Ricci V., Mulè G., … Logrieco A. F., 2010. Identification, mycotoxin risk and pathogenicity of *Fusarium* species associated with fig endosepsis in Apulia, Italy. *Food Additives & Contaminants: Part A: Chemistry, Analysis, Control, Exposure & Risk Assessment. Foreword* 27(5): 718–728. https://doi.org/10.1080/19440040903573040.

Morgounov A., Keser M., Kan M., Küçükçongar M., Özdemir F., … Qualset C.O., 2016. Wheat landraces currently grown in Turkey: distribution, diversity, and use. *Crop Science* 56(6):1–13. https://doi.org/10.2135/cropsci2016.03.0192.

Mousavi Khaneghah A., Farhadib A., Nematollahic A., Vasseghiand Y., Fakhrie Y., 2020. A systematic review and meta-analysis to investigate the concentration and prevalence of trichothecenes in the cereal-based food. *Trends in Food Science & Technology* 102:193–202. https://doi.org/10.1016/j.tifs.2020.05.026.

Mulè G., Susca A., Stea G., Moretti A., 2004. A species-specific PCR assay based on the calmodulin partial gene for identification of *Fusarium verticillioides*, *F. proliferatum* and *F. subglutinans*. *European Journal of Plant Pathology* 110: 495–502. doi: 10.1023/B:EJPP.0000032389.84048.71.

Nazari L., Pattori E., Manstretta V., Terzi V., Morcia C., … Rossi V., 2018. Effect of temperature on growth, wheat head infection, and nivalenol production by *Fusarium poae*. *Food Microbiology* 76: 83–90. https://doi.org/10.1016/j.fm.2018.04.015.

Niehaus E.M., Von Bargen K.W., Espino J.J., Pfannmuller A., Humpf H.U., Tudzynski B., 2014. Characterization of the fusaric acid gene cluster in *Fusarium fujikuroi*. *Applied Microbiology Biotechnology* 98(4): 1749–1762. doi: 10.1007/s00253-013-5453-1.

Nicholson P., Simpson D.R., Weston G, Rezanoor H.N., Lees A.K., … Joyce D., 1998. Detection and quantification of *Fusarium culmorum* and *Fusarium graminearum* in cereals using PCR assays. *Physiological and Molecular Plant Pathology* 53: 17–37.

Nielsen L.K., Jensen J.D. Nielsen G.C., Jensen J.E., Spliid N.H., … Jorgensen L.N., 2011. Fusarium head blight of cereals in Denmark: species complex and related mycotoxins. *Phytopathology* 101(8): 960–969. https://doi.org/10.1094/PHYTO-07-10-0188.

O'Donnell, K., Cigelnik, E., Nirenberg, H.I., 1998. Molecular systematics and phylogeography of the *Gib-*

berella fujikuroi species complex. *Mycologia* 90(3): 465–493. https://doi.org/10.1080/00275514.1998.12026933O'Donnell K, Sutton DA, Rinaldi MG., 2009. Novel multilocus sequence typing scheme reveals high genetic diversity of human pathogenic members of the *Fusarium incarnatum-equiseti* and *F. chlamydosporum* species complexes within the United States. *Journal of Clinical Microbiology* 47(12): 3851– 3861. https://doi.org/ 10.1128/JCM.01616-09.

O'Donnell K., McCormick S. P., Busman M., Proctor R. H., Ward T. J., … Geiser D. M., Alberts J. F., Rheeder J. P., 2018. Toxigenic *Fusarium* species: identity and mycotoxicology revisited. *Mycologia* 110(6): 1058– 1080. https://doi.org/10.1080/00275514.2018.1519773.

Pecoraro F., Giannini M., Beccari G., Covarelli L., Filippini G., … Prodi A., 2018. Comparative studies about fungal colonization and deoxynivalenol translocation in barley plants inoculated at the base with *Fusarium graminearum, Fusarium culmorum* and *Fusarium pseudograminearum. Agricultural and Food Science* 27(1): 74–83. https://dx.doi.org/10.23986/afsci.67704.

Parry D. W, Bayles R. A, Priestley R. H., 1985. Resistance of winter wheat varieties to ear blight caused by *Fusarium avenaceum* and *F. culmorum. Tests of Agrochemicals and Cultivars* 6: 164–165.

Parry D. W., Nicholson, P., 1996. Development of a PCR assay to detect *Fusarium poae* in wheat. *Plant Pathology* 45(2): 383–391. https://doi.org/10.1046/j.1365-3059.1996.d01-133.x.

Pereyra S., Dill-Macky, R., 2021. *Fusarium* species recovered from wheat and barley grains in Uruguay, pathogenicity and deoxynivalenol content. *Agrociencia Uruguay* 14 (2): 33–44. https://doi.org/10.31285/AGRO.14.625.

Prodi A., Purahong W., Tonti S., Salomoni D., Nipoti P., … Pisi A., 2011. Difference in chemotype composition of *Fusarium graminearum* populations isolated from durum wheat in adjacent areas separated by the Apennines in Northern-Central Italy. *Plant Pathology Journal* 27(4): 354–359. http://dx.doi.org/10.5423/PPJ.2011.27.4.354.

Ronquist F., Teslenko M., Van der Mark P., Ayres D. L., Darling A., … Huelsenbeck J. P., 2012. MrBayes 3.2: Efficient bayesian phylogenetic inference and model choice across a large model space. *Systematic Biology* 61(3): 539–542. https://doi.org/10.1093/sysbio/sys029.

Rigorth K. S., Finckh M. R., Šišić A., 2021. First report of *Fusarium venenatum* causing foot and root rot of wheat (*Triticum aestivum*) in Germany. *Plant Disease* 105(6): 1855. https://doi.org/10.1094/PDIS-10-20-2202-PDN.

Savary S., Willocquet L., Pethybridge S.J., Esker P., McRoberts N., Nelson A., 2019. The global burden of pathogens and pests on major food crops. *Nature Ecologia & Evolution* 3(3): 430–439 https://doi.org/10.1038/s41559-018-0793-y.

Scherm B., Balmas V., Spanu F., 2013. *Fusarium culmorum*: causal agent of foot and root rot and head blight on wheat. *Molecular Plant Pathology* 14: 323–41. https://doi.org/10.1111/mpp.12011.

Senatore M. T., Ward T. J., Cappelletti E., Beccari G., McCormick S. P., … Laraba I., O'Donnell K., Prodi A., 2021. Species diversity and mycotoxin production by members of the *Fusarium tricinctum* species complex associated with Fusarium head blight of wheat and barley in Italy. *International Journal of Food Microbiology* 358. https://doi.org/10.1016/j.ijfoodmicro.2021.109298.

Senatore M.T., Prodi A., Tini F., Balmas V., Infantino A., … Beccari G., 2023. Different diagnostic approaches for the characterization of the fungal community and *Fusarium* species complex composition of Italian durum wheat grain and correlation with secondary metabolite accumulation. *Journal of The Science of Food and Agriculture* 103(9): 4251–4719. https://doi.org/ 10.1002/jsfa.12526.

Shah L., Ali A., Yahya M., Zhu Y., Wang S., … Ma C., 2018. Integrated control of Fusarium head blight and deoxynivalenol mycotoxin in wheat. *Plant Pathology* 67(3): 532–548. https://doi.org/10.1111/ppa.12785.

Shikur Gebremariam, E. S., 2015. *Determination of Fusarium Species Associated with Crown Rot of Wheat in Turkey and Assessment of Resistance Status of Some Wheat Genotypes to Fusarium culmorum*. PhD Thesis, Ankara University Graduate School of Natural and Applied Sciences, 132 pp.

Shikur Gebremariam, E., Sharma-Poudyal, D., Paulitz, T. C., Erginbas-Orakci, G., Karakaya, A., Dababat, A. A., 2018. Identity and pathogenicity of *Fusarium* species associated with crown rot on wheat (*Triticum* spp.) in Turkey. *European Journal of Plant Pathology* 150(2): 387–399. https://doi.org/10.1007/s10658-017-1285-7.

Smiley R. W., Gourlie J. A., Easley S. A., Patterson L. M., 2005. Pathogenicity of fungi associated with the wheat crown rot complex in Oregon and Washington. *Plant Disease* 89(9): 949–957. https://doi.org/10.1094/PD-89-0949.

Stanković S., Lević J., Ivanović D., Krnjaja V., Stanković G., Tančić S., 2012. Fumonisin B1 and its co-occurrence with other fusariotoxins in naturally-contaminated wheat grain. *Food Control* 23: 384–388. https://doi.org/10.1016/j.foodcont.2011.08.003.

Summerell B.A., 2019. Resolving *Fusarium*: current status of the genus. *Annual Review of Phytopathology* 57: 323–339. https://doi.org/10.1146/annurev-phyto-082718-100204.

Tamura K., Stecher G., Kumar, S., 2021. MEGA11: Molecular Evolutionary Genetics Analysis Version 11. *Molecular Biology and Evolution* 38(7): 3022–3027. https://doi.org/ 10.1093/molbev/msab120.

Tian Y., Zhang D., Cai P., Lin H., Ying H., Hu Q., Wu A., 2022. Elimination of *Fusarium* mycotoxin deoxynivalenol (DON) via microbial and enzymatic strategies: Current status and future perspectives. *Trends in Food Science & Technology* 124: 96–107. https://doi.org/10.1016/j.tifs.2022.04.002.

Torbati M., Arzanlou M., Sandoval-Denis M., Crous P.W., 2019. Multigene phylogeny reveals new fungicolous species in the *Fusarium tricinctum* species complex and novel hosts in the genus *Fusarium* from Iran. *Mycological Progress* 18: 119–133. https://doi.org/10.1007/s11557-018-1422-5.

Torres-Cruz T. J., Whitaker B., Proctor R. H., Laraba I., Kim H.-S., … Geiser D. M., 2022. FUSARIUM-ID v.3.0: An updated downloadable resource for *Fusarium* species identification. *Plant Disease* 106(6):1610–1616. https://doi.org/10.1094/PDIS-09-21-2105-SR.

Tunalı B., Nicol J., Erol F. Y., Altiparmak G., 2006. Pathogenicity of Turkish crown and head scab isolates on stem bases on winter wheat under greenhouse conditions. *Plant Pathology Journal* 5(2): 143–149. doi: 10.3923/ppj.2006.143.149.

Tunalı B., Nicol J. M., Hodson D., Uçkun Z., Büyük O., … Bağci S. A., 2008. Root and crown rot fungi associated with spring, facultative, and winter wheat in Turkey. *Plant Disease* 92(9): 1299–1306. https://doi.org/10.1094/PDIS-92-9-1299.

TÜİK, 2021. Türkiye İstatistik Kurumu (in Turkish) Available at: https://data.tuik.gov.tr/Kategori/GetKategori?p=Tarim-111. Accessed March 1, 2023.

Turco S., Grottoli A., Drais MI., De Spirito C., Faino L., … Mazzaglia A., 2021. Draft genome sequence of a new *Fusarium* isolate belonging to *Fusarium tricinctum* species complex collected from hazelnut in central Italy. *Frontiers in Plant Science* (12). https: //doi.org/10.3389/fpls.2021.788584.

Ünal F., Dolar F. S., Tekiner N., Yeğin N. Z., 2017. Molecular identification, virulens and genetic diversity of *Fusarium* species on wheat. *Eurasian Journal of Agricultural research* 1(2): 13–22.

Ünüsan N., 2019. Systematic review of mycotoxins in food and feeds in Turkey. *Food Control* 97: 1–14. https://doi.org/10.1016/j.foodcont.2018.10.015.

Waalwijk C., Kastelein P., De Vries I., Kerényi Z., Van Der Lee T., … Kema G., 2003. Major changes in *Fusarium* spp. in wheat in the Netherlands. *European Journal of Plant Pathology* 109: 743–754. https://doi.org/10.1023/A:1026086510156.

Wang M. M., Chen Q., Diao Y. Z., Duan W. J., Cai L., 2019. *Fusarium incarnatum-equiseti* complex from China. *Persoonia* 43: 70–89. https://doi.org/10.3767/persoonia.2019.43.03.

Wright D. G., Thomas G. J., Loughman R., Fuso-Nyarko J., Bullock S., 2010. Detection of *Fusarium graminearum* in wheat grains in Western Australia. *Australasian Plant Disease Notes* 5: 82–84. https://doi.org/10.1071/DN10029.

Xia J. W., Sandoval- Denis M., Crous P. W., Zhang X. G., Lombard L., 2019. Numbers to names - restyling the *Fusarium incarnatum-equiseti species complex*. *Persoonia* 43: 186–221. https://doi.org/ 10.3767/persoonia.2019.43.05.

Xu X., Nicholson P., 2009. Community ecology of fungal pathogens causing wheat head blight. *Annual Review of Phytopathology* 47: 83–103. https://doi.org/10.1146/annurev-phyto-080508-081737.

Zhou H., He X., Wang S., Ma Q., Sun B., … Li H., 2019. Diversity of the *Fusarium* pathogens associated with crown rot in the Huanghuai wheat-growing region of China. *Applied Microbiology* 21(8): 2740–2754. https://doi.org/10.1111/1462-2920.14602.

Phytopathologia Mediterranea
The international journal of the
Mediterranean Phytopathological Union

Firenze University Press
www.fupress.com/pm

New or Unusual Disease Reports

Detection of hibiscus chlorotic ringspot virus, citrus exocortis viroid and citrus viroid VI in China rose from Italy using high-throughput sequencing

Giuseppe PARRELLA[1,*], Chantal FAURE[2], Armelle MARAIS[2], Elisa TROIANO[1,4], Thierry CANDRESSE[2]

[1] *Institute for Sustainable Plant Protection of National Research Council (IPSP-CNR), 80055 Portici, Italy*
[2] *University of Bordeaux, INRAE, UMR BFP, CS 20032, 33882 Villenave d'Ornon CEDEX, France*
[3] *University of Naples "Federico II", Department of Biology, 80126, Naples, Italy*
[4] *Enbiotech s.r.l., 84012, Angri (SA), Italy*
*Corresponding author. E-mail: giuseppe.parrella@ipsp.cnr.it

Summary. In Spring 2024, a symptomatic plant of China rose (*Hibiscus rosa-sinensis*) showing leaf yellowing and deformation, located in the province of Naples (South Italy), was re-sampled for further investigations. Total RNAs were purified from leaves and subjected to Illumina HTS analysis. Results confirmed that the plant was infected by hibiscus chlorotic ringspot virus (HCRSV), citrus exocortis viroid (CEVd), and citrus viroid VI (CVd-VI). The two viroids had not been previously detected in China rose. HTS results were confirmed by RT-PCR in the re-sampled plant, and in three nearby China rose plants with the same symptoms, using specific primer pairs for the three pathogens, followed by Sanger sequencing and BLAST analysis of the sequences. Different results obtained can be due to differing sensitivity and specificity in HTS-based detection of plant viruses. This is the first report of multiple infections by HCRS, CEVd and CVd-VI in China rose, which is also a new host for both of the viroids.

Keywords. HCRSV, CEVd, CVd-VI, mixed infections, NGS

OPEN ACCESS

Citation: Parrella, G., Faure, C., Marais, A., Troiano, E., & Candresse, T. (2024). Detection of hibiscus chlorotic ringspot virus, citrus exocortis viroid and citrus viroid VI in China rose from Italy using high-throughput sequencing. *Phytopathologia Mediterranea* 63(2): 255-257. doi: 10.36253/phyto-15435

Accepted: July 29, 2024

Published: September 15, 2024

Data Availability Statement: All relevant data are within the paper and its Supporting Information files.

Competing Interests: The Author(s) declare(s) no conflict of interest.

Editor: Safaa Kumari, International Center for Agricultural Research in the Dry Areas (CARDA), Terbol Station, Lebanon.

ORCID:
GP: 0000-0002-0412-4014
AM: 0000-0003-2482-1543
ET: 0000-0001-7755-4915
TC: 0000-0001-9757-1835

Hibiscus rosa-sinensis Linn. (*Malvaceae*), also known as China rose, is a popular ornamental shrub in Italy, and is frequently found near private and public buildings and in parks and gardens. China rose is affected by several diseases that are significant factors in reducing yield and quality. This host can be infected by viroids and viruses from several families, and previous reports have highlighted the phytosanitary status of Chine rose in Italy (De Stradis *et al*., 2008; Luigi *et al*., 2013; Parrella and Mignano, 2024). Recently, an siRNA HTS analysis applied to *H. rosa-sinensis* leaves with generalized yellowing revealed the association of hibiscus chlorotic ringspot virus (HCRSV) infection with these symptoms (Parrella and Mignano, 2024).

Nevertheless, since the symptoms observed were different from those attributed to HCRSV (Pourrahim *et al.*, 2013), other viruses or viroids, not previously identified, were suspected to be present in the same plant (Figure 1). A new HTS analysis was carried out on the plant, using leaf tissues collected in spring, with the aim to determine if additional pathogens were present.

Total RNAs were purified from leaves of the previously analysed symptomatic plant (Parrella and Mignano, 2024), and following a ribodepletion step, these were subjected to Illumina HTS (2 × 150 nt). After quality trimming, a total of 20,902,880 reads were obtained and assembled *de novo* (CLC Genomics Workbench 21, Qiagen). Contigs were annotated by Blastn and BlastX analyses against the GenBank database, resulting in the identification of single contigs for citrus exocortis viroid (CEVd), citrus viroid VI (CVd-VI) and HCRSV.

The single identified HCRSV contig was a near complete genome. It integrated 414,901 reads (2.0% of total reads), with a 13,614x average coverage, and had greatest nucleotide similarity (99.4%) with the Ita-1 isolate (GenBank OR891792) previously identified from the same plant (Parrella and Mignano, 2024). The single identified CEVd contig represented a complete genome and integrated 425 reads (0.002% of total reads) for a 158x average coverage. This had greatest nucleotide similarity (99.2%) with a severe variant from *Gynura aurantiaca* in the United States of America (isolate CEVdg-S; GenBank AF298177). The single identified CVd-VI contig also corresponded to a complete genome. It integrated 175 reads (0.0008% of the total reads) for a 70x average coverage, and had greatest nucleotide similarity (91.3%) with the Kaki13-5 isolate from *Diospyros kaki* in Japan (GenBank AB366017). Therefore, the identified contig was quite divergent from all previously identified CVd-VI isolates, as confirmed by phylogenetic relationships among sequences of the different isolates available in GenBank (Figure 2).

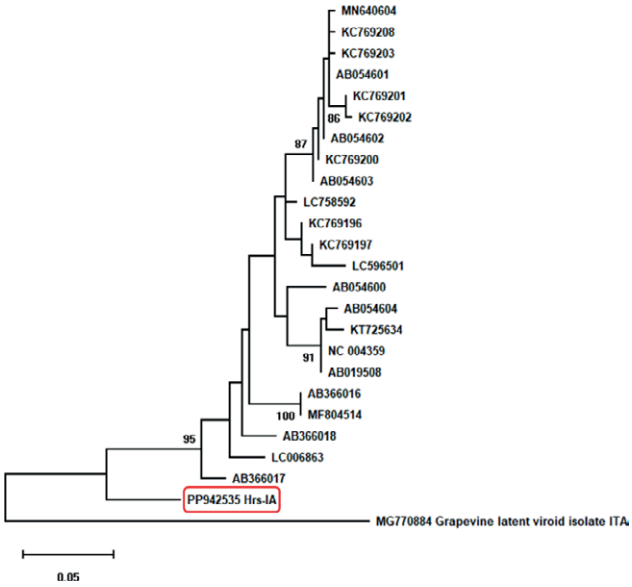

Figure 2. Phylogenetic relationships among the whole genomes of citrus viroid VI isolates obtained from GenBank (n = 23), based on a maximum-likelihood analysis and the Kimura-2 parameter method implemented in Mega X (Kumar *et al.*, 2018). The tree had the greatest log likelihood (-1382.63) generated using 1000 bootstrap replicates. The sequence of the grapevine latent viroid genome (Acc. No. MG770884) was used as the outgroup. Bootstrap values >70% are indicated near the branches. The position of the Hibiscus isolate of citrus viroid VI (named Hrs-1A; Acc. No. PP942535) is highlighted by a red box.

Figure 1. Yellowing symptoms observed on the leaves of the *Hibiscus rosa-sinensis* analysed in the present study.

The HCRSV contig and the complete genomes of the CEVd and CVd-VI isolates have been deposited in GenBank (respective Acc. Nos. PP942537, PP942536 and PP942535). In addition, the presence of these three pathogens in China rose was confirmed by the RT-PCR analysis in the original plant and in three additional symptomatic plants from the same location. HCRSV was detected using the primer pairs HCRSV-2F/HCRSV-3R (Parrella and Mignano, 2024); CVd-VI was detected using the CVd-VI-F/CVd-VI-R primers described by Cao *et al.* (2017), and CEVd was detected with primers CEVd-F/CEVd-R described by Abualrob *et al.* (2024).

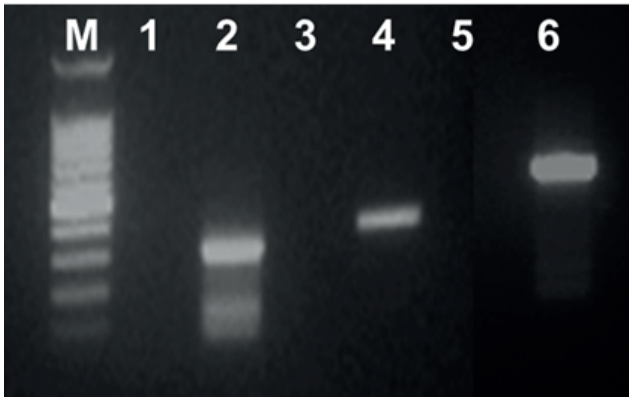

Figure 3. Validation of the HTS results by RT-PCR using a specific primer pairs for CVd-VI (lane 2; 326 bp), CEVd (lane 4; 371 bp), and HCRSV (lane 6; 697 bp) infections in the original and re-analyzed *Hibiscus rosa-sinensis* plant. Lanes 1, 3 and 5 are the negative controls for each RT-PCR. M is the 100 bp ladder.

Amplicons obtained by RT-PCR were further sequenced from both ends at Macrogen (Milano, Italy), and the sequences obtained were found to be 100% identical to the respective contigs obtained by HTS (Figure 3).

Different sensitivity and specificity in HTS-based detection of plant viruses have been recently reported. In particular, RNA-Seq approaches demonstrated better performance than small RNA-Seq (Di Gaspero *et al*., 2022) This could explain why, in the first siRNA-based HTS analysis of the China rose leaf sample, the two viroids were not identified (Parrella and Mignano, 2024). Alternatively, it is possible that the analysis of samples collected in two different periods (late summer, by Parrella and Mignano (2024) and spring, in the present study) may have contributed to the different results. This was likely to be due to differences in accumulations in plant tissues of the two viroids during the two different seasons.

With the increased use of HTS analyses for plant virome characterization, multiple infections by viruses and/or viroids have become increasingly evident, particularly in perennial plants. The present study detected multiple infections in China rose plants, involving HCRSV (already reported, Parrella and Mignano, 2024), and the two viroids CEVd and CVd-VI, for all of which China rose is a new host. In addition, these results are the first detection of CVd-VI in Italy.

ACKNOWLEDGEMENTS

The HTS analyses of China rose sample reported in this paper were carried out as a transnational service access, in the frame of the European Union-funded EVA-Global infrastructure project H2020 (grant agreement No. 871029-EVA-GLOBAL).

LITERATURE CITED

Abualrob A., Alabdallah O., Kubaa R.A., Naser S.M., Alkowni R., 2024. Molecular detection of Citrus exocortis viroid (CEVd), Citrus viroid-III (CVd-III), and Citrus viroid-IV (CVd-IV) in Palestine. *Scientific Report* 14: 423.

Cao M., Wu Q., Yang F., Wang X., Li R., Zhou C., Li Z., 2017. Molecular characterization and phylogenetic analysis of Citrus viroid VI variants from citrus in China. *European Journal of Plant Pathology* 149: 885–893.

De Stradis A., Parrella G., Vovlas C., Ragozzino A., 2008. Vein yellowing of Hibiscus rosa-sinensis caused by Eggplant mottled dwarf virus in southern Italy. *Journal of Plant Pathology* 90: 359–361.

Di Gaspero G., Radovic S., De Luca E., Spadotto A., Magris G., … Marroni F., 2022. Evaluation of sensitivity and specificity in RNA-Seq-based detection of grapevine viral pathogens. *Journal of Virological Methods* 300: 114383.

Luigi M., Manglli A., Tomassoli L., Faggioli F., 2013. First report of Hop stunt viroid in Hibiscus rosa-sinensis in Italy. *New Disease Report* 27: 14.

Kumar S., Stecher G., Li M., Knyaz C., Tamura K., 2018. MEGA X: molecular evolutionary genetic analysis across computing platform. *Molecular Biology and Evolution* 35: 1547–1549.

Parrella G., Mignano A., 2024. First report of hibiscus chlorotic ringspot virus infecting *Hibiscus rosa-sinensis* in Italy. *Plant Disease* 108: 828.

Pourrahim R., Ghobakhlo A., Farzadfar S., 2013. Biological and molecular detection of Hibiscus chlorotic ringspot virus infecting *Hibiscus rosa-sinensis* in Iran. *Phytopathologia Mediterranea* 52: 528–531.

Phytopathologia Mediterranea
The international journal of the
Mediterranean Phytopathological Union

Firenze University Press
www.fupress.com/pm

Research Papers

Deciduous fruit trees and grapevines as alternative crops in *Dematophora necatrix* (syn. *Rosellinia necatrix*) infested soils

Mery DAFNY-YELIN[1,*], Jehudith Clara KOHAVI-MOY[1], Tirtza ZAHAVI[2], Shlomit DOR[3], Amber HILL[4], Shlomi KFIR[1]

[1] *Northern Agricultural Research and Development, MIGAL, Galilee Technology Center, Kiryat Shemona 11016, Israel*
[2] *Extension Service, Ministry of Agriculture and Rural Development, Israel*
[3] *MIGAL, Galilee Technology Center, Kiryat Shemona 11016, Israel*
[4] *Tel Hai Academic College, Upper Galilee, 9977, Qiryat Shemona, 1220800, Israel*
*Corresponding author. E-mail: merydy@gmail.com

Summary. White root rot, caused by *Dematophora necatrix* (syn. *Rosellinia necatrix*), affects deciduous trees. A *D. necatrix* infection-distribution survey found widespread disease in apple and cherry orchards in northern Israel bordering a Mediterranean forest, although the forest trees were unaffected. Because cherry and apple orchards must be abandoned due to long fungal survival in infested soils, alternative deciduous fruit trees and grapevines were assessed for growth in these *D. necatrix*-infested orchards. In the field, grapevine rootstocks and the almond–peach rootstock GF-677 were most tolerant to *D. necatrix*-infested soil. Apple was the most sensitive crop, with the rootstock Hashabi being more tolerant than PI80 or MM104. The Mediterranean forest tree *Pistacia atlantica*, which can serve as a rootstock for pistachio, was as sensitive as kiwifruit and apple, and persimmon rootstock sensitivity was not different from grapevine. Those results show that beside the above mentioned crops, vineyards can also replace apple orchards in *D. necatrix*-infested soils and so broadens the list of possible crops for the local farmers in a Mediterranean climate at altitudes above 440 m above sea level. This has also been observed in a commercial 10-year-old vineyard of 'Shiraz' grapevines grafted on SO4 rootstock. The almond-peach rootstock GF-677 can also be grown in infested soil, but in commercial orchards requires additional treatment for adequate disease control.

Keywords. Apple rootstock, GF-677 almond–peach rootstock, grapevine rootstock, tolerant crops.

OPEN ACCESS

Citation: Dafny-Yelin, M., Kohavi-Moy, J.C., Zahavi, T., Dor, S., Hill, A., & Kfir, S. (2024). Deciduous fruit trees and grapevines as alternative crops in *Dematophora necatrix* (syn. *Rosellinia necatrix*) infested soils. *Phytopathologia Mediterranea* 63(2): 259-268. doi: 10.36253/phyto-15307

Accepted: July 21, 2024

Published: September 15, 2024

Data Availability Statement: All relevant data are within the paper and its Supporting Information files.

Competing Interests: The Author(s) declare(s) no conflict of interest.

Editor: Ilaria Pertot, Centro Agricoltura, Alimenti, Ambiente, University of Trento, Italy.

ORCID:
MD-Y: 0000-0001-9652-0964
JCK-M: 0009-0005-8636-7413
TZ: 0000-0003-3435-5961
SD: 0009-0003-2936-4051
AH: 0000-0001-6902-990X

INTRODUCTION

The disease white root rot is caused by the ascomycete fungus *Dematophora necatrix* Hartig, (syn. *Rosellinia necatrix*). *Dematophora necatrix* is a soilborne pathogen that has been reported to infect 170 plant species from 30 families, including deciduous trees (apple, pear, plum and almond), olives, some citrus species, avocado, mango and macadamia (Pliego *et al.*, 2011). Development

of this disease occurs in sensitive trees, where the roots become covered with white mycelium and decay, the leaves turn yellow and fall, and the affected trees wither and die soon after symptom appearance. In Israel, apple and cherry orchards are mostly affected (Dafny-Yelin *et al.,* 2018). Infected trees do not recover and must be uprooted. Replacement of the infected trees in apple or cherry orchards where the soils are infested is not possible, so the land must be abandoned for production of these fruit.

In Japan, grapevine is considered to be very sensitive to *D. necatrix* infection (Arakawa *et al*., 2002), but the plants can overcome infections with the use of fungicides (Kanadani *et al*., 1998). In Israel, grapevines became infected after inoculation with *D. necatrix*, but in naturally infested soil under field conditions, no plants became infected (Sztejnberg and Madar, 1980).

Tolerance to white root rot has been shown in the apple rootstocks M7 and MM109 (Gupta and Verna, 1978). In addition, SangBum *et al.* (2000) showed that a *Malus sieversii* seed lot was resistant to a Korean *D. necatrix* isolate, where 32 out of 159 clones of *Malus* germplasm exhibited slow development of *D. necatrix* infections or had no necrotic symptoms. In avocado plants, Zumaquero *et al.* (2019) characterized expression of different genes in tolerant and susceptible avocado rootstocks.

In Israel, Sztejnberg *et al.* (1983) reported that persimmon was survived for 6 years in *D. necatrix* infested soil, without any signs of disease symptoms. Citrus and mango rootstocks, and *Passiflora edulis*, were also tolerant to the disease (Sztejnberg and Madar, 1980). Most of the infested soils in Israel are in the northern part of the country, at altitudes 440-1100 m above sea level (Dafny-Yelin *et al*., 2018). This area is suitable for deciduous fruit trees and grapevines, but not for citrus or mango.

An infection-distribution survey by Dafny-Yelin *et al.* (2018) showed that white root rot was widespread in plots bordering a Mediterranean forest, but the infections did not appear to harm the trees in that forest. From farmer viewpoints, *Pistacia atlantica*, which grows in these forests, can be used as a rootstock for pistachio (Picchioni *et al*., 1990).

The present research aimed to identify alternative crops that could be grown in *D. necatrix*-infested soils to broadens the list of possible crops for the local farmers.

MATERIALS AND METHODS

Plant material

The following rootstocks and crops were tested:

(i) apple rootstocks Hashabi 13-14, Malling Merton series MM104, MM109 and MM106, and PI80 from Pillnitzer 'Supporter' (a semi-dwarf apple rootstock from Pillnitz in Dresden). All apple plants were 2 years old at planting day, and was obtained from the Tesler Nursery, Moshav Nov, Israel, except for the apple plants in the Metula plot that were not grafted and were only 1 year old at planting day.

(ii) GF-677 rootstock, a peach–almond hybrid which can be used as a rootstock for almond and peach, was obtained from plant nurseries in Rosh HaNikra, Israel, and was 1 year old at planting day.

(iii) grapevine rootstocks 101-14 MGT, 110 Richter, 1103 Paulsen, 140 Ruggeri and SO4 (*Vitis labrusca*), all grafted with Cabernet Sauvignon (*Vitis vinifera*). Grapevine plants were 6 months old, from the Machmid Nursery in Umm al-Fahm, and the Dor-onn and Zimnavoda Nursery in Zikhron Ya'akov, Israel.

(iv) persimmon rootstocks *Diospyros virginiana* and *Diospyros lotus* were from Haskelberg Nursery, Kfar Vitkin, Israel, and were 2 years old.

(v) *Actinidia deliciosa* (kiwifruit) var. Hayward (not grafted, self-rooted) 1-year-old plants from Fuga Agricultural Marketing Ltd., Yesud HaMa'ala, Israel.

(vi) *Pistacia atlantica* forest trees (not commercial rootstocks), 1-year-old plants from KKL Nursery, Golani junction, Israel.

Resistant fruit crops and grapevines in naturally infested plots

Experimental plots were chosen based on the presence of dead apple trees with typical *D. necatrix* mycelia in the roots. Experimental trees were planted between the orchard trees (except in Mas'ada where the entire plot was replanted). During the years of the experiment, the nearby orchard trees (or the trees between the experimental trees) were also monitored for indication of active disease (data not shown).

The field experiment included five plots. These were:

(1) Cabernet Sauvignon vines grafted on five rootstocks, including 101-14 MGT, 110 Richter, 1103 Paulsen, 140 Ruggeri, and SO4, planted in Metula orchards (Lat. 35.569, Long. 33.278, altitude of 442 m above sea level) in June 2013 (distribution map presented in Supplementary Figure 1);

(2) mainly non-grafted rootstocks, including —GF-677 (used for peach and almonds), Hashabi 13-14 (for apples), persimmon rootstocks *D. virginiana* and *D. lotus*, and *P. atlantica*, along with self-rooted kiwifruit var. Hayward, planted in Metula next to plot (1) (above) in July 2013 (Supplementary Figure 2);

(3) grapevines, fruit and forest trees grown together, with the plant material the same as in Metula

(above) with one exception. Hashabi 13-14 apple rootstock was grafted with var. Starking (Scarlet-spur type). The experiment was planted in Mas'ada (Lat. 33.237, Long. 35.780, 1034 m above sea level) in March 2013 (Supplementary Figure 3);

(4) apple tree var. Sundowner was grafted on the five different apple rootstocks, including Hashabi, MM106, MM109, PI80, MM104 from Tesler Nursery, and was planted in Manara orchard (Lat. 33.187, Long. 35.543, 848 m above sea level) in March 2018. The fungicide Ohayo (a.i. 0.5% fluazinam) was applied on the day of planting, at the rate of 2 L of 5 g L^{-1} Ohayo per tree via irrigation (as recommended in Dafny-Yelin *et al*., 2019). Two additional applications of the fungicide were applied at 1.5 and 2.5 months after planting (Supplementary Figure 4);

(5) similar experiment to (4) (above), planted in Sasa orchard (Lat. 33.022, Long. 35.400, 830 m above sea level) in March 2018, with the following exceptions: (i) the apple tree variety was Cripps Pink , (ii) to give the trees in Sasa the good establishment conditions, soil solarization was carried out in the summer of 2017, a year before planting. Ohayo fungicide was applied on the day of planting and one additional application was applied 2.5 months after planting (Supplementary Figure 5).

The grapevines were trained vertically and pruned each year. The weight of pruned tissues from each plant was measured as an index of plant vigour. For the other plant species, trunk circumferences were measured as indices of plant vigour. In Mas'ada in the last year of experiments, grapevine yield parameters were measured at harvest. For the other crops, trunk circumferences and tree heights (except for kiwifruit and grapevine) were measured in eack plot in the last experimental year. For all plants, in April to November, viability was recorded using the following key: 0 = dead plant, 1 = weak plant, 2 = healthy plant with no new vegetative growth, or 3 = healthy plant with normal development. Daily areas under the viability curves (AUC) were calculated based on ca. 20 monitoring times, at least five per year at minimum intervals of 1 month.

All experiments were planted in randomized blocks, in five (1st and 3rd plots) or six (2nd, 4th and 5th plots) replicates, except for *P. atlantica* in the 1st plot that was planted in six replicates, and 101-14 MGT and 110 Richter grapevine rootstocks that were planted in seven replicates. Plots 1 to 3 were planted in May 2013. Most replicates contained five trees, except for GF-677, which had four trees per replica. The trees were planted 0.5 m apart. Plots 4 and 5 were planted in March 2018. Each replica consisted of at least three trees (except for PI80 which had one tree in one of the replicas), and trees were planted *ca*. 1.5 m apart.

Statistical analyses

ANOVA and Pearson's chi-squared test for contingency analysis were carried out using JMP 13 software (SAS Institute, 2016). The statistical significance of treatment effects was determined using honestly significant difference (HSD), at $P \leq 0.05$, or Student's t-test [least significant difference (LSD), $P \leq 0.05$] for pairs. Normality (Shapiro–Wilk or Anderson–Darling tests) and homoscedasticity (Levene's test) of the results with or without square-root or Log+1 transformations were the conditions ($P > 0.05$) for running the ANOVA test; otherwise, non-parametric contingency analysis was performed. Where specified, Bonferroni corrections were applied to correct the critical alpha level, due to multiple chi-squared tests conducted. Effects of experimental blocks were also evaluated to estimate *D. necatrix* infection and aggressiveness in the orchards. In the apple rootstock experiment, contingency analysis was conducted only between the Hashabi–PI80 and Hashabi–MM104 pairs.

RESULTS

Comparisons between fruit crops and grapevines in naturally infested soils

To find potential alternative crops for farmers, and to give them the best alternatives based on farm geographical locations, comparisons between fruit crops and grapevines were made on two farms located in different geographical regions: (i) Metula in the Galilee region at 442 m above sea level, and (ii) Mas'ada in the Golan Heights at 1034 m above sea level. In the naturally infested soil in Mas'ada (Figure 1A), there were statistically significant differences between the crops in the number of wilting trees at the end of the experiment ($\chi^2 = 82.7577$, $P < 0.0001$), and no effect of block was detected ($\chi^2 = 10.7023$, $P = 0.0301$).

Almond and grapevine were the most resistant plants, with, respectively, 96.0% and 86.4% of plants still viable 5 years after planting. Almond was more tolerant than apple ($\chi^2 = 35.507$, $P < 0.0001$), kiwifruit ($\chi^2 = 18.015$, $P < 0.0001$), *P. atlantica* ($\chi^2 = 18.075$, $P < 0.0001$) and persimmon ($\chi^2 = 8.567$, $P = 0.034$). Persimmon plants showed 72.2 and 53.3% survival with *D. virginiana* and *D. lotus* rootstocks, respectively. Apple rootstocks were the most sensitive, with only 12% of the

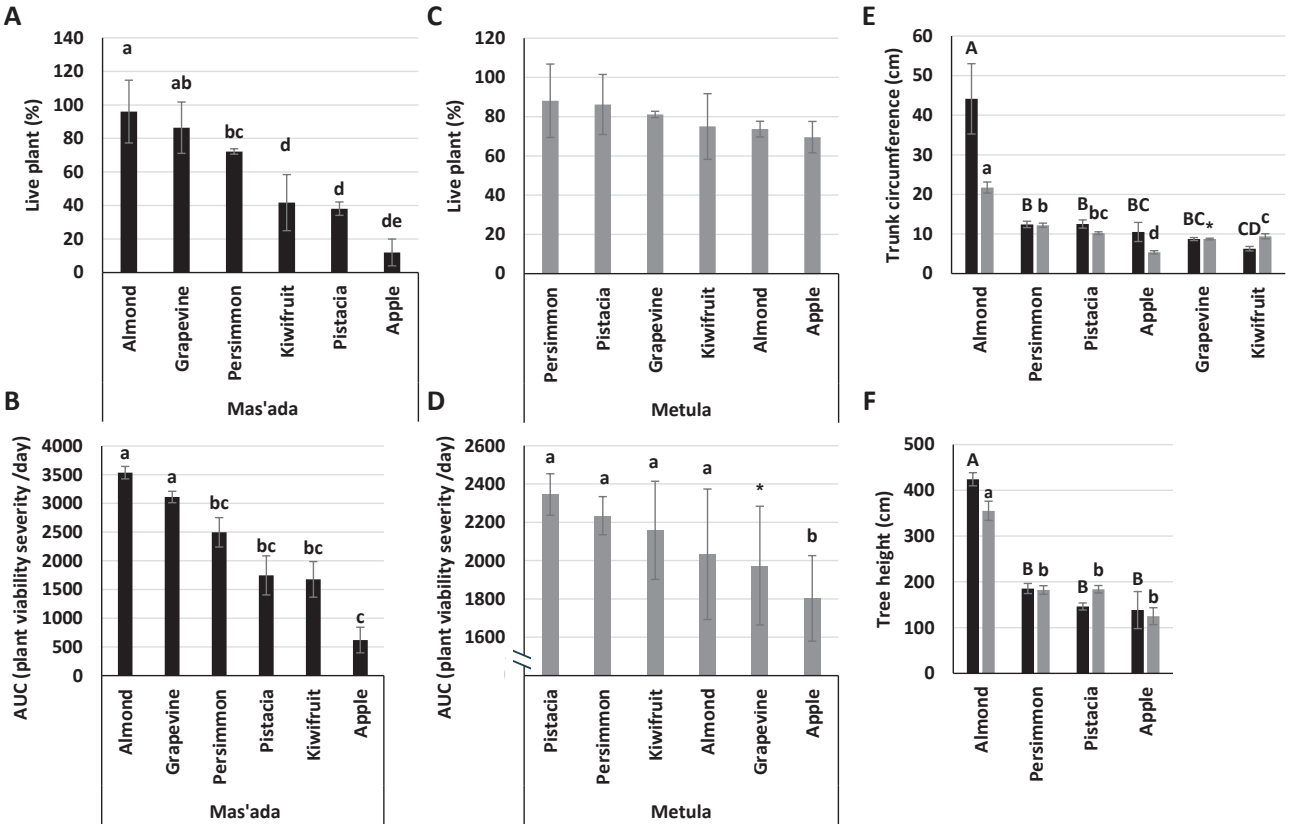

Figure 1. Mean parameters in *Dematophora necatrix*-infested soil for Mas'ada and Metula plants. (A) Percentage of live 5-year-old trees and (B) areas under the curves (AUC) for plant viability (0 = dead plant to 3 = live plant with good growth) over time (by days) in Mas'ada. Different letters indicate statistically significant differences ($P < 0.01$) between crops, as shown from contingency analyses, and Pearson tests after Bonferroni corrections, for 15 comparisons. (C) Mean percentages of live 3-year-old trees, and (D) mean AUC in Metula. Different letters accompanying the means indicate statistically significant differences ($P < 0.05$) between crop types, as indicated by contingency analyses, and Pearson tests without Bonferroni corrections. (E) Mean trunk circumferences of surviving trees. Black bars, Mas'ada plots; different uppercase letters indicate differences ($P < 0.05$) between crops as indicate from contingency analyses and Pearson tests after Bonferroni correction, for 15 comparisons. Gray bars, Metula plots; different lowercase letters indicate differences ($P < 0.05$) indicated from HSD after Log+1 transformations. (F) Mean tree heights. Black bar, Mas'ada plot; different letters indicate differences ($P < 0.05$) shown from HSD, after square root transformations. Gray bar, Metula plot; different letters indicate differences ($P < 0.05$), shown from contingency analyses, and Pearson tests after Bonferroni corrections, for six comparisons. Asterisks indicate that grapevines in Metula were not taken into consideration in the statistical analyses because they were planted in a separate plot nearby.

plants surviving after 5 years. Plant survival of *P. atlantica* and kiwifruit were, respectively, 38.1 and 40.0%, with no significant difference ($P > 0.05$) compared to the apple Hashabi rootstock (Figure 1A). AUC for plant viability per day gave statistically significant differences among crops ($\chi^2 = 88.9121$, $P < 0.0001$). Apple trees had the smallest AUCs, and almond and grapevine had the greatest, indicating that they were less sensitive than persimmon, *Pistacia*, kiwifruit and apple (Figure 1B).

In the Metula experiment the number of live apple plants was lowest (69.6%; Figure 1C), the number of live persimmon plants was highest (88.1%), while 26.3% of almonds and only 4.0% of Mas'ada plants were wilted. There was no significant difference ($\chi^2 = 4.8432$, $P = 0.3038$) between the crops for numbers of dead plants at the end of the experiment in 2015 (Figure 1C). For viability indices (AUC), there were significant differences between the crop types ($\chi^2 = 24.1618$, $P < 0.0001$), where apples had the lowest AUC values (lowest viability, and greatest severity), that were different from *Pistacia* (non-parametric comparison for each pair using the Wilcoxon method $P < 0.0001$), persimmon ($P < 0.0001$), kiwifruit ($P = 0.0098$), and almond ($P = 0.0234$), (Figure 1D). In Metula and in Mas'ada, block also had significant effects on AUC values ($\chi^2 = 88.9121$ for Metula and 13.4844 for Mas'ada, $P < 0.0001$, Wilcoxon test).

In the Metula and Mas'ada plots, at the end of the experiment (third and fifth years, respectively), trunk

circumferences of GF-677 were greatest (mean = 217 mm for Metula, and 441 mm for Mas'ada (Figure 1E), and the trees were the tallest (mean = 3.55 m in the third year for Metula and 4.24 m in the fifth year for Mas'ada. (Figure 1F). This indicates suggests that the disease affected plant growth differently based on the host sensitivities to *D. necatrix*, but that the pathogen did not kill the plants. No effect of block on plant height ($P > 0.05$) was detected in Metula or Mas'ada. However, in Mas'ada, there was a significant effect of block on the trunk circumference (after square root transformation, F = 5.9485, $P = 0.0013$).

Most of the plants that wilted died in the first year, up to 72% of the apple trees in Mas'ada. In general, for all crops, most of the trees died in the first 3 years. In Mas'ada, only a single plant or no plant from each crop wilted in the fourth year, and no wilting was seen in the fifth year of the study (Table 1). In grapevine, 78–92% of the plants were healthy after years 3 and 5 of the experiment. The main damage occurred in the first or second years of the study. For rootstock 1103 Paulsen in Mas'ada, and SO4 in Mas'ada and Metula, plant death was observed in less than 5% of the rootstocks after the second year of the study.

In Mas'ada, no statistically significant differences were observed between grapevine rootstocks for mean trunk circumference ($\chi^2 = 4.9029$, $P = 0.2974$), pruning weight ($\chi^2 = 4.0556$, $P = 0.3985$), yield (F = 1.0463, $P = 0.3872$), or AUC ($\chi^2 = 4.1664$, $P = 0.3840$; Table 2). In Metula, there were no effects on mean trunk circumference (F = 3.3069, $P = 0.0135$) or AUC for plant viability per day ($\chi^2 = 1.8664$, $P = 0.7603$). However, statistically significant differences were detected for mean pruning weights (F = 7.2734, $P < 0.0001$). Plants grafted on the 1103 Paulsen rootstock had greater pruning weights than plants grafted on the 110 Richter rootstock (F = 3.3867, $P = 0.0120$), with no effect of block (F = 0.568, $P = 0.7243$) or the block × crop interactions (F = 1.4983, $P = 0.2082$; Table 2).

Table 1. Mean proportions Sensitivity of fruit trees and grapevines to *D. necatrix* in naturally infested soil in the orchard. Dead plants were calculated as percentage of live plants at the beginning of each year.

		Percentage of dead plants each year (dead plants/live plants at the beginning of the year)				
Crop	Rootstock	2013	2014	2015	2016	2017
Mas'ada						
Almond	GF-677	0.0 (0/25)	0.0 (0/25)	4.0 (1/25)	0.0 (0/24)	0.0 (0/24)
Apple	Hashabi	72.0 (18/25)	14.3 (1/7)	50.0 (3/6)	0.0 (0/3)	0.0 (0/3)
Grapevine	101-14 MGT	8.0 (2/25)	0.0 (0/23)	0.0 (0/23)	0.0 (0/23)	0.0 (0/23)
	110 Richter	8.0 (2/25)	0.0 (0/23)	0.0 (0/23)	0.0 (0/23)	0.0 (0/23)
	1103 Paulsen	8.0 (2/25)	0.0 (0/23)	4.4 (1/23)	4.5 (1/22)	0.0 (0/23)
	140 Ruggeri	8.0 (2/25)	0.0 (0/23)	0.0 (0/23)	0.0 (0/23)	0.0 (0/23)
	SO4	4.0 (1/25)	4.2 (1/24)	4.3 (1/23)	0.0 (0/22)	0.0 (0/22)
Kiwifruit	Hayward	37.5 (9/24)	6.7 (1/15)	14.3 (2/14)	7.7 (1/13)	0.0 (0/12)
Persimmon	*D. virginiana*	11.1 (2/18)	6.3 (1/16)	13.3 (2/15)	0.0 (0/13)	0.0 (0/13)
	D. lotus	33.3 (5/15)	10.0 (1/10)	11.1 (1/9)	0.0 (0/8)	0.0 (0/8)
Pistacia	*atlantica*	38.1 (8/21)	15.4 (2/13)	27.3 (3/11)	0.0 (0/8)	0.0 (0/8)
Metula						
Almond	GF-677	26.32 (5/19)	0.0 (0/14)	0.0 (0/14)		
Apple	Hashabi	4.35 (1/23)	27.3 (6/17)	0.0 (0/16)	n.d.	n.d.
Grapevine	101-14 MGT	7.40 (2/27)	8.0 (2/25)	0.0 (0/23)	n.d.	n.d.
	110 Richter	25.00 (7/28)	4.8 (1/21)	0.0 (0/21)	n.d.	n.d.
	1103 Paulsen	21.4 (6/28)	0.0 (0/22)	0.0 (0/22)	n.d.	n.d.
	140 Ruggeri	7.4 (2/27)	0.0 (0/25)	0.0 (0/25)	n.d.	n.d.
	SO4	10.7 (3/28)	8.0 (2/25)	4.4 (1/23)	n.d.	n.d.
Kiwifruit	Hayward	12.5 (3/24)	4.8 (1/21)	10.0 (2/20)	n.d.	n.d.
Persimmon	*D. virginiana*	5.9 (1/17)	6.3 (1/16)	0.0 (0/15)	n.d.	n.d.
	D. lotus	0.0 (0/25)	12.0 (3/25)	0.0 (0/22)	n.d.	n.d.
Pistacia	*atlantica*	6.9 (2/29)	3.7 (1/27)	3.9 (1/26)	n.d.	n.d.

n.d., not detected.

Table 2. Mean plant growth indices of different live grapevine rootstocks in a soil that was naturally infested with *Dematophora necatrix*, at the end of 2017 in Mas'ada (n = 15 to 23 plants) and 2015 in Metula (n = 20 to 25 plants). The AUC for plant vitality / day calculated for all tested plants (n=24-25 plants in Mas'ada, n=30 plants in Metula).

Grapevine	Yield weight (g)	Trunk circumference (cm)	Pruning weight (kg)	AUC
Mas'ada (2017)				
101-14 MGT	904.9 ± 188.7	100.0 ± 7.14	1.3 ± 0.3	3220.0 ± 188.2
110 Richter	533.8 ± 122.5	74.8 ± 10.0	0.6 ± 0.1	2706.0 ± 302.6
1103 Paulsen	595.5 ± 130.0	101.0 ± 4.4	1.0 ± 0.1	3196.0 ± 188.6
140 Ruggeri	961.5 ± 205.0	82.8 ± 9.7	0.9 ± 0.2	3162.0 ± 215.5
SO4	836.5 ± 178.4	76.7 ± 9.4	0.7 ± 0.1	3286.0 ± 188.7
Metula (2015)				
101-14 MGT	998.4 ± 114.4	86.0 ± 4.6	2.4 ± 0.2 ab	2038.4 ± 148.5
110 Richter	1162.0 ± 125.8	91.1 ± 5.1	1.8 ± 0.2 c	1780.3 ± 176.8
1103 Paulsen	1251.65 ± 167.7	93.5 ± 4.2	2.7 ± 0.2 a	1901.2 ± 170.0
140 Ruggeri	1042.48 ± 132.6	84.9 ± 4.6	1.8 ± 0.2 bc	2069.0 ± 152.4
SO4	865.52 ± 121.0	82.1 ± 4.5	1.9 ± 0.2 bc	2081.8 ± 129.9

Different letters indicate significant difference by LSD ($P < 0.05$).

Comparison between apple rootstocks in naturally infested soils

To find potential solutions for growers who wish to continue growing apples, apple rootstocks were compared in naturally infested soil in two field plots located 22 km apart at similar altitude in the Galilee region. Hashabi was the most tolerant rootstock, with 82% (18 of 22) healthy trees in Manara and 87% (20 of 23) in Sasa. PI80 and MM104 were the most sensitive rootstocks, with 50% (eight of 16) PI80 trees surviving and 48% (ten of 21) of MM104 trees surviving. In Manara, statistically significant differences were found between Hashabi and PI80 ($\chi^2 = 4.34$; $P = 0.0372$) and Hashabi compared to MM104 ($\chi^2 = 5.532$; $P = 0.0187$), but not between blocks ($P > 0.05$). In addition, among the viable trees, Hashabi had an additional benefit in the infested soil compared to the other rootstocks, in terms of growth parameters of trunk circumference and tree height. In Sasa, MM109 and MM104 had the greatest growth parameters (Figure 2). There were no effects of block or rootstock × block interaction in either plot ($P > 0.05$).

DISCUSSION

This study examined the sensitivity of fruit crops and grapevine species to the pathogenic fungus *D. necatrix* in Mas'ada and Metula, with emphasis on species suitability for growth in the north of Israel, in the Golan Heights and in Galilee regions.

In the naturally *D. necatrix*-infested orchards, according to measures of trunk diameter and plant height, the GF-677 rootstock, which can be grafted with stone fruit trees such as peach and almond, produced the largest trees in the experimental plot. This is the first study to demonstrate that GF-677 rootstock can be grown in *D. necatrix*-infested soils. As a result, several infested commercial apple orchards in Metula were replaced in recent years with nectarine or peach trees on the GF-677 rootstock. In two of the three commercial plots, no tree mortality was seen for 2 years, and the trees developed normally. The third plot was monitored for 8 years after the crop replacement, and the orchard remained well-developed. However, each year, *ca.* 8 to 9% of the trees were replaced, similar to previous findings by Sztejnberg and Madar (1980). They observed that peach and almond species are very susceptible to *D. necatrix* in pots. Pinochet (2010) also reported that peaches grafted on GF-677 rootstock are very sensitive to *D. necatrix*, with an observed 18% mortality rate of trees growing in infested soil. The present study results showed that the GF-677 rootstock was less sensitive than the apple Hashabi rootstock, and can be grown in soil infested with *D. necatrix*, but additional steps must be taken to deal with the disease, such as solar treatments (Sztejnberg *et al.*, 1987) or use of pesticides (Gupta and Gupta, 1992; Dafny-Yelin *et al.*, 2019). In addition, more peach rootstocks should be tested in Israel to find better ones, as Pinochet (2010) reported that Replantpac (Rootpac R), a plum–almond hybrid rootstock, was suitable for replanting in *D. necatrix*-infested soils.

The grapevines in the field experiment survived, with approx. 85% surviving and mortality decreased each year. These results were similar to those of Sztejnberg and

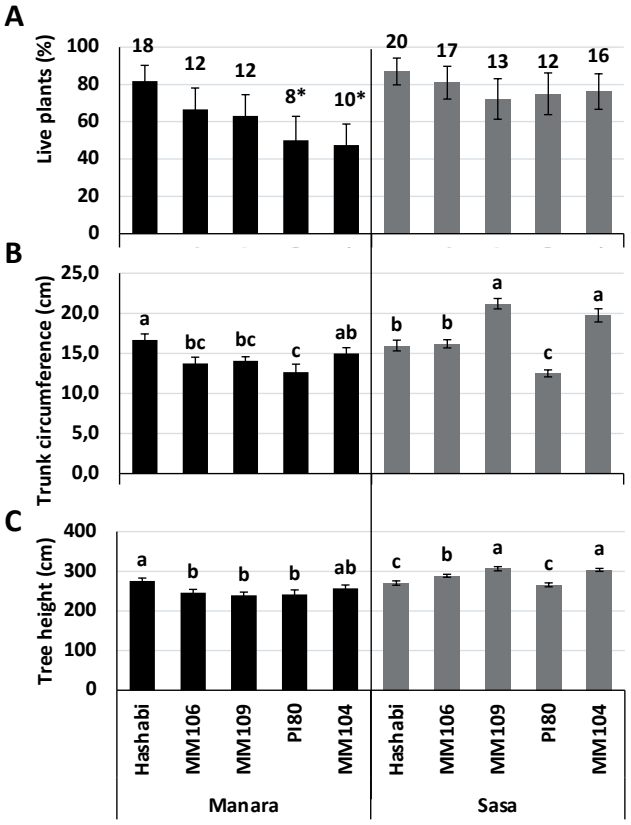

Figure 2. Mean apple rootstock parameters in *D. necatrix*-infested soils in Manara and Sasa. (A) Health of 5-year-old apple trees on different rootstocks (planted in March 2018, and tested in September 2022). The numeral above each column is the number of trees that survived. Asterisks indicates differences ($P < 0.05$) compared to the Hashabi survivors in each plot (contingency analyses). (B) Mean trunk circumferences of surviving trees. Different letters indicate differences ($P < 0.01$) between rootstocks in each plot (LSD tests). (C) Mean tree heights. Different letters indicate differences ($P < 0.05$) between rootstocks in each plot. Black histograms, Manara plots; gray histograms, Sasa plots.

Madar (1980), who showed that vines on different rootstocks were not damaged for 2 years in a naturally infested agricultural area. Mansoori and Dorostkar (2008) reported that most seedlings derived from *Vitis vinifera* and hybrid varieties died within 150 d in artificially infested pots, and the varieties were defined as susceptible. In contrast, seedlings of 'Bidaneh Sephid Gazvin' and 'Bidaneh Ghermez Gazvin' remained alive. Wine grapes in Israel are grown in areas where white root rot occurs in apple and cherry (Dafny-Yelin *et al.,* 2018), but no mortality occurs in grapevine plots as a result of the disease. This may be due to the low levels of irrigation applied in vineyards (500 to 2500 m^3 ha^{-1} per season (Zahavi, personal communication), compared to the *ca.* 10-fold greater irrigation rates applied for apple and cherry (Peres *et al.*, 2018).

In parallel to the experiments reported here, a study was carried out in Moshav Margaliot, where there was high infestation of cherry trees grafted on MM2 rootstock. In the summer of 2013, the farmer replaced this crop with a Shiraz scion grafted on the SO4 rootstock. Ten years after planting, the plot has remained healthy, bearing fruit, and no vines have been damaged by white root rot (Dafny-Yelin, personal communication).

Apple is known to be very susceptible to *D. necatrix* infections (Gupta, 1978; Sztejnberg *et al.*, 1987; Dafny-Yelin *et al.*, 2018; 2019), in agreement with the present study results in Mas'ada, where 88% of the apple trees (variety Starking Scarlet-spur, grafted on Hashabi rootstock) had died after the third year. In the Metula plot, the Hashabi rootstock was much less sensitive than in the Mas'ada plot, with less than a third of the trees having died during the same period.

Growth parameters of all plants that survived till the end of the experiment were monitored. Although these parameters of the various host species cannot predict plant survival, they can provide estimates of crop fitness in infested plots. The apple plants that survived in Metula developed at a lower rate than expected after 3 years, where healthy plants did not develop new growth and reached an average height of 1.25 m and trunk circumference of ca. 5 cm. This contrasted with GF-677 which developed new growth, and reached 3.5 m height and trunk circumference of more than 20 cm. In Metula, 27% of the trees wilted, whereas in Mas'ada, only 4% of the plants died. These differences may be due to other factors that affect plant and fungal development, such as irrigation regimes, the root system volumes, and soil type and depth. The interaction of rootstock and scion could also affect rootstock sensitivity, as the apple trees in Metula were not grafted. Rootstock–scion interactions are important because auxin, the growth regulator produced in the shoots, has effects on root development and elongation (Soumelidou *et al.*, 1994; Hooijdonk *et al.*, 2010).

Sharma *et al.* (2013) assessed resistance of apple rootstocks in a pot trial with artificially infested soil, and showed that the commercial rootstocks MM106, M4, M9, M26, M27 and M7 were very sensitive to *D. necatrix* infection. Gupta and Verma (1978) showed that M7 and MM109 were partially resistant in the field 500 d after infection. In the present study, similarly to Sharma *et al.* (2013) in naturally infested soil, none of the apple rootstocks exhibited immune reactions. However, apple trees that were grafted on Hashabi were less sensitive than those on the other assessed rootstocks in two plots (Figure 2). The trees were less damaged in Sasa than in Manara probably because the soil in Sasa had been solarized before planting. Solarization has

been found useful for young trees under Israel's climatic conditions (Sztejnberg *et al.*, 1987), and in other areas in the world where apples (Gupta, 1978; Kanadani *et al.*, 1998) or avocado (López-Herrera and Zea-Bonilla, 2007; Arjona-López *et al.*, 2020) are grown in infested soils. In healthy Israeli plots, Hashabi plants had the optimum rootstock for apple growth (Assaf, 1995), and in the *D. necatrix*-infested plot in Manara, this rootstock gave the best performance as indicated by trunk circumference. The semi-dwarf rootstock PI80 was the weakest, as expected, with the least mean trunk circumference and tree height (Figure 2, and Fischer, 1996). However, since introduction of new apple rootstocks, Hashabi is no longer commonly used in commercial orchards.

Persimmon survived in the Metula experimental plots at an average of *ca.* 90%, greater survival than for the other crops; in Mas'ada, survival rate of Metula was less than for almond trees, but similar to that for grapevines. Sztejnberg *et al.* (1983) reported survival of persimmon trees for 6 years with no signs of disease, suggesting that this was due to high phenol contents in the roots of this species.

Kiwifruit is a *D. necatrix*-sensitive crop (Pliego *et al.*, 2011). In the present study, kiwifruit was found to be less susceptible to the pathogen than apple. Similar to grapevine, kiwifruit is grown in Israel in plots that are close to infected apple and cherry orchards (Dafny-Yelin *et al.*, 2018), and no mature kiwifruit plots with mortality due to *D. necatrix* have been seen. This suggests that kiwifruit can overcome the white root rot in commercial plots.

Overall, grapevine and peach rootstocks were the most tolerant of *D. necatrix* soil infestations, without any significant differences between the assessed rootstocks. Apple was the most sensitive crop. Among apple rootstocks, Hashabi was more resistant to *D. necatrix* infections than PI80 or MM104 rootstocks. Kiwifruit and *Pistacia* were as sensitive as apple, while persimmon rootstock sensitivity did not differ significantly from that of the grapevine rootstocks.

CONCLUSIONS

This study has demonstrated the relative sensitivity of different fruit crop species (including grapevine) to the pathogenic fungus *D. necatrix*, in different regions of Israel. Grapevines commercial rootstocks and the almond-peach rootstock GF-677 had promising tolerance to *D. necatrix*-infested soil, offering an alternative for orchard replacement, particularly in the northern regions of Israel such as the Golan Heights and Galilee areas. Despite susceptibility to white root rot in controlled experiments, GF-677 exhibited resilience in commercial orchards, although additional disease management practices were required in the field. The present study also highlighted the importance of selecting appropriate host rootstocks, with Hashabi showing greatest resistance among apple varieties. The necessity for crop replacements for management of soilborne diseases underscores the challenges faced by farmers, necessitating further research to identify optimal rootstocks for sustainable agriculture in *D. necatrix*-infested areas. The present study has contributed valuable insights for agricultural practices aimed at mitigating the impacts of soil-borne pathogens on fruit crop production in Israel.

FUNDING

This work was supported by the "Plant Production & Marketing Board".

AUTHOR CONTRIBUTIONS

Mery Dafny-Yelin and Tirtza Zahavi conceived the study, the experimental design and the data analyses; Jehudith Clara Kohavi-Moy and Shlomit Dor conducted data collection; Shlomi Kfir took care of the experiment plots; Mery Dafny-Yelin wrote the first draft of the manuscript of this paper; and all authors commented on all previous versions of the manuscript. Amber Hill and Tirtza Zahavi reviewed and edited the manuscript of the paper, and all the authors read and approved the final manuscript.

ACKNOWLEDGMENTS

The authors thank the Vinberd family from Metula, Orchard Kibbutz Sasa and Orchard Kibbutz Manara, and the farmer Faiz Safady from Mas'ada who helped locate the experimental sites and was responsible for irrigation, and Soliman Farchat who took care of the experiment plots. Camille Vainstein assisted with proofreading the manuscript of this paper.

LITERATURE CITED

Arakawa M., Nakamura H., Uetake Y., Matsumoto N., 2002. Presence and distribution of double-stranded RNA elements in the white root rot fungus *Rosellinia necatrix*. *Mycoscience* 43: 21–26.

Arjona-López J.M., Capote N., Melero-Vara J.M., López-Herrera C.J., 2020. Control of avocado white root rot by chemical treatments with fluazinam in avocado orchards. *Crop Protection* 131: 105100. https://doi.org/10.1016/j.cropro.2020.105100.

Assaf R., 1995. Les Hashabi, nouveaux porte-greffes pour la culture du pommier en Israël II-Comportement dans différentes conditions de culture. *Fruits* 50(2), 133–143. https://revues.cirad.fr/index.php/fruits/article/view/35469/36534.

Dafny-Yelin M., Mairesse O., Moy J., Dor S., Malkinson, D., 2018. Genetic diversity and infection sources of *Rosellinia necatrix* in northern Israel. *Phytopathologia Mediterranea* 57(1): 37–47. https://www.jstor.org/stable/26458735.

Dafny-Yelin M., Dor S., Mairesse, O., Moy J., 2019. The control of white root rot of apple tree caused by *Rosellinia necatrix* by fluazinam and prochloraz. *Pesticides and Bio Fertilizers*. https://www.auctoresonline.org/article/the-control-of--white-root-rot-of-apple-tree-caused-by-rosellinia-necatrix-by-fluazinam-and-prochloraz.

Fischer M., 1996. Pillnitzer Supporter 4 (Pi 80) – A semi-dwarf apple rootstock from Dresden-Pillnitz, in *VI International Symposium on Integrated Canopy, Rootstock, Environmental Physiology in Orchard Systems Acta Horticolturae* 451, 99–104. https://doi.org/10.17660/ActaHortic.1997.451.7

Gupta V.K., 1978. Possible use of carbendazim in the control of *Dematophora* root rot of apple. *Indian Phytopathology* 30: 527–531. https://www.cabdirect.org/cabdirect/abstract/19791354768.

Gupta V.K., Verma K.D., 1978. Comparative susceptibility of apple root-stocks to *Dematophora necatrix*. *Indian Phytopathology* 31(3): 377–378. https://www.researchgate.net/publication/339657987.

Gupta V.K., Gupta S.K., 1992. Management of white root rot of apple with fungicide drenching. *Indian Phytopathology* 45(2): 239–240. https://epubs.icar.org.in/index.php/IPPJ/article/view/21628.

Hooijdonk V., Woolley D.J., Warrington I.J., Tustin D.S., 2010. Initial alteration of scion architecture by dwarfing apple rootstocks may involve shoot-root-shoot signalling by auxin, gibberellin, and cytokinin. *Journal of Horticultural Science and Biotechnology* 85(1): 59–65. https://doi.org/10.1080/14620316.2010.11512631.

Kanadani G., Date H., Nasu H., 1998. Effect of fluazinam soildrench on white root rot of grapevine. *Annals of the Phytopathological Society of Japan* 64: 139–141. https://www.jstage.jst.go.jp/article/jjphytopath1918/64/2/64_2_139/_pdf.

López-Herrera C.J., Zea-Bonilla T., 2007. Effects of benomyl, carbendazim, fluazinam and thiophanate methyl on white root rot of avocado. *Crop Protection* 26(8): 1186–1192. https://doi.org/10.1016/j.cropro.2006.10.015.

Mansoori B., Dorostkar M., 2008. Reactions of some grape cultivars to *Dematophora necatrix*. *Vitis* 47(4): 231–233.

Peres M., Grinblet Y., Doron I., 2018. Irrigation coefficients and water doses for deciduous plantations. Israel Ministry of Agriculture and Rural Development Extension Service – Professional Publications. In Hebrew.

Picchioni G.A., Miyamoto S., Storey J.B., 1990. Salt effects on growth and ion uptake of pistachio rootstock seedlings. *Journal of the American Society for Horticultural Science* - ASHS 115(4): 647–653. https://doi.org/10.21273/JASHS.115.4.647.

Pinochet J., 2010. 'Replantpac' (Rootpac® R), a plum–almond hybrid rootstock for replant situations. *HortScience* 45(2): 299–301. https://doi.org/10.21273/HORTSCI.45.2.299.

Pliego C., López-Herrera C., Ramos C., Cazorla F.M., 2011. Developing tools to unravel the biological secrets of *Rosellinia necatrix*, an emergent threat to woody crops. *Molecular Plant Pathology* 13(3): 226–239. https://doi.org/10.1111/j.1364-3703.2011.00753.x.

SangBum L., KiSung K., Aldwinckle H.S., 2000. Resistance of selected *Malus* germplasm to *Rosellinia necatrix*. *Journal of the American Pomological Society* 54(4): 219–228.

Sharma Y.P., Pramanick K.K., Sharma S.K., Kashyap P., 2013. Disease reaction of apple germplasm to white root rot (*Dematophora necatrix*). *Indian Journal of Horticulture* 70(1): 130–134.

Soumelidou K., Morris D.A., Battey N.H., Barnett J.R., John P., 1994. Auxin transport capacity in relation to the dwarfing effect of apple rootstocks. *Journal of Horticultural Science* 69(4): 719–725. https://doi.org/10.1080/14620316.1994.11516505.

Sztejnberg A., Madar Z., 1980. Host range of *Dematophora necatrix*, the cause of white root rot disease in fruit trees. *Plant Disease* 64: 662–664.

Sztejnberg A., Azaizia H., Chet I., 1983. The possible role of phenolic compounds in resistance of horticultural crops to *Dematophora necatrix* Hartig. *Journal of Phytopathology* 107(4):318–326. https://doi.org/10.1111/j.1439-0434.1983.tb00551.x.

Sztejnberg A., Freeman S., Chet I., Katan J., 1987. Control of *Rosellinia necatrix* in soil and in apple orchard by solarization and *Trichoderma harzianum*. *Plant Disease* 71(4): 365–369.

Zumaquero A., Martínez-Ferri E., Matas A.J., Reeksting B., Olivier N.A., Pliego-Alfaro F., …Pliego C., 2019. *Rosellinia necatrix* infection induces differential gene expression between tolerant and susceptible avocado rootstocks. *PLoS One* 14(2): e0212359.

Phytopathologia Mediterranea
The international journal of the
Mediterranean Phytopathological Union

Firenze University Press
www.fupress.com/pm

Research Papers

Montmorillonite nanoclay triggers immunity responses in wheat against *Puccinia striiformis* f. sp. *tritici*, and suppresses uredospore germination

Younes M. RASHAD[1,*], Mohamed HAFEZ[2], Mohamed BOUROUAH[3], Ahmed M. ABD-ELGAWAD[4], Hany H.A. EL-SHARKAWY[5]

[1] *Plant Protection and Biomolecular Diagnosis Department, Arid Lands Cultivation Research Institute (ALCRI), City of Scientific Research and Technological Applications (SRTA-City), New Borg El-Arab City, 21934, Egypt*
[2] *Land and Water Technologies Department, Arid Lands Cultivation Research Institute (ALCRI), City of Scientific Research and Technological Applications (SRTA-City), New Borg El-Arab, 21934, Egypt*
[3] *Hahn-Schickard-Gesellschaft für angewandte Forschung e V., Wilhelm-Schickard-Straße 10, 78052 Villingen Schwenningen, Germany*
[4] *Plant Production Department, College of Food & Agriculture Sciences, King Saud University, P.O. Box 2460 Riyadh 11451, Saudi Arabia*
[5] *Mycology Research and Diseases Survey Department, Plant Pathology Research Institute, Agricultural Research Center, Giza, Egypt*
*Corresponding author. E-mail: younesrashad@yahoo.com

Summary. *Puccinia striiformis* f. sp. *tritici* causes the important disease, yellow rust of wheat (*Triticum aestivum*). Montmorillonite nanoclay (MNC) is naturally occurring and biodegradable. This study assessed *in vitro* anti-germination effects of MNC on *P. striiformis* uredospores. Application of MNC at 150 mg L^{-1} completely inhibited uredospore germination, and MNC at 100 mg L^{-1} reduced yellow rust severity in wheat plants by 89%. Expression of defense-related genes was increased after MNC treatment at 100 mg L^{-1}, by 5.23-fold for jasmonate and ethylene-responsive factor 3 (*JERF3*), 4.89-fold for chitinase class II (*CHI II*), and 2.37-fold for pathogenesis-related protein 1 (*PR1*). Applying MNC at 100 mg L^{-1} also activated the antioxidant enzymes POD to 62.1 unit min^{-1} g^{-1} fresh wt, PPO to 21.6 units min^{-1} g^{-1} fresh wt, and CAT to 36.6 units min^{-1} g^{-1} fresh wt. MNC also enhanced phenolic content in wheat leaves (to 1489.53 mg 100 g^{-1} f. wt), and reduced lipid oxidation levels (to 5.6 µmol MDA g^{-1} fresh wt). MNC at 100 mg L^{-1} also mitigated damaging effects of *P. striiformis* infections on host leaf cell ultrastructure, increased leaf photosynthetic pigments, and increased wheat plant growth. These results show that MNC has potential as a natural control agent for yellow rust of wheat, although field testing of MNC is necessary before this material can be recommended for wheat production.

Keywords. Nanoclay, host resistance, defense, *Triticum aestivum*, yellow rust.

OPEN ACCESS

Citation: Rashad, Y.M., Hafez, M., Bourouah, M., Abd-ElGawad, A.M., & El-Sharkawy, H.H.A. (2024). Montmorillonite nanoclay triggers immunity responses in wheat against *Puccinia striiformis* f. sp. *tritici*, and suppresses uredospore germination. *Phytopathologia Mediterranea* 63(2): 269-281. doi: 10.36253/phyto-15291

Accepted: August 5, 2024

Published: September 15, 2024

Data Availability Statement: All relevant data are within the paper and its Supporting Information files.

Competing Interests: The Author(s) declare(s) no conflict of interest.

Editor: Alessandra Lanubile, Università Cattolica del Sacro Cuore, Piacenza, Italy.

ORCID:
YMR: 0000-0002-7702-8023
MH: 0000-0001-9269-2128
MB: 0009-0001-3311-3816
AMA-E: 0000-0002-5903-6329
HHAE-S: 0000-0002-9386-6852

INTRODUCTION

Nanoclays are clay minerals consisting of particles in nanometer size ranges (1 to 100 nm). These minerals are classified as phyllosilicates, and are composed of stacked layers of aluminum and silicon oxides (Nazir *et al*., 2016). Nanoclays are known for their widespread presence in different environments, their high cation exchange capacity, affordability, and overall non-toxic nature. These properties allow them to form polymer nanocomposites which are carriers for active compounds and bioagents. These polymer nanocomposites have extensive applications in medicine, agriculture, and other technological applications, forming the nanoclay technology (Hafez *et al*., 2022).

Nanoclay research has focused on harnessing potential of materials in several fields (Merino *et al*., 2021). Agricultural uses of different nanoclay types, including montmorillonite, have been studied mainly for their antimicrobial activities (Yousef *et al*., 2023) and aflatoxin B1 detoxification potential in animal feeds (Soltan *et al*., 2022). Rashad *et al*. (2021a) reported effective spraying of silica nanoparticles (at 150 ppm) against downy mildew of grapevines, caused by *Plasmopara viticola*. A reduction (82%) in the disease severity and induction in the plant defense responses were recorded. Guilger-Casagrande *et al*., (2024) found that nanoparticles of iron oxide and titanium dioxide had high insecticidal potential on larvae of the crop pests *Helicoverpa armigera* and *Spodoptera frugiperda*, recording up to 76% mortality of these insects.

Montmorillonite is a clay mineral (smectite category), and consists of a layer of alumina enclosed between two layers of silica. Montmorillonite nanoclay (MNC) is widely used as a nanocomposite to form nano antimicrobials and pesticides against several plant diseases (Hossain *et al*., 2023). Oliveira-Pinto *et al*. (2022) reported effective potential of MNC alone or supplemented with *Satureja montana* essential oil, for control of bacterial spot in tomato, caused by *Xanthomonas euvesicatoria*. Antimicrobial, antioxidant, and defense triggering activities of MNC have been discussed as disease management strategies. Sundaresha *et al*. (2022) found that spraying potato plants with multigene-targeted dsRNA molecules carried on nanoclay particles reduced severity of late blight and inhibited growth and sporulation of *Phytophthora infestans*. In general, nanoparticles can be used to control different plant diseases, either as alone as protectants (Rashad et al., 2021a) or as carriers for fungicides or other antimicrobial substances (Worrall *et al*., 2018).

Wheat (*Triticum aestivum*) is the main staple diet for much of the world population. However, this crop is adversely affected by many fungal pathogens that are production threats. *Puccinia striiformis* Westend. f. sp. *tritici* Eriks, which causes stripe rust (yellow rust) of wheat, is a destructive pathogen that threatens wheat production (Chen *et al*., 2014). This obligate biotrophic basidiomycete fungus) is a heteroecious pathogen, infecting two alternate hosts (wheat and *Berberis* spp.) during its life cycle (Zhao *et al*., 2011). Under suitable climatic conditions, stripe rust infections can result in a severe wheat grain yield reduction of up to 100%. Fast growth, sporulation intensity, variability, and long-distance dispersal of air-borne *P. striiformis* uredospores are key properties that enable the fungus to cause severe yield damage (Chen *et al*., 2014).

Control of stripe rust has been widely studied using different agents to overcome development of *P. striiformis* race variability and rust resistance in wheat. El-Sharkawy *et al*. (2023a) achieved 88% reduction in yellow rust of wheat when sprayed with the endophyte *Epicoccum nigrum* Link (HE20). However, studies are lacking on impacts of MNC against wheat stripe rust. The present research was designed to investigate: 1) the inhibitory potential of MNC on *P. striiformis* uredospore germination; 2) disease control potential of MNC in greenhouse tests; 3) effects of MNC on transcriptomic profiles of defense genes in wheat plants; and 4) the effects of MNC applications on physiology, ultrastructure, and development of wheat plants.

MATERIALS AND METHODS

Fungal and plant materials

For the greenhouse experiment, infection of wheat plants was carried out using fresh uredospores of *P. striiformis* race 174E191. These spores were obtained from the Plant Pathology Research Institute, Agricultural Research Center (ARC), Giza, Egypt. To prepare inoculum, uredospores were suspended in sterilized water and adjusted to concentration of 10^4 spore mL^{-1} using a haemocytometer. Tween 80 (Sigma-Aldrich) was added at 0.3%, and gum Arabic (Stanton) was added to standardized uredospore suspensions at 35 g L^{-1}. The wheat cultivar Gemmaza 11 was used in experiments, and was obtained from ARC in Egypt.

Montmorillonite clay (MNC) preparation

The MNC used in this study was purchased from Egypt Bentonite and Derivatives Co., Alexandria, Egypt. To prepare MNC, montmorillonite clay parti-

cles were firstly modified with the organic surfactant CETAB (Sigma Aldrich) as described by Bujdáková *et al*. (2018). The modified MNC was ground using a planetary mill (PM 100, Verder Scientific) for 5 h at 300 rpm (reverse rotation), followed by 600 rpm (vial rotation) with nine zirconia grinding balls (35 mm diam.) and 12 (12 mm) (9:1 mass:mass) to obtain nano-scale particles (Soltan *et al*., 2022).

Characterization of MNC

To determine shape and size of MNC particles, dry nanoclay particles were put on a brass holder, coated with gold, and examined using a scanning electron microscope (SEM, JEOL-JSM-6360-LA), under vacuum and at accelerating voltage 20 Kv. To determine the element content of MNC, nanoclay particles were coated with gold and examined using an energy-dispersive X-ray spectroscope (EDX-Max), at a working voltage of 30 Kv. Functional groups in the MNC were identified using a Fourier-transform-infrared spectrophotometer (FTIR) (Shimadzu FTIR-8400S) equipped with a deuterated triglycine sulfate detector.

Assessment of the suppressive potential of MNC

Suppressive potential of MNC was tested against uredospore germination using the agar plate method *in vitro*. Petri plates (8 cm diam.) containing water agar (Merck) supplemented with MNC to obtain final concentrations of 10, 8, 6, 4, or 2% were each inoculated with 200 uredospores. Water agar plates without added MNC served as experimental controls. Three biological replicates and three technical replicates were applied for each treatment. The plates were incubated at 9°C for 1 d, and uredospore germination was assessed, and percentage of germination suppression was calculated.

Evaluation of MNC for wheat rust control

Plastic pots (20 cm diam.), each containing 10 kg sterile soil, were each planted with ten wheat seeds that had been previously surface sterilized by soaking in hypochlorite solution (0.05%) for 1.5 min, then in ethyl alcohol (75%) for 1.5 min. The pots were fertilized twice, first at seed sowing and then 7 weeks later. For each fertilization, nitrogen, (1 g per pot) phosphorus (1.5 g) and potassium (1 g) were applied. At 60 d after sowing, the resulting wheat plants were sprayed with MNC solution (at 100, 150, or 200 mg L^{-1} water) until run-off. A set of plants sprayed with Crwan fungicide (El-Helb Pest. and Chem., Egypt) at 3 mL L^{-1} served as positive controls. For inoculations, suspensions of *P. striiformis* uredospores were sprayed onto the plants (at booting growth stage) 3 d after the experimental treatments were applied. For negative controls, a set of plants were sprayed with water. Fifteen pots per treatment were used, and all pots were irrigated twice each week. All plants were arranged in a completely randomized experimental design in a greenhouse (20°C/17°C, 14 h light/10 h dark daily regime, and 75-90 % humidity). Treatments assessed were: untreated uninoculated (control; C), untreated plus *P. striiformis* inoculated (P), fungicide treated plus inoculated (F + P), MNC at 100 mg L^{-1} plus inoculated (N1 + P), MNC at 150 mg L^{-1} plus inoculated (N2 + P), or MNC at 200 mg L^{-1} plus inoculated (N3 + P).

Stripe severity was assessed in the plants at 14 d after inoculation (dai), according to the scale of Peterson *et al*. (1948). Average disease severity coefficients were calculated by multiplying severity percentages by values according to disease type: resistant = 0.2, moderately resistant = 0.4, moderately susceptible = 0.8, and susceptible = 1 (Johnston and Browder, 1966).

Impact of MNC on wheat gene expression

Wheat leaves (second upper leaf) from the assessed treatments were sampled at 3 d after inoculation (dai) (booting stage). Total RNA was extracted from sampled leaves using a RNA extraction kit (Qiagen), following the manufacturer's instructions. The reverse transcription mixture contained RNA (30 ng, 2.5 µL), 10× buffer solution (3 µL), oligo (dT) primer (8 pmol μL^{-1}, 5 µL), dNTPs (13 mM, 2.5 µL), RT enzyme (Biolabs, (0.4 µL), and sterile RNase-free water (7.6 µL). The reaction was carried out at 42°C for 1.5 h, then at 85°C for 10 min. cDNA was prepared using a thermocycler (Sure-Cycler 8800, Agilent Technologies). The quantitative real-time PCR (qPCR) contained cDNA (55 ng; 2.5 µL), SYBR Green Mix (13 µL, Bioloine), forward and reverse primers (10 pmol μL^{-1}, 1.5 µL for each), and sterile water (1.5 µL). Triplicate qPCR reactions (biological and technical) were carried out as follows: one cycle at 95°C for 3 min, 40 cycles, each of 95°C for 15 s, 56°C for 30 s, and 72°C for 30 s. β-actin was used as the reference gene. The primer sequences used are indicated in Table 1. The Rotor-Gene-6000-system (Qiagene) was used for the qPCR. The comparative CT method ($2^{-\Delta\Delta CT}$, Livak and Schmittgen, 2001) was used to calculate the gene expression, using triplicate samples (biological and technical).

Table 1. Primer sequences used in quantitative real-time PCR to study transcriptional expression of the defense-related genes jasmonate and ethylene-responsive factor 3 (*JERF3*), chitinase class II (*CHI II*), and Pathogenesis-related protein 1 (*PR1*) in wheat leaves after application of montmorillonite nanoclay at 100 mg L^{-1}.

Gene name	Abbreviation	Sequence (5'-3')
Jasmonate and ethylene-responsive factor 3	*JERF3*-F	GCCATTTGCCTTCTCTGCTTC
	JERF3-R	GCAGCAGCATCCTTGTCTGA
Chitinase class II	*CHI II*-F	GCGTTGTGGTTCTGGATGACA
	CHI II-R	CAGCGGCAGAATCAGCAACA
Pathogenesis-related protein 1	*PR1*-F	ACTTGGCATCCCGAGCACAA
	PR1-R	CTCGGACACCCACAATTGCA
β-actin	*β-actin-F*	GTGGGCCGCTCTAGGCACCAA
	β-actin-R	CTCTTTGATGTCACGCACGATTTC

Effects of MNC on the biochemical indicators in wheat leaves

At 3 dai, wheat leaves from each treatment (second upper leaf from each plant) were sampled for biochemical analyses. Total phenolic compounds were estimated as described by Malik and Singh (1980), using the Folin–Ciocalteu reagent. Peroxidase (POD) activity was determined as described by Maxwell and Bateman (1967), and polyphenol oxidase (PPO) was determined as described by Galeazzi *et al.* (1981). Catalase (CAT) activity was determined as described by Chance and Maehly (1955). Lipid peroxidation, expressed as malondialdehyde, was estimated at 14 dai in wheat leaves, as described by HongBo *et al.* (2005). The method of Harborne (1984) was used to measure photosynthetic pigments. Four samples were used for assessments of each treatment.

Transmission electron microscopy (TEM)

Wheat leaves were sampled from the different experimental treatments at 7 dai. The samples were cut into small segments (1 cm^2) and dehydrated using serial dilutions of ethyl alcohol (10 to 100%) for 10 min at each concentration). The samples were treated with propylene oxide for 15 min, and then put into gelatin capsules containing Araldite® for 1 h. The samples were then incubated at 65°C for 62 h. A Reichert ultramicrotome was used for the ultrathin sectioning. The obtained sections (thickness 70 to 90 nm) were stained by uranyl acetate (2%) then lead citrate (3%). Examination of the samples was carried out using a trans-mission electron microscope (JEM-1230, JEOL Ltd), as described by Hayat (2000).

Effects of MNC on the plant growth

From each treatment, ten plants were randomly selected at 30 dai (ripening stage), and were uprooted, washed with tap water, then measured for plant heights (cm), dry weights (g) of shoots and roots, and leaf areas (cm^2). Leaf areas were measured using ImageJ software, while plant heights were determined using a flexible graduated tape measure. Plant weights were measured after the plants had been sampled were oven-dried (80°C for 48 h).

Statistical analyses

Normality of raw data was assessed by Shapiro tests before analysis of variance. One-way analysis of variance was applied to raw data. The experimental design was completely randomized ($y_{ij} = \mu_i + \varepsilon_{ij}$). Comparisons of means were carried out using Tukey's HSD test ($P \leq 0.05$) with CoStat package version 6.4) (CoStat, 2005).

RESULTS

Characterization of MNC

The MNC used in this study was characterized using different techniques to elucidate its structure and physicochemical features. SEM observation showed glomerations of MNC particles with layered surfaces, showing that the material had normal form of montmorillonite clay (Figure 1).

Figure 2 shows the FTIR analysis of MNC. The FTIR spectrum revealed existence of interlayer –OH peaks at wavenumbers 3693 and 3626 cm^{-1}, which is characteristic for vibrations of OH in montmorillonite. Additionally, the absorption band at wavenumber of 1633 cm^{-1} is attributed to –OH bending in adsorbed H_2O, and the peak at wavenumber 1089 cm^{-1} is characteristic for Si–O–Si vibration (out-of-plane). Furthermore, the peak at wavenumber of 992 cm^{-1} is character-

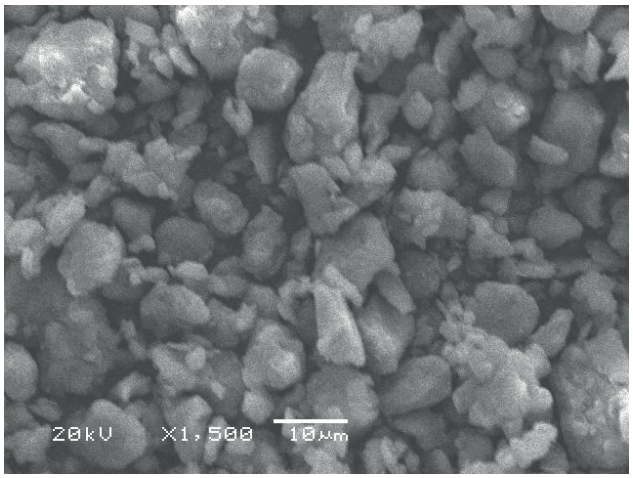

Figure 1. Scanning electron micrograph of the montmorillonite nanoclay used in this study. The cracked and rough particle surface morphology and agglomerations of particles with layered surfaces indicate normal form of the montmorillonite clay.

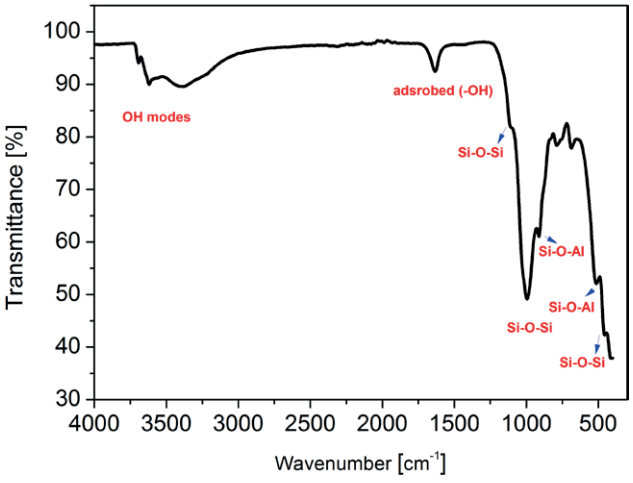

Figure 2. Fourier transformed infrared spectrum showing the functional groups in used montmorillonite nanoclay used in this study. The spectrum shows existence of the interlayer –OH peaks at 3693 and 3626 cm^{-1}. The absorption band at 1633 cm^{-1} is due to –OH bending. The peak at 1089 cm^{-1} is characteristic for the Si–O–Si vibration. The peak at 992 cm^{-1} is characteristic of in-plane Si–O–Si vibration. The area at 900 cm^{-1} is attributed to stretching of Si–O–Al. Vibration of Si–O–Al is also represented by the peak at 531 cm^{-1}, while that of Si–O–Si is represented by the peak at 472 cm^{-1}. The peak at 512 cm^{-1} is characteristic to vibration of Si–O–Al, while that at 462 cm^{-1} is characteristic to Si–O–Si vibration.

istic of in-plane Si–O–Si vibration, and the area at wavenumber 900 cm^{-1} is attributable to stretching of Si–O–Al. Bending vibration of Si–O–Al was represented by the peak at wavenumber of 531 cm^{-1}, while that of Si–O–Si was indicated by the peak at wavenumber of 472 cm^{-1}.

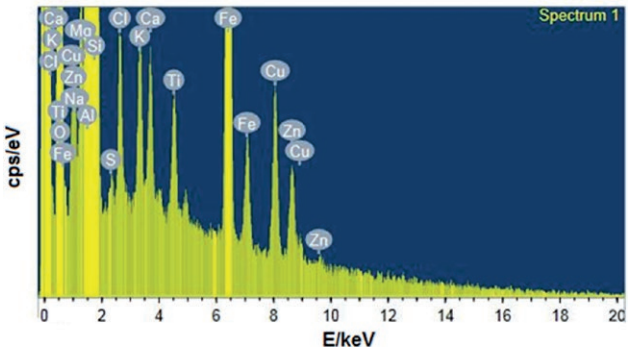

Figure 3. The energy-dispersive X-ray spectrum showing the elemental composition of the montmorillonite nanoclay used in this study. Element analysis showed presence of Na, Mg, Al, Si, K, and Ca. Other elements (S, Cl, Fe, Ti, Cu and Zn) were presented as traces.

Moreover, the peak at wavenumber of 512 cm^{-1} is characteristic of bending vibration of Si–O–Al, while the peak at wavenumber 462 cm^{-1} is characteristic to Si–O–Si bending vibration.

EDX analysis also showed that the major elements in the MNC were Na, Mg, Al, Si, K, and Ca, and other elements such as S, Cl, Fe, Ti, Cu and Zn were present as traces. The EDX spectrum is shown in Figure 3.

In vitro *assessment of suppressive potential of MNC*

Potential of MNC to suppress germination of *P. striiformis* uredospores was investigated *in vitro* (Table 2). Untreated uredospores exhibited normal germination (94.5 ± 2.44%). Treating uredospores with MNC at 150 or 200 mg L^{-1} completely suppressed germination, while treating them with MNC at 100 mg L^{-1} suppressed germination (89.2 ± 1.58%) compared to the untreated uredospores.

Assessments off disease severity

Table 3 shows effects of application of MNC on stripe rust at 14 dai. The pathogen caused 93.3% severity of stripe rust. Application of the fungicide reduced (by 96.5%) severity of the disease. Application of MNC at 100, 150, and 200 mg L^{-1} considerably reduced the disease severity leading, respectively, to reductions of 82.1, 82.1, and 78.6%, when compared with the control inoculated treatment (P). No differences ($P \leq 0.05$) were recorded between the three tested concentrations of MNC. Treatment (P) gave an average of 93.3% average coefficient of infection. The lowest average coefficient of infection (0.66%) was recorded from the F + P treatment

Table 2. Mean *in vitro* proportions of germination and inhibition of *Puccinia striiformis* f. sp. *tritici* uredospores treated with montmorillonite nanoclay (MNC) at different concentrations[a].

Treatment		Germination (%)	Inhibition (%)
Control		94.5 ± 2.4 a	0.0 c
MNC (mg L^{-1})	100	10.2 ± 1.3 b	89.2 ± 1.6 b
	150	0.0 c	100.0 a
	200	0.0 c	100.0 a
P-value ≤ 0.05			

[a]Means accompanied by different letters in each column are significantly different, according to Tukey's HSD test. Each value is the mean of three replicates ± SD. Anova significance values were as follows: germination (df = 5, F = 672.1); inhibition (df = 5, F = 1753.5).

Table 3. Mean stripe rust severity, reduction proportions and average coefficients of infection, after spraying wheat plants with montmorillonite nanoclay (MNC) at 14 days after inoculation with the pathogen[a].

Treatment	Disease severity (%)	Reduction (%)	Average coefficient infection (%)
C	0 c	0 c	0 d
P	93.3 ± 2.3 a	0 c	93.3 ± 2.3 a
F + P	3.3 ± 0.7 c	96.5 ± 3.1 a	0.66 ± 0.1 d
N1 + P	16.7 ± 1.1 b	82.1 ± 2.0 b	6.68 ± 1.1 c
N2 + P	16.5 ± 1.1 b	82.1 ± 1.8 b	6.68 ± 1.0 c
N3 + P	20.4 ± 1.2 b	78.6 ± 1.1 b	16.0 ± 1.7 b
P-value ≤ 0.05			

[a]Means accompanied by different etters in each column are significantly different according to Tukey's HSD test. Each value is the mean of ten replicates ± SD. Anova significance values were as follows: disease severity (df = 5, F = 640.2), reduction (df = 5, F = 1735.9), and average coefficient infection (df = 5, F = 1742.3). Non-sprayed and uninfected plants (C), non-sprayed and infected plants (P), plants sprayed with fungicide and inoculated (F + P), plants sprayed with MNC at 100 mg L^{-1} and inoculated (N1 + P), plants sprayed with MNC at 150 mg L^{-1} and inoculated (N2 + P), and plants sprayed with MNC at 200 mg L^{-1} and inoculated (N3 + P).

while application of MNC at 100, 150, or 200 mg L^{-1} led, respectively, to mean average coefficients of infection of 6.68, 6.68, and 16.0%

Effects of MNC on gene expression in wheat leaves

Transcriptional expression of *JERF3*, *CHI II*, and *PR1* in plant leaves following application of MNC at 100 mg L^{-1} is illustrated in Figure 4. Stripe rust infections did not affect the relative expression of *JERF3* and *CHI II*, while it led to a downregulation of *PR1*, compared to the control treatment (C). In contrast, spraying of the infected plants caused increased expression of the defensive genes *JERF3* (5.23-fold increase), *CHI II* (4.89-fold increase), and *PR1* (2.37-fold increase) when compared with the control plants.

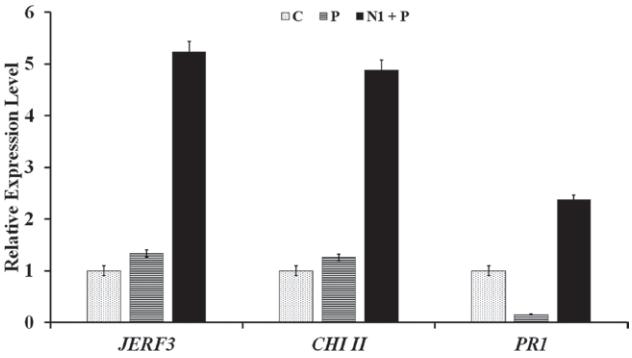

Figure 4. Mean relative transcriptional expression levels of the defense-related genes jasmonate-ethylene-responsive factor 3 (*JERF3*), chitinase II (*CHI II*), and the pathogenesis-related protein 1 (*PR1*) in wheat leaves in response to infections with *Puccinia striiformis* f. sp. *tritici* and application of the montmorillonite nanoclay (MNC) at 100 mg L^{-1}. The different coloured histograms indicate means for non-treated and uninfected plants (C), non-treated and infected plants (P), and plants sprayed with MNC at 100 mg L^{-1} and infected (N1 + P). Histograms for each gene which were superscripted with different letters are significantly different according to Tukey's HSD test ($P \leq 0.05$). For each treatment, three biological and three technical samples were used. Bars indicate the standard errors of the means.

Effects of MNC on plant defense biochemicals

Spraying the infected wheat plants with MNC affected production of several anti-oxidative stress enzymes, phenolic compounds, and lipid oxidation, at 3 dai (Table 4). Biochemical analyses showed that infections reduced activity of the enzymes POD, PPO, and CAT, and reduced phenolic contents, while infection increased lipid peroxidation, compared to the control treatment. Application of the fungicide activated POD and CAT, and enhanced the phenolic contents of the treated plants. Activity of PPO was not affected, and lipid oxidation was reduced by inoculation compared with treatment (P). MNC at most of the assessed concentrations activated POD, PPO, and CAT, (except for POD at MNC, 200 mg L^{-1}), and also increased wheat phenolic contents, while MNC reduced lipid oxidation, compared with treatment (P). The greatest enzymes activities and phenolic contents were recorded for the MNC treatments at 100 and 150 mg L^{-1}. The lowest mean lipid peroxida-

Table 4. Mean concentrations of enzymes, phenolic contents, and lipid peroxidation in wheat plants 3 d after inoculation with *Puccinia striiformis* f. sp. *tritici* and application of treatments with montmorillonite nanoclay (MNC) [a].

Treatment	Peroxidase (Unit $min^{-1}g^{-1}$ f. wt)	Polyphenol oxidase (Unit $min^{-1}g^{-1}$ f. wt)	Catalase (Unit $min^{-1}g^{-1}$ f. wt)	Phenolic content (mg.100 g^{-1} f. wt)	Lipid peroxidation (µmol MDA g^{-1} f. wt)
C	45.6 ± 3.6 b	8.0 ± 0.7 c	16.2 ± 2.3 c	862.6 ± 13.3 c	3.7 ± 0.3 e
P	26.5 ± 2.2 c	5.8 ± 0.6 d	12.6 ± 2.1 d	763.1 ± 10.2 d	13.2 ± 0.9 a
F + P	40.0 ± 2.5 b	6.9 ± 0.8 d	15.2 ± 1.5 c	824.3 ± 9.9 c	9.8 ± 0.9 b
N1 + P	62.1 ± 4.7 a	21.6 ± 1.4 a	36.6 ± 4.1 a	1489.5 ± 24.1 a	5.6 ± 1.0 d
N2 + P	60.1 ± 3.9 a	19.8 ± 1.1 ab	37.9 ± 3.9 a	1463.9 ± 22.4 a	7.2 ± 0.4 c
N3 + P	49.1 ± 1.5 b	18.2 ± 1.8 b	28.7 ± 3.8 b	1232.5 ± 21.8 b	9.6 ± 1.0 b
P-value ≤ 0.05					

[a]Means accompanied by different sletters in each column are significantly different according to Tukey's HSD test. Each value is the mean of ten replicates ± SD. Anova significance values were as follows: peroxidase (df = 5, F = 10.5), polyphenol oxidase (df = 5, F = 165.7), catalase (df = 5, F = 40), phenolic content (df = 5, F = 31.9), and lipid peroxidation (df = 5, F = 59.6). The treatments were: non-sprayed and uninoculated (C); non-sprayed and inoculated (P); sprayed with fungicide and inoculated (F + P); sprayed with MNC at 100 mg L^{-1} and inoculated (N1 + P); sprayed with MNC at 150 mg L^{-1} and inoculated (N2 + P); or sprayed with MNC at 200 mg L^{-1} and inoculated (N3 + P).

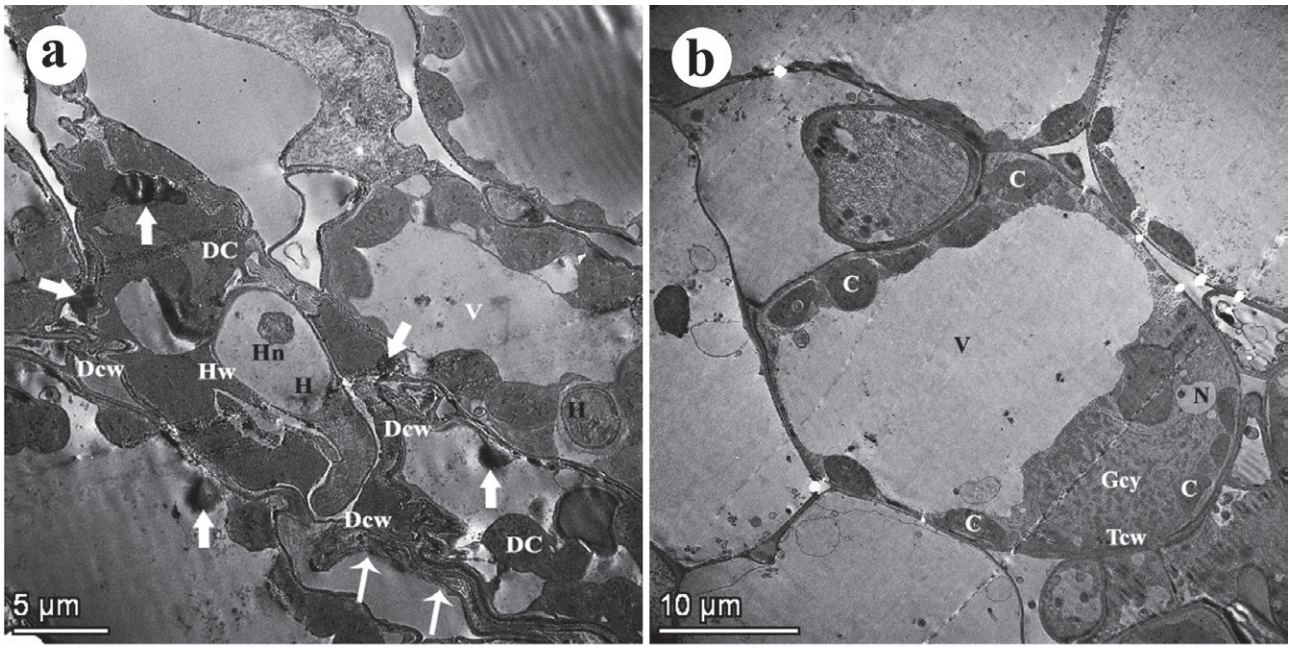

Figure 5. Transmission electron micrographs showing the cellular ultrastructure of wheat leaves which were infected with stripe rust and treated or not treated with montmorillonite nanoclay at 100 mg L^{-1} 7 d after the inoculation with the pathogen. a) an untreated inoculated leaf, and b) an infected leaf which was sprayed with montmorillonite nanoclay. H, haustoria; Hw, haustorium wall; Hn, haustorium nucleus; Dcw, decomposed cell wall; DC, degenerated chloroplast; V, vacuole; Tcw, thick cell wall; N, nucleus; C, chloroplast; Gcy,: granulated cytoplasm. Narrow arrows indicate intercellular fungal mycelium, while the broad arrows indicate electron dense bodies.

tion level (5.60 µmol MDA g^{-1} fresh weight) in the infected plants was recorded from MNC at 100 mg L^{-1}.

TEM observations

Effects of MNC (100 mg L^{-1}) application on ultrastructure of infected wheat cells are illustrated in Figure 5. Transmission electron micrographs showed that untreated inoculated leaves leaf contained large haustoria penetrating the mesophyll cells and growing between them. Host stress effects were also observed in the infected cells, including disorganization of the cells, degeneration of many chloroplasts, presence of electron dense bodies, and decomposition of some cell walls (Fig-

ure 5a). In contrast, tissue of the infected plant which had been treated with MNC did not show these disruptions. Cells from this tissue had normal organization and were enclosed by thick walls surrounding normal chloroplasts, and had large vacuoles, granulated cytoplasm, and normal nuclei (Figure 5b).

Effects of MNC on wheat photosynthetic pigments

Spraying MNC affected photosynthetic pigments in the infected wheat leaves at 14 dai (Table 5). Treatment (P) reduced chlorophyll *a* and *b* contents, and carotenoids, compared with treatment (C). Treatment (F + P) led to increases in all assessed pigments, compared with treatment (P). Application of MNC at all concentrations also increased contents of chlorophyll *a* and *b*, and carotenoids content, compared with treatment (P). The greatest amounts of total pigments were in the infected wheat sprayed with MNC at 100 or 150 mg L^{-1}, with both treatments resulting in means of 4.62 mg MNC g^{-1} fresh weight.

Effects of spraying MNC on plant growth

Treatment (P) (treatment of wheat plants with MNC) reduced all the assessed plant growth parameters, compared to treatment (C) (Table 6). Application of the fungicide enhanced all these growth parameters, compared to treatment (P), while spraying the infected wheat by MNC at 100, 150, or 200 mg L^{-1} increased all the

Table 5. Mean photosynthetic pigment contents in wheat leaves 14 d after inoculation with *Puccinia striiformis* f. sp. *tritici* and application of treatments with montmorillonite nanoclay (MNC) [a].

Treatment	Chlorophyll *a* (mg g^{-1} fresh weight)	Chlorophyll *b* (mg g^{-1} fresh weight)	Carotenoids (mg g^{-1} fresh weight)	Total pigments (mg g^{-1} fresh weight)
C	2.3 ± 0.2 b	1.0 ± 0.2 b	0.3 ± 0.06 c	3.5 ± 0.4 c
P	1.4 ± 0.2 d	0.8 ± 0.1 c	0.1 ± 0.05 d	2.3 ± 0.5 d
F + P	1.9 ± 0.1 c	1.0 ± 0.1 b	0.3 ± 0.02 b	3.1 ± 0.2 c
N1 + P	2.9 ± 0.4 a	1.4 ± 0.2 a	0.3 ± 0.04 b	4.6 ± 0.6 a
N2 + P	2.9 ± 0.4 a	1.3 ± 0.1 a	0.4 ± 0.08 a	4.6 ± 0.6 a
N3 + P	2.8 ± 0.2 ab	1.0 ± 0.2 b	0.5 ± 0.05 a	4.2 ± 0.5 b
P-value ≤ 0.05				

[a] Means accompanied by different letters in each column are significantly different, according to Tukey's HSD test. Each value is the mean of ten replicates ± SD. Anova significance values were: Chlorophyll *a* (df = 5, F = 14.9), Chlorophyll *b* (df = 5, F = 1.6), caroteniods (df = 5, F = 3.2), and total pigments (df = 5, F = 13.2). Treatments applied were: non-sprayed and uninoculated (C), non-sprayed and inoculated (P), sprayed with the fungicide and infoculatted (F + P), sprayed with MNC at 100 mg L^{-1} and inoculated (N1 + P), sprayed with MNC at 150 mg L^{-1} and inoculated (N2 + P), or sprayed with MNC at 200 mg L^{-1} and infected (N3 + P).

Table 6. Mean wheat plant parameters 30 d after inoculation with *Puccinia striiformis* f. sp. *tritici* and application of treatments with fungicide or montmorillonite nanoclay (MNC) [a].

Treatment	Plant height (cm)	Shoot dry weight (g)	Root dry weight (g)	Leaf area (cm^2)
C	56.4 ± 1.6 b	2.1 ± 0.4 bc	0.4 ± 0.01 c	18.3 ± 0.9 b
P	45.1 ± 1.3 c	1.2 ± 0.2 d	0.2 ± 0.04 e	11.1 ± 1.1 c
F + P	60.0 ± 3.6 ab	2.1 ± 0.3 c	0.3 ± 0.01 c	18.0 ± 1.1 b
N1 + P	51.1 ± 4.0 b	2.3 ± 0.3 b	0.5 ± 0.07 a	35.6 ± 4.5 a
N2 + P	69.0 ± 3.1 a	3.2 ± 0.7 a	0.5 ± 0.08 b	32.2 ± 4.1 a
N3 + P	53.3 ± 2.6 b	2.2 ± 0.6 b	0.3 ± 0.07 d	18.2 ± 1.2 b

[a]Means accompanied by different letters in each column are significantly different, according to Tukey's HSD test ($P \leq 0.05$). Each value represents the mean of ten replicates ± SD. Anova significance values were as follows: mean plant height (df = 5, F = 7.2); mean shoot dry weight (df = 5, F = 7.8); mean root dry weight (df = 5, F = 75.5);,mean leaf area (df = 5, F = 13).Non-sprayed and non-inoculated leaves (C); non-sprayed and inoculated leaves (P); leaves sprayed with fungicide and inoculated (F + P); leaves sprayed with MNC at 100 mg L^{-1} and inoculated (N1 + P); leaves sprayed with MNC at 150 mg L^{-1} and inoculated (N2 + P); leave sprayed with MNC at 200 mg L^{-1} and inoculated (N3 + P).

growth parameters. However, MNC at 150 mg L^{-1} gave the greatest increases in plant height, shoot dry weight and leaf area. Spraying *P. striiformis* infected plants with MNC at 150 mg L^{-1} usually improved the plant growth, and more so than the fungicide.

DISCUSSION

Several previous studies have focused on potential solutions for control of stripe rust in wheat, due to the importance of this disease which can cause up to complete yield losses in disease-conducive climatic conditions (El-Sharkawy *et al*., 2023 a and b). In the present study, the wheat stripe rust control potential of MNC was evaluated. Direct suppressive effects of MNC on uredospore germination was demonstrated *in vitro*, where applications of MNC at 150 or 200 mg L^{-1} completely suppressed germination, while MNC at 100 mg L^{-1} led to a strong germination inhibition (89.2 %). This anti-germination activity is consistent with the results of Iconaru *et al.* (2019), who reported antifungal potential of montmorillonite against growth of *Candida albicans*. This inhibitory potential was attributed to silicon and aluminum ions released from montmorillonite clay. However, due to nano size of the MNC particles assessed in this study, their contents of metal ions were greater than that in the micro sized particles of montmorillonite layer which led to increased antifungal activity.

Inhibitory potential of aluminum ions has been previously reported, and is causes imbalance of cellular ionic contents and inhibits messenger calmodulin protein (Kolaei *et al*., 2013). Reductions in spore germination caused by silicon ions were attributed to disruption of fungal spore plasma membranes, leading to leakage of cell contents (Liu *et al*., 2010). This may have been the cause of reductions in uredospore germination after MNC treatments observed in the present study. Uredospores germinate rapidly (within 3 h) before stomatal penetration, so suppression of germination is likely to control *P. striiformis tritici* by reducing inoculum loads. Direct inhibitory effects of MNC on uredospores played an important role in controlling rust in wheat plants.

Data obtained in the present study showed that spraying MNC at 100 mg L^{-1} gave greater than 80% reductions in stripe rust, compared to the untreated-inoculated control treatment [treatment (P)]. To investigate the mechanisms of disease control caused by MNC, expression profiles of *JERF3*, *CHI II*, and *PR1* were assessed in infected wheat leaves which were treated with MNC at 100 mg L^{-1}. Results showed that application of MNC at 100 mg L^{-1} gave overexpression of these genes. The response factor *JERF3* activates defense-related and stress-responsive genes in plants (Zhang *et al*., 2010). Rashad *et al.* (2021b) found that banana plants exhibiting upregulation of *JERF3* had increased tolerance to biotic and abiotic stresses. These plants also overexpressed multiple stress-responsive genes. *CHI II* is a defensive gene encoding for chitinase, and activates hydrolysis of chitin. This compound is a major component of fungal cell walls, and chitinase degrades glycoside bonds (Poria *et al*., 2021). Production of chitinase has potential for protection of wheat plants against invasion by *P. striiformis*, by degrading cell walls of penetrating haustoria and impairing their function. *PR1* encodes for the pathogenesis-related protein 1, a stress responsive protein which accumulates against various stresses, and is used as a marker for triggered plant defense, particularly within the salicylic acid pathway (Li *et al*., 2021). This protein has multiple functions, including signal transduction, cell wall rigidification, and fungitoxic potential. Farrakh *et al.* (2018) recorded overexpression of *PR1* in *P. striiformis*-infected wheat. They found that the *PR1* gene affected race-specific immunity regulated by *Yr* genes. In contrast, results obtained in the present study showed that stripe rust did not affect relative expression of *JERF3* and *CHI II*, while it led to downregulation of *PR1*, compared to control plants. This result is similar to those of Rashad *et al.* (2024), who reported downregulation of six of 13 polyphenol genes in response to stripe rust. Breakdowns of immunity to *P. striiformis* have been reported in different wheat varieties (Gultyaeva *et al*., 2022).

Spraying MNC on the infected wheat plants activated the antioxidant enzymes POD, PPO, and CAT, and increased phenolic contents, while this material also lowered lipid oxidation levels. Reactive oxygen species have important roles in virulence of *P. striiformis*. This pathogen produces superoxide radicals, hydrogen peroxide, and hydroxyl radicals through infection processes, which are important for uredospore germination and fungal development in plants (Wang *et al*., 2020). Therefore, induction by MNC of these antioxidant enzymes mitigate infection impacts on plant cells, and reduce pathogen virulence. This result was supported by the TEM observations (Figure 5b), which showed mitigation of stress in infected plants that were sprayed with MNC.

POD and CAT enzymes catalyze oxidative reactions by breaking down hydrogen peroxide (Vidossich *et al*., 2012). The enzyme PPO catalyzes oxidation of phenols to quinones, that are more toxic to *P. striiformis* than phenols (Zhang, 2023). Phenolic compounds such as phenolic acids, flavonoids, and flavonols have defense functions in plants through multiple antifungal effects (Rashad *et*

al., 2020a), and are used as markers for induced resistance in plants (Rashad *et al*., 2018). Rashad *et al.* (2020b) reported that induced resistance against garlic white rot (caused by *Sclerotium cepivorum*) , was accompanied with increases in total phenols. In addition, lignin deposition is an important host defense mechanism for restricting penetration of *P. striiformis* into plant cells and limiting nutrient intake by haustoria (El-Sharkawy *et al*., 2023b). These observations demonstrated the induction of immunity responses by MNC applications to in the infected wheat plants.

Spraying MNC onto wheat plants increased all the evaluated growth parameters, while high rate of MNC reduced some parameters. Most nanoparticles have cytotoxic and genotoxic effects at high concentrations, which may negatively affect plant physiological processes (Rashad *et al*., 2021a). Reduction of infection due to application of MNC mitigated effects of *P. striiformis* on plant growth. Spraying with MNC enhanced contents of chlorophyll *a* and *b*, and carotenoids. These photosynthetic pigments are essential for plant growth, and they are indicators of host physiological status under environmental stresses (Al-Askar *et al*., 2014; Esteban *et al*., 2015). Rust diseases destroy chloroplast ultrastructure in wheat leaves, as was observed from the TEM observations in the present study (Figure 5a). This leads to decreased chlorophyll *a* and *b*, and carotenoids, and reduced photosynthetic activity. Furthermore, thylakoid membranes and proteins are also destroyed (Chen *et al*., 2015). El-Sharkawy *et al.* (2023a) found that wheat rust adversely affects photosynthetic contents in host leaves. Analysis of MNC in the present study indicated that it contained plant nutrient including Mg, Na, S, K, Ca, Fe, Cu, and Zn. Mg ions are the central components of chlorophyll molecules, and activate plant enzyme system in plants and are involved in protein synthesis. The other elements have growth-enhancing effect on plants, and are also involved in cell wall rigidity, enzymes activation, protein synthesis, and other important plant metabolic processes (Ishfaq *et al*., 2022).

CONCLUSIONS

This study has demonstrated the suppressive effects of MNC on *P. striiformis tritici* uredospore germination, and ability of this nanoclay to induce wheat defensive responses against stripe rust. The study showed that overexpression of *JERF3*, *CHI II*, and *PR1* followed MNC treatments. Additionally, spraying MNC activated POD, PPO, and CAT enzymes, increased plant phenolic contents, and reduced lipid oxidation in wheat leaves. MNC applications also reduced the damaging effects of the pathogen on the leaf cell ultrastructure, and enhanced contents of photosynthetic pigments and plant growth. MNC is biodegradable and naturally occurring, so is environmentally "friendly". Based on these results, MNC has promise as a natural control agent against yellow rust of wheat. However, further evaluation of MNC under field conditions is necessary before practical disease control can be recommended.

ACKNOWLEDGMENTS

The authors are grateful to Prof. Abu Bakr A. Amine of SRTA-City for his assistance with physical characterization of MNC. They also acknowledge funding support for the reported research from The Researchers Supporting Project number RSPD2024R676, at King Saud University, Riyadh, Saudi Arabia.

AUTHOR CONTRIBUTIONS

Y.M. Rashad contributed to the research concept, formal analyses, investigation, and manuscript preparation, writing, and revision. A.M. Abd-ElGawad contributed to the resources and revision of the manuscript. M. Hafez and M. Bourouah contributed to data analyses and revision of the manuscript. H.E. El-Sharkawy contributed to investigation, and data curation. All the authors have read and agreed to publication of the final version of the manuscript.

LITERATURE CITED

Al-Askar A.A., Abdulkhair W.M., Rashad Y.M., Hafez E.E., Ghoneem K.M., Baka Z.A., 2014. Streptomyces griseorubens E44G: A Potent Antagonist Isolated from Soil in Saudi Arabia. *Journal of Pure and Applied Microbiology* 8: 221–230.

Bujdáková H., Bujdáková V., Májeková-Koščová H., Gaálová B., Bizovská V., … Bujdák J., 2018. Antimicrobial activity of organoclays based on quaternary alkylammonium and alkylphosphonium surfactants and montmorillonite. *Applied Clay Science* 158: 21–28. https://doi.org/10.1016/j.clay.2018.03.010.

Chance B., Maehly A.C.B.T.-M. in E., 1955. Assay of catalases and peroxidases: In: *Methods in Enzymology*, Academic Press, 764–775.

Chen W., Wellings C., Chen X., Kang Z., Liu T., 2014. Wheat stripe (yellow) rust caused by *Puccinia strii-*

formis f. sp. *tritici*. *Molecular Plant Pathology* 15: 433–446. https://doi.org/10.1111/mpp.12116.

Chen Y.E., Cui J.M., Su Y.Q., Yuan S., Yuan M., Zhang H.Y., 2015. Influence of stripe rust infection on the photosynthetic characteristics and antioxidant system of susceptible and resistant wheat cultivars at the adult plant stage. *Frontiers in Plant Science* 6: 779. https://doi.org/10.3389/fpls.2015.00779.

CoStat, 2005. *Cohort Software*. 798 Lighthouse Ave., PMB 320 Monterey, USA.

El-Sharkawy H.H.A., Rashad Y.M., Elazab N.T., 2023a. Biocontrol potential of the endophytic *Epicoccum nigrum* HE20 against stripe rust of wheat. *Pesticide Biochemistry and Physiology* 194: 105517. https://doi.org/10.1016/j.pestbp.2023.105517.

El-Sharkawy H.H.A., Rashad Y.M., Elazab N.T., 2023b. Induction of multiple defense responses in wheat plants against stripe rust using mycorrhizal fungi and Streptomyces viridosporus HH1. *BioControl* 68(5): 525–535. https://doi.org/10.1007/s10526-023-10207-4.

Esteban R., Barrutia O., Artetxe U., Fernández-Marín B., Hernández A., García-Plazaola J.I., 2015. Internal and external factors affecting photosynthetic pigment composition in plants: A meta-analytical approach. *New Phytologist* 206: 268–280. https://doi.org/10.1111/nph.13186.

Farrakh S., Wang M., Chen X., 2018. Pathogenesis-related protein genes involved in race-specific all-stage resistance and non-race specific high-temperature adult-plant resistance to *Puccinia striiformis* f. sp. *tritici* in wheat. *Journal of Integrative Agriculture* 17: 2478–2491. https://doi.org/10.1016/S2095-3119(17)61853-7.

Galeazzi M.A.M., Sgarbieri V.C., Constantinides S.M., 1981. Isolation, purification and physicochemical characterization of polyphenol oxidase (PPO) from a dwarf variety of banana (*Musa cavendishii*, L). *Journal of Food Science* 46: 150–155. https://doi.org/10.1111/j.1365-2621.1981.tb14551.x.

Guilger-Casagrande M., Migliorini B.B., Germano-Costa T., Bilesky-José N., Harada L.K., … Lima R., 2024. *Beauveria bassiana* biogenic nanoparticles for the control of Noctuidae pests. *Pest Management Science* 80: 1325–1337. https://doi.org/10.1002/ps.7863.

Gultyaeva E., Shaydayuk E., Kosman E., 2022. Virulence Diversity of Puccinia striiformis f. sp. Tritici in Common Wheat in Russian Regions in 2019–2021. *Agriculture (Switzerland)*.

Hafez M., Ahmed A.A., Mohamed A.E., Rashad MM., 2022. Influence of environmental-friendly bio-organic ameliorants on abiotic stress to sustainable agriculture in arid regions: A long term greenhouse study in northwestern Egypt. *Journal of King Saud University - Science* 34(6): 102212.

Harborne J.B., 1984. *Phytochemical Methods: A guide to Modern Techniques of Plant Analysis*. London: Chapman and Hall.

Hayat M.A., 2000. *Principles and Techniques of Electron Microscopy*. Biological Applications, 4th edition. Cambridge University Press, Cambridge, United Kingdom.

HongBo S., ZongSuo L., MingAn S., 2005. Changes of anti-oxidative enzymes and MDA content under soil water deficits among 10 wheat (*Triticum aestivum* L.) genotypes at maturation stage. *Colloids and Surfaces. B, Biointerfaces*, Netherlands 45: 7–13. https://doi.org/10.1016/j.colsurfb.2005.06.016.

Hossain S.I., Kukushkina E.A., Izzi M., Sportelli M.C., Picca R.A., … Cioffi N., 2023. A Review on Montmorillonite-Based Nanoantimicrobials: State of the Art. *Nanomaterials* 13(5): 848

Iconaru S.L., Groza A., Stan G.E., Predoi D., Gaiaschi S., … Chapon P., 2019. Preparations of Silver/Montmorillonite Biocomposite Multilayers and Their Antifungal Activity. *Coatings* 9: 817.

Ishfaq M., Wang Y., Yan M., Wang Z., Wu L., … Li X., 2022. Physiological Essence of Magnesium in Plants and Its Widespread Deficiency in the Farming System of China. *Frontiers in Plant Science* 13: 802274.

Johnston C.O., Browder L.E., 1966. Seventh revision of the international register of physiologic races of *Puccinia recondita* f. sp. *tritici*. *Plant Disease Reporter* 50: 756–760.

Kiani T., Mehboob F., Hyder M.Z., Zainy Z., Xu L., … Farrakh S., 2021. Control of stripe rust of wheat using indigenous endophytic bacteria at seedling and adult plant stage. *Scientific Reports* 11: 14473. https://doi.org/10.1038/s41598-021-93939-6.

Kolaei E.A., Cenatus C., Tweddell R.J., Avis T.J., 2013. Antifungal activity of aluminium-containing salts against the development of carrot cavity spot and potato dry rot. *Annals of Applied Biology* 163: 311–317. https://doi.org/10.1111/aab.12056.

Li S., Wang Z., Tang B., Zheng L., Chen H., … Liu D., 2020. A Pathogenesis-Related Protein-Like Gene Is Involved in the Panax notoginseng Defense Response to the Root Rot Pathogen. *Frontiers in Plant Science* 11: 610176.

Liu J., Zong Y., Qin G., Li B., Tian S., 2010. Plasma membrane damage contributes to antifungal activity of silicon against penicillium digitatum. *Current Microbiology* 61: 274–279. https://doi.org/10.1007/s00284-010-9607-4.

Livak K.J., Schmittgen T.D., 2001. Analysis of relative gene expression data using real-time quantitative PCR and the 2-ΔΔCT method. *Methods* 25: 402–408. https://doi.org/10.1006/meth.2001.1262.

Malik C. P. and Singh M. B., 1980. Estimation of total phenols. In: *Plant Enzymology and Histo-Enzymology*. Kalyani Publishers, New Delhi.

Maxwell D.P., Bateman D.F., 1967. Changes in the activities of some oxidases in extracts of Rhizoctonia-infected bean hypocotyls in relation to lesion maturation. *Phytopathology* 57: 132–136.

Merino D., Tomadoni B., Salcedo M.F., Mansilla A.Y., Casalongué C.A., Alvarez V.A., 2021. Nanoclay as Carriers of Bioactive Molecules Applied to Agriculture. In: *Handbook of Nanomaterials and Nanocomposites for Energy and Environmental Applications: Volumes 1-4* (O.V. Kharissova, L.M. Torres-Martínez and B.I. Kharisov, ed.), Cham, Springer International Publishing, 433–454.

Nazir M.S., Mohamad Kassim M.H., Mohapatra L., Gilani M.A., Raza M.R., Majeed K., 2016. Characteristic Properties of Nanoclays and Characterization of Nanoparticulates and Nanocomposites. In: *Engineering Materials* (M. Jawaid, A. el K. Qaiss and R. Bouhfid, ed.), Singapore, Springer Singapore, 35–55.

Oliveira-Pinto P.R., Mariz-Ponte N., Gil R.L., Cunha E., Amorim C.G., … Santos C., 2022. Montmorillonite Nanoclay and Formulation with *Satureja montana* Essential Oil as a Tool to Alleviate Xanthomonas euvesicatoria Load on *Solanum lycopersicum*. *Applied Nano* 126–142.

Peterson R.F., Campbell A.B., Hannah A.E., 1948. A diagrammatic scale for estimating rust intensity on leaves and stems of cereals. *Canadian Journal of Research* 26c: 496–500. https://doi.org/10.1139/cjr48c-033.

Poria V., Rana A., Kumari A., Grewal J., Pranaw K., Singh S., 2021. Current perspectives on chitinolytic enzymes and their agro-industrial applications. *Biology* 10(12):1319. https://doi.org/10.3390/biology10121319.

Rashad Y.M., Aseel D.G., Hafez E.E., 2018. Antifungal potential and defense gene induction in maize against Rhizoctonia root rot by seed extract of Ammi visnaga (L.) Lam. *Phytopathologia Mediterranea* 57: 73–88. https://doi.org/10.14601/Phytopathol_Mediterr-21366.

Rashad Y., Aseel D., Hammad S., 2020a. Phenolic Compounds Against Fungal and Viral Plant Diseases. In: *Plant Phenolics in Sustainable Agriculture* (R. Lone, R. Shuab and A.N. Kamili, ed.), Singapore, Springer Singapore, 201–219.

Rashad Y.M., Abbas M.A., Soliman H.M., Abdel-Fattah G.G., Abdel-Fattah G.M., 2020b. Synergy between endophytic Bacillus amyloliquefaciens GGA and arbuscular mycorrhizal fungi induces plant defense responses against white rot of garlic and improves host plant growth. *Phytopathologia Mediterranea* 59: 169–186. https://doi.org/10.14601/Phyto-11019.

Rashad Y.M., El-Sharkawy H.H.A., Belal B.E.A., Abdel Razik E.S., Galilah D.A., 2021a. Silica Nanoparticles as a Probable Anti-Oomycete Compound Against Downy Mildew, and Yield and Quality Enhancer in Grapevines: Field Evaluation, Molecular, Physiological, Ultrastructural, and Toxicity Investigations. *Frontiers in Plant Science* 12: 763365.

Rashad Y.M., Fekry W.M.E., Sleem M.M., Elazab N.T., 2021b. Effects of Mycorrhizal Colonization on Transcriptional Expression of the Responsive Factor JERF3 and Stress-Responsive Genes in Banana Plantlets in Response to Combined Biotic and Abiotic Stresses. *Frontiers in Plant Science* 12: 742628.

Rashad, Y.M., El-Sharkawy, H.A., Abdalla, S.A., Ibrahim, O. M. and Elazab N.T., 2024. Unraveling the regulation effect of the endophyte Epicoccum nigrum HE20 on the polyphenol biosynthetic pathways genes in wheat against stripe rust. *BMC Plant Biology* 24:

Soltan Y.A., Morsy A.S., Hashem N.M., Elazab M.A.I., Sultan M.A., … Sallam S.M.A., 2022. Potential of montmorillonite modified by an organosulfur surfactant for reducing aflatoxin B1 toxicity and ruminal methanogenesis *in vitro*. *BMC Veterinary Research* 18: 387. https://doi.org/10.1186/s12917-022-03476-1.

Sundaresha S., Sharma S., Bairwa A., Tomar M., Kumar R., … Chakrabarti S.K., 2022. Spraying of dsRNA molecules derived from Phytophthora infestans, along with nanoclay carriers as a proof of concept for developing novel protection strategy for potato late blight. *Pest Management Science* 78: 3183–3192. https://doi.org/10.1002/ps.6949.

Vidossich P., Alfonso-Prieto M., Rovira C., 2012. Catalases versus peroxidases: DFT investigation of H2O 2 oxidation in models systems and implications for heme protein engineering. *Journal of Inorganic Biochemistry* 117: 292–297. https://doi.org/10.1016/j.jinorgbio.2012.07.002.

Wang X., Che M.Z., Khalil H.B., McCallum B.D., Bakkeren G., … Saville B.J., 2020. The role of reactive oxygen species in the virulence of wheat leaf rust fungus *Puccinia triticina*. *Environmental Microbiology* 22: 2956–2967. https://doi.org/10.1111/1462-2920.15063.

Worrall E.A., Hamid A., Mody K.T., Mitter N., Pappu H.R., 2018. Nanotechnology for plant disease management. *Agronomy* 8(12): 285.

Yousef H.A., Fahmy H.M., Arafa F.N., Abd Allah M.Y., Tawfik Y.M., … Bassily M.E., 2023. Nanotechnology in pest management: advantages, applications, and challenges. *International Journal of Tropical Insect Science* 43: 1387–1399. https://doi.org/10.1007/s42690-023-01053-z.

Zhang H., Liu W., Wan L., Li F., Dai L., … Huang R., 2010. Functional analyses of ethylene response factor JERF3 with the aim of improving tolerance to drought and osmotic stress in transgenic rice. *Transgenic Research* 19: 809–818. https://doi.org/10.1007/s11248-009-9357-x.

Zhang S., 2023. Recent Advances of Polyphenol Oxidases in Plants. *Molecules* 28(5): 2158.

Zhao J., Zhang H., Yao J., Paul S., 2011. Identifcation of Berberis spp. as alternate hosts of *Puccinia striiformis* f. sp. *tritici* in China. *Borlaug Global Rust Initiative workshop*, *Mycosystema* 30: 167.

Phytopathologia Mediterranea
The international journal of the
Mediterranean Phytopathological Union

Firenze University Press
www.fupress.com/pm

Research Papers

Prevalence and characterization of *Burkholderia gladioli* in Iran, from bacterial dry rot of saffron corms (*Crocus sativus* L.)

Mahmoud-Reza KARIMI-SHAHRI[1], Mohammad ZAKIAGHL[2]

[1] *Department of Plant Protection, Razavi-Khorasan Agricultural and Natural Resources Research Center, (AREEO), Mashhad, Iran*
[2] *Department of Plant Protection, College of Agriculture, Ferdowsi University of Mashhad, Mashhad, Iran*
The authors contributed equally to this research.
Corresponding authors. E-mail: zakiaghl@um.ac.ir; karimi_in@yahoo.com

Summary. Iran is the main world producer of saffron (*Crocus sativus* L.), but a bacterial disease continues to threaten saffron production, causing severe flower failure, rot on flowering tubes, delayed vegetative growth, premature yellowing of leaves, bare patches in saffron farms, reddish-brown lesions in the germination zones of roots, and rot of saffron corms. Field surveys in Razavi-Khorasan and Southern-Khorasan provinces revealed high incidence of Burkholderia gladioli dry rot symptoms in saffron farms, with symptoms observed during flowering on leaves and corms. Twenty-four bacterial isolates from symptomatic saffron corms from different parts of Iran were characterized. These bacteria were identified as *Burkholderia gladioli*, based using phenotypic characteristics, species-specific PCR, and sequencing analyses of the 16S rRNA and 16S-23S intergenic transcribed spacer regions. All 24 isolates triggered hypersensitive reactions in tobacco and pelargonium leaves, although pathogenicity tests showed that only 21 isolates were capable of causing rots on saffron corms.

Keywords. Saffron dry rot, pathogenicity, phenotypic tests, molecular identification.

OPEN ACCESS

Citation: Karimi-Shahri, M.R., & Zakiaghl, M. (2024). Prevalence and characterization of *Burkholderia gladioli* in Iran, from bacterial dry rot of saffron corms (*Crocus sativus* L.). *Phytopathologia Mediterranea* 63(2): 283-294. doi: 10.36253/phyto-15326

Accepted: August 19, 2024

Published: September 15, 2024

Data Availability Statement: All relevant data are within the paper and its Supporting Information files.

Competing Interests: The Author(s) declare(s) no conflict of interest.

Editor: Jesus Murillo, Public University of Navarre, Spain.

ORCID:
M-RK-S: 0000-0003-3183-457X
MZ: 0000-0001-5032-8344

INTRODUCTION

Burkholderia (Yabuuchi *et al.*, 1992) comprises aerobic, Gram-negative and rod-shaped bacteria, and includes more than 60 species, some of which are plant growth-promoting, endophytic and antifungal biocontrol agents (Compant *et al.,* 2008). Other species are important pathogens for humans, animals and plants (Coenye and Vandamme, 2003; Suárez-Moreno *et al.,* 2012). Important plant pathogens include *B. andropogonis* (bacterial leaf stripe of sorghum and maize; Li and De Boer 2005), *B. caryophylli* (bacterial wilt of carnation; EPPO, 2006), *B. gladioli* (bacterial blight of gladiolus; McCulloch, 1921), *B. glumae* (bacterial panicle blight of rice; Nandakumar *et al.,* 2009), and *B. plantarii* (seedling blight of rice; Wang *et al.,* 2016). Although *B. gladioli* was originally described as the causal agent of gladiolus

blight, this species has been found to be pathogenic on other plants, and four pathovars of *B. gladioli* have been identified based on their host ranges. These pathovars are: *B. gladioli* pv. *alliicola* (Bga) (formerly *Pseudomonas alliicola*), causing onion rot; *B. gladioli* pv. *gladioli* (Bgg) (formerly *Pseudomonas marginata*), responsible for leaf and corm rot of gladiolus and iris, and also affecting other plants (Saddler, 1994); *B. gladioli* pv. *agaricicola*, causing soft rot of mushrooms (*Agaricus bitorquis*) (Lincoln *et al*., 1991; Yabuuchi *et al.,* 1992; Ura *et al.,* 2006; Nandakumar *et al.,* 2009; Kowalska *et al.,* 2015; Moon *et al.,* 2017); and *B. gladioli* pv. *cocovenenans* (formerly *Pseudomonas cocovenenans*), which causes rot of coconut rot and producing the human toxin bongkrekic acid (Jiao *et al.,* 2003).

Burkholderia gladioli pv. *gladioli* was first identified in China (Xu and Ge, 1990), and later in Sardinia (Italy) (Fiori *et al.,* 2011), as a destructive pathogen of saffron. In addition, the bacterium has been considered a quarantine pathogen that causes soft rot during growth and storage of many vegetables, leading to significant economic losses in China (Lee *et al.,* 2012; 2021). This pathogen has been detected in onion growing areas in the United States, Bulgaria, Korea, and elsewhere (Lee *et al.,* 2005).

Several methods have been developed for detection and identification of *Burkholderia* species, including culture in a semi-selective medium (Castro-González *et al.,* 2011), pathogenicity assays (Nandakumar *et al.,* 2009), multiplex PCR (Maeda *et al.,* 2006), and real-time PCR (Thibault *et al.,* 2004). Sequence analysis of the 16S ribosomal RNA gene (rRNA) is a powerful tool for understanding phylogenetic and evolutionary relationships in bacteria (Woo *et al.,* 2003). Nevertheless, *Burkholderia* species show a high degree of similarity in their 16S rRNA gene sequences (Vermis *et al.,* 2002; Chiarini *et al.,* 2006), so the 23S rRNA or the internal transcribed spacer (ITS) region of the 16-23S rRNA has been used in addition to the 16S rRNA, for improved species (Liguori *et al.,* 2011).

Saffron (*Crocus sativus* L., *Iridaceae*) is a reliable industrial and medicinal plant. Propagation of saffron is vegetative from corms, as the plant is a sterile triploid (3n = 24) that does not produce seeds (Koocheki and Khajeh-Hosseini, 2020). Iran is the world leader in saffron production, growing approx. 408 tons of saffron from 112,000 ha in 2021. Approximately 60% of cultivated saffron area is in the three provinces of Khorasan (UNIDO, 2022). However, due to the lack of packaging, marketing and production of saffron-based edible products, a significant portion of Iranian saffron is distributed by other countries. In recent years, saffron production in Iran has faced challenges. In many farms, saffron bloom, a measure of potential yield, is not reached. In addition, in some farms vegetative growth of saffron is delayed, leading to formation of small daughter corms that do not flower in the following season. Saffron corms may also fail to germinate, and bare patches occur in affected fields.

The present paper describes isolation, identification, and prevalence of the bacterial pathogen *B. gladioli* from diseased saffron corms in Iran. This research used pathogenicity assessments, and physiological, biochemical, and molecular characteristics to characterize this pathgen.

MATERIALS AND METHODS

Field survey and sample collection

Saffron fields in Razavi-Khorasan and South-Khorasan provinces of Iran were surveyed for Burkholderia gladioli dry rot (BGR) in saffron corms from 2016 to 2022. Field symptoms on affected plants were early leaf yellowing followed by drying in the autumn and winter seasons. Corm samples were collected from October (before saffron blooming) until June. A total of 455 corm samples were collected from 108 saffron fields in different regions (Table 1). The samples were kept at 4°C until analyses.

Isolation and purification of bacteria

Isolations were carried out as reported by Fiori *et al.* (2011). Corms were washed in tap water and then disinfected by immersion in 0.5% sodium hypochlorite for 5 min. Diseased scale tissues were then cut into 10-15 mm cubes from the edges of symptomatic areas using a sterilized scalpel. Fragments of these tissues were then disinfected in ethanol for 30 s, and washed several times in sterile water. Each sample was then ground in a sterile mortar with Tris-HCl buffer (50 mM, pH 7.0). The resulting suspensions were streaked onto Petri plates containing nutrient agar (NA). The plates were then incubated at 28°C for 48 h. Resulting colonies were subcultured twice onto NA, and then stored at 4°C in sterile 0.1 M $MgSO_4$ for short-term use. The isolates were also maintained at -80°C in nutrient broth medium containing 50 % (v/v) glycerol for long-term storage.

Pathogenicity assays

The isolates were grown in Luria Bertani (LB) broth at 28°C until OD_{600} = 2. Resulting cells were pelleted by

Table 1. Farm locations in Iran from which saffron samples were harvested, including numbers of farms sampled, incidence of Burkholderia gladioli dry rot, and numbers of *Burkholderia gladioli* isolates obtained.

District	Years of sampling	Location	Number of farms	Number of infected samples	Number of isolates
Razavi-Khorasan Province					
Sabzevar	2018-2019	35°56'N/57°30'E	22	0	0
Torbat-e Heydariyeh	2016-2017	35°25'N/ 59°09'E	55	23	13
Zaveh	2016-2019	35°15'N/ 59°43'E	168	62	42
Bajestan	2019-2020	34°34'N/58°12'E	15	15	15
Rashtkhar/ Khaf	2018-2019	34°26'N/60°09'E	3	3	3
Mahvelat	2018-2019	35°02'N/58°40'E	24	0	0
Torbat-e-Jam	2018-2019	35°20'N/60°37'E	10	10	2
Chenaran	2019-2020	36°43'N/ 59°00'E	9	9	9
Gonabad	2019-2020	34°26'N/58°52'E	15	15	15
Fariman	2018-2019	35°43'N/60°01'E	3	3	3
Neyshabur	2020-2021	36°25'N/58°37'E	5	5	5
Quchan	2021-2022	37°09'N/58°35'E	8	8	8
Average of incidence in Razavi-Khorasan Province				45.4	
South-Khorasan Province					
Boshruyeh	2018-2020	34°06'N/57°23'E	19	15	5
Tabas	2018-2019	33°26'N/56°48'E	4	0	0
Ferdows	2018-2019	33°51'N/58°01'E	7	0	0
Sarayan	2020-2021	33°28'N/58°19'E	13	5	5
Qaen	2018-2019	33°39'N/59°15'E	23	4	0
Zirkuh	2018-2019	33°32'N/60°10'E	8	3	0
Birjand	2018-2019	33°05'N/59°10'E	11	0	0
Sarbisheh	2018-2019	32°29'N/60°03'E	18	2	0
Khosf	2018-2019	32°19'N/58°38'E	13	8	0
Nehbandan	2018-2019	31°26'N/59°43'E	2	2	0
Average of incidence in South-Khorasan province				33.1	
Overall average of incidence				42.2	

centrifugation at 7,000 rpm for 2 min, and then resuspended in sterile distilled water.

Hypersensivity reaction (HR) tests of selected isolates were conducted using tobacco (*Nicotiana tabacum* 'Samsun') and pelargoniums leaves. A bacterial suspension of each isolate was prepared in 1×PBS buffer using a 24 h culture in LB broth, and was adjusted to 5×10^8 cfu mL^{-1}. The bacterial suspension was then injected into the intercellular spaces of leaves, and positive pathogenicity was recorded where complete collapse of the tissues occurred after 24 h. The test was repeated at least twice with each isolate. Healthy corms of saffron were peeled, washed with running water, disinfected by dipping in 0.5% sodium hypochlorite for 2 min, disinfected in 70% ethanol for 30 s and then washed with sterile water. For each isolate, four corms were inoculated at 1 cm depth on two opposite sides of each corm with a 20 µL aliquot of the bacterial suspension, using a syringe. Control corms were mock inoculated with sterile distilled water. Each isolate was also inoculated into onion and carrot disks, by adding a drop of the bacterial suspension onto injured surfaces. Controls were mock inoculated with sterile distilled water. The inoculated material was maintained in a high humidity chamber at 28°C for symptom development. Re-isolations were made from diseased material, as described above. Some saffron corms were also wounded with a laboratory needle to make a 5 mm long scratch on each corm, and these were each inoculated with 20 µL of suspension (5×108 cfu mL^{-1}) from a 24 h culture, and were then planted into pots containing a sterile commercial soil, and these were maintained in a greenhouse at 28°C for 7 d. Plants and corms were checked regularly for symptom development. Re-isolations were made from the inoculated corms, and from shoots and leaves that developed from the inoculated corms.

Phenotypic tests of bacterial isolates

Physiological and biochemical characteristics of the bacterial isolates were determined, as described by Holt (1994). Culture tubes each containing saline solution, were each inoculated with 150 µL of bacterial suspension (5×10^8 cfu mL^{-1}). The tubes were then incubated at 28°C for 24 h. Twenty-four selected bacterial isolates were characterized by Gram staining, colony morphology, catalase and oxidase production, oxidative/fermentative metabolism of glucose, starch and gelatin hydrolysis, and H_2S production. Utilization of glucose, lactose, maltose, galactose, arabinose, raffinose, dextrose, sucrose, citrate, adonitol, mannitol, sorbitol, and urease and arginine decarboxylase activity, were also assessed. Abilities of the isolates to grow at pHs of 4 to 9, in 3% NaCl 3%, and at 41°C were also assayed (Table 2). The phenotypic data were analyzed by cluster analyses using Pearson correlation coefficient similarity indices (http://genomes.urv.cat/UPGMA/).

Molecular characterization of bacteria

For PCR identifications, total DNA was extracted using the DNA extraction kit (DNP™) (Sinaclon), according to the manufacturer's instructions for Gram-negative bacteria. PCRs were carried out using universal primers 16S-27F (5'-AGAGTTTGATCMTGGCTCAG-3') and 16S-1492R (5'-TACGGYTACCTTGTTACGACTT-3'); CMG16-1 (5'-AGAGTTTGATCMTGGCTCAG-3') and CMG16-2 (5'-CGAAGGATATTAGCCCTC-3'); GLA-f (5'-CGAGCTAATACCGCGAAA-3') and GLA-r (5'-AGACTCGAGTCAACTGA-3'); and LP1 (5'-GGGGGGTCCATTGCG-3') and LP4 (5'-AGAAGCTCGCGCCACG-3') designed on 16S and 23S rRNA sequences (Whitby *et al.,* 2000; Furuya *et al.,* 2002; Fiori *et al.,* 2011; Stoyanova *et al.,* 2011b; Li *et al.,* 2019). A 869-bp fragment of the *Burkholderia recA* gene was also amplified using a specific primer pair BUR1 (5'-GATCGA(AG)AAGCAGTTCGGCAA-3') and BUR2 (5'-TTGTCCTTGCCCTG(AG)CCGAT-3') (Payne *et al.,* 2005). Each reaction contained 10 µL of Amplicon 2× ready to use PCR master mix, 1 µM of each primer, 1 µL of genomic DNA in a total volume of 20 µL. The PCR program consisted of an initial denaturation of 97°C for 7 min followed by 30 cycles of denaturation each at 95°C for 30 s, annealing at 57°C for 60 s, and extension at 72°C for 80 s. The PCR products were subjected to electrophoresis in a 1% agarose gel containing DNA Safe Stain (Sinaclon) in TBE buffer (pH 8.0), and photographed. The PCR products were cloned into the pGT19 vector (Vivantis), according to the manufacturer's recommendations, and were Sanger sequenced by Pishgam Co., Iran. Phylogenetic trees were constructed using the neighbor-joining method, with the General Time Reversible nucleotides substitution model with 500 bootstrap replicates, using MegaX software (Tamura *et al.,* 2011).

RESULTS

Prevalence of BGR in saffron farms of Iran

Of the 455 samples taken, 192 showed BGR symptoms. BGR incidence in Razavi-Khorasan was 45.4% (153 of 337 samples), and the greatest incidence was observed in Zaveh and Torbat-e-Heydarieh districts. In South Khorasan province, incidence was 33.1% (39 of 118 samples), and the greatest incidence was observed in Beshrouye (79% of samples infected. In some farms, no Bgg was detected (Table 1).

A total of 125 isolates were obtained from the 192 saffron corms. From these 125 isolates, 21 isolates from saffron farms in Razavi-Khorasan, which had the greatest BGR incidence, were selected for subsequent for phenotypic and pathogenicity tests, based on the type and severity of host plant symptoms and colony morphology. In addition, two isolates from diseased saffron corms from Kermanshah, one isolate from a diseased saffron corm from Afghanistan, and a Bgg isolate from an onion, were used for comparisons.

Symptoms of BGR in the field

Symptoms of BGR on saffron plants could be categorized into three distinct types.

1) Symptoms during flowering. Symptoms during the flowering period in November were absence of flowering or decreased numbers of flowers, and decreased quantity and quality of flower stigmas. BGR caused rot and collapse in underground shoots. Infested saffron plants had decayed sheaths, while newly formed sprouts exhibited tissue burning and browning. These shoots were incapable of emergence from soil, saffron shoot rot led to reduction in flower production and appearance of bare patches in affected areas on the affected farms (Figure 1).
2) Symptoms on leaves. These symptoms became evident after the leaves had fully grown. Affected leaves showed symptoms of yellowing and necrosis, and corms were shorter than those of the healthy corms. BGR manifested as irregular bare patches in saffron farms, and patches were observed throughout different sections of individual farms. BGR triggered premature yellowing of saffron leaves. During midwin-

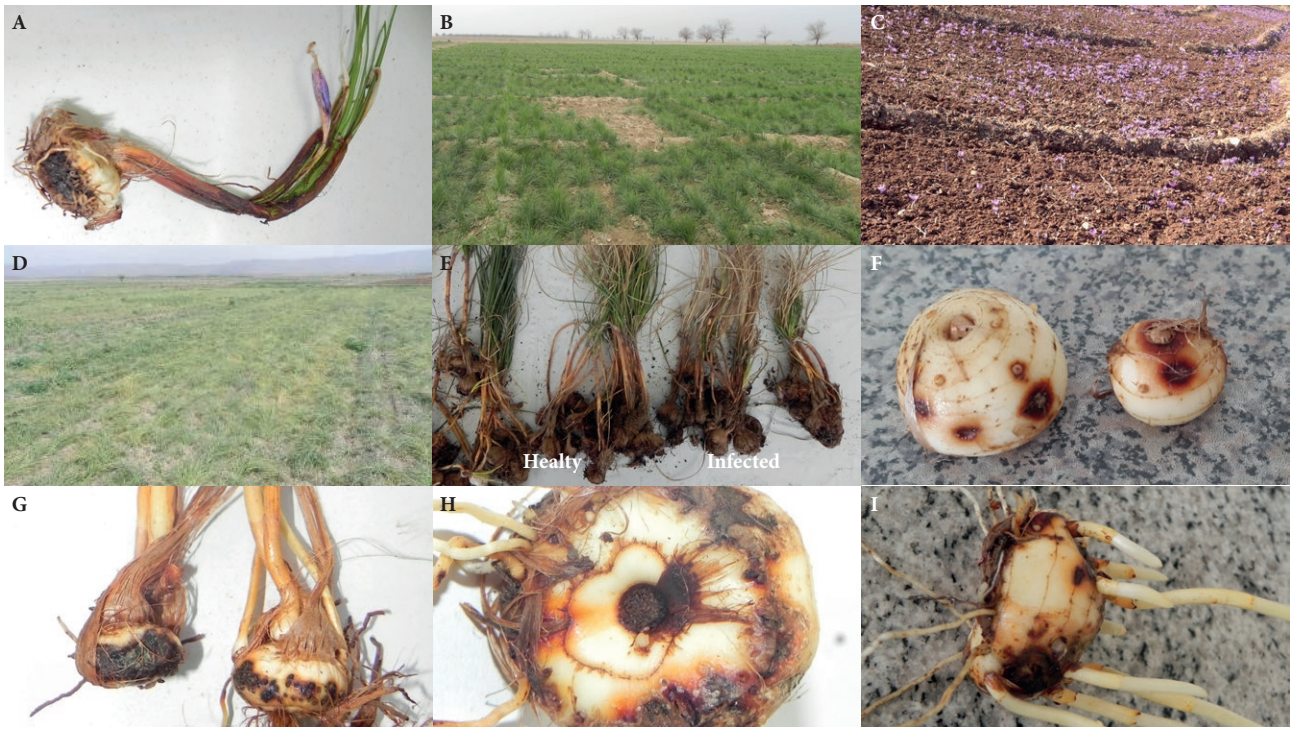

Figure 1. Symptoms of BGR in naturally infected saffron plants and corms. (A) burning and browning in newly formed sprout tissues; (B) bare patches in saffron farms; (C) flowering failure; (D) premature yellowing of saffron leaves; (E) yellowing and necrosis at the ends of leaves; (F) ring-shaped red to brown lesions on saffron corms; (G) progressive spread of lesions to larger areas of necrosis; (H) ring-shaped red to brown lesions within the root germination zone in o saffron corm; (I) a large number of weak flowering tubes from the lateral buds of a corm with emerging leaves.

ter, most infected saffron leaves turned yellow and fell (Figure 1).

3) Symptoms on corms. These symptoms were predominantly manifested on the mother corms, and were characterized by a distinctive ring-shaped red-brown discolouration precisely within the root germination zones. These zones progressively decayed and extended into the deeper layers of each corm. BGR was initially manifested as burnt spots, and gradually extended to cover an increasing area. Affected tissue surfaces acquired glistening appearance, occasionally covered by a thin gray layer. Lateral buds of infected corms began to grow and produced large numbers of weak cataphylls that exhibited abnormal growth, and had necrosis and red discolouration, flowering failure and also produced very small daughter corms (Figure 1).

Pathogenicity tests

The results of the pathogenicity tests with BGR-associated bacteria are shown in Figure 2. A necrotic zone or rot lesion at least 2 mm beyond the inoculation site was considered as evidence of infection in all the pathogenicity tests. All 24 selected isolates induced HR after inoculations of tobacco and pelargonium leaves. Inoculation of saffron corms with BGR isolates resulted in development of lesions with black necrosis around the inoculation site. Water-soaked lesions appeared 4 to 8 d post inoculation (dpi), and these lesions rapidly enlarged and turned dark-brown to black lesions within 7 to 10 dpi. Negative controls displayed small wounding sites without further development in 10 d. Symptoms were similar to those observed in the greenhouse, as shown in Figure 2.

Most of the isolates were infectious on saffron corms, except isolates 110, 126 and 160. Isolate 126 was obtained from onion, and isolates 110 and 160 were obtained from saffron corms with BGR symptoms. The most severe corm symptoms were caused by isolates 169 and 255. Symptoms included necrosis and rotting, which could be superficial or deep. Based on symptom severity, a 0 to 5 rating scale was established, in which isolates inducing complete rot and tissue decay were scored as 5, and non-pathogenic isolates scored 0. The isolates were assigned into six groups (Figure 3).

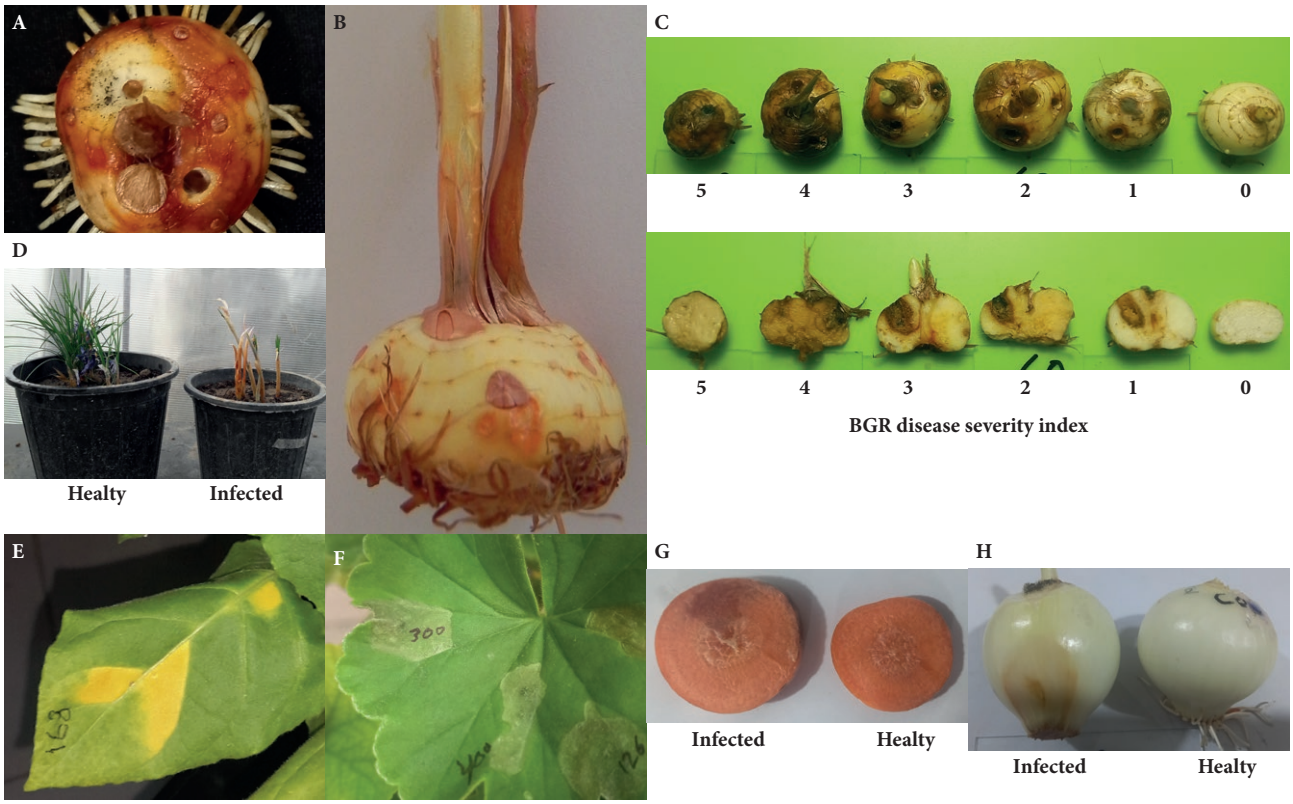

Figure 2. Results of pathogenicity tests of *B. gladioli* isolates on different plants. (A) Severe red-brown discolouration on an inoculated saffron corm; (B) rotted, twisted and truncated flowering tubes turned orange in inoculated corms; (C) disease severity rating scales for BGR on entire (upper) and cross sections (lower) of corms; (D) yellowing, tip necrosis and growth delay of leaves from inoculated corms; (E) HR in a tobacco leaf; (F) HR response in a pelargonium leaf; (G) watery rot on carrot discs; (H) severe watery decay on onions.

Cataphylls of inoculated saffron corms turned orange, and became twisted and truncated, and the flowers did not emerge from the tubes. The leaves of the inoculated corms showed yellowing and tip necroses (Figure 2). The pathogen was re-isolated from inoculated and symptomatic corms, their 16s RNA fragments were amplified with PCR, and the amplified fragments were identical to those of the inoculated bacterial strains, thus fulfilling Koch's postulates.

With the exception of isolates 110, 148, 149, 150 and 160, the remaining isolates caused watery rot on carrot discs, and in onions, and with the exception of isolates 149, 150, 160, 168, 169, 250, 251, 262, 300 and 400, the remaining isolates caused watery rot (Figure 2).

Based on the pathogenicity test data for saffron, the BGR-associated isolates were categorized into six groups (correlation coefficient 94%) (Figure 3).

Physiological and biochemical tests of BGR-associated isolates

The results of the most relevant phenotypic tests are listed in Table 2. Most of the assessed islotes were oxidase and catalase positive and hydrolyzed gelatin, and most were positive for arginine decarboxylase activity, and grew in 3% NaCl. Some of the isolates grew at 41°C, but none produced indole or acidified glucose. There were differences among the isolates for their profiles of utilization of carbohydrate sources, and urease activity. Results of the morphological, physiological and biochemical characteristics showed that all 24 BGR-associated isolates were identified as *B. gladioli* (with 82 to 98% probability). However, some differences were observed, and according to the phenotype tests, the isolates clustered into four groups. Nine isolates (102, 155, 161, 169, 252, 255, 262, SA4 and SA14), nine isolates (106, 110, 126, 147, 148, 151, 160, 168 and 300), five isolates (149, 150, 250, 251 and 400) and one isolate (176) were categorized into four phenotypic groups of BGR-associated bacteria (Figure 3, Table 2).

Molecular identifications

Molecular identification of the BGR-associated isolates was achieved by PCR amplification of the rRNA and *recA* gene. Expected fragments of 1500, 470 and 300 bp belonging to the 16S rRNA and 16S-23S rRNA

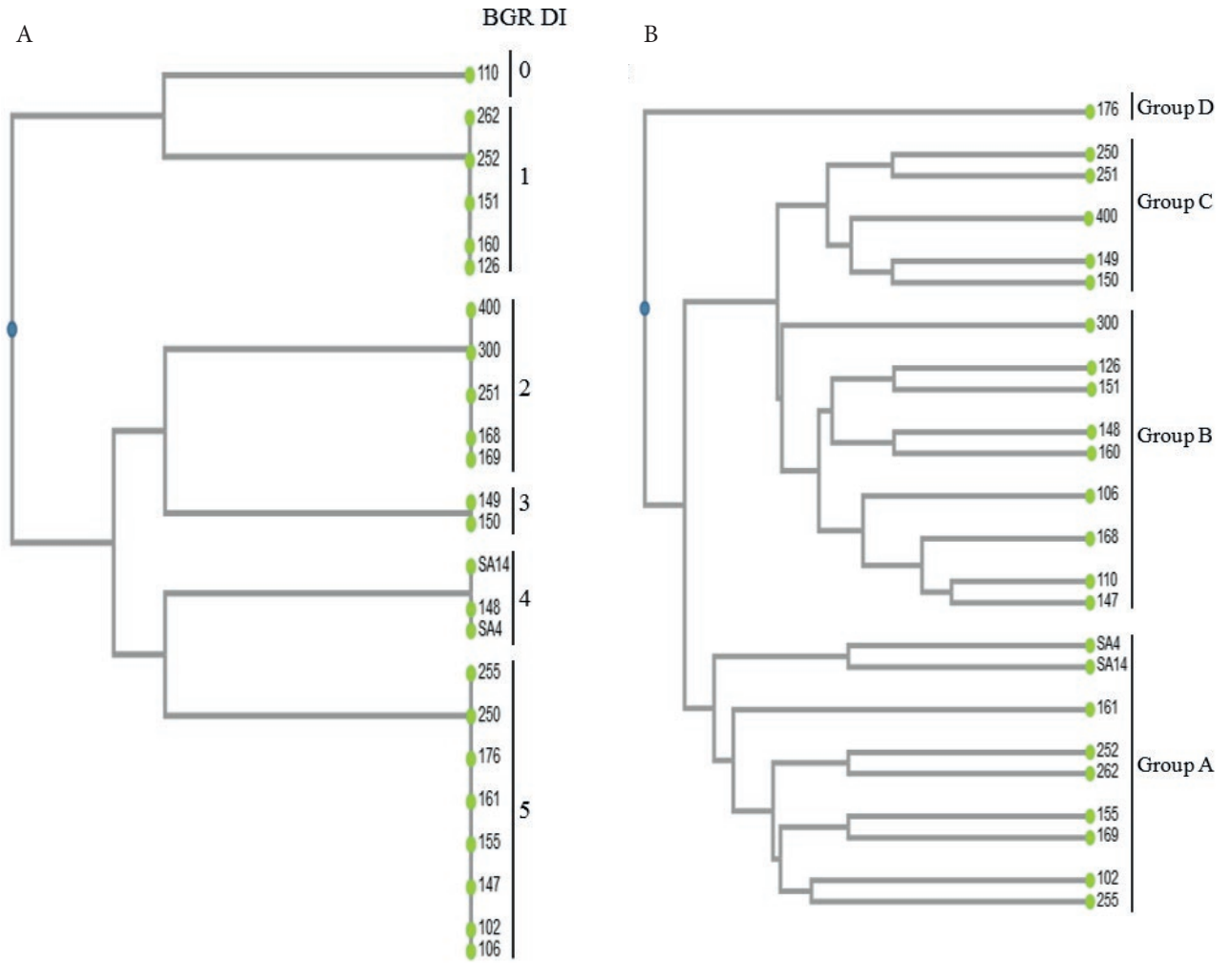

Figure 3. Representative dendrograms of clustering of 24 BGR-associated isolates, based on disease severity scale on saffron corms (A); and diversity in physiological and biochemical characteristics (B). DI = disease index.

ITS region were amplified from all isolates, using the primer pairs 27F/1492R (1500 bp), CMG16-1/CMG16-2 (470 bp) and GLA-f/GLA-r (300 bp). An approx.i700 bp fragment of the 23S rRNA was amplified from most of the isolates using the LP1/LP4 primer pair, but amplification was unsuccessful from isolates 14 of 24. In most isolates (18 of 24), the expected *Burkholderia recA*-related fragment of 869 bp was amplified with the BUR1/BUR2 primer pair. A 470 bp fragment of the 16S rRNA from two isolates (110 from phenotype group A, and 155 from group B) was cloned and sequenced. The sequences were deposited in GenBank with accession numbers PQ120996 and PQ120997. These sequenced fragments of the BGR-associated isolates showed 97 to 99.5% similarity with other *Burkholderia gladioli* isolates deposited in GenBank, and were put in *B. gladioli* group in the phylogentic tree (Figure 4 A). In a phylogenetic tree, *B. gladioli* pv. *gladioli* isolates from saffron isolates from Italy, India and Iran clustered in a separate clade from other *B. gladioli* pathovars (Figure 4 B). *Burkholderia gladioli* isolates from saffron had, in the 16S rRNA gene, 99.5 to 99.9% similarity to *B. gladioli* pv. *gladioli* 99.5 to 100% similarity to *B. gladioli* pv. *alliicola*, and 99.1 to 99.7% similarity to *B. gladioli* pv. *agaricicola*. The 16S rRNA fragments from two isolates of *B. gladioli* had 97.3 to 98.5% similarity to homologous sequences from *B. cepacia* and showed 92.5 to 96.4% similarity to those of other *Burkholderia* species.

DISCUSSION

In this study, a polyphasic approach was used, by combining pathogenicity, biochemical and molecular

Table 2. Main characteristics of bacterial isolates from saffron.

Characteristic	Group A	Group B	Group C	Group D	*B. gladioli* pv. *gladioli* CFBP2427[a] (Fiori *et al.,* 2011)
Gram reaction	-	-	-	-	-
Colony colour	Yellowish/ orange-milky	Milky	Milky	Milky	
Oxidase	+/-	+/-	+	+	+
Catalase	+	+/-	+	-	+
Arginine decarboxylase	-/+	+	+	-	
Hydrolysis of: gelatin	+	+	+	-	+
Hydrolysis of starch	+/-	+/-	+	+	-
O-F Glucose test	+/-	+/-	+/-	+/-	+/-
Growth at: pH 4	+	+	+	+	+
pH 8	+	+	+	+	+
pH 9	+	+	+	+	-
Growth in 3% NaCl	+	+	+	-	+
Growth at 41° C	-/+	-/+	-/+	-	-/+
Utilization of					
Raphinose	+/-	-/+	+/-	+	
Arabinose	-/+	-/+	+	+	
Adonitol	+	-	-	-	+
Glucose	$+^{w}$	$+^{w}$	$+^{w}$	$+^{w}$	+
Dextrose	+	-/+	+	-	
Maltose	++	+/-	+	++	-
Sucrose	-	-	-	-	
Lactose	+	-	-	+	
Galactose	-/+	-/+	-	+	
Urease	+	++	+	+	

[a] CFBP 2427 is the pathotype strain of *Burkholderia gladioli* pv. *gladioli*
+ = positive; - = negative; -/+ = mostly negative, but positive in some isolates; +/- = mostly positive, but negative in some isolates; ++ = strongly positive; $+^{w:}$ weakly positive.

test to identify and characterize a collection of bacterial isolates causing dry rot of saffron corms in Iran. The main symptom of the disease was reddish-brown lesions on saffron corms, which spread to the inner corm tissues. In many cases, the corms were completely rotted. The colonies of isolated bacteria were milky-yellowish and round in 2 day cultures, and secreted yellowish pigments into the culture media. Based on results of biochemical and physiological tests, 24 isolates were initially identified as *B. gladioli*. These isolates were also categorized into six groups based on disease severity indices on saffron corms, and four groups determined from results of physiological and biochemical tests. No correlation was found between the BGR disease indices and the phenotypic grouping of the isolates or their geographical distributions. *B. gladioli* is a heterogeneous species with variations in phenotypic and genetic characteristics; its differentiation is mainly based on host range (Sadler, 1994; Coenye *et al.,* 1999; Nandakumar *et al.,* 2009; Castro-González *et al.,* 2011; Fiori *et al.,* 2011).

Due to the high degree of phenotypic similarity between *B. gladioli*, *B. glumae* (Coenye and Vandamme 2003; Coenye *et al.,* 1999), and *B. cepacia* (Baxter *et al.,* 1997), biochemical characterization if these bacteria is not accurate for precise identification of *B. gladioli*. PCR with *B. gladioli*-specific primers was used to increase detection sensitivity, specificity, and simplicity, and for more rapid identifications than from phenotypic methods. Specific fragments of *B. gladioli* fragments were amplified from selected Iranian isolates. Sequences of 16S and 23S rRNA have been used for rapid identification and differentiation of *B. gladioli* from *B. cepacia*, *B. multivorans*, *B. vietnamiensis*, *B. mallei*, *B. pseudomallei* and *Ralstonia pickettii* (Bauernfeind *et al.,* 1998). BLAST analysis showed that the BGR-associated isolates were most similar to *Burkholderia* species. Comparison of the 16S rRNA sequence of the Iranian BGR-associated saffron isolates revealed 99.5 to 99.9% nucleotide similar-

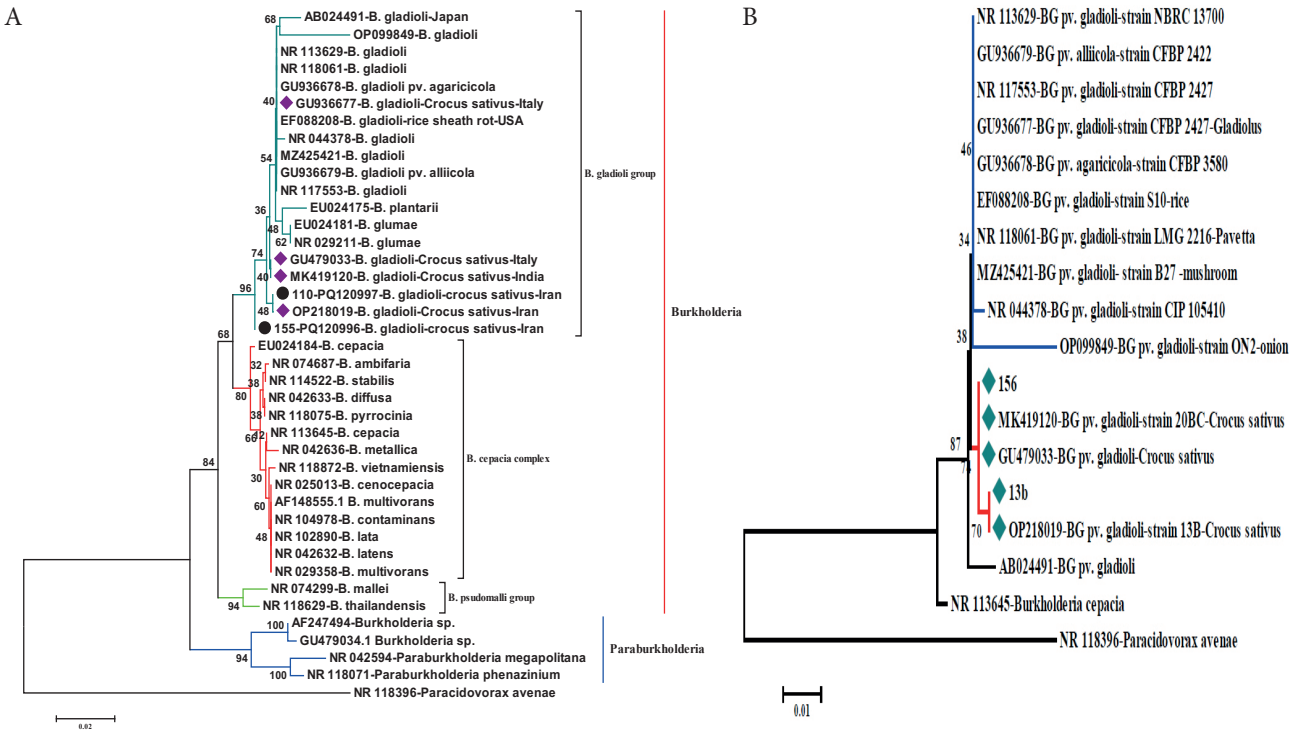

Figure 4. Neighbor-joining phylogenetic tree based on partial sequences of the 16S rRNA gene of *Burkholderia* species (A) and 16S-23S rRNA ITS region of *Burkholderia gladioli* pathovars (B). Numbers on branch nodes are percentage bootstrap values based on 1,000 replicates. *Paracidovorax avenae* was used as an outgroup. Bar shows substitutions per nucleotide position. • indicates represented *Burkholderia gladioli* isolates from saffron (*Crocus sativus*) from Iran, and ♦ indicates isolates from owther countries.

ity with other *B. gladioli* isolates (Gee *et al.,* 2003; Kim *et al.,* 2009). Similarity of this fragment with sequences from other *Burkholderia* species was in the range 92.5 to 96.4%. Phylogenetic analysis of the 16S rRNA gene placed the BGR-associated isolates in the *Burkholderia* group, close to the *B. gladioli* group. Due to the similarity of the 16S rRNA sequence from *B. gladioli* and *B. glumae* (Nandakumar *et al.*, 2009), the 16S-23S rRNA ITS region was used to distinguish *B. gladioli* from *B. glumae* (Furuya *et al.,* 2002). In the phylogenetic tree, the Iranian saffron BGR-associated isolates were placed next to *B. gladioli* isolates.

Bgg is pathogenic to gladiolus, orchids, *Crocus* spp., rice, and fern, and other plant species (Sadler, 1994; Ura *et al.,* 2006; Compant *et al.,* 2008; Nandakumar *et al.,* 2009). Sequence analysis of the 16S rRNA of the Iranian saffron BGR-associated isolates showed similarity of 99.1 to 100% with the pathovars Bgg and Bga of *B. gladioli*.

To determine the pathovars of the Iranian BGR-associated isolates, pathogenicity tests were carried in onion as a possible alternative host. Presumptive Bgg isolates caused dry rot in onion, but possible Bga gave soft rot and internal rot in onion (Lee *et al.,* 2005). Most of the BGR-associated isolates caused soft rot in onion, making it possible that BGR-associated saffron isolates from Iran are Bga. However, phylogenetic analyses of some BGR-associated isolates using the 16S-23S rRNA ITS region showed that they were very similar to pathovar *gladioli*. These results indicate that the causal agent of saffron dry rot in Iran could be *B. gladioli* pv. *gladioli*. Recently, *B. gladioli* has been reported from saffron, garlic and wild mushrooms in Iran (Abachi *et al.,* 2024; Hamidizade *et al.* 2024; Khezri *et al.,* 2023), but the present report is the first from Iran, where biochemical and molecular characterization have been achieved for the pathogen causing bacterial dry rot of saffron Iranian saffron *B. gladioli* strains possess pathogenicity characteristics that overlap with Bgg and Bga pathovars of *B. gladioli*. This shows that using phenotypic pathovar-oriented assays to classify *B. gladioli* strains should be replaced by phylogenetic or phylogenomic analyses for identification of this pathogen (Abachi *et al.*, 2024).

Inoculation by injection of saffron corms with the BGR-associated isolates, or through wounds in the corm skins, caused lesions in the corms. These results agree with the observations of Fiori *et al.* (2011). Nevertheless, the severity of symptoms depended on virulence of the different isolated bacteria.

It has been reported that *Burkholderia* is more frequently isolated from rhizospheres of plants than from bulk soil of the same field (Marques *et al.,* 2014). *Burkholderia gladioli* has been identified as an endophyte in coffee (Vega *et al.,* 2005) and soybean (Kuklinsky-Sobral *et al.,* 2004), but not as an endophyte in saffron (Marques *et al.,* 2015; Sharma *et al.,* 2015; Xuan *et al.,* 2016). However, Ahmad *et al.* (2022) reported *B. gladioli* as an endophyte in saffron, so it is still unclear whether *B. gladioli* is in the rhizosphere community of *Crocus* species. Studies have shown that toxoflavin produced by *B. gladioli* and *B. glumae* is an important pathogenic factor causing grain wilt in rice and rot in many crops (Jeong *et al.,* 2003; Jung *et al.,* 2011). Inoculation with toxoflavin led to infections in crops such as tomato, sesame, eggplant and bell pepper (Jeong *et al.,* 2003; Nandakumar *et al.,* 2009). The reddish-brown lesions on saffron corms could be due to the presence of toxoflavin. Therefore, further investigation is required on the role of toxoflavin production in regulating pathogenicity of *B. gladioli* in saffron.

LITERATURE CITED

Abachi H., Moallem M., Taghavi S.M., Hamidizade M., Soleimani A., … Osdaghi E., 2024. Garlic bulb decay and soft rot caused by the cross-kingdom pathogen *Burkholderia gladioli*. *Plant Disease* 108: 684–693. https://doi.org/10.1094/PDIS-08-23-1603-RE

Ahmad T., Bashir A., Farooq S., Riyaz-Ul-Hassan S., 2022. *Burkholderia gladioli* E39CS3, an endophyte of *Crocus sativus* L., induces host resistance against corm-rot caused by *Fusarium oxysporum*. *Journal of Applied Microbiology* 132: 495–508. https://doi.org/10.1111/jam.15190

Baxter I.A., Lambert P.A., Simpson I.N., 1997. Isolation from clinical sources of *Burkholderia cepacia* possessing characteristics of *Burkholderia gladioli*. *Journal of Antimicrobial Chemotherapy* 39: 169–175. https://doi.org/10.1093/jac/39.2.169

Bauernfeind A., Roller C., Meyer D., Jungwirth R., Schneider I., 1998. Molecular procedure for rapid detection of *Burkholderia mallei* and *Burkholderia pseudomallei*. *Journal of Clinical Microbiology* 36: 2737–2741. https://doi.org/10.1128/jcm.36.9.2737-2741.1998

Castro-González R., Martínez-Aguilar L., Ramírez-Trujillo A., Estada-de los santos P., Cballero-Mellado J., 2011. High diversity of culturable *Burkholderia* species associated with sugarcane. *Plant Soil* 345: 155–169. https://doi.org/10.1007/s11104-011-0768-0

Chiarini L., Bevivino A., Dalmastri C., Tabacchioni S., Visca P., 2006. *Burkholderia cepacia* complex species: health hazards and biotechnological potential. *Trends Microbiology* 14: 277–86. https://doi.org/10.1016/j.tim.2006.04.006

Coenye T., Vandamme P., 2003. Diversity and significance of *Burkholderia* species occupying diverse ecological niches. *Enviromental Microbiology* 5: 719–29. https://doi.org/10.1046/j.1462-2920.2003.00471.x

Coenye T., Schouls L. M., Govan J. R. W., Kersters K., Vandamme P., 1999. Identification of *Burkholderia* species and genomovars from cystic fibrosis patients by AFLP fingerprinting. *International Journal Systematic Bacteriology* 49: 1657–1666. https://doi.org/10.1099/00207713-49-4-1657

Compant S., Nowak J., Coenye T., Clément C., Ait Barka E., 2008. Diversity and occurrence of *Burkholderia* spp. in the natural environment. *FEMS Microbiology Review* 32: 607–626. https://doi.org/10.1111/j.1574-6976.2008.00113.x

EPPO. 2006. PM 7/58 (1) *Burkholderia caryophylli*. *Bulletin OEPP/EPPO Bulletin* 36: 95–98. https://doi.org/10.1111/j.1365-2338.2006.00918.x

Fiori M., Ligios V., Schiaffino A., 2011. Identification and characterization of *Burkholderia* isolates obtained from bacterial rot of saffron (*Crocus sativus* L.) grown in Italy. *Phytopathologia Mediterranea* 50: 450–461. https://dx.doi.org/10.14601/Phytopathol_Mediterr-8730

Furuya N., Ura H., Iiyama K., Matsumoto M., Takeshita M., Takanami Y. 2002. Specific oligonucleotide primers based on sequences of the 16S–23S rDNA spacer region for the detection of *Burkholderia gladioli* by PCR. *Journal General Plant Pathology* 68: 220–224. https://doi.org/10.1007/PL00013080

Gee J.E., Sacchi C.T., Glass M.B., De B.K., Weyant R.S., …Popovic T., 2003. Use of 16S rRNA gene sequencing for rapid identification and differentiation of *Burkholderia pseudomallei* and *B. mallei*. *Journal Clinical Microbiology* 41: 4647–54. https://doi.org/10.1128/JCM.41.10.4647-4654.2003

Hamidizade M., Taghavi S.M., Soleimani A., Bouazar M., Abachi H., Portier P., Osdaghi E., 2024. Wild mushrooms as potential reservoirs of plant pathogenic bacteria: a case study on *Burkholderia gladioli*. *Microbiology Spectrum* 12(4): e03395-23. https://doi.org/10.1128/spectrum.03395-23

Holt J.G., 1994. *Bergey's Manual of Determinative Bacteriology*. 9th ed. Lippincott Williams and Wilkins, Baltimore, MD, USA.

Jeong Y., Kim J., Kim S., Kang Y., Nagamatsu T., Hwang I., 2003. Toxoflavin produced by *Burkholderia glumae*

causing rice grain rot is responsible for inducing bacterial wilt in many field crops. *Plant Disease* 87: 890–895. https://doi.org/10.1094/PDIS.2003.87.8.890

Jiao Z., Kawamura Y., Mishima N., Yang R., Li N., Liu X., Ezaki T., 2003. Need to differentiate lethal toxin-producing strains of *Burkholderia gladioli*, which cause severe food poisoning: description of *B. gladioli* pathovar *cocovenenans* and an emended description of *B. gladioli*. *Microbiology and Immunology* 47: 915–25. https://doi.org/10.1111/j.1348-0421.2003.tb03465.x

Jung W.-S., Lee J., Kim M.-I., Ma J., Nagamatsu T., … Rhee S. 2011. Structural and functional analysis of phytotoxin toxoflavin-degrading enzyme. *PLoS ONE* 26: e22443. https://doi.org/10.1371/journal.pone.0022443

Khezri M., Karimi Shahri M.R., Ghasemi A. 2023. Bacterial rot disease of saffron corm and leaf. *Plant Pathology Science* 12: 74–83. Doi: 10.2982/PPS.12.1.74

Kim J., Oh J., Choi O., Kang Y., Kim H., … Hwang I., 2009. Biochemical evidence for ToxR and ToxJ binding to the *tox* operons of *Burkholderia glumae* and mutational analysis of ToxR. *Journal Bacteriology* 191: 4870–4878. http://dx.doi.org/10.1128/JB.01561-08

Koocheki A., Khajeh-Hosseini M., 2020. *Saffron: Science, Technology and Health*. Woodhead Publishing, 580 pp. eBook ISBN: 9780128187401.

Kowalska B., Smolińska U., Oskiera M., 2015. *Burkholderia gladioli* associated with soft rot of onion bulbs in Poland. *Journal Plant Pathology* 97: 37–43. http://www.jstor.org/stable/24579128

Kuklinsky-Sobral J., Araújo W.L., Mendes R., Geraldi I.O., Pizzirani-Kleiner A.A., Azevedo J.L., 2004. Isolation and characterization of soybean-associated bacteria and their potential for plant growth promotion. *Enviromental Microbiology* 6: 1244–51. https://doi.org/10.1111/j.1462-2920.2004.00658.x

Lee C.J., Lee J.T., Kwon J.H., Kim B.C., Park W. 2005. Occurrence of bacterial soft rot of onion plants caused by *Burkholderia gladioli* pv. *alliicola* in Korea. *Australasian Plant Pathology* 34: 287–292. https://doi.org/10.1071/AP05024

Lee C.J., Lee J.T., Kim Y.T., Jhune C.S., Cheong J.C., Park W., 2012. Phytopathogenicity of *Burkholderia gladioli* pv. *alliicola* CH1 and production of PGase isozymes. *Research in Plant Disease* 18: 240–244. https://doi.org/10.5423/rpd.2012.18.3.240

Lee C.J., Lee J.T. Park H.S., Lee E., Min G., 2021. Molecular analysis of the pathogenicity-related polygalacturonase gene *pehA* of *Burkholderia gladioli* pv. *alliicola* isolated from onion (*Allium cepae*. L). *Physiological and Molecular Plant Pathology* 115: 101670. https://doi.org/10.1016/j.pmpp.2021.101670

Li X., De Boer SH., 2005. First Report of *Burkholderia andropogonis* causing leaf spots of *Bougainvillea* sp. in Hong Kong and clover in Canada. *Plant Disease* 89: 1132. https://doi.org/10.1094/PD-89-1132A

Li X., Li Y., Wang R., Wang Q., Lu L., 2019. Toxoflavin produced by *Burkholderia gladioli* from *Lycoris aurea* is a new broad-spectrumffungicide. *Applied Enviromental Microbiology* 85: e00106-19. https://doi.org/10.1128/AEM.00106-19

Liguori A.P., Warrington S.D., Ginther J.L., Pearson T., Bowers J., Glass M.B., … Tuanyok A., 2011. Diversity of 16S-23S rDNA internal transcribed spacer (ITS) reveals phylogenetic relationships in *Burkholderia pseudomallei* and its near-neighbors. *PLoS One* 6: e29323. https://doi.org/10.1371/journal.pone.0029323

Lincoln S.P., Fermor T.R., Stead D.E., Sellwood J.E. 1991. Bacterial soft rot of *Agaricus bitorquis*. *Plant Pathology* 40: 136–144. https://doi.org/10.1111/j.1365-3059.1991.tb02302.x.

Maeda Y., Shinohara H., Kiba A., Ohnishi K., Furuya N., … Hikichi Y., 2006. Phylogenetic study and multiplex PCR-based detection of *Burkholderia plantarii*, *Burkholderia glumae* and *Burkholderia gladioli* using *gyrB* and *rpoD* sequences. *International Journal of Systematic and Evolutionary Microbiology* 56: 1031–1038. https://doi.org/10.1099/ijs.0.64184-0

McCulloch L., 1921. A bacterial disease of gladiolus. *Science* 54: 115–116. doi: 10.1126/science.54.1388.115

Marques J.M. da Silva T.F., Vollu R.E., Blank A.F., Ding G.C., … Smalla K., 2014. Plant age and genotype affect the bacterial community composition in the tuber rhizosphere of field-grown sweet potato plants. *FEMS Microbiology Ecology* 88: 424–435. https://doi.org/10.1111/1574-6941.12313

Marques J.M., da Silva T.F., Vollú R.E., de Lacerda J.R.M., Blank A.F., … Seldin L., 2015. Bacterial endophytes of sweet potato tuberous roots affected by the plant genotype and growth stage. *Applied Soil Ecology* 96: 273–281. https://doi.org/10.1016/j.apsoil.2015.08.020

Moon H., Park H.J., Jeong A., Han S.W., Park C.J., 2017. Isolation and identification of *Burkholderia gladioli* on *Cymbidium* orchids in Korea. *Biotechnology and Biotechnological Equipment* 31: 280–288. https://doi.org/10.1080/13102818.2016.1268069

Nandakumar R., Shahjahan A.K.M., Yuan X.L., Dickstein E.R., Groth D.E., … Rush M.C., 2009. *Burkholderia glumae* and *B. gladioli* cause bacterial panicle blight in rice in the southern United States. *Plant Disease* 93: 896–905. https://doi.org/10.1094/PDIS-93-9-0896

Payne G.W., Vandamme P., Morgan SH., Lipuma J.J., Coenye T., … Mahenthiralingam E., 2005. Development of a *recA* gene-based identification approach for

the entire *Burkholderia* genus. *Applied Environmental Microbiology* 71: 3917–27. https://doi.org/10.1128/AEM.71.7.3917-3927.2005

Saddler G.S. (ed.) 1994. *Burkholderia gladioli* pv. *gladioli*. *IMI Descriptions of Fungi and Bacteria*, Vol. 122. CAB International, Wallingford, UK, 1218 pp.

Sharma T., Kaul S., Dhar M.K., 2015. Diversity of culturable bacterial endophytes of saffron in Kashmir, India. *Springerplus* 4: 661. https://doi.org/10.1186/s40064-015-1435-3

Stoyanova M., Hristova P., Petrov N., Moncheva P., Bogatzevska N. 2011a. Method for differentiating *Bukholderia gladioli* pathovars. *Science & Technology* 1(6): 15-19.

Stoyanova M., Kizheva Y., Chipeva V., Bogatzevska N., Moncheva P. 2011b. Phytopathogenic *Burkholderia* species in bulbs plants in Bulgaria. *Biotechnology & Biotechnological Equipment* 25(3): 2477–2483. https://www.researchgate.net/publication/260236547

Suárez-Moreno Z.R., Caballero-Mellado J., Coutinho B.G., Mendonça-Previato L., James E.K., Venturi V. 2012. Common features of environmental and potentially beneficial plant-associated *Burkholderia*. *Microbial Ecology* 63: 249–66. https://doi.org/10.1007/s00248-011-9929-1

Tamura K., Peterson D., Peterson N., Stecher G., Nei M., Kumar S. 2011. MEGA5: Molecular evolutionary genetics analysis using Maximum Likelihood, Evolutionary Distance, and Maximum Parsimony methods. *Molecular Biology and Evolution* 28: 2731–2739. https://doi.org/10.1093/molbev/msr121

Thibault F.M., Valade E., Vidal D.R., 2004. Identification and discrimination of *Burkholderia pseudomallei*, *B. mallei*, and *B. thailandensis* by real-time PCR targeting type III secretion system genes. *Journal Clinical Microbiology* 42: 5871–5874. https://doi.org/10.1128/jcm.42.12.5871-5874.204

United Nations Industrial Development Organization (UNIDO), 2022. Online: http://open.unido.org

Ura H., Furuya N., Iiyama K., Hidaka M., Tsuchiya K., Matsuyma M., 2006. *Burkholderia gladioli* associated with symptoms of bacterial grain rot and leaf-sheath browning of rice plants. *Journal General Plant Pathology* 72: 98–103. https://doi.org/10.1007/s10327-005-0256-6

Vega F.E., Pava-Ripoll M., Posada F., Buyer J.S., 2005. Endophytic bacteria in *Coffea arabica* L. J. *Basic Microbiology* 45: 371–380. https://doi.org/10.1002/jobm.200410551

Vermis K., Coenye T., Mahenthiralingam E., Nelis H.J., Vandamme P., 2002. Evaluation of species-specific recA-based PCR tests for genomovar level identification within the *Burkholderia cepacia* complex. *Journal Medical Microbiology* 51: 937–940. https://doi.org/10.1099/0022-1317-51-11-937Wang M., Wei P., Cao M., Zhu L., Lu Y., 2016. First Report of Rice Seedling Blight Caused by *Burkholderia plantarii* in North and Southeast China. *Plant Disease* 100: 645. https://doi.org/10.1094/PDIS-07-15-0765-PDN

Whitby P.W., Carter K.B., Hatter K.L., LiPuma J.J., Stull T.L., 2000. Identification of members of the *Burkholderia cepacia* complex by species-specific PCR. *Journal Clinical Microbiology* 38: 2962–5. https://doi.org/10.1128/JCM.38.8.2962-2965.2000

Woo P.C., Ng K.H., Lau S.K., Yip K.T., Fung A.M., … Yuen K.Y., 2003. Usefulness of the MicroSeq 500 16S ribosomal DNA-based bacterial identification system for identification of clinically significant bacterial isolates with ambiguous biochemical profiles. *Journal Clinical Microbiology* 41: 1996–2001. https://doi.org/10.1128/jcm.41.5.1996-2001.2003Xu C.X., Ge Q.X. 1990. A preliminay study on corm rot of *Crocus sativus* L. *Acta Agriculturae, Universitatis Zhejiangensis* 16 (suppl. 2): 241–246

Xuan L.N.T., Van Dung T., Hung N.N., Diep C.N., 2016. Isolation and characterization of endophytic and rhizopheric bacteria associated sweet-potato plants cultivated on soils of the Mekong Delta. *Vietnam* 6: 129–149. https://doi.org/10.20959/wjpps20169-7671

Yabuuchi E., Kosako Y., Oyaizu H., Yano I., Hotta H., … Arakawa M., 1992. Proposal of *Burkholderia* gen. nov. and transfer of seven species of the genus *Pseudomonas* homology group II to the new genus, with the type species *Burkholderia cepacia* (Palleroni and Holmes 1981) comb. nov. *Microbiology and Immunology* 36: 1251–1275. https://doi.org/10.1111/j.1348-0421.1992.tb02129.x

Phytopathologia Mediterranea
The international journal of the
Mediterranean Phytopathological Union

Firenze University Press
www.fupress.com/pm

Research Papers

Identification and fungicide screening of *Phyllosticta capitalensis* causing leaf spot on sweet viburnum in China

Wen LI[1], Yixuan RUAN[1], Zhengping BIAN[2], Yueqiu HE[1], Kai FENG[1], Liang LIU[1], Zhilong WANG[1,*], Feng HUANG[3,*]

[1] *Ningbo City College of Vocational Technology, Ningbo Zhejiang, China*
[2] *Ningbo Forest Farm, Ningbo Zhejiang, China*
[3] *Plant Protection Research Institute, Guangdong Academy of Agricultural Sciences, Key Laboratory of Green Prevention and Control on Fruits and Vegetables in South China Ministry of Agriculture and Rural Affairs, Guangdong Provincial Key Laboratory of High, Guangzhou, Guangdong, China*
*Corresponding authors. E-mail: wangzhl01@163.com, rm12407@126.com

Summary. Sweet viburnum (*Viburnum odoratissimum* Ker-Gawl.) is a widely used ornamental plant, which has dense branches and leaves, and fast spreading and evergreen habit. In October 2022, leaf spot symptoms were observed in a hedge of sweet viburnum in Yuanshi Garden, Ningbo, China. Fungi were isolated from symptomatic leaves, and were identified using morphological characteristics and phylogenetic analyses of partial sequences of internal transcribed spacer (ITS), actin (*act*), and translation elongation factor 1-alpha (*tef*1-α), and were evaluated in pathogenicity tests. The causal agent of sweet viburnum leaf spot was identified to be *Phyllosticta capitalensis*. Effects of seven fungicides on *P. capitalensis* were assessed *in vitro*. Fungicide EC_{50}s (mg L^{-1}) against *P. capitalensis* were: 270.77 for 75% chlorothalonil (WP); 0.02 for 250 g L^{-1} azoxystrobin SC; 0.27 for 10% difenconazole WDG; 0.02 for 75% trifloxystrobin + tebuconazole WDG, 9.03 for 35% fluopyram + tebuconazole SC, 5.90 for 500 g L^{-1} fluazinam SC, and 89.11 for 10% prothioconazole SC. Among these, azoxystrobin SC and trifloxystrobin + tebuconazole WDG could be used for control of viburnum leaf spot. This is the first report of *P. capitalensis* causing leaf spot of sweet viburnum, and this study provides guidance for chemical management sweet viburnum leaf spot, and on other host plants.

Keywords. Chemical control, new disease, pathogen identification, phylogeny.

Citation: Li, W., Ruan, Y., Bian, Z., He, Y., Feng, K., Liu, L., Wang, Z., & Huang, F. (2024). Identification and fungicide screening of *Phyllosticta capitalensis* causing leaf spot on sweet viburnum in China. *Phytopathologia Mediterranea* 63(2): 295-301. doi: 10.36253/phyto-15455

Accepted: July 31, 2024

Published: September 15, 2024

Data Availability Statement: All relevant data are within the paper and its Supporting Information files.

Competing Interests: The Author(s) declare(s) no conflict of interest.

Editor: Alan J.L. Phillips, University of Lisbon, Portugal.

ORCID:
WL: 0000-0002-0983-7910
YR: 0009-0004-1956-1833
ZB: 0009-0008-7439-175X
YH: 0009-0002-8988-9012
KF: 0009-0000-4501-7883
LL: 0000-0001-8044-1006
ZW: 0000-0001-8734-1729
FH: 0000-0002-8406-5068

INTRODUCTION

Viburnum, including almost 200 species, is a large genus of flowering shrubs (Landis *et al.*, 2021), of which sweet viburnum (*Viburnum odoratissimum* Ker-Gawl.) is a shrub native to the Himalayas and Japan. Due to its attributes of fast and spreading growth, dense branches, evergreen leaves, and attractive flowers, sweet viburnum has been widely used as ornamental plants (Shober *et al.*, 2017).

Several fungi and viruses have been reported causing diseases on sweet viburnum. The positive-sense RNA virus designated as 'Viburnum-like virus'

was recently isolated from sweet viburnum, and siRNA sequencing indicated that this virus actively replicates within the host and elicits antiviral defence mechanisms (Gao *et al*., 2024). *Erysiphe hedwigii* causes powdery mildew, and *Colletotrichum gloeosporioides* causes anthracnose of sweet viburnum (Yang *et al*., 2015; Cho *et al*., 2016; Michael *et al*., 2022), and economically important leaf spot diseases are caused by *Diaporthe eres*, *Corynespora cassiicola*, *Alternaria* spp., and *Neofusicoccum parvum* (Qiu *et al*., 2021; Ma *et al*., 2022; Zhang *et al*., 2022a; Wan *et al*., 2023). Occasionally, these leaf spot diseases can kill their host plants. Thus, it is important to identify the causative pathogens, and assessment potential management methods for these diseases.

The present study outlines observation, isolation and description of the pathogen responsible for leaf spot on sweet viburnum leaves. Assessments were also made of the activity of different fungicides as potential agents for control of this disease.

MATERIALS AND METHODS

Pathogen isolation and morphology

To identify the pathogen associated with the disease, 20 symptomatic leaves were collected from ten different sweet viburnum plants. Pathogen isolation was carried out using methods described by Li *et al*. (2021a). Leaf tissue was excised from lesion margins, and was surface sterilized with 75% ethanol for 30 sec. rinsed three times in sterile distilled water, then immersed in 10% sodium hypochlorite for 5 min, and again washed three times in distilled water, followed by drying on sterile filter paper. The excised leaf pieces were then cut into small segments (1 cm^2) and transferred to Petri plates containing potato dextrose agar (PDA: 20% diced potato, 2% glucose, 1.5% agar, and distilled water.). The plates were then incubated at 28°C for 2 d under a 12 h light, 12 h dark regime. Nine individual resulting colonies were selected and transferred to fresh PDA plates, and after incubation were preserved in 10% glycerol at -80°C for future use. Morphology of the colonies on PDA was observed from the upper and lower sides of the plates after 5 d incubation. Conidium morphology was examined using a Leica DM3000 microscope system, and the morphology and sizes of 50 conidia were assessed.

Pathogenicity testing

To confirm the pathogenicity of the isolated fungus, Koch's postulates were assessed for one of the isolates ("F2") obtained. Wounds were created on leaf surfaces of healthy sweet viburnum plants by pricking. Mycelium plugs from fungal colonies in PDA cultures were then placed onto the wounded sites. PDA without fungi was used for inoculation controls. The plants were then maintained in a growth chamber at 25°C and 85% relative humidity. Photographs of developing disease symptoms were taken at 10 to 20 d post-inoculation. Subsequently, the fungi were re-isolated from the inoculated leaf tissues and identified using the methods described above.

DNA extraction, amplification, and sequencing

For accurate identification, genomic DNA was extracted from the samples using the TIANamp Genomic DNA Kit (Cat. No 4992254, Tiangen Biotech (Beijing) Co. Ltd), following the manufacturer's instructions. Partial sequences of the ribosomal internal transcribed spacer (ITS), actin (*act*) and translation elongation factor 1-alpha (*tef*1) were amplified and sequenced, as described by Wikee *et al*., (2013) and Li *et al.* (2021a), and the nucleotide sequences were deposited in GenBank. Multiple alignments of concatenated ITS, *act* and *tef1*-α sequences were carried out using MEGA 7 with default settings. A concatenated phylogenetic tree was constructed using the Maximum Likelihood method (ML) with JTT model, as implemented in MEGA 7 (Jones *et al*., 1992). The fungus strains used in this study are listed in Table 1.

Fungicide tests

In vitro fungicide activity against *P. capitalensis* was assessed following the method of Li *et al.* (2021b). Seven fungicides were selected, including 75% chlorothalonil WP, 250 g L^{-1} azoxystrobin SC, 10% difenconazole WDG, 75% trifloxystrobin + tebuconazole WDG (25% trifloxystrobin, 50% tebuconazole), 35% fluopyram + tebuconazole SC (17.5% fluopyram, 17.5% tebuconazole), 500 g L^{-1} fluazinam SC, and 10% prothioconazole SC. The concentrations of each fungicide used in PDA plates for the tests are shown in Table 2. Disks were excised from the edges of colonies on PDA plates at 5 d post inoculation using a 6 mm diam. sterilized punch. The side of each disk containing fungal hyphae was positioned at the center of each PDA plate. The inoculated plates were incubated at 28°C in the dark. PDA plates without fungicide were used as the negative experimental controls. Diameters of resulting colonies were measured at 5 d post-inoculation. Each treatment was con-

Table 1. Fungus strains used in this study.

Species	GenBank No.		
	ITS	*tef*	*act*
Phyllosticta ampelicida CBS 111645	JN692542	EU683653	JN692518
Phyllosticta brazilianiae LGMF 333	JF343574	JF343595	JF343658
Phyllosticta capitalensis CPC 20251	KC291333	KC342553	KC342530
Phyllosticta capitalensis CPC 20256	KC291337	KC342557	KC342534
Phyllosticta capitalensis CPC 20257	KC291338	KC342558	KC342535
Phyllosticta capitalensis F2	PP785331	PP788704	PP788703
Phyllosticta capitalensis JFRL-03-40	ON076573	ON081651	ON081650
Phyllosticta capitalensis LC 0002	KC291350	KC342570	KC342547
Phyllosticta citriasiana CBS 123370	FJ538355	FJ538413	FJ538471
Phyllosticta citribraziliensis LGMF09	JF261436	JF261478	JF343618
Phyllosticta citricarpa CBS 102374	FJ538313	GU349053	FJ538429
Phyllosticta citrichinaensis ZJUCC 2010152	JN791664	JN791515	JN791589
Phyllosticta hypoglossi CBS 101.72	FJ538365	FJ538423	FJ538481
Phyllosticta kerriae MUCC 17	AB454266	KC342576	AB704209
Guignardia mangiferae IMI 260576	JF261459	JF261501	JF343641
Phyllosticta owaniana CBS 776.97	FJ538368	FJ538426	FJ538484
Phyllosticta paracapitalensis CPC 26517	KY855622	KY855951	KY855677
Phyllosticta paracitricarpa CPC 27169	KY855635	KY855964	KY855690
Phyllosticta podocarpi CBS 111646	AF312013	KC357671	KC357670
Phyllosticta spinarum CBS 292.90	JF343585	JF343606	JF343669
Phyllosticta ampelicida CBS 111645	JN692542	EU683653	JN692518

ducted at least three times. Toxicity regression equations and EC_{50} values were calculated using Data Processing System (DPS 7.05).

RESULTS

Disease symptoms and pathogen isolation

In October 2022, sweet viburnum plants cultivated in Ningbo Yuanshi Park showed extensive necroses on the leaf tips or edges. The necroses developed from light to dark yellow, eventually drying to scorched appearance. During the subsequent infection stage, minute black spots emerged, which later developed into conidiomata (Figures 1, a and b). As the disease lesions expanded across entire leaves the leaves abscised from the tree. Approx. 30% of the sweet viburnum plants in the Park exhibited these symptoms, which significantly impeded their growth. After 7 d of incubation, isolated fungal colonies each had a white margin surrounding a dark green centre (Figure 1c). Conidia in the cultures were hyaline, oval-shaped and tapered at the ends, each with a hyaline, unstable apical appendage, measuring 2.7 to 5.2 µm in length. Conidia were of mean dimensions 6.6 to 14.3 × 5.2 to 8.1 µm (n=50) (Figure 1 d). Based on the colony morphology, the fungus was determined to be a member of the *Phyllosticta* species (Damm *et al.*, 2009; Wikee *et al.*, 2013).

Pathogenicity test

To determine if the isolates could induce the symptoms observed in the field, Koch's postulates were assessed on 20 1-year-old sweet viburnum plants. At 14 d after inoculation, leaf spot symptoms appeared on the leaves inoculated with isolate F2, while the control plants showed no symptoms. By 21 d post-inoculation, 80% of the inoculated plants displayed typical leaf spots accompanied by conidiomata within areas of necroses (Figure 2, a and b). The inoculated fungus was subsequently re-isolated from the inoculated leaf tissues, confirming that isolate F2 represented the pathogen responsible for the leaf spot in sweet viburnum plants.

Phylogenetic analysis

For accurate identification of the pathogen, a multilocus phylogenetic analysis was conducted using concat-

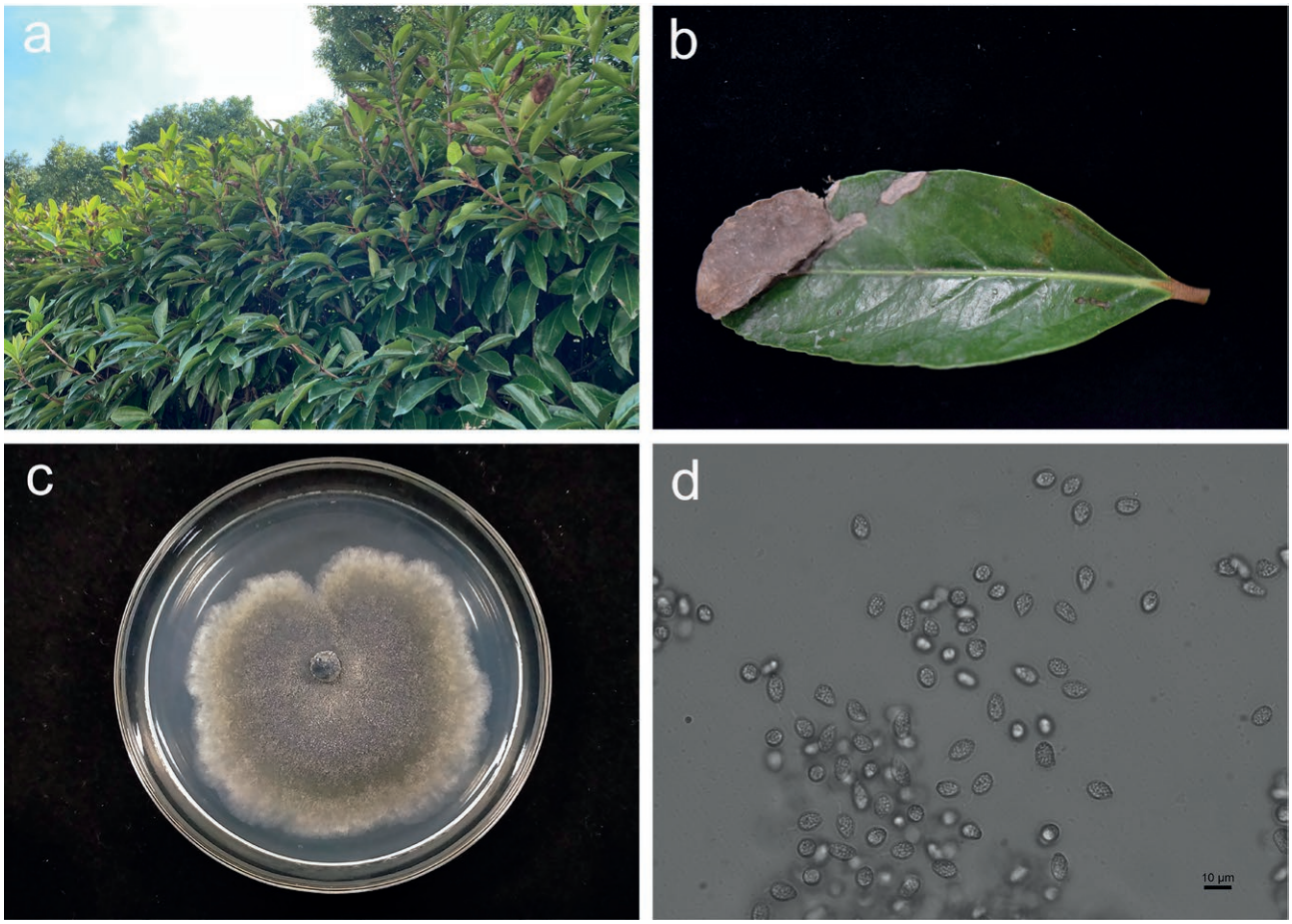

Figure 1. Disease symptoms and pathogen isolation. a and b, Disease symptoms on affected sweet viburnum leaves. c, Colony of *Phyllosticta capitalensis* grown on a PDA plate for 7 days at 28°C. d, Conidia of *P. capitalensis* observed under a light microscope at 200× magnification.

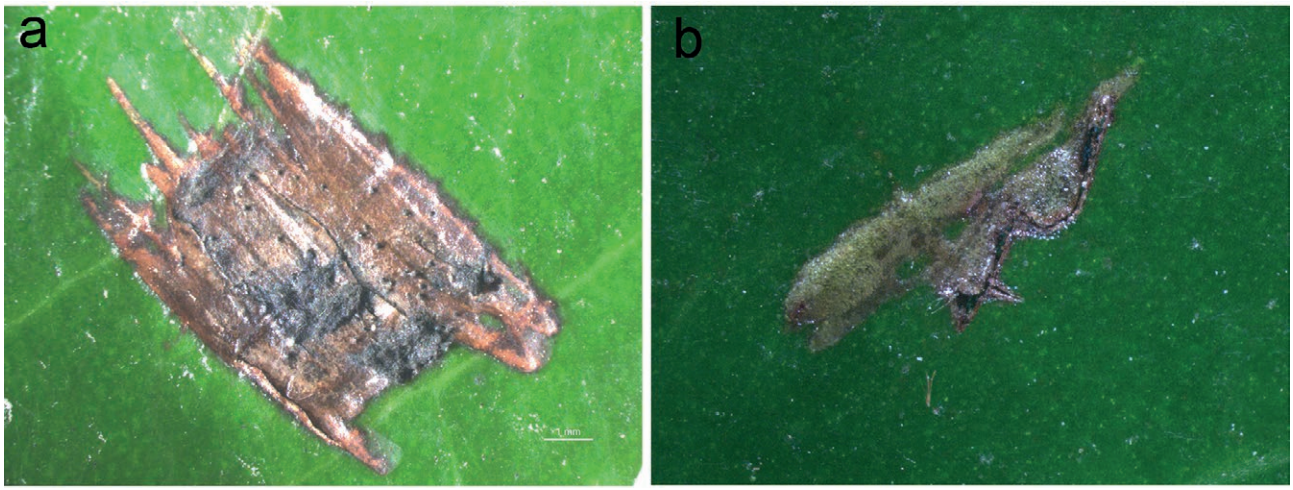

Figure 2. Pathogenicity test. Koch's postulates were conducted by inoculating healthy plants with fungal mycelium PDA plugs (2 a) or PDA plug inoculation controls (Figure 2 b). These photographs were taken at 21 d post inoculation.

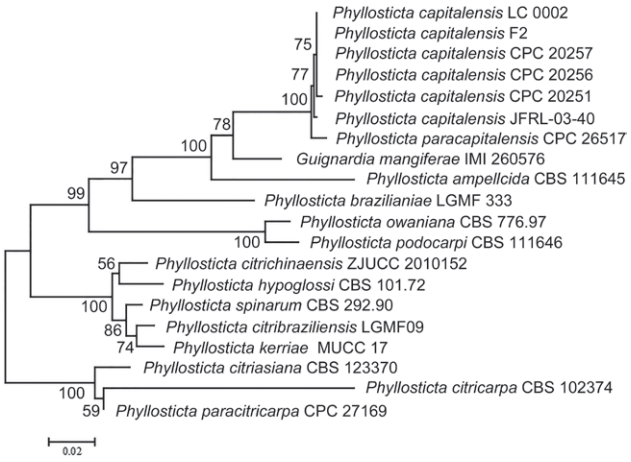

Figure 3. Phylogenetic tree for *Phyllosticta capitalensis* isolate F2 and closely related *Phyllosticta* species. Results were inferred from the concatenated sequences of ITS, *act* and *tef*1-α.

enated sequences of ITS, *act* and *tef*1-α genes from the 20 representative isolates, including isolate F2. The phylogenetic tree obtained (Figure 3) showed that isolate F2 is within the *P. capitalensis* clade, which is supported by moderate bootstrap support value of 77 %.

In vitro *fungicide tests*

The sensitivity of *P. capitalensis* to seven common fungicides was assessed. The results indicated that the EC_{50} values for the seven fungicides assessed against *P. capitalensis* were: 270.77 for 75% chlorothalonil WP, 0.02 for 250 g L^{-1} azoxystrobin SC, 0.27 for 10% difenconazole WDG, 0.02 for 75% trifloxystrobin + tebuconazole WDG, 9.03 for 35% fluopyram + tebuconazole SC, 5.90 for 500 g L^{-1} fluazinam SC, and 89.11 for 10% prothioconazole SC (Table 2). Among the tested fungicides, azoxystrobin and trifloxystrobin + tebuconazole exhibited the greatest antifungal activity against *P. capitalensis*. In contrast, chlorothalonil and prothioconazole exhibited limited efficacy against this pathogen.

DISCUSSION

Phyllosticta capitalensis has been recognized as an endophyte with a broad host range (Glienke-Blanco *et al*., 2002; Silva and Pereira 2007; Silva *et al*., 2008; Wikee *et al*., 2013; Bogas *et al*., 2022). Additionally, it has also been identified as an important pathogen responsible for leaf spot and black spot diseases on many plant species (Glienke *et al*., 2011; Wang *et al*., 2012; Zhang *et al*., 2022b; Jiang *et al*., 2023). While sweet viburnum leaf spot diseases caused by *Alternaria* (Qiu *et al*., 2021) and leaf blotch caused by *C. siamense* (Li *et al*., 2023) have been documented, the present report is the first of *P. capitalensis* as a pathogen affecting sweet viburnum.

Plant pathogen identification and pesticide screening for disease management assessments are important for developing effective disease control. For example, two microbial pathogens, *Streptomyces* sp. and *C. gloeosporioides*, cause leaf spot diseases on sweet cherry in Beijing, China (Ji *et al*., 2022). Upon pathogen identification, 10% difenconazole had the greatest inhibitory effect on mycelium growth of *P. capitalensis*, followed by 250 g L^{-1} of pyrazole ether ester, 50% imidacloprid, and 2% pyrimidine nucleoside antibiotics. These pesticides are the first choice for the chemical control the leaf spot of sweet cherry (Wu *et al*., 2015). *Phyllosticta capitalensis* isolates from leaf spots of *Polygonatum cyrtonema* were best targeted by triadimefon (Cui *et al*., 2023). Together with the present study, these fungicides plus 10% difenconazle WDG are likely to be good choices for control of leaf spot diseases caused by *P. capitalensis*.

Table 2. Growth inhibition activity of seven fungicides against *Phyllosticta capitalensis* F2

Fungicide	Concentrations assessed $(mg\ L)^{-1}$	Toxicity regression equation	EC_{50} $(mg\ L^{-1})$	Correlation coefficient *r*
75% chlorothalonil	1, 2, 4, 8, 16	$y = 4.4005 + 1.3858x$	270.77	0.9131
250g/L azoxystrobin	1, 2, 4, 8, 16	$y = 5.6516 + 0.1769x$	0.02	0.8963
10% difenconazole	0.125, 0.25, 0.5, 1, 2	$y = 6.0058 + 0.3913x$	0.27	0.8526
75% trifloxystrobin + tebuconazole	0.5, 1, 2 4, 8	$y = 6.8191 + 0.4820x$	0.02	0.8952
35% fluopyram + tebuconazole	0.5, 1, 2, 4 8	$y = 6.0194 + 0.9760x$	9.03	0.9158
500g/L fluazinam	0.125, 0.25, 0.5, 1, 2	$y = 6.8488 + 1.5041x$	5.90	0.9857
10% prothioconazole	0.125, 0.25, 0.5, 1, 2	$y = 5.1066 + 2.1279x$	89.11	0.9759

ACKNOWLEDGEMENT

This research was funded by the research project Green Pest Control Technology for Important Economic Crops in Ningbo (project no. 2024Z274).

LITERATURE CITED

Bogas A.C., Cruz F.P.N., Lacava P.T., Sousa C.P., 2022. Endophytic fungi: an overview on biotechnological and agronomic potential. *Brazilian Journal of Biology* 84: e258557. https://doi.org/10.1590/1519-6984.258557

Cho S.E., Lee S.H., Lee S.Y., Lee C.K., Shin H.D., 2016. First report of powdery mildew caused by *Erysiphe hedwigii* on *Viburnum awabuki* in Korea. *Plant Disease* 100: 2533. https://doi.org/10.1094/PDIS-06-16-0836-PDN

Cui X.Y., Dan Y.R., Li J.J., Ma W.L., Tang Z.X., … Liu M. 2023. Identification, biological characterization and inhibitory effect of fungicides on the pathogen causing *Polygonatum cyrtonema* leaf spot. *Acta Phytopathologica Sinica* 53(6): 1038-1046.

Damm U., Woudenberg J.H.C., Cannon P.F., Crous P.W., 2009. *Colletotrichum* species with curved conidia from herbaceous hosts. *Fungal Diversity* 39: 1–119. https://doi.org/10.1016/j.riam.2009.11.001

Gao Y.W., Xu Z.T., Li P., Hu X.D., Chen J.P., … Li Y.Y., 2024. Complete genome analysis of a novel narnavirus in sweet viburnum (*Viburnum odoratissimum*). *Archives of Virology* 169: 90. https://doi.org/10.1007/s00705-024-06000-y

Glienke-Blanco C., Aguilar-Vildoso C.I., Vieira M.L.C., Barroso P.A.V., Azevedo J.L. 2002. Genetic variability in the endophytic fungus *Guignardia citricarpa* isolated from citrus plants. *Genetics and Molecular Biology* 25: 251–255. https://doi.org/10.1590/S1415-47572002000200021

Glienke C., Pereira O., Stringari D., Fabris J., Kava-Cordeiro V., … Crous P.W. 2011. Endophytic and pathogenic *Phyllosticta* species, with reference to those associated with citrus black spot. *Persoonia* 26: 47–56. https://doi.org/10.3767/003158511X569169

Jiang A.M., Hou H.G., Jiang G.H., Fan C.L., Wei J.G., … Wei J.F., 2023. First report of leaf spot caused by *Phyllosticta capitalensis* on *Illicium difengpi* in China. *Plant Disease* 107: 937. https://doi.org/10.1094/PDIS-01-22-0164-PDN

Ji S.X., Zhou Y.Y., Zong X.Y., Li X.H., Zhang W., Yan J.Y., 2022. Toxicity test of thirteen fungicides on two main pathogens causing sweet cherry leaf spot disease. *Northern Horticulture* 18: 37–41. https://doi.org/10.11937/bfyy.20220934

Jones D.T., Taylor W.R., Thormton J.M., 1992. The rapid generation of mutation data matrices from protein sequences. *Computer Applications in the Biosciences* 8(3): 275–282. https://doi.org/10.1093/bioinformatics/8.3.275

Landis M.J., Eaton D.A.R., Clement W.L., Park B., Spriggs E.L., … Donoghue M.J., 2021. Joint phylogenetic estimation of geographic movements and biome shifts during the global diversification of *Viburnum*. *Systematic Biology* 70: 67–85. https://doi.org/10.1093/sysbio/syaa027

Li W., He Y.Q., Fu T., Lin L., Liu F., … Wang G.L., 2021a. First report of *Colletotrichum siamense* causing anthracnose on *Zinnia elegans* in China. *Plant Disease* 105: 1226. https://doi.org/10.1094/PDIS-04-20-0803-PDN

Li W., He Y.Q., Wang J.Y., Wang G.L., Wang Z.L., 2021b. Isolation and identification of pathogen causing anthracnose on *Zinnia elegans* Jacq. and screening of control fungicides. *Chinese Journal of Pesticide Science* 23(2): 341–347. https://doi.org/10.16801/j.issn.1008-7303.2021.0017

Li H., Liao Y.C.Z., Wan Y., Li D.W., Zhu L.H., 2023. *Colletotrichum siamense*, a novel causal agent of *Viburnum odoratissimum* leaf blotch and its sensitivity to fungicides. *Journal of Fungi* 9: 882. https://doi.org/10.3390/jof9090882

Ma Y.W., Ye L., Dong S.Y., Huai B.Y., Tan G.J., 2022. First report of *Neofusicoccum parvum* causing leaf spot on coral trees (*Viburnum odoratissimum*) in China. *Plant Disease* 106: 3000. https://doi.org/10.1094/PDIS-12-21-2799-PDN

Michael J.B., Uwe B., Donald H.P., 2022. Phylogeny and taxonomy of the genera of *Erysiphaceae*, part 1: Golovinomyces. *Mycologia* 114: 964–993. https://doi.org/10.1080/00275514.2022.2115419

Qiu C., Zhang Y., Liu Z., 2021. First Report of *Alternaria* spp. causing leaf spot on sweet viburnum in China. *Plant Disease* 105: 2253. https://doi.org/2253.10.1094/PDIS-06-20-1407-PDN

Shober A.L., Koeser A.K., Mclean D.C., Hasing G., Moore K.K., 2017. Nitrogen fertilizer rate, timing, and application method affects growth of sweet viburnum and nitrogen leaching from simulated planting beds. *HortScience: A Publication of the American Society for Horticultural Science* 52(1): 1–8. https://doi.org/10.21273/HORTSCI11114-16

Silva M., Pereira O.L., 2007. First report of *Guignardia endophyllicola* leaf blight on *Cymbidium* (*Orchidaceae*) in Brazil. *Australasian Plant Disease Notes* 2: 31–32. https://doi.org/10.1071/DN07015

Silva M., Pereira O.L., Braga I.F., Leli S.M., 2008. Leaf and pseudobulb diseases on *Bifrenaria harrisoniae* (*Orchidaceae*) caused by *Phyllosticta capitalensis* in Brazil. *Australasian Plant Disease Notes* 3: 53–56. https://doi.org/10.1071/DN08022

Wan Y., Wu S., Si Y.Z., Li D.W., Zhu L.H., 2023. First report of *Diaporthe eres* causing leaf spot of *Viburnum odoratissimum* var. awabuki in China. *Plant Disease* 107: 954. https://doi.org/10.1094/PDIS-05-22-1187-PDN

Wang X., Chen G., Huang F., Zhang J., Hyde K.D., Li H., 2012. *Phyllosticta* species associated with citrus diseases in China. *Fungal Diversity* 52: 209–224. https://doi.org/10.1007/s13225-011-0140-y

Wikee S., Lombard L., Crous P.W., Nakashima C., Motohashi K., … Hyde K.D., 2013. *Phyllosticta capitalensis*, a widespread endophyte of plants. *Fungal Diversity* 60: 91–105. https://doi.org/10.1007/s13225-013-0235-8

Wu S.P., Chen X.J., Liu Z.Y., 2015. Identification of *Fatsia japonica* grey spot pathogen and screening of fungicides. *Southwest China Journal of Agricultural Sciences* 28: 1130–1134.

Yang X.X., Yue S.S., Gao L.X., Cheng J.S., Xie J.T., Fu Y.P., 2015. First report of anthracnose caused by *Colletotrichum gloeosporioides* on *Viburnum odoratissimum* in China. *Plant Disease* 99: 1647. https://doi.org/10.1094/PDIS-04-15-0417-PDN

Zhang T., Liu H., Song Q., Liu J., Yang Q., … Li D., 2022a. First report of leaf spot caused by *Corynespora cassiicola* on *Viburnum odoratissimum* var. *awabuki* (Sweet Viburnum) in China. *Plant Disease* 106: 1062. https://doi.org/10.1094/PDIS-04-21-0849-PDN

Zhang W.H., Su D., 2022b. First report of *Phyllosticta capitalensis* causing black freckle disease on *Rubus chingii* in China. *Plant Disease* 106: 1517. https://doi.org/10.1094/PDIS-05-21-1031-PDN

Phytopathologia Mediterranea
The international journal of the
Mediterranean Phytopathological Union

Firenze University Press
www.fupress.com/pm

Research Papers

Interactions between bois noir and the esca disease complex in a Chardonnay vineyard in Italy

Francesco PAVAN, Elena CARGNUS, Davide FRIZZERA, Marta MARTINI*, Paolo ERMACORA

Department of Agricultural, Food, Environmental and Animal Sciences, University of Udine, Via delle Scienze 206, 33100 Udine, Italy
*Corresponding author. E-mail: marta.martini@uniud.it

Summary. Grapevine yellows bois noir (BN) and the grapevine trunk disease esca complex (EC) cause serious yield losses in European vineyards and are often widespread in the same vineyard. In a Chardonnay vineyard in north-eastern Italy, evolution of the two diseases from 2007 to 2020 was compared and their possible interaction was investigated. Evolution of symptomatic grapevines over the 16 years was very different between the two diseases, with a substantial linear increase for BN and an exponential increase for EC. The BN increase from one year to another was associated with the abundance of *Hyalesthes obsoletus*, the BN-phytoplasma vector, whereas the exponential increase in EC was likely due to the amount of inoculum and the increased size of pruning cuts over time. The courses of the two diseases were also very different, with a much greater occurrence of dead grapevines from EC than from BN. Some grapevines showed symptoms of both diseases, but the probability was less that a grapevine symptomatic for BN or EC showed symptoms of the other disease. Examinations of the spatial distribution of the two diseases showed dissociation between them. Data indicated that mechanisms of induced defense were involved in the lower probability that a grapevine affected by one showed symptoms of the other.

Keywords. Grapevine yellows, phytoplasmas, grapevine trunk diseases, symptom evolution, induced defense.

OPEN ACCESS

Citation: Pavan, F., Cargnus, E., Frizzera, D., Martini, M., & Ermacora, P. (2024). Interactions between bois noir and the esca disease complex in a Chardonnay vineyard in Italy. *Phytopathologia Mediterranea* 63(2): 303-314. doi: 10.36253/phyto-15052

Accepted: August 10, 2024

Published: September 15, 2024

Data Availability Statement: All relevant data are within the paper and its Supporting Information files.

Competing Interests: The Author(s) declare(s) no conflict of interest.

Editor: Josep Armengol Forti, Polytechnical University of Valencia, Spain.

ORCID:
FP: 0000-0001-9111-2144
EC: 0000-0002-2107-6245
DF : 0000-0002-8809-2768
MM: 0000-0002-7271-5297
PE: 0000-0003-0757-7956

INTRODUCTION

Grapevine age positively influences yields, rooting depths, plant resilience and wine quality (Riffle *et al.*, 2022), so factors that influence grapevine longevity can compromise the economic sustainability of vineyards. In European vineyards, yield losses, often associated with early grapevine death, are caused by grapevine yellows (GYs) [i.e., flavescence dorèe (FD) and bois noir (BN)] (Garau *et al.*, 2007; Belli *et al.*, 2010; Pavan *et al.*, 2012; Romanazzi *et al.*, 2013), and trunk diseases [esca complex (EC), in particular)] (Larignon and Dubos, 1997; Mugnai *et al.*, 1999; Bertsch *et al.*, 2013; Bruez *et al.*, 2013; De la Fuente *et al.*, 2016).

GYs are associated with phytoplasmas that colonize phloem vessels (Santi *et al*., 2013; Angelini *et al*., 2018), and are vectored by auchenorrhyncha phloem-feeding insects (Alma *et al*., 2019). Bois noir (BN), unlike FD, is widespread in all Euro-Mediterranean grape-growing regions (Angelini *et al*., 2018). BN is associated with '*Candidatus* Phytoplasma (*Ca*. P.) solani' (subgroup 16SrXII-A) (Quaglino *et al*., 2013; Angelini *et al*., 2018), and the most important vector of this pathogen is the planthopper *Hyalesthes obsoletus* Signoret (*Homoptera, Cixiidae*) (Maixner, 1994; Alma *et al*., 2019; Kosovac *et al*., 2019).

Different susceptibilities and sensitivities of grapevine cultivars to BN have been reported (Bellomo *et al*., 2007; Garau *et al*., 2007; Panassiti *et al*., 2015; Zahavi *et al*., 2013). After symptom appearance, the course of the disease in BN-symptomatic grapevines during subsequent vegetative seasons can lead to recovery or death of the infected grapevines (Osler *et al*., 1993, 2002; Garau *et al*., 2007; Pavan *et al*., 2012; Zahavi *et al*., 2013). In general, recovery from GYs involves phytoplasma-induced grapevine response mechanisms (Musetti *et al*., 2007; Albertazzi *et al*., 2009; Romanazzi *et al*., 2009; Landi and Romanazzi, 2011; Margaria and Palmano, 2011; Santi *et al*., 2013; Paolacci *et al*., 2017; Bertazzon *et al*., 2019; Pacifico *et al*., 2019; Mátai *et al*., 2020; Pagliarani *et al*., 2020; Nutricati *et al*., 2023). Furthermore, fungal and bacterial endophytes have been suggested to affect grapevine recovery from GYs (Martini *et al*., 2009; Bulgari *et al*., 2016).

Grapevine trunk diseases (GTDs) are caused by fungi that penetrate host plants through wood wounds and invade the vascular systems (Bertsch *et al*., 2013; Bruez *et al*., 2013; Claverie *et al*., 2020). Esca complex (EC) is the most widespread GTD, and is characterised by inner necrosis in grapevine wood tissues and external plant symptoms ("tiger-striped" leaves or "black measles" on the berries) (Larignon and Dubos, 1997; Mugnai *et al*., 1999; Graniti *et al*., 2000; Úrbez-Torres, 2011; Mondello *et al*., 2018; Fischer and Peighami-Asnaei, 2019; Nerva *et al*., 2019; Bruez *et al*., 2020). When grapevines show typical leaf symptoms, the EC is defined as grapevine leaf stripe disease (GLSD), whereas when grapevines dry out and die, the EC shows apoplectic symptoms (Surico *et al*., 2006; Surico, 2009). Grapevines can produce defensive compounds in response to wood invasion by esca-associated fungi (Ramírez-Suero *et al*., 2014; Stempien *et al*., 2018; Goufo *et al*., 2019). Activity of non-pathogenic fungi (e.g., *Epicoccum* spp., *Pythium oligandrum*, *Trichoderma* spp.) or bacteria [e.g., *Bacillus pumilus* (S32), *Paenibacillus* sp. (S19)] in preventing EC fungal infections has been reported, and different mechanisms were considered, including production of inhibitory compounds, competition for nutrients and space, triggering of grapevine resistance, and interference with pathogenicity genes of esca-associated fungi (Haidar *et al*., 2016; Del Frari *et al*., 2019; Bigot *et al*., 2020; Yacoub *et al*., 2020; Romeo- Oliván *et al*., 2022). Susceptibility to EC can be influenced by *V. vinifera* cultivar, rootstock genotype, and cultivar × rootstock combination (Fischer and Peighami-Ashnaei, 2019). Chardonnay was classified as intermediate in EC susceptibility (Borgo *et al*., 2016).

No studies have been reported on comparative evolution of GYs and EC within the same vineyard, or the possible interaction between the GYs and EC. For this purpose, grapevines in a large Chardonnay vineyard in north-eastern Italy were annually monitored from 2007 to 2020. This allowed comparison of the evolution of the two diseases at vineyard level, and determination of whether the two diseases can coexist in individual host plants. This also would give knowledge of the degree of interaction (none, synergistic, or antagonistic) between the two in manifestation of host symptoms.

MATERIALS AND METHODS

Vineyard studied

The study was conducted from 2007 to 2020, in a vineyard in north-eastern Italy (Friuli Venezia Giulia region, Gorizia district, Cormons locality; 45°56'34"N, 13°26'45"E, 44 m a.s.l.). The vineyard was planted in 2000, with approx. 3.5 ha of Chardonnay R8 clone grafted onto SO4. The vineyard had 21 rows of length 370 m (westernmost row) to 408 m (easternmost row). The grapevines were trained to the double-arched Guyot system, and were at spacing of 3.5 m between rows and 1.0 m within rows.

In the vineyard, the only GY detected up to 2022 was BN. All the 128 GY symptomatic samples randomly collected and analysed by qPCR/HRM from 2010 to 2021 tested positive for '*Ca*. P. solani' and negative for FD phytoplasma (Mori *et al*., 2020; Pavan *et al*., 2024; Martini *et al*., unpublished data). No symptoms of virus or soil-borne diseases were observed in the vineyard.

During the years of the study, FD had not been reported in the vineyards of the wine-growing area where the vineyard was located, but mandatory insecticide treatments against *Scaphoideus titanus* were applied each year, at the beginning of July. Since the active ingredients used were not basipetal systemic insecticides (organophosphate in the early years, thiamethoxam more recently), the insecticides would not have affected *H. obsoletus* nymphs living in the roots of herbaceous plants. Even against *H. obsoletus* adults, the efficacy of insecticides is not high, as

the insects emerge gradually and can colonize vineyards, even from outside. Only mechanical weeding was used in the vineyard. After winter pruning, no fungicide treatments were applied to protect the pruning cuts.

Sampling and data analyses

Mapping of the vineyard

In 2007, the vineyard rows and plants were mapped, by referring each grapevine to a row (numbered 1 to 21, starting from the west), a supporting pole along the row (numbered from the north end of each row), and a position (designated a, b, c, or d) between neighbouring poles. From 2007 to 2020, each grapevine was checked each year in early September, by the same observers every year, to determine which plants showed GY or EC symptoms. Replacement of dead grapevines occurred in only a few rows in 2019, but newly planted grapevines were not considered in this study.

Grapevines with BN symptoms were identified based on their characteristic GY symptoms, including leaf rolling, sectorial leaf blade discolourations, poorly lignified and falling shoots, and shriveled berries. Grapevines with the GLSD form of EC were identified based on tiger-striped leaves or black measles on the berries. Grapevines with the apoplexy form of EC were identified based on necrosis and shoots without leaves. Since these symptoms were visible both in grapevines that had or had not previously manifested GLSD symptoms, death of these plants was attributed to EC, even when the GLSD form of EC had not previously manifested. The grapevines that died from BN could not be confused with those that died from EC, as BN-affected plants had green shoots in the previous year, which only in the following year were necrotic due to frost damage, as they were not lignified.

Symptom evolution in BN and EC symptomatic grapevines

Annual records were made to check whether grapevines were affected by BN, and if the symptoms were noted for the first time. In subsequent sampling years, these grapevines were assigned to three categories: "still symptomatic", "asymptomatic", or "dead". Grapevines that became asymptomatic were recorded as "recovered" only after three consecutive years without symptoms, and taking into account that pollarding can mask GY symptoms for some years (Pavan *et al.*, 1997; Mutton *et al.*, 2002). Grapevines that did not have lignified shoots at the time of sampling, or that did not sprout in the following year, were considered dead. The annual sampling of grapevines affected by BN allowed recording of the evolution of symptoms for individual grapevines, from the year of the first symptom appearance (year = 0) to year n (maximum n = 13 for grapevines that showed symptoms in the first sampling year).

For each grapevine exhibiting EC symptoms, the following details were noted: (i) the year in which symptoms first appeared, and whether they were in the form of GLSD or apoplexy, and (ii) the year in which apoplexy occurred for grapevines that had previously exhibited GLSD symptoms. To determine when the grapevines affected by EC showed apoplexy (0, or more years), only grapevines during the period 2015 to 2020 were considered, which enabled certainty for exclusion of grapevines that could have presented symptoms of GLSD in the years preceding the start of mapping.

Interactions between BN- and EC-affected grapevines

For comparison of symptom evolution of BN and EC with time, and disease interactions, the grapevines were grouped into those displaying symptoms of only BN or EC, or of both diseases. For both diseases, the following parameters were calculated: (i) Proportions (%) of dead grapevines to total live grapevines in 2007; (ii) Proportions (%) of dead grapevines to total symptomatic grapevines; (iii) Accumulated numbers of dead grapevines; (iv) Accumulated numbers of total symptomatic grapevines (symptomatic live plus dead grapevines). Grapevines with symptoms of both diseases over the sampling years were also divided into three groups: (1) grapevines that showed EC symptoms for the first time in years following their first year of exhibiting BN symptoms; (2) grapevines showing EC symptoms for the first time one or more years after recovering from BN; or (3) grapevines that showed BN symptoms for the first time in the years following their first year of exhibiting EC symptoms.

Fisher's exact test was used to compare two proportions in each dataset, while Rayan's test was used to compare three proportions. Dynamics of BN or EC dead grapevines over the years were determined using polynomial regressions of best fit to the experimental data for the two diseases.

Comparisons of spatial distribution of BN- and EC-symptomatic grapevines

SADIE red-blue analysis (Perry *et al.*, 1999) was used to determine spatial distributions of cumula-

tive BN- and EC-symptomatic grapevines within the vineyard. The sampling units were groups of 16 grapevines (four inter-poles), and the total number of grapevines with symptoms of either or both diseases in each year was determined for each 16 plant unit. This analysis identified areas with high-density counts (disease patches) or low or zero counts (gaps), and calculated indices of clustering (vi; vj) for each unit, which measured local contribution to either patch or gap. The clustering significance ($\alpha = 0.05$) for each variable was determined by comparing the mean values of vi and vj with their corresponding values under the null hypothesis (Perry *et al.*, 1999).

A two-dimensional map depicting the spatial distribution of local clustering indices (vi; vj) for each variable was generated using linear kriging with SURFER (Golden Software 191 Inc.). The red-blue analysis datasets were then used to assess similarity between spatial patterns of BN-symptomatic grapevines and EC-symptomatic grapevines. An algorithm was used to derive overall indices of spatial association (X_k), and their statistical significance (P_x) was determined through a randomisation test (Perry and Dixon, 2002). This test determined if the spatial patterns of two variables were associated ($P_x < 0.025$), unassociated ($0.025 \leq P_x \leq 0.975$), or dissociated ($P_x > 0.975$), with association indicating the coincidence of a patch cluster for one variable with a patch cluster for the other, or the coincidence of two gaps, and dissociation indicating that a patch for one variable coincides with a gap for the other (Perry, 1998).

RESULTS

Evolution of grapevines affected by BN

In the first sampling year (2007), 199 grapevines had symptoms of BN, and cumulative numbers of grapevines with these symptoms rose to 831 in the last sampling year (2020). The status of most of the grapevines affected by BN changed to "recovered" or "dead" in the years following the first onset of symptoms (Figure 1). A substantial proportion of the grapevines (11%) showed symptoms for at least 13 years, highlighting that the infection can last for many years. Probability of recovery of a symptomatic grapevine was greater in the first few years than later, as more than half of recovered plants were recorded within the following 3 years. Likelihood of a symptomatic grapevine dying was also greater in the first few years than later, as more than two-thirds of symptomatic plants died within the first 5 years after first symptom observation.

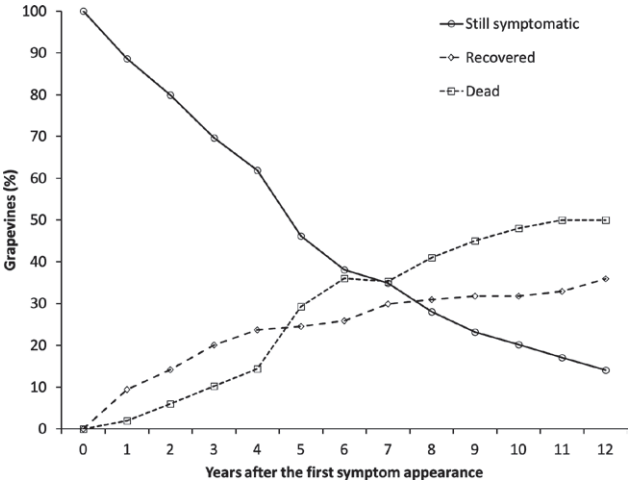

Figure 1. Proportions of grapevines that from 1 to 13 years after first appearance of BN symptoms (year 0) either remained symptomatic, recovered, or died.

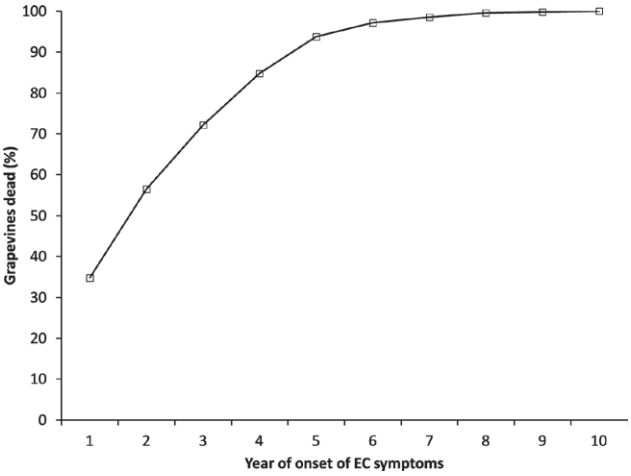

Figure 2. Proportions of dead grapevines during the first 10 years following the occurrence of EC symptoms. Grapevines that were dead at year = 1 exhibited the apoplexy form of EC without first showing the GLSD form.

Evolution of grapevines affected by EC

From 2015 to 2020, 1126 grapevines died for apoplexy. Apoplexy was observed in a third of the grapevines without them having previously shown GLSD symptoms (Figure 2). Over 95% of the grapevines with GLSD symptoms exhibited apoplexy within 5 years. Three grapevines died 9 years after first showing GLSD symptoms, and two grapevines did not develop apoplexy more than 9 years (10 and 12, respectively) after the first appearance of GLSD symptoms in 2008, which increased initially very slowly.

Table 1. Mean percentages of grapevines dead from 2008 to 2020 after showing symptoms of BN or EC, or both diseases, calculated on the total number of live vines in 2007 and on the number of symptomatic vines. Means in each column accompanied by the same letter are not different ($P > 0.05$).

Symptoms	Dead grapevines (%)	
	Calculated on total live in 2007	Calculated on symptomatic
BN exclusively	2.96 b	27.55 a
EC exclusively	24.45 c	86.26 c
Both BN and EC	0.74 a	69.51 b

Comparisons of BN and EC evolution

From 2008 to 2020, 2236 grapevines died (29.2% of the live grapevines in 2007), 1952 of which had EC symptoms, 227 had BN symptoms, and 57 had symptoms of both diseases. The proportion of dead grapevines from EC was eight times greater ($P \leq 0.05$) than from BN (Table 1). Approx. 1% of the grapevines died after showing symptoms of both diseases. Grapevine deaths from EC started 1 year after the BN deaths, but accumulated death numbers subsequently increased more rapidly, as the ratios of EC deaths to BN deaths rose from 2.0 in 2009 to 8.6 in 2020 (Figure 3 A). The trend towards increases in dead grapevines over time was sinusoidal for BN ($Y = -0.2486X^3 + 1502X^2 - 3E + 06X + 2E+09$; $R^2 = 0.9947$), and more than proportional for EC ($Y = 13.41X^2 - 53854X + 5E + 07$; $R^2 = 0.9968$).

Considering the total number of symptomatic grapevines (i.e. "symptomatic alive" plus "dead"), the differences between BN and EC were less marked (Figure 3 B). From 2007 to 2020, 2262 grapevines exhibited symptoms of EC, 831 of BN, and 82 of both diseases. The number of accumulated symptomatic grapevines was greater for BN up to 2013 and greater for EC in the subsequent years.

The EC / BN ratio of the total number of affected grapevines (2.74) was three times smaller than that of the dead grapevines (8.60), due to the different mortality rates between the EC and BN. The percentage of "dead" grapevines relative to the total of "symptomatic" grapevines was greater ($P \leq 0.05$) for EC than for BN, with EC being three times greater than BN (Table 1). There was also a smaller proportion of grapevines that died with symptoms of both diseases than grapevines dying only with EC symptoms ($P \leq 0.05$).

Interactions between BN and EC

The percentage of grapevines displaying EC symptoms was less among grapevines that had exhibited BN

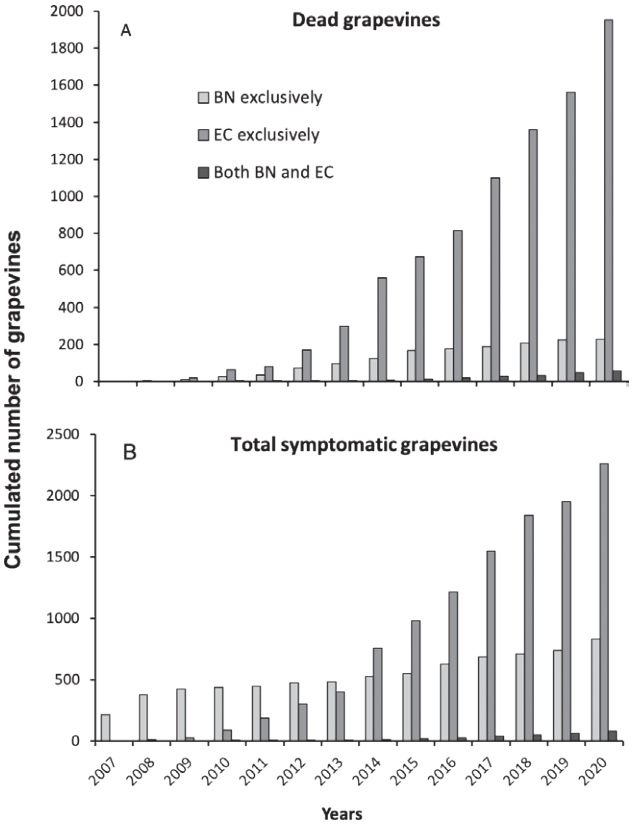

Figure 3. Accumulated numbers of dead and total symptomatic grapevines ("symptomatic alive" and "dead") due to EC, BN or both diseases during the years 2007 to 2020.

symptoms in previous years than among those that had never shown BN symptoms (Figure 4 A). Within the BN-symptomatic grapevines, the recovered grapevines showed greater proportions with EC symptoms than the non-recovered grapevines (Figure 4 B), but were still less likely to show EC symptoms than grapevines that never showed BN symptoms (Figure 4, A and B).

The percentage of grapevines succumbing to EC was less in those that had previously exhibited symptoms of BN than in those that had never shown BN symptoms (Figure 4 C). The proportion of dead grapevines among symptomatic ones (86.3%) was greater ($P = 0.017$; Fisher's exact test) for those without previous BN symptoms than for those with prior BN symptoms (76.0%). Within the BN-symptomatic grapevines, the recovered grapevines died from EC at a greater proportion than the non-recovered grapevines (Figure 4 D), but they still died at lower percentage ($P \leq 0.05$) than grapevines that had never exhibited BN symptoms (Figure 4, C and D).

Among grapevines that displayed GLSD symptoms, only seven plants (2.3%) later had symptoms of BN, and this contrasted with grapevines that had never exhibited

GLSD symptoms, which had a greater rate (13.8%) of BN symptoms ($P < 0.00001$; Fisher's exact test).

Spatial distribution of BN- and EC-symptomatic grapevines

The distribution of BN-symptomatic grapevines was aggregated. The most important patches were found in the first 100 m from the northern edge of the vineyard (vi = 6.365, $P_{vi} < 0.001$), while gaps occurred in the remaining vineyard area and predominantly in the south-western part of the vineyard (vj = - 5.691; $P_{vj} < 0.001$) (Figure 5 A).

The distribution of EC-symptomatic grapevines was aggregated. The most significant patches occurred along the eastern edge of the vineyard, between the central and southern parts (vi = 5.08; $P_{vi} < 0.001$), while gaps occurred along the western vineyard edge in the first 100 m from the northern edge (vj = -5.312, $P_{vj} < 0.001$) (Figure 5 B).

The distributions of BN- and EC-symptomatic grapevines were dissociated, with the areas of greatest dissociation coinciding with the major patches of BN- and EC-symptomatic grapevines (X_k = - 0.25; $P_x > 0.999$) (Figure 8 C).

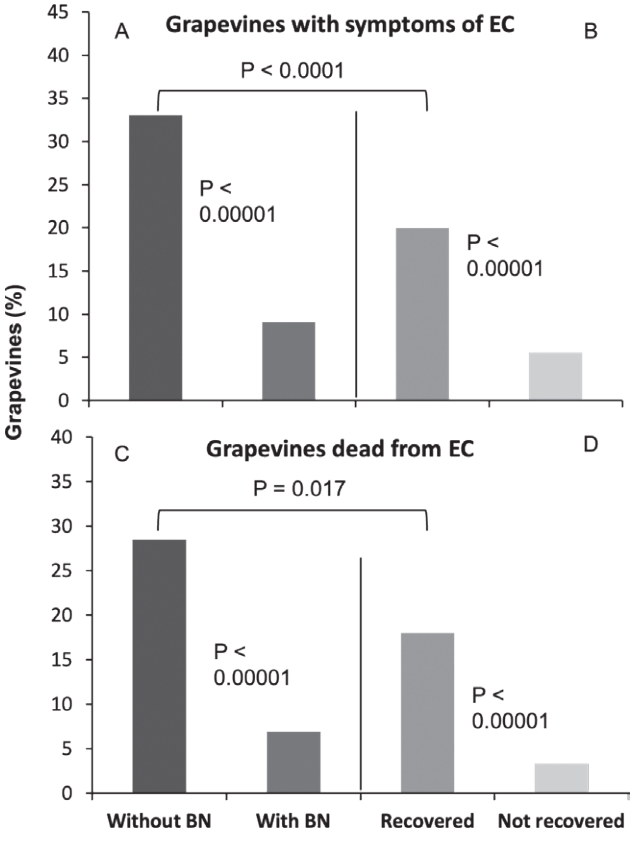

Figure 4. Mean proportions (%) of grapevine plants with symptoms of EC, and among these, percentages of dead vines that never showed BN symptoms (without BN; 4 A), or had previously shown symptoms of BN (with BN) (4 C). Among the BN symptomatic vines, the percentages of those "Recovered" or "Not recovered" (i.e., still symptomatic; 4 B) at the occurrence of EC symptoms, or dead from EC (4 D), are indicated.

DISCUSSION

This 14-year-long descriptive epidemiology study was carried out in a large vineyard, and aimed to investigate potential synergistic or antagonistic interactions between two important grapevine diseases. The selected vineyard was in a wine-growing area where the exclusive presence of BN among GY had been reported until the last study year (2020), and also during the monitoring survey conducted in 2021 and 2022 seasons. This made it possible to obtain descriptive results, as discussed below.

Evolution of grapevines affected by BN

In the vineyard studied, 50% of the grapevines died, and 10% still showed BN symptoms 13 years after first detection of these symptoms. This evolution was less favourable than that observed for the same cultivar (Chardonnay) in a multi-year study (1987–2000) conducted in ten vineyards in another wine-growing area of north-eastern Italy (Friuli Venezia Giulia region, Pordenone district: Pavan *et al.*, 2012). In that study: (i) only 10% of the affected grapevines had died after 9 years (45% in the present study), and only 1.1% of grapevines showed symptoms after 13 years (11% after 13 years in the present study). These differences could be due to differing virulence of the phytoplasma strains (Langer and Maixner, 2004; Pierro *et al.*, 2022), or to differing host susceptibility. Differences in grapevine susceptibility could have been due to differences in clone-rootstock combinations and/or grapevine training systems. In the study of Pavan *et al.* (2012), many clone-rootstock combinations were assessed, including some polyclonal vineyards, and the grapevine training system was Sylvoz. In the present study, the vineyard was monoclonal, and the training system was double-arched Guyot. In the Pavan *et al.* (2012) study, there were three to five canes originating from points of each permanent horizontal trunk, the canes were distant from each other, and the symptoms only rarely seriously affected all the canes. The affected plants also almost always had some lignified shoots. In the present study, each grapevine had two canes originating from the trunk heads, and

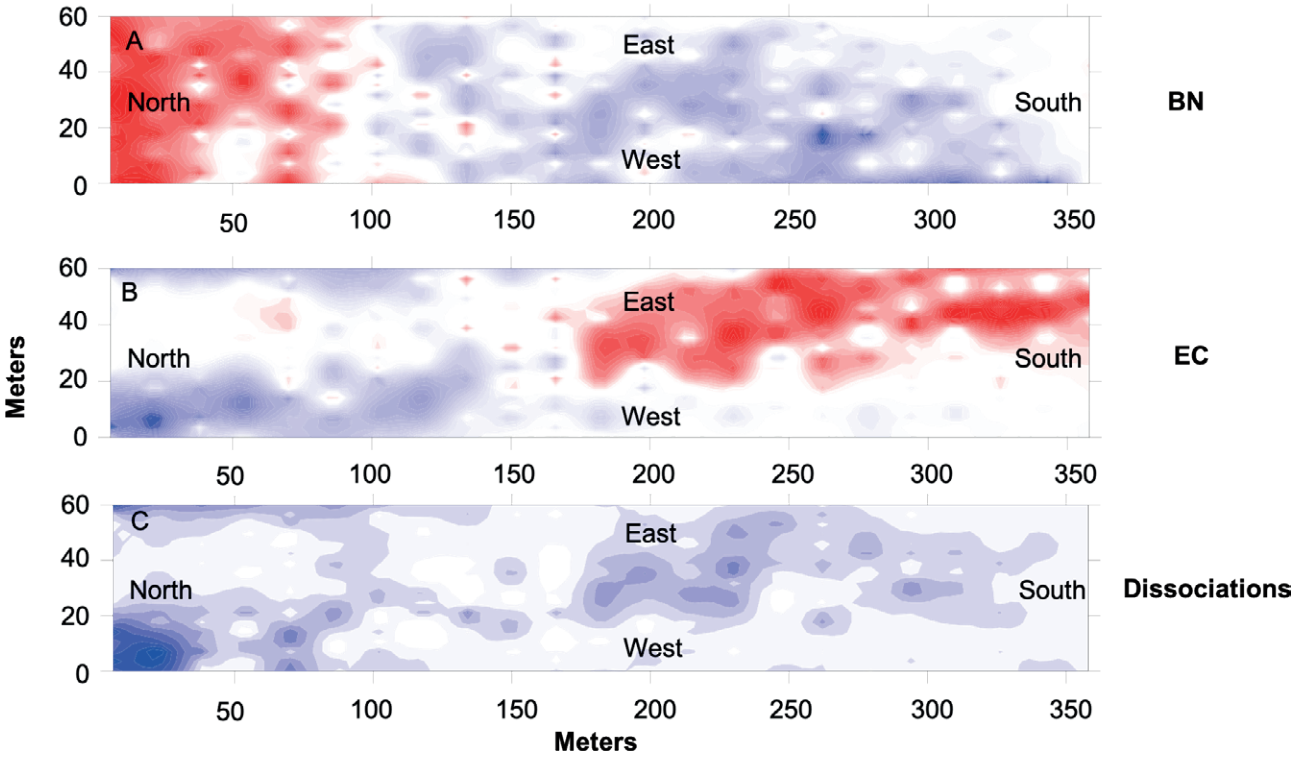

Figure 5. Spatial distributions of BN and EC symptomatic grapevines (cumulative numbers over sampling years from 2007 to 2020). Red areas indicate aggregation (patches: vi ≥ 1.5), and blue areas indicate dispersion (gaps: vj ≤ -1.5). The map of Dissociations has blue areas indicating areas with statistically significant dissociations between the two diseases.

the symptoms often affected both canes. As there were no lignified shoots, these were probably killed by winter frosts, so the grapevines did not sprout in the following springs.

Comparisons of BN and EC evolution

The appearance of BN before EC is explained by the different epidemiology of the two diseases. For BN, the likelihood that a healthy grapevine may become infected does not depend on the vineyard age, but depends on the number of infectious vectors that can inoculate grapevines with BN phytoplasmas, regardless of grapevine age. In contrast, the likelihood that grapevines are affected by trunk diseases increases with vineyard age, because the overall numbers of pruning cuts increase with time, favouring fungal infections (Mugnai *et al.*, 1999; Amponsah *et al.*, 2011; Kovacs *et al.*, 2017). With increasing vineyard age and EC progression, pathogen inoculum related to EC also increases with time, increasing infection probability. Although EC appeared after BN in the studied vineyard, the number of grapevines affected by EC at the end of the survey years was three times greater than for BN. This occurred because the increase in BN over study period was substantially linear, with some fluctuations. In contrast, the increase in EC was more than proportional. This difference between the two disease syndromes could be due to BN inoculum not originating from the grapevines, which are the final hosts of the phytoplasma (Maixner, 2010; Alma *et al.*, 2019). For EC, the infected grapevines are the inoculum sources. For BN, primary inoculum arrives from other host plants via *H. obsoletus*, so the pathogen inoculum is likely to be relatively stable, which may explain the low variability in increase with time. In contrast, EC inoculum derives from infected grapevines whose numbers increase with time. This explains the greater than proportional increase in EC-affected grapevines. However, some annual variation in rate of increase also occurs for BN, because the number of infectious vectors can vary relative to the number of host plants that are sources of BN phytoplasma, and relative to the population density of the vector *H. obsoletus* (Mori *et al.*, 2008; 2012; 2020; Panassiti *et al.*, 2015).

In the present study, EC was more harmful to the grapevines than BN, as indicated by the greater number of symptomatic grapevines and the greater incidence of dead grapevines among those infected.

Interactions between BN and EC

Grapevines previously affected by BN were less likely to show symptoms of EC and die from EC than grapevines without BN. However, the probability that grapevines exhibited symptoms of EC was greater for BN-recovered grapevines than for those still symptomatic, although the likelihood of EC symptoms was always less than for grapevines that had never shown BN symptoms. These two data sets could suggest that in BN-infected grapevines, there are specific defense mechanisms induced by infections that prevent EC infections or symptom expression, and that these mechanisms are less present in BN-recovered grapevines (therefore no longer symptomatic) than in those that have not recovered (therefore still symptomatic) but have active defense mechanisms.

It is known that induced defense in host plants confers resistance, not only towards the pathogen that activated the resistance mechanisms, but also against other pathogens (Sticher *et al*., 1997; Durrant and Dong, 2004; Vlot *et al*., 2021; Cooper and Ton, 2022). Activation of defense mechanisms is well documented for GYs. Recent studies have shown that concentrations of defense compounds (phenolic substances), including stilbenoids, flavonols and flavanols, are increased in the presence of BN or FD infections (Rusjan *et al*., 2015; Pagliarani *et al*., 2020; Casarin *et al*., 2023). Other studies have reported that after infection of grapevines with '*Ca*. P. solani', most jasmonic acid (JA) and salicylic acid (SA) biosynthetic genes are up-regulated, as compared to uninfected plants (Paolacci *et al*., 2017; Rotter *et al*., 2018; Dermastia, 2019). In stably recovered plants, increased levels of endogenous H_2O_2 and increased concentrations of specific stilbenoids, including viniferin, have been demonstrated (Musetti *et al*., 2007; Gambino *et al*., 2013; Pagliarani *et al*., 2020). Activation of defense genes is also linked to JA-dependent signalling, and suppression of SA-dependent signalling is important for establishment and maintenance of host recovery (Paolacci *et al*., 2017; Pagliarani *et al*., 2020). The role of mechanisms of induced resistance in recovered grapevines has been indirectly confirmed by the efficacy of resistance inducers in improving the recovery of BN-affected grapevines (Romanazzi *et al*., 2009).

EC infections also significantly reduce the likelihood of BN infections. In this case, it would be the EC infections that induce traits in grapevines that act as resistance factors against phytoplasmas. Several reports have indicated involvement of upregulations of the phenylalanine ammonia-lyase (PAL) gene, which encodes the first enzyme of the phenylpropanoid pathway, along with the chalcone synthase (CHS) and stilbene synthase (STS) genes, coding for enzymes of the flavonoid and stilbenoid pathways (Kenfaoui *et al*., 2022; Garcia *et al*., 2022). Recent data also suggested a JA-dependent signalling mechanism activated after invasion of wood by EC-associated fungi, that induces accumulation of secondary metabolites such as phytoalexins and pathogenesis-related proteins (PRs) (Goufo *et al*., 2020). EC-symptomatic plants are also unattractive for the vector *H. obsoletus*, as happened in grapevines treated with a chemical elicitor emitting volatiles that repelled adult planthoppers (Minuz *et al*., 2020).

Grapevines previously symptomatic for BN were less likely to show EC symptoms, and non-BN symptomatic plants were more likely than BN symptomatic plants to develop EC symptoms, probably influenced the spatial distribution of grapevines with symptoms of each disease. This might explain why where there are patches of one disease there are gaps of the other, and *vice versa*. The present study has therefore highlighted that spatial distribution of a disease within a crop can be influenced by the presence of a separate pathogen.

LITERATURE CITED

Albertazzi G., Milc J., Caffagni A., Francia E., Roncaglia E., … Pecchioni N., 2009. Gene expression in grapevine cultivars in response to Bois Noir phytoplasma infection. *Plant Science* 176: 792–804.

Alma A., Lessio F., Nickel H., 2019. Insects as phytoplasma vectors: Ecological and epidemiological aspects. In: *Phytoplasmas: Plant Pathogenic Bacteria—II, Transmission and Management of Phytoplasma—Associated Diseases* (A. Bertaccini, P.G. Weintraub, G.P. Rao, N. Mori, ed.) Springer, Singapore, 1–25.

Amponsah N.T., Jones E.F., Ridgway H.J., Jaspers M.V., 2011. Identification, potential inoculum sources and pathogenicity of botryosphaeriaceous species associated with grapevine dieback disease in New Zealand. *European Journal of Plant Pathology* 131: 467–482.

Angelini E., Constable F., Duduk B., Fiore N., Quaglino F., Bertaccini A., 2018. Grapevine phytoplasmas. In: *Phytoplasmas: Plant Pathogenic Bacteria—I, Characterisation and Epidemiology of Phytoplasma—Associated Diseases* (G.P. Rao, A. Bertaccini, N. Fiore, L.W. Liefting, ed.) Springer, Singapore, 123–152.

Belli G., Bianco P.A., Conti M., 2010. Grapevine yellows in Italy: past, present and future. *Journal of Plant Pathology* 92: 303–326.

Bellomo C., Carraro L., Ermacora P. Pavan F., Osler R., … Governatori G., 2007. Recovery phenomena in

grapevines affected by grapevine yellows in Friuli Venezia Giulia. *Bulletin of Insectology* 60: 235–236.

Bertazzon N., Bagnaresi P., Forte V., Mazzucotelli E., Filippin L., … Angelini E., 2019. Grapevine comparative early transcriptomic profiling suggests that Flavescence dorée phytoplasma represses plant responses induced by vector feeding in susceptible varieties. *BMC Genomics* 20: 526.

Bertsch C., Ramirez-Suero M., Magnin-Robert M., Larignon P., Chong J., … Fontaine F., 2013. Grapevine trunk diseases: complex and still poorly understood. *Plant Pathology* 62: 243–265.

Bigot G., Sivilotti P., Stecchina M., Lujan C., Freccero A. Mosetti, D., 2020. Long-term effects of *Trichoderma asperellum* and *Trichoderma gamsii* on the prevention of esca in different vineyards of Northeastern Italy. *Crop Protection* 137: 105264.

Borgo M., Pegoraro G., Sartori E., 2016. Susceptibility of grape varieties to esca disease. In: *39th World Congress of Vine and Wine*, BIO Web of Conferences, 7: 01041. DOI: 10.1051/bioconf/20160701041.

Bruez E., Lecomte P., Grosman J., Doublet B., Bertsch C., … Gu.rin-Dubrana L., 2013. Overview of grapevine trunk diseases in France in the 2000s. *Phytopathologia Mediterranea* 52: 262–275.

Bruez E., Vallance J., Gautier A., Laval V., Compant, … Rey P., 2020. Major changes in grapevine wood microbiota are associated with the onset of esca, a devastating trunk disease. *Environmental Microbiology* 22: 5189–5206.

Bulgari D., Casati P., Quaglino F., Bianco P. A., Compant S., Mathieu F., 2016. Endophytic bacteria associated with grapevine plants: putative candidates for phytoplasma containment. In: *Biocontrol of Major Grapevine Diseases: Leading Research,* CABI, Wallingford, UK, 215–230.

Casarin S., Vincenzi S., Esposito A., Filippin L., Forte V., Bertazzon N., 2023. A successful defence strategy in grapevine cultivar 'Tocai friulano' provides compartmentation of grapevine Flavescence dorée phytoplasma. *BMC Plant Biology 23*(1): 161.

Claverie M., Notaro M., Fontaine F., Wery J., 2020. Current knowledge on Grapevine Trunk Diseases with complex etiology: a systemic approach. *Phytopathologia Mediterranea* 59(1): 29–53.

Cooper A., Ton J. 2022. Immune priming in plants: from the onset to transgenerational maintenance. *Essays Biochemistry* 66: 635–646. https://doi.org/10.1042/ebc20210082.

De la Fuente M., Fontaine F., Gramaje D., Armengol J., Smart R., … Corio-Costet M.F., 2016. Grapevine Trunk Diseases. A Review. In: International Organisation of Vine and Wine , OIV. (Ed.), 1st edition, Paris, France, 24 p. ISBN : 979-10-91799-60-7.

Dermastia M., 2019. Plant Hormones in Phytoplasma Infected Plants. *Frontiers in Plant Science* 10: 477.

Durrant W.E., Dong X., 2004. Systemic acquired resistance. *Annual Review of Phytopathology* 42: 185–209.

Del Frari G., Cabral A., Nascimento T., Ferreira R. B., Oliveira H., 2019. *Epicoccum layuense* a potential biological control agent of esca-associated fungi in grapevine. *PloS ONE* 14, e0213273.

Fischer M., Peighami-Ashnaei S., 2019. Grapevine, esca complex, and environment: the disease triangle. *Phytopathologia Mediterranea* 58: 17–37.

Gambino G., Boccacci P., Margaria P., Palmano S., Gribaudo I., 2013. Hydrogen peroxide accumulation and transcriptional changes in grapevines recovered from Flavescence dorée disease. *Phytopathology* 103: 776–784. https://doi.org/ 10.1094/PHYTO-11-12-0309-R

Garau R., Sechi A., Prota V.A., Moro G., 2007. Productive parameters in Chardonnay and Vermentino grapevines infected with "bois noir" and recovered in Sardinia. *Bulletin of Insectology*, 60(2) 233–234.

García J.A., Garrido I., Ortega A., del Moral J., Llerena, J.L., Espinosa F., 2022. Physiological and Molecular Responses of Vitis vinifera cv. Tempranillo Affected by Esca Disease. *Antioxidants* 11: 1720. https://doi.org/10.3390/ antiox11091720.

Goufo P., Cortez I., 2020. A lipidomic analysis of leaves of esca-affected grapevine suggests a role for galactolipids in the defense response and appearance of foliar symptoms. *Biology* 9(9): 268.

Goufo P., Marques A.C., Cortez I., 2019. Exhibition of local but not systemic induced phenolic defenses in *Vitis vinifera* L. affected by brown wood streaking, grapevine leaf stripe, and apoplexy (escacomplex). *Plants* 8 (10): 412.

Graniti A., Surico G., Mugnai L., 2000. Esca of grapevine: a disease complex or a complex of diseases? *Phytopathologia Mediterranea* 39: 16–20.

Haidar R., Roudet J., Bonnard O., Dufour M. C., Corio-Costet M. F., … Fermaud M., 2016. Screening and modes of action of antagonistic bacteria to control the fungal pathogen *Phaeomoniella chlamydospora* involved in grapevine trunk diseases. *Microbiological Research* 192: 172–184.

Kenfaoui J., Radouane N., Mennani M., Tahiri A., El Ghadraoui L., … Barka, E. A., 2022. A panoramic view on Grapevine Trunk Diseases threats: Case of Eutypa dieback, Botryosphaeria dieback, and Esca disease. *Journal of Fungi* 8(6): 595.

Kosovac A., Jakovljević M., Krstić O., Cvrković T., Mitrović M., … Jović J., 2019. Role of plant-special-

ized Hyalesthes obsoletus associated with *Convolvulus arvensis* and *Crepis foetida* in the transmission of '*Candidatus* Phytoplasma solani'-inflicted bois noir disease of grapevine in Serbia. *European Journal of Plant Pathology* 153: 183–195.

Kovacs C., Balling P., Bihari Z., Nagy A., Sandor E., 2017. Incidence of grapevine trunk diseases is influenced by soil, topology and vineyard age, but not by *Diplodia seriata* infection rate in the Tokaj Wine Region, Hungary. *Phytoparasitica* 45: 21–32.

Landi L., Romanazzi G., 2011. Seasonal variation of defense-related gene expression in leaves from bois noiraffected and recovered grapevines. *Journal of Agricultural and Food Chemistry* 59: 6628–6637.

Langer M., Maixner M., 2004. Molecular characterisation of grapevine yellows associated phytoplasmas of the stolbur-group based on RFLP-analysis of non-ribosomal DNA. *Vitis* 43, 191–199.

Larignon P., Dubos B., 1997. Fungi associated with esca disease in grapevine. *European Journal of Plant Pathology* 103: 147–157.

Maixner M., 1994. Transmission of German grapevine yellows (Vergilbungskrankheit) by the planthopper *Hyalesthes obsoletus* (Auchenorrhyncha: Cixiidae). *Vitis* 33: 103–104.

Maixner M., 2010. Phytoplasmas epidemiological systems with multiple plant hosts. In *Phytoplasmas: Genomes, Plant Hosts and Vectors*; (P.G. Weintraub, P. Jones, ed.), CABI Publishing: Wallingford, UK, 213–232.

Margaria P., Palmano S., 2011. Response of the *Vitis vinifera* L. cv. 'Nebbiolo' proteome to Flavescence dorée phytoplasma infection. *Proteomics* 11: 212–224.

Martini M., Musetti R., Grisan S., Polizzotto R., Borselli S., Pavan F., Osler R., 2009. DNA-dependent detection of the grapevine fungal endophytes *Aureobasidium pullulans* and *Epicoccum nigrum*. *Plant Disease* 93: 993–998.

Mátai A., Teszlák P., Jakab G., 2020. Recovery of *Vitis vinifera* L. cv. 'Kékfrankos' from 'bois noir' disease. *European Journal of Plant Pathology* 156(3): 987–991.

Minuz R.L., Mancini V., Ruschioni S., Mozzon M., Foligni R., … Riolo P., 2020. Volatiles emitted by resistance inducer-treated grapevines affect *Hyalesthes obsoletus* behavioural responses. *Bulletin of Insectology* 73: 117–123.

Mondello V., Larignon P., Armengol J., Kortekamp A., Vaczy K., … Fontaine F. 2018. Management of grapevine trunk diseases: knowledge transfer, current strategies and innovative strategies adopted in Europe. *Phytopathologia Mediterranea* 57: 369–383.

Mori N., Pavan F., Bondavalli R., Reggiani N., Paltrinieri S., Bertaccini A., 2008. Factors affecting the spread of "Bois Noir" disease in north Italy vineyards. *Vitis* 47(1): 65–72.

Mori N., Pavan F., Reggiani N., Bacchiavini M., Mazzon L., … Bertaccini A., 2012. Correlation of bois noir disease with nettle and vector abundance in northern Italy vineyards. *Journal of Pest Science* 85(1): 23–28.

Mori N., Cargnus E., Martini M., Pavan F., 2020. Relationships between *Hyalesthes obsoletus*, its herbaceous hosts and Bois noir epidemiology in northern Italian vineyards. *Insects* 11: 606.

Mugnai L., Graniti A., Surico G., 1999. Esca (Black Measles) and brown wood-streaking: two old and elusive diseases of grapevines. *Plant Disease* 83: 404–418.

Musetti R., Marabottini R., Badiani M., Martini M., Toppi L.S., … Osler R., 2007. On the role of H_2O_2 in the recovery of grapevine (*Vitis vinifera* cv. Prosecco) from Flavescence dorée disease. *Functional Plant Biology* 34(8): 750–758.

Mutton P., Boccalon W., Bressan S., Coassin C., Colautti M., … Villani A., 2002. Legno nero della vite in vigneti di Chardonnay del Friuli-Venezia Giulia. *Informatore Fitopatologico* 52(1): 52-59.

Nerva L., Turina M., Zanzotto A., Gardiman M., Gaiotti F., … Chitarra W., 2019. Isolation, molecular characterization and virome analysis of culturable wood fungal endophytes in esca symptomatic and asymptomatic grapevine plants. *Environmental Microbiology* 21: 2886–2904.

Nutricati E., Pascali M., de Negro C., Bianco P.A., Quaglino F., … Luvisi A., 2023. Signalling cross-talk between salicylic and gentisic acid in the *'Candidatus* Phytoplasma solani' interaction with Sangiovese grapevines. *Plants* 12: 14.

Osler R., Carraro L., Loi N., Refatti E., 1993. Symptom expression and disease occurrence of a yellow disease of grapevine in northeastern Italy. *Plant Disease* 77: 496–498.

Osler R., Zucchetto C., Carraro L., Frausin C., Mori N., Pavan F., Vettorello G., Girolami V., 2002. Trasmissione di flavescenza dorata e legno nero e comportamento delle viti infette. *L'Informatore Agrario* 58 (19): 61–65.

Pacifico D., Margaria P., Galetto L., Legovich M., Abbà S., … Palmano S., 2019. Differential gene expression in two grapevine cultivars recovered from "flavescence dorée". *Microbiological Research* 220: 72–82.

Pagliarani C., Gambino G., Ferrandino A., Chitarra W., Vrhovsek U., … Schubert, A. 2020. Molecular memory of Flavescence dorée phytoplasma in recovering grapevines. *Horticulture Research* 7: 126.

Panassiti B., Hartig F., Breuer M., Biedermann R., 2015. Bayesian inference of environmental and biotic fac-

tors determining the occurrence of the grapevine disease 'bois noir'. *Ecosphere* 6: 143.

Paolacci A.R., Catarcione G., Ederli L., Zadra C., Pasqualini S., … Ciaffi M., 2017. Jasmonate-mediated defence responses, unlike salicylate-mediated responses, are involved in the recovery of grapevine from *bois noir* disease. *BMC PlantBiology* 17: 118.

Pavan F., Carraro L., Vettorello G., Pavanetto E., Girolami V., Osler R., 1997. Flavescenza dorata nei vigneti delle colline trevigiane. *L'Informatore Agrario* 53(10): 73–78.

Pavan F., Mori N., Bressan S., Mutton P., 2012. Control strategies for grapevine phytoplasma diseases: Factors influencing the profitability of replacing symptomatic plants. *Phytopathologia Mediterranea* 51: 11–22.

Pavan F., Frizzera D., Martini M., Lujan C., Cargnus E., 2024. Is the removal of nettles along ditches effective in controlling Bois noir in vineyards? *Agronomy* 14: 643.

Perry J. N., 1998. Measures of spatial pattern for counts. *Ecology* 79: 1008–1017.

Perry J.N., Dixon P.M., 2002. A new method to measure spatial association for ecological count data. *Écoscience* 9(2): 133–141.

Perry J. N., Winder L., Holland J.M., 1999. Red-blue plots for detecting clusters in count data. *Ecology Letters* 2: 106–113.

Pierro R., de Pascali M., Panattoni A., Passera A., Materazzi A., … Quaglino F., 2022. In silico three-dimensional (3D) modeling of the SecY protein of *'Candidatus* Phytoplasma solani' strains associated with grapevine "bois noir" and its possible relationship with strain virulence. *International Journal of Plant Biology* 13(2): 15–30.

Quaglino F., Zhao Y., Casati P., Bulgari D., Bianco P.A., … Davis R.E., 2013. '*Candidatus* Phytoplasma solani', a novel taxon associated with stolbur-and bois noir-related diseases of plants. *International Journal of Systematic and Evolutional Microbiology* 63: 2879–2894.

Ramírez-Suero M., Bénard-Gellon M., Chong J., Laloue H., Stempien E., … Bertsch C., 2014. Extracellular compounds produced by fungi associated with Botryosphaeria diebackinduce differential defence gene expression patterns and necrosis in *Vitis vinifera* cv. Chardonnay cells. *Protoplasma* 251(6): 1417–1426.

Riffle V.L., Alvarez Arredondo J., Lomonaco I., Appel C., Catania A.A., … Casassa L.F., 2022. Vine age affects grapevine performance, grape and wine chemical and sensory composition of cv. Zinfandel from California. *American Journal of Enology and Viticulture* 73: 277–293. https://doi.org/10.5344/ajev.2022.22014

Romanazzi G., D'Ascenzo D., Murolo S., 2009. Field treatment with resistance inducers for the control of grapevine Bois noir. *Journal of Plant Pathology* 91(3): 677–682.

Romanazzi G., Murolo S., Feliziani E., 2013. Effects of an innovative strategy to contain grapevine Bois noir: field treatment with resistance inducers. *Phytopathology* 103(8): 785–791.

Romeo-Oliván A., Chervin J., Breton C., Lagravère T., Daydé J., … Gaur R.K., 2022. Comparative transcriptomics suggests early modifications by vintec® in grapevinetrunk of hormonal signaling and secondary metabolism biosynthesis in response to *Phaeomoniella chlamydospora* and *Phaeoacremonium minimum*. *Frontiers in Microbiology* 13: 898356.

Rotter A., Nikolić P., Turnšek N., Kogovšek P., Blejec A., Gruden K., Dermastia M., 2018.

Statistical modeling of long-term grapevine response to *'Candidatus* Phytoplasma solani' infection in the field. *European Journal of Plant Pathology* 150: 653–668.

Rusjan D., Mikulic-Petkovsek M., 2015. Phenolic responses in 1-year-old canes of *Vitis vinifera* cv. Chardonnay induced by grapevine yellows (Bois noir). *Australian Journal of Grape and Wine Research* 21(1): 123–34.

Santi S., Grisan S., Pierasco A., De Marco F., Musetti R., 2013. Laser microdissection of grapevine leaf phloem infected by stolbur reveals site-specific gene responses associated to sucrose transport and metabolism. *Plant, Cell and Environment* 36(2): 343–355.

Stempien E., Goddard M.L., Leva Y., Bénard-Gellon M., Laloue H., … Chong J., 2018. Secreted proteins produced by fungi associated with *Botryosphaeria* dieback trigger distinct defense responses in *Vitis vinifera* and *Vitis rupestris* cells. *Protoplasma* 255(2): 613–628.

Sticher L., Mauch-Mani B., Métraux J. P., 1997. Systemic acquired resistance. *Annual Review of Phytopathology* 35: 235–270.

Surico G., 2009. Towards a redefinition of the diseases within the esca complex of grapevine. *Phytopathologia Mediterranea* 48: 5–10.

Surico G., Mugnai L., Marchi G., 2006. Older and more recent observations on esca: a critical overview. *Phytopathologia Mediterranea* 45: 68–86.

Úrbez-Torres J.R., 2011. The status of Botryosphaeriaceae species infecting grapevines. *Phytopathologia Mediterranea* 50: S5–S45

Vlot A., Sales C.J.H., Lenk M., Bauer K., Brambilla A., … Nayem S., 2021. Systemic propagation of immunity in plants. *New Phytologist* 229(3): 1234–1250.

Yacoub A., Magnin N., Gerbore J., Haidar R., Bruez E., … Rey P., 2020. The biocontrol root-oomycete, *Pythium oligandrum*, triggers grapevine resistance and shifts

in the transcriptome of the trunk pathogenic fungus, *Phaeomoniella chlamydospora*. *International Journal of Molecular Sciences* 21: 18.

Zahavi T., Sharon R., Sapir G., Mawassi M., Dafny-Yelin M., Naor V., 2013. The long-term effect of Stolbur phytoplasma on grapevines in the Golan Heights. *Australian Journal of Grape and Wine Research* 19(2): 277–284.

Phytopathologia Mediterranea
The international journal of the
Mediterranean Phytopathological Union

Firenze University Press
www.fupress.com/pm

Short Notes

Characterization and genetic diversity of grapevine Pinot gris virus in Serbian vineyards

Sanja ŽIVKOVIĆ[1,*], Bojana VASILIJEVIĆ[2], Tanja VASIĆ[1], Debasis MITRA[3], Darko JEVREMOVIĆ[2]

[1] *University of Niš, Faculty of Agriculture, Kosančićeva 4, 37000 Kruševac, Serbia*
[2] *Fruit Research Institute, Kralja Petra I 9, 32102 Čačak, Serbia*
[3] *Department of Microbiology, Graphic Era (Deemed to be University), 566/6 Bell Road, Clement Town, Dehradun, 248002 Uttarakhand, India*
*Corresponding author. E-mail: zivkovic.sanja@ni.ac.rs

Summary. Sixty-five samples of grapevine from commercial vineyards in the Rasina district of Serbia were tested for the presence of grapevine Pinot gris virus (GPGV), using the reverse transcription-polymerase chain reaction. Fourteen samples of the grapevine varieties 'Red Globe', 'Victoria' and 'Preobraženje' were infected with GPGV. All the infected plants showed symptoms of leaf chlorotic mottling, puckering, and deformation, stunting, and reduced yields. The coding regions of the movement and coat protein (MP/CP) and a region of the RNA-dependent RNA polymerase (RdRP) domains of eight virus isolates were sequenced. Phylogenetic analyses of these genomic regions showed high nucleotide similarity among the Serbian GPGV isolates. This study is the first to describe genetic diversity of GPGV isolates in Serbia.

Keywords: *Vitis vinifera* L., RT-PCR, detection, phylogenetic analyses.

OPEN ACCESS

Citation: Živković, S., Vasilijević, B., Vasić, T., Mitra, D., & Jevremović, D. (2024). Characterization and genetic diversity of grapevine Pinot gris virus in Serbian vineyards. *Phytopathologia Mediterranea* 63(2): 315-321. doi: 10.36253/phyto-15465

Accepted: September 5, 2024

Published: September 15, 2024

Data Availability Statement: All relevant data are within the paper and its Supporting Information files.

Competing Interests: The Author(s) declare(s) no conflict of interest.

Editor: Nihal Buzkan, Kahramanmaraş Sütçü Imam University, Turkey.

ORCID:
SŽ: 0000-0002-4451-4957
BV: 0000-0002-9906-6522
TV: 0000-0002-1834-9484
DM: 0000-0003-0525-8812
DJ: 0000-0002-2983-9198

INTRODUCTION

More than 80 viruses naturally infect grapevines (*Vitis vinifera* L.) (Fuchs, 2020). Grapevine fanleaf virus (GFLV), grapevine leafroll-associated viruses (GLRaVs), and grapevine red blotch virus (GRBV) are economically important pathogens that cause severe damage to various plant organs, resulting in low grape yields and reduced berry quality. Most viruses are present in grapevines in mixed infections, although their influence on host plants is minor or unknown.

Grapevine Pinot gris virus was discovered in Trentino, Italy, in 2003, on the cultivar 'Pinot Gris' (Giampetruzzi *et al*., 2012). GPGV is a positive-sense single-stranded RNA virus (*Trichovirus, Betaflexiviridae*) (Tarquini *et al*., 2018). This virus causes chlorotic mottling, puckering, and deformation of 'Pinot Gris' grapevine leaves (Giampetruzzi *et al*., 2012; Martelli, 2014). Stunting, grapevine leaf mottling and deformation (GLMD), discolouration, blistering, and significant yield losses have also been reported on other grapevine cultivars (including 'Traminer,' 'Chardonnay', 'Riesling', and

'Tocai') (Giampetruzzi *et al*., 2012; Malossini *et al*., 2012; Martelli *et al*., 2014; Saldarelli *et al*., 2015; Gentili *et al*., 2017). Latent infections can also be caused by GPGV (Giampetruzzi *et al*., 2012; Saldarelli *et al*., 2013; Eichmeier *et al*., 2016a; 2016b; 2017). GPGV has been frequently identified in mixed infections with other viruses that infect grapevines, making it difficult to determine its influence on vine health. The virus has been reported in numerous countries, including in Europe (Armenia, Belgium, Bosnia and Herzegovina, Croatia, Czech Republic, France, Georgia, Germany, Greece, Hungary, Italy, Moldova, Montenegro, North Macedonia, Poland, Portugal, Romania, Russia, Serbia, Slovakia, Slovenia, Spain, Switzerland, Türkiye, Ukraine, and the United Kingdom), in Asia (China, Lebanon, Iran, Japan, Pakistan, and South Korea), Africa (Algeria), and in South America (Argentina) (EPPO, 2024). Hily *et al*. (2020) hypothesized a scenario for GPGV dispersal from an Asian origin to Europe and other world grape producing countries. Movement and exchange of GPGV infected host propagation material (potted vines, cuttings, rootlings, and budwood) is the primary mode for transmission of the virus. Bertazzon *et al*. (2020) reported rapid transmission of GPGV in Italian vineyards, and the grape leaf blister mite (*Colomerus vitis* Pagenstecher) is a putative GPGV vector (Malagnini *et al*., 2016). GPGV does not spread mechanically through pruning or harvesting machinery.

The presence of GPGV in Serbia was confirmed by Bertazzon *et al*. (2016), in one sample from an unknown grapevine cultivar. Since then, no further research has been reported on GPGV presence in this country. The aim of the present study was to investigate presence and genetic diversity of GPGV in Serbia.

MATERIALS AND METHODS

From 2020 to 2022, 65 samples of grapevine leaves were collected from the Rasina district, which is an important grape-producing region in Serbia. Samples were collected from symptomatic and asymptomatic plants. Symptomatic plants had shortened internodes, deformed leaves, and leaf chloroses and mottling. Each sample consisted of five to six leaves picked from different parts of an individual plant. Leaf petiole samples were ground in extraction bags (Flexo), in 2% cetyltrimethylammonium bromide (CTAB) buffer, as described for total nucleic acid (TNA) extraction by Li *et al*. (2008). Reverse transcription (RT) reactions were carried out in two steps with random hexamer $pd(N)_6$ primers and Maxima Reverse Transcriptase (Thermo Scientific). Polymerase chain reactions (PCR) were carried out using two GPGV-specific primer pairs. For the first PCR, the primer pair GPGVRepF/GPGVRepR was used, spanning the RNA-dependent RNA polymerase (RdRp) domain of the replicase gene (525 bp) (Saldarelli *et al*., 2015). The primer pair GPGVDetF/GPGVDetR, spanning the end of the movement protein (MP) and the beginning of the coat protein (CP) gene (585 bp), was used for the second PCR (Saldarelli *et al*., 2015). Polymerase chain reactions were carried out in a TPersonal thermocycler (Biometra), with each reaction containing 1× DreamTaq Green Buffer, 0.2 mM dNTPs, 2.5 mM $MgCl_2$, 0.2 mM each primer, and 0.05U of Green Taq DNA polymerase (ThermoScientific). The thermal cycling conditions were as follows: 5 min at 94°C; 30 cycles each of 30 s at 94°C, 30 s at 55°C, and 60 s at 72°C; and a final step of 10 min at 72°C. Amplicons were visualized using 1.5% agarose gel electrophoresis.

All GPGV-infected samples were additionally tested for the presence of nine other viruses capable of infecting grapevines (GFLV, GRSPaV, GFkV, GLRaV1, GLRaV3, GVA ArMV, GVB, and GlRaV-2), using multiplex RT-PCR as described by Gambino and Gribaudo (2006).

Genetic diversity of the GPGV isolates was assessed by sequencing the amplified products of eight isolates (Table 1) (Macrogen Europe Laboratory, the Netherlands). BioEdit software (Hall, 1999) was used to assemble the raw sequences obtained. Phylogenetic relationships were reconstructed using a Maximum Likelihood (ML) tree, using MEGA11 software (Tamura *et al*., 2021). A phylogenetic tree was generated using the ML method with 1000 bootstrap replications.

RESULTS AND DISCUSSION

The expected 525 bp and 585 bp fragments were obtained in 17% (14 of the 65 tested samples). These results indicate limited distribution of GPGV in the Rasina district of Serbia. GPGV was confirmed in three grapevine cultivars ('Red Globe,' 'Victoria' and 'Preobraženje'), which had symptoms of stunted canes with shortened internodes, chlorotic mottling, and leaf deformation (Figures 1 and 2). GPGV-infected samples were collected from two vineyards located in the village of Božurevac. GPGV-infected samples of 'Victoria' originated from a 15-year-old vineyard, while samples from 'Red Globe' and 'Preobraženje' were taken from a nearby 3-year-old vineyard.

To further characterize the detected virus, fragments of the RdRP and MP/CP genes from eight isolates

Figure 1. Shortened internodes, deformed leaves and stunting of shoots in a GPGV-infected grapevine of 'Red Globe'.

Figure 2. Leaf deformation, chlorosis and mottling in a GPGV-infected grapevine of 'Victoria'.

were selected and partially sequenced (Table 1). Sequences were deposited in NCBI GenBank under accession numbers OP279698 to OP279713. When compared, the detected Serbian GPGV isolates had 97.3 to 100% nucleotide sequence similarities in the RdRP fragments, and 97.6 to 100% similarities in the MP/CP fragments. The sequences from the isolates were compared with those of other GPGV isolates available in the NCBI GenBank database. BLAST analysis of the RdRP sequences showed the greatest (99.62%) nt sequence similarity with isolates from Spain (KY404083), Switzerland (ON237610), and Slovakia (KF134125). Nucleotide sequences of the MP/CP gene showed greatest similarity (98.98 to 99.66%) with isolates from Russia (ON033806) and Hungary (ON360686). In the reconstructed phylogenetic tree with MP/CP sequences, the Serbian isolates clustered into three separate subclusters (Figure 3). In the RdRP sequence phylogenetic tree, the GPGV isolates were clustered into two subclusters (Figure 4). The clustering of the Serbian isolates confirms their close relatedness, and indicates that the samples originated from the same locality. The older vineyard of 'Victoria' grapevines may have been the source of GPGV, that spread to the adjacent younger plants of 'Red Globe' and 'Preobraženje'.

Table 1. Grapevine Pinot gris virus isolates characterized in this study.

Isolate	Year of isolation	Host cultivar	NCBI accession numbers RdRp gene	NCBI accession numbers MP/CP gene
RS-GPGV-1	2021	'Red Globe'	OP279698	OP279706
RS-GPGV-4	2021	'Red Globe'	OP279699	OP279707
RS-GPGV-6	2021	'Red Globe'	OP279700	OP279708
RS-GPGV-8	2021	'Red Globe'	OP279701	OP279709
RS-GPGV-12	2021	'Preobraženje'	OP279702	OP279710
RS-GPGV-13	2021	'Preobraženje'	OP279703	OP279711
RS-GPGV-14	2021	'Victoria'	OP279704	OP279712
RS-GPGV-15	2021	'Victoria'	OP279705	OP279713

In addition to GPGV, other viruses were detected by RT-PCR in the samples tested. GFLV, GFkV, GRSPaV, and GLRaV1 were detected in all the GPGV-infected

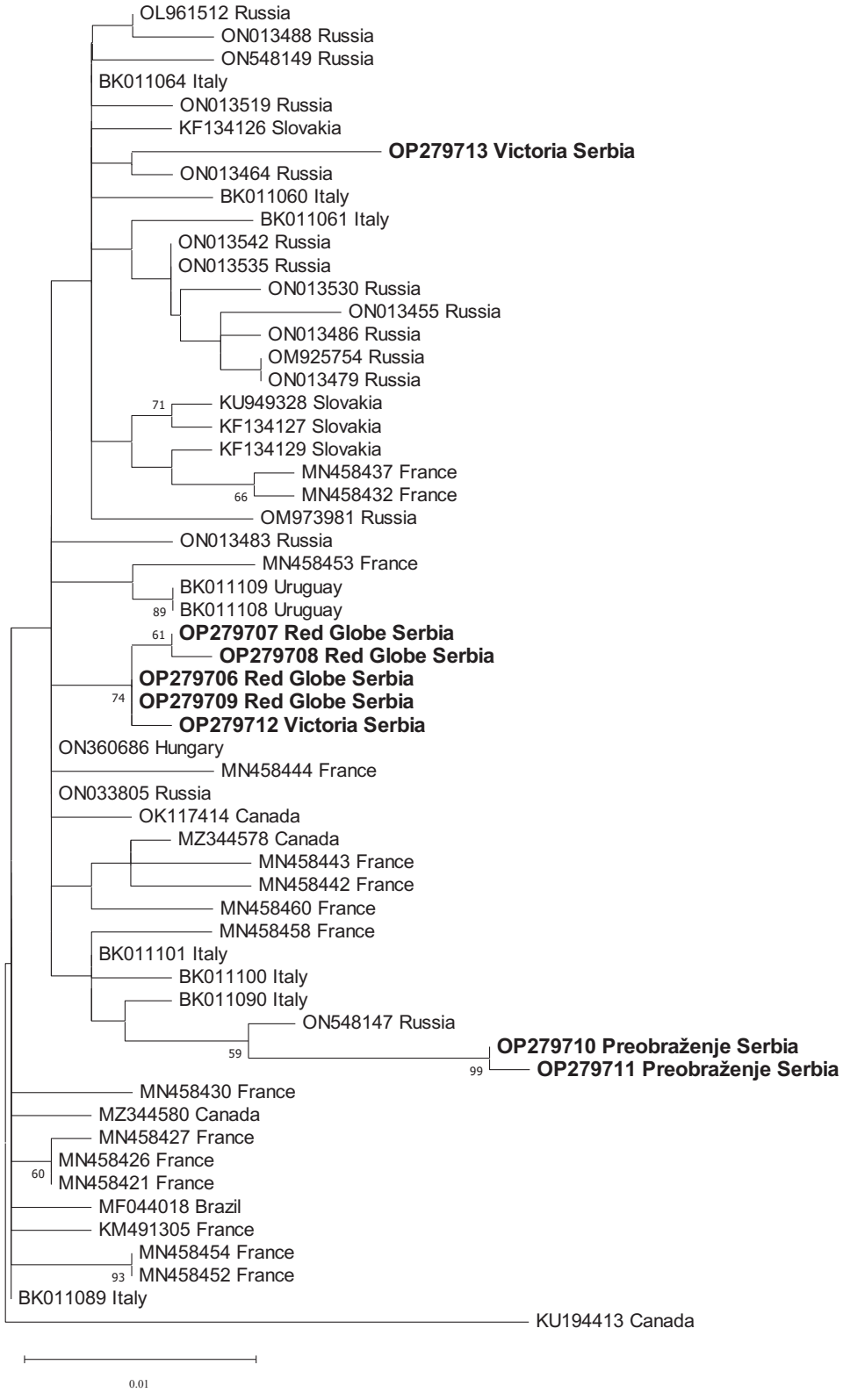

Figure 3. Phylogenetic analysis of partial MP/CP sequences of 58 grapevine Pinot gris virus isolates retrieved from NCBI. Phylogenies were inferred with ML method based on Kimura 3-parameter model with gamma distribution (MEGA11). Bootstrap values (> 50%) are displayed next to respective branches. The NCBI accession numbers are in parentheses. Serbian isolates are in bold font.

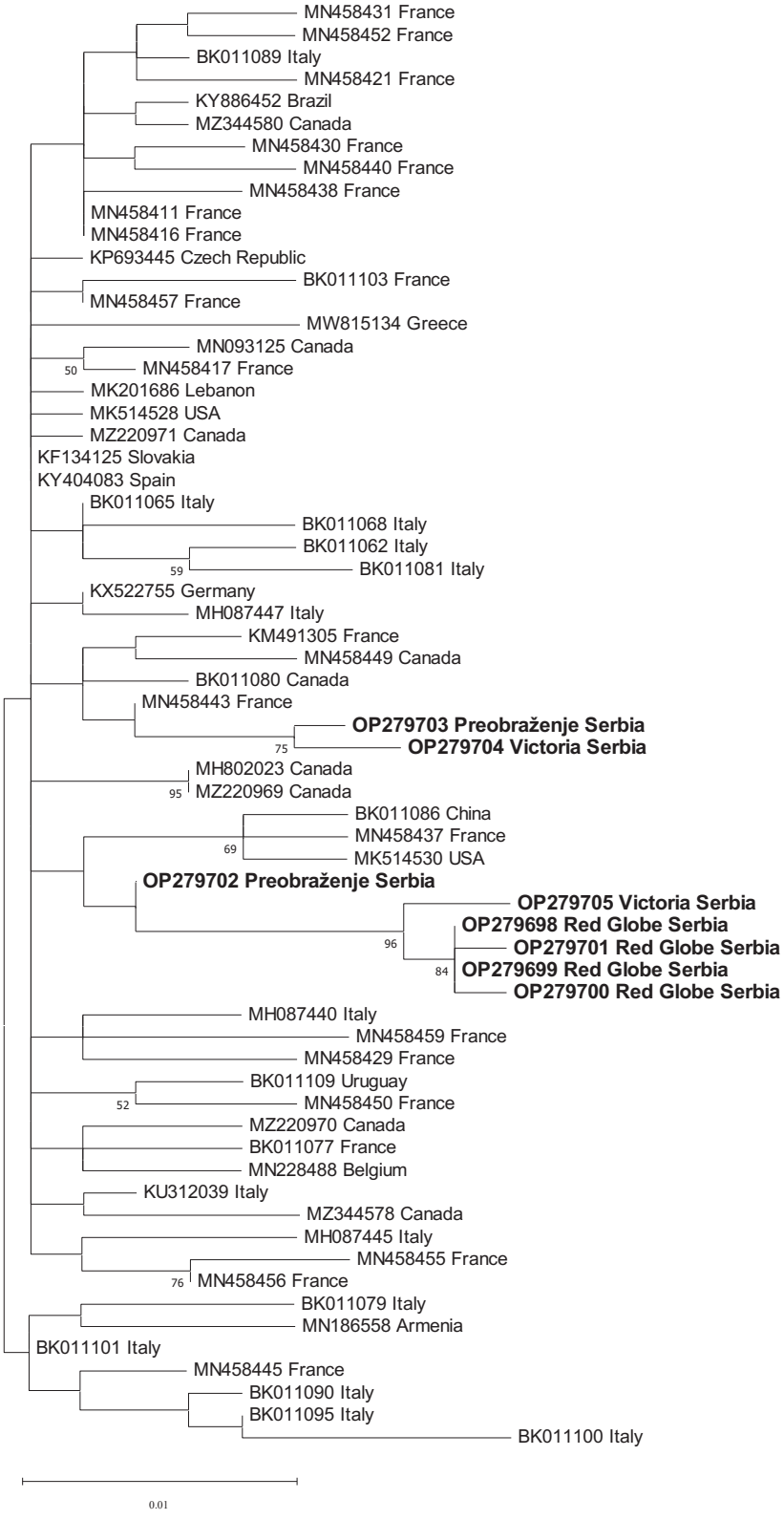

Figure 4. Phylogenetic analysis of partial RdRP sequences of 65 grapevine Pinot gris virus isolates. Phylogenies were inferred with ML method based on Kimura 3-parameter model with gamma distribution (MEGA11). Bootstrap values (> 50%) are displayed next to respective branches. The NCBI accession numbers are in parentheses. Serbian isolates are in bold font.

samples. In varieties 'Preobraženje' and 'Victoria', GFkV and GRSPaV were also confirmed.

All the GPGV-infected samples showed typical symptoms, as described by Giampetruzzi *et al*. (2012). The most significant symptom found in all infected vines was plant stunting, followed by shortened internodes and chlorotic leaves. Saldarelli *et al*. (2015) detected GPGV in asymptomatic samples, but in the present study GPGV was not confirmed in samples with no symptoms. Other viruses that caused similar symptoms (GFLV and GFkV) were detected in all 14 GPGV-positive samples from Serbia. Therefore, it cannot be confirmed which virus was the primary cause of the disease symptoms, or whether the symptoms resulted from mixed virus infections.

The presence of symptoms in infected grapevines depends on the genetic variability of GPGV isolates (Tarquini *et al*., 2018). In addition, the expression of symptoms correlates with different virus variants and/or virus titres. Bertazzon *et al*. (2017) confirmed that symptomatic grapevines have a greater GPGV titres than asymptomatic grapevines. The frequency of manifestation of symptoms has been found to be affected by soil and terrain types (Angelini *et al*., 2015).

The Serbian GPGV isolates showed high nucleotide similarities in both genomic regions examined. Analyses of the nucleotide sequences of partial MP and CP genes showed that the Serbian GPGV isolates were closely related to Russian and Hungarian isolates. Considering the RdRP domain, the Serbian isolates were closely related to Spanish, Swiss, and Slovakian isolates.

This is the first comprehensive study of GPGV in Serbia. Further research should be carried out to characterize the incidence and prevalence of GPGV in vineyards across all districts of the country.

ACKNOWLEDGEMENTS

This research was supported by the Ministry of Science, Technological Development and Innovation of the Republic of Serbia, under the contract numbers, 451-03-65/2024-03/200383 and 451-03-66/2024-03/200215.

LITERATURE CITED

Angelini E, Bazzo I., Bertazzon N., Filippin L., Forte V., 2015. A new disease in the vineyard: Grapevine. leaf mottling and deformation. *The Australian & New Zealand Grapegrower and Winemaker* 622: 56–59.

Bertazzon N., Filippin L., Forte V., Angelini E., 2016. Grapevine Pinot gris virus seems to have recently been introduced to vineyards in Veneto, Italy. *Archives of Virology* 161(3): 711–714. https://doi.org/10.1007/s00705-015-2718-2

Bertazzon N., Forte V., Filippin L., Causin R., Maixner M., Angelini E., 2017. Association between genetic variability and titre of Grapevine Pinot gris virus with disease symptoms. *Plant Pathology* 66: 949–959. doi: 10.1111/ppa.12639

Bertazzon N., Forte V., Angelini E., 2020. Fast transmission of grapevine 'Pinot gris' virus (GPGV) in vineyard. *Vitis* 59: 29–34. https://doi.org/10.5073/vitis.2020.59.29-34

Eichmeier A., Peňázová E., Pavelková R., Mynarzová Z., Saldarelli P., 2016a. Detection of grapevine pinot gris virus in certified grapevine stocks in Moravia, Czech Republic. *Journal of Plant Pathology* 98: 155–157. https://doi.org/10.4454/JPP.V98I1.043

Eichmeier A., Komínková M., Komínek P., Baránek M., 2016b. Comprehensive virus detection using next generation sequencing in grapevine vascular tissues of plants obtained from the wine regions of bohemia and Moravia (Czech Republic). *PloS One* 11, e0167966. https://doi.org/10.1371/journal.pone.0167966.

Eichmeier A., Pieczonka K., Peňázová E., Pečenka J., Gajewski Z., 2017. Occurrence of grapevine pinot gris virus in Poland and description of asymptomatic exhibitions in grapevines. *Journal of Plant Diseases and Protection* 124: 407–411. https://doi.org/10.1007/s41348-017-0076-x

EPPO, 2024. GPGV distribution. Available at: https://gd.eppo.int/taxon/GPGV00/distribution. Retrieved 10 May 2024.

Fuchs, M., 2020. Grapevine viruses: a multitude of diverse species with simple but overall poorly adopted management solutions in the vineyard. *Journal of Plant Pathology* 102: 643–653. https://doi.org/10.1007/s42161-020-00579-2

Gambino G., Gribaudo I., 2006. Simultaneous detection of nine grapevine viruses by multiplex reverse transcription-polymerase chain reaction with coamplification of a plant RNA as internal control. *Phytopathology* 96(11): 1223–1229. https://doi.org/10.1094/PHYTO-96-1223

Gentili A., Prota V., Moro G., Schianchi N., Di Lucca E., Luigi M., Faggioli F., 2017. Identification of grapevine 'Pinot gris' virus in Sardinia and Lazio (South and Central Italy). *Journal of Plant Pathology* 99: 527–535. https://doi.org/10.4454/JPP.V99I2.3872

Giampetruzzi A., Roumi V, Roberto R, Malossini U, Yoshikawa N, … Saldarelli P. 2012. A new grapevine virus discovered by deep sequencing of virus– And

viroid–derived small RNAs in cv pinot gris. *Virus Research* 163: 262–268. https://doi.org/10.1016/j.virusres.2011.10.010

Hall T.A., 1999. BioEdit: a user-friendly biological sequence alignment editor and analysis program for Windows 95/98/NT. *Nucleic Acid Symposium Series* 41: 95–98.

Hily J.M., Poulicard N., Candresse T., Vigne E., Beuve M., … Lemaire O., 2020. Datamining, genetic diversity analyses, and phylogeographic reconstructions redefine the worldwide evolutionary history of grapevine pinot gris virus and grapevine berry inner necrosis virus. *Phytobiomes Journal* 4(2): 165–177. https://doi.org/10.1094/PBIOMES-10-19-0061-R

Li R., Mock R., Huang Q., Abad J., Hartung J., Kinard G., 2008. A reliable and inexpensive method of nucleic acid extraction for the PCR-based detection of diverse plant pathogens. *Journal of Virological Methods* 154: 48–55. https://doi.org/10.1016/j.jviromet.2008.09.008

Malagnini V., de Lillo E., Saldarelli P., Beber R., Duso C., … Gualandri V., 2016. Transmission of grapevine Pinot gris virus by *Colomerus vitis* (Acari: Eriophyidae) to grapevine. *Archives of Virology* 161(9): 2595-2599. https://doi.org/10.1007/s00705-016-2935-3

Malossini U., Moscon R., Ferrazza M., Bianchedi P., Varner M., Credi R., 2012. Caratteristiche vegeto-produttive di viti Pinot grigio e Traminer aromatico affette da una nuova virosi segnalata in Trentino [Vegetative-productive characteristics of Pinot grigio and Traminer aromatico vines affected by a new virus reported in Trentino]. In: *Proceedings IV Convegno Nazionale di Viticoltura: CONAVI.TO*, 10–12 July, 2012, Asti, Italy, 37 (abstract).

Martelli G.P., 2014. Directory of virus and virus-like diseases of the grapevine and their agents. *Journal of Plant Pathology* 96: 105–120. https://doi.org/10.4454/JPP.V96I1SUP

Saldarelli P., Beber R., Novelli L., Bianchedi P., Credi R., … Gualandri V., 2013. Studies on a new grapevine disease in Trentino vineyards. *Journal of Plant Pathology* 95: S4.60

Saldarelli P., Giampetruzzi A., Morelli M., Malossini U., Pirolo C., Bianchedi P., Gualandri V., 2015. Genetic variability of Grapevine Pinot gris virus and its association with grapevine leaf mottling and deformation. *Phytopathology* 105: 555–563. https://doi.org/10.1094/PHYTO-09-14-0241-R

Tamura K., Stecher G., Kumar S., 2021. MEGA11: Molecular Evolutionary Genetics Analysis version 11. *Molecular Biology and Evolution* 38: 3022–3027. https://doi.org/10.1093/molbev/msab120

Tarquini G., Ermacora P., Bianchi G.L., De Amicis F., Pagliari L., … Musetti R., 2018. Localization and subcellular association of Grapevine Pinot Gris Virus in grapevine leaf tissues. *Protoplasma* 255(3): 923–935. https://doi.org/10.1007/s00709-017-1198-5

Finito di stampare da
Logo s.r.l. – Borgoricco (PD) – Italia

Mediterranean Phytopathological Union

Founded by Antonio Ciccarone

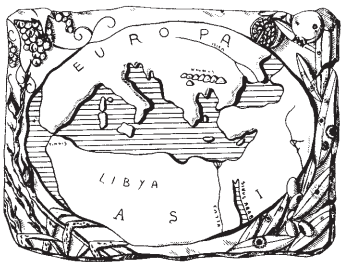

The Mediterranean Phytopathological Union (MPU) is a non-profit society open to organizations and individuals involved in plant pathology with a specific interest in the aspects related to the Mediterranean area considered as an ecological region. The MPU was created with the aim of stimulating contacts among plant pathologists and facilitating the spread of information, news and scientific material on plant diseases occurring in the area. MPU also intends to facilitate and promote studies and research on diseases of Mediterranean crops and their control.
The MPU is affiliated to the International Society for Plant Pathology.

MPU Governing Board

Affiliated Societies

Arab Society for Plant Protection (ASPP), http://www.asplantprotection.org/
French Society for Phytopathology (FSP), http://www.sfp-asso.org/
Hellenic Phytopathological Society (HPS), http://efe.aua.gr/
Israeli Phytopathological Society (IPS), http://www.phytopathology.org.il/
Italian Phytopathological Society (SIPAV), http://www.sipav.org/
Portuguese Phytopathological Society (PPS), http://www.spfitopatologia.org/
Spanish Society for Plant Pathology (SEF), http://www.sef.es/sef/

2024 MPU Membership Dues

Institutional MPU Membership: : € 200.00 (college and university departments, libraries and other facilities or organizations). Beside the open-access on-line version of *Phytopathologia Mediterranea*, the print version can be received with a € 50 contribution to mail charges (total € 250,00 to receive the print version). Researchers belonging to an Institution which is a member of the Union are entitled to publish with a reduced page contribution, as the Individual Regular members.
Individual Regular MPU Membership*: € 50.00 (free access to the open-access on-line version of Phytopathologia Mediterranea and can get the print version with a contribution to mail charges of € 50 (total € 100,00 to receive the print version).

*Students can join the MPU as a Student member on the recommendation of a Regular member. Student MPU members are entitled to a 50% reduction of the membership dues (proof of student status must be provided).

Payment information and online membership renewal and subscription at www.mpunion.com

For subscriptions and other information visit the MPU web site:
www.mpunion.com
or contact us at: Phone +39 39 055 2755861/862 – E-mail: phymed@unifi.it

Phytopathologia Mediterranea

Volume 63, August, 2024

Contents

Direttore responsabile: Giuseppe Surico • Autorizzazione del Tribunale di Firenze n. 4923 del 5-1-2000 • *Printed by* Logo S.r.l. - Padova, October 2024